

**SOLID-STATE HYDROGEN-DEUTERIUM EXCHANGE MASS
SPECTROMETRY OF LYOPHILIZED PEPTIDES**

by

Rajashekar Kammari

A Dissertation

Submitted to the Faculty of Purdue University

In Partial Fulfillment of the Requirements for the degree of

Doctor of Philosophy



Department of Industrial and Physical Pharmacy

West Lafayette, Indiana

August 2020

THE PURDUE UNIVERSITY GRADUATE SCHOOL
STATEMENT OF COMMITTEE APPROVAL

Dr. Elizabeth M. Topp, Chair

Department of Industrial and Physical Pharmacy

Dr. Lynne S. Taylor

Department of Industrial and Physical Pharmacy

Dr. Gregory T. Knipp

Department of Industrial and Physical Pharmacy

Dr. Weiguo A. Tao

Department of Biochemistry

Approved by:

Dr. Rodolfo Pinal

Dedicated to my parents, grandparents, and siblings

ACKNOWLEDGMENTS

I would like to thank Dr. Elizabeth M. Topp, my research advisor, with immense gratitude for her invaluable guidance throughout my Ph.D. education. I honestly believe that without her support, this work would not have been possible. I am forever grateful for the opportunity to work on exciting projects, and I am sure I will miss the wonderful days that I spent in Topp lab at Purdue University. I extend my sincere thanks to the research committee members, Dr. Lynne S. Taylor, Dr. Gregory T. Knipp, and Dr. Weiguo A. Tao, for their valuable time, scientific input, and guidance. I appreciate Mary Ellen Hurt, Nancy Cramer, and Delayne Graham for their administrative help.

I am thankful to all Topp lab members, especially Dr. Shenbaga Moorthy, Dr. Mohamed AbouGhaly, and Dr. Ehab Moussa, for their helpful suggestions. I sincerely thank the LyoHub facility at Purdue University for training and allowing us to use lyophilization equipment. Many thanks to fellow graduate researchers in the Department of Industrial and Physical Pharmacy for their help with my presentations, fun times, and stimulating discussions over coffee breaks. I am indebted to Dr. Andreas Sophocleous for an internship opportunity in the Biopharmaceutical Product Sciences department at GlaxoSmithKline. I thank Dr. Jainik Panchal (Merck & Co., Inc.) and Dr. Lokesh Kumar (Genentech, Inc.) for the industrial collaboration opportunities and valuable scientific inputs.

I am incredibly grateful to my parents and grandparents for their constant motivation and for inspiring me to pursue my career goals. I express my heartfelt thanks to my brother, sister, and brother-in-law, for supporting me over the years. Finally, I would like to thank my niece and nephew for their unconditional love and support.

TABLE OF CONTENTS

LIST OF TABLES	9
LIST OF FIGURES	10
LIST OF ABBREVIATIONS.....	18
ABSTRACT.....	20
CHAPTER 1. INTRODUCTION	22
1.1 Therapeutic proteins.....	22
1.2 Protein instability in the solid-state.....	24
1.2.1 Physical instability.....	24
1.2.2 Chemical instability	26
1.3 Solid-state protein characterization techniques	29
1.4 Solid-state hydrogen-deuterium exchange mass spectrometry (ssHDX-MS)	32
1.4.1 Fundamentals of hydrogen-deuterium exchange in solution.....	34
1.4.2 Hydrogen-deuterium exchange in proteins with higher-order structure.....	35
1.4.3 Factors affecting hydrogen-deuterium exchange in solution.....	39
1.4.4 Mechanistic models for solid-state hydrogen-deuterium exchange	42
1.5 Specific aims and hypotheses	44
1.6 Overall approach.....	46
1.7 References.....	48
CHAPTER 2. SOLID-STATE HYDROGEN-DEUTERIUM EXCHANGE MASS SPECTROMETRY (ssHDX-MS) OF LYOPHILIZED POLY-D, L-ALANINE.....	57
2.1 Abstract.....	57
2.2 Introduction.....	58
2.3 Materials and methods	62
2.3.1 Sample preparation by lyophilization.....	62
2.3.2 Solution HDX-MS.....	63
2.3.3 Solid-state HDX-MS (ssHDX-MS).....	63
2.3.4 Dynamic vapor sorption	64
2.3.5 Powder X-ray diffraction (PXRD).....	65
2.3.6 Solid state FT-IR.....	65

2.3.7	Modulated differential scanning calorimetry (MDSC).....	65
2.4	Results.....	66
2.4.1	Physical characterization of lyophilized solids by PXRD.....	66
2.4.2	Thermal analysis of lyophilized samples by MDSC	67
2.4.3	Secondary structure of peptides after lyophilization by FT-IR	67
2.4.4	Residual moisture content by DVS.....	68
2.4.5	Vapor sorption by DVS	68
2.4.6	Mass spectrometric characterization of PDLA.....	71
2.4.7	Solution state HDX-MS.....	71
2.4.8	Solid-state HDX-MS	73
2.4.9	Effect of RH on ssHDX-MS.....	76
2.5	Discussion.....	76
2.6	Conclusions.....	84
2.7	Supporting information.....	84
2.8	References.....	85
CHAPTER 3. PRE-HYDRATION AND THE REVERSIBILITY OF SOLID-STATE HYDROGEN-DEUTERIUM EXCHANGE		89
3.1	Abstract.....	89
3.2	Introduction.....	90
3.3	Materials and methods	94
3.3.1	Materials	94
3.3.2	Lyophilization.....	94
3.3.3	Powder X-ray diffraction (PXRD).....	95
3.3.4	Pre-hydration and ssHDX-MS.....	95
3.3.5	Reversibility of ssHDX-MS	96
3.3.6	Statistical analysis.....	97
3.4	Results.....	97
3.4.1	Physical characterization by PXRD.....	97
3.4.2	Effect of pre-hydration on ssHDX-MS kinetics	99
3.4.3	Reversibility of ssHDX-MS	101
3.4.4	Comparison of the forward and reverse ssHDX-MS reactions	101

3.5	Discussion.....	105
3.5.1	Pre-hydration and ssHDX-MS.....	105
3.5.2	Reversibility of ssHDX-MS	105
3.5.3	Limiting solution for deuterated peptide concentration, high RH.....	106
3.5.4	Steady-state solution for plateau level of deuterated peptide	108
3.6	Conclusions.....	111
3.7	Supporting information.....	111
3.8	References.....	111
CHAPTER 4. EFFECTS OF PEPTIDE SECONDARY STRUCTURE ON SOLID-STATE HYDROGEN-DEUTERIUM EXCHANGE		114
4.1	Abstract.....	114
4.2	Introduction.....	115
4.3	Materials and methods	118
4.3.1	Materials	118
4.3.2	Lyophilization.....	119
4.3.3	Circular dichroism spectroscopy (CD)	119
4.3.4	Fourier transform infrared spectroscopy (FTIR).....	120
4.3.5	Powder X-ray diffraction (PXRD).....	120
4.3.6	Solution HDX-MS.....	120
4.3.7	Solid-state HDX-MS (ssHDX-MS).....	121
4.3.8	Statistical analysis.....	121
4.4	Results.....	122
4.4.1	Peptide secondary structure in solution by CD.....	122
4.4.2	Peptide secondary structure after lyophilization.....	123
4.4.3	Solid physical form by PXRD	124
4.4.4	Solution-state HDX-MS	126
4.4.5	Solid-state HDX-MS	127
4.4.6	Effect of RH on ssHDX-MS.....	130
4.4.7	Effect of peptide secondary structure on ssHDX-MS	131
4.5	Discussion.....	136
4.6	Conclusions.....	141

4.7 Supporting information.....	141
4.8 References.....	142
CHAPTER 5. CONCLUSIONS.....	146
APPENDIX A. SUPPORTING INFORMATION FOR CHAPTER 2.....	149
APPENDIX B. SUPPORTING INFORMATION FOR CHAPTER 3.....	162
APPENDIX C. SUPPORTING INFORMATION FOR CHAPTER 4.....	171
VITA.....	189

LIST OF TABLES

Table 4.1. Number of protected amide bonds for model peptides in various formulations, as measured in ssHDX-MS studies at 11% and 23% RH 137

APPENDIX TABLES

Table A1. A list of PDLA peptides detected on MS analysis. Initial mass spec analysis data shows the presence of several peptides (6 amino acid length to 44 amino acid length) and their corresponding masses, m/z values and retention times are shown in table-A1 159

Table A2. Statistical analysis for a_D vs D_{max} 160

Table A3. Statistical analysis for $1/a_D$ vs A_0/D_{max} 161

Table C1. Effect of RH on the D_{max} (Da) values of Peptide A and Peptide B formulations (n=3, mean \pm SE)..... 184

Table C2. Effect of RH on the HDX rate constant values (k, h^{-1}) of Peptide A and Peptide B formulations (n=3, mean \pm SE)..... 184

Table C3. Effect of secondary structure on the D_{max} (Da) values of Peptide A formulations in comparison with corresponding unstructured PDLA peptides (n=3, mean \pm SE)..... 185

Table C4. Effect of secondary structure on the D_{max} (Da) values of Peptide B formulations in comparison with corresponding unstructured PDLA peptides (n=3, mean \pm SE)..... 185

Table C5. Effect of secondary structure on the HDX rate constant values (k, h^{-1}) of Peptide A formulations in comparison with corresponding unstructured PDLA peptides (n=3, mean \pm SE).
..... 186

Table C6. Effect of secondary structure on the HDX rate constant values (k, h^{-1}) of Peptide B formulations in comparison with corresponding unstructured PDLA peptides (n=3, mean \pm SE).
..... 186

Table C7. Calculation of approximate number of structural H-bonds in myoglobin using protein sequence structure information from PDB 187

Table C8. Number of protected amide bonds for myoglobin in various formulations, as measured in ssHDX-MS studies 188

LIST OF FIGURES

- Figure 1.1.** Hydrogen-deuterium exchange reaction mechanisms in solution. (a) base catalysis, (b) acid catalysis by N-protonation, and (c) acid catalysis by O-protonation 35
- Figure 1.2.** Schematic representation of the solvent penetration model 37
- Figure 1.3.** Schematic representation of the relayed imidic acid model 38
- Figure 1.4.** Schematic representation of the Linderstrom-Lang model. (a) local unfolding events, or (b) global unfolding events..... 38
- Figure 1.5.** Chemical hydrogen exchange rate vs. pH profile in a poly-D, L-alanine peptide 40
- Figure 2.1.** Powder X-ray diffraction profiles of lyophilized PDLA formulations show amorphous characteristics for sucrose, trehalose and excipient-free formulations and crystalline characteristics for mannitol, sodium chloride and guanidine HCl formulations 66
- Figure 2.2.** T_g values of amorphous lyophilized PDLA formulations as a function of RH. Samples showed deliquescence for $T_g < 20^\circ\text{C}$ ($n=3$, mean \pm SD) 67
- Figure 2.3.** Solid state FT-IR spectra of PDLA peptides after lyophilization. 68
- Figure 2.4.** Moisture content in lyophilized PDLA formulations measured with dynamic vapor sorption (DVS): A) Residual moisture content in lyophilized poly-DL-alanine formulations at $t=0$, B) Equilibrium moisture content at 6 % RH, 11 % RH and 23 % RH and C) Equilibrium moisture content at 43 % RH, 57 % RH ($n=1$). 70
- Figure 2.5.** Solution state hydrogen deuterium exchange mass spectrometry (HDX-MS) of PDLA formulations containing: A) sucrose, B) trehalose, C) mannitol, D) sodium chloride, E) guanidine hydrochloride or F) no excipient (“excipient free”). Deuterium incorporation data are shown for eight PDLA peptides from the polydisperse mixture having different amino acid (AA) chain length: 15 AA (blue), 18 AA (red), 22 AA (green), 25 AA (purple), 27 AA (orange), 29 AA (black), 31 AA (brown) and 34 AA (dark blue). $n=3$, mean \pm SD; error bars not shown when less than the height of the symbol..... 72
- Figure 2.6.** Solid state hydrogen deuterium exchange mass spectrometry (ssHDX-MS) of PDLA formulations containing: A) sucrose, B) trehalose, C) mannitol, D) sodium chloride, E) guanidine HCl or F) no excipient (“excipient-free”). Data shown for 22 amino acid peptide. $n=3$, mean \pm SD; error bars not shown when less than the height of the symbol..... 75

Figure 2.7. A_0/D_{\max} as a function of $1/a_D$ for lyophilized PDLA peptides at RH < 50% in formulations containing: A) sucrose, B) trehalose, C) mannitol, D) sodium chloride, E) guanidine HCl or F) no excipient (excipient-free), where $a_D = (\%RH/100)$ at equilibrium. D_{\max} was calculated from the back exchange corrected percentage deuterium uptake mono-exponential fits and A_0 is theoretical percentage of exchangeable amide groups (=100). Data shown for a 22 amino acid peptide, n=3; dotted lines represent 95% CI of the best fit line..... 80

Figure 2.8. Apparent exchange rate constant (k_{ap}) as a function of a_D for lyophilized PDLA peptides at RH < 50% in formulations containing: A) sucrose, B) trehalose, C) mannitol, D) sodium chloride, E) guanidine HCl or F) no excipient (“excipient-free”), where $a_D = (\%RH/100)$ at equilibrium. Data shown for a back exchange corrected 22 amino acid peptide, n=3, dotted lines represent 95% CI of the best fit line. 82

Figure 3.1. PXRD diffractograms of PDLA formulations immediately after lyophilization (t_0), after pre-hydration for 12 h at 6% RH or 11% RH: (A) sucrose, (B) trehalose, (C) mannitol, (D) sodium chloride, (E) guanidine HCl, and (F) no excipient (“excipient free”)..... 98

Figure 3.2. The maximum extent of deuterium (D_{\max}) and deuteration rate constant (k) values of non-prehydrated (open bar) and pre-hydrated (hatched bar) PDLA formulations lyophilized with various excipients. (A) D_{\max} at 6% RD (Case-1), (B) D_{\max} at 11% RD (Case-2), (C) k at 6% RD (Case-1), (D) k at 11% RD (Case-2), Data shown for an 18 amino acid length PDLA peptide; n=3, mean \pm SE; error bars not shown when less than the height of the symbol. 100

Figure 3.3. Comparison of the forward and reverse ssHDX-MS kinetics for PDLA formulations deuterated at 6% RD (forward) followed by deuterium removal at 0% RH (reverse) (Case-3a). Formulations contained (A) sucrose, (B) trehalose, (C) mannitol, (D) sodium chloride, (E) guanidine HCl, and (F) no excipient (“excipient free”). Solid line indicates fit of the forward ssHDX reaction to a mono-exponential association model, dotted line indicates fit of the reverse ssHDX reaction to a mono-exponential decay model; see text for details. Data shown for an 18 amino acid length PDLA peptide, n=3, mean \pm SD. error bars not shown when less than the height of the symbol..... 102

Figure 3.4. Comparison of the forward and reverse ssHDX-MS kinetics for PDLA formulations deuterated at 6% RD (forward) followed by deuterium removal at 6% RH (reverse) (Case-3b). Formulations contained (A) sucrose, (B) trehalose, (C) mannitol, (D) sodium chloride, (E) guanidine HCl, and (F) no excipient (“excipient free”). Solid line indicates fit of the forward ssHDX reaction to a mono-exponential association model, dotted line indicates fit of the reverse ssHDX reaction to a mono-exponential decay model; see text for details. Data shown for an 18 amino acid length PDLA peptide, n=3, mean \pm SD. error bars not shown when less than the height of the symbol..... 103

Figure 3.5. Comparison of the forward and reverse ssHDX-MS kinetics for PDLA formulations deuterated at 6% RD (forward) followed by deuterium removal at 43% RH (reverse) (Case-3c). Formulations contained (A) sucrose, (B) trehalose, (C) mannitol, (D) sodium chloride, (E) guanidine HCl, and (F) no excipient (“excipient free”). Solid line indicates fit of the forward

ssHDX reaction to a mono-exponential association model, dotted line indicates fit of the reverse ssHDX reaction to a mono-exponential decay model; see text for details. Data shown for an 18 amino acid length PDLA peptide, n=3, mean \pm SD. error bars not shown when less than the height of the symbol..... 104

Figure 3.6. The reverse ssHDX reaction rate constant values, k_b , for PDLA formulations deuterated at 6% RD (open bar) or 11% RD (hatched bar) followed by deuterium removal at 43% RH (Case-3c, Case-4c). Data shown for an 18 amino acid length PDLA peptide; n=3, mean \pm SE. 107

Figure 3.7. Effect of RH on the plateau level of deuterated peptide in de-labeling (reverse exchange) experiments conducted at (A) low RH (0%, 6% or 11%) or (B) high RH (43%). P•D represents deuterated peptide (B, Eqn. 3.5), E• represents a non-volatile excipient acting as a deuterium acceptor (Z•, Eqn. 3.5), PH represents protonated peptide (A, Eqn. 3.5) and E•D represents deuterated excipient (Z•D, Eqn. 3.5). At low RH (A), non-volatile excipients serve as deuterium acceptors during reverse exchange. These deuterated excipients remain in the solid and can serve as deuterium donors for the forward reaction (Eqn. 3.6; not shown). At high RH (B), sorbed H₂O serves as a deuterium acceptor and DHO (or D₂O, not shown) is generated as a reaction product. Volatile DHO and/or D₂O can be removed from the solid into the vapor phase, reducing the concentration of deuterium donors for the forward reaction (Eqn. 3.6). 110

Figure 4.1. Circular dichroism (CD) spectra of Peptide A (i.e., Ac-(A₄K)₃A-NH₂) and Peptide B (i.e., Ac-KA₁₂K-NH₂) in solution show peaks characteristic of α -helix and β -sheet secondary structures, respectively..... 122

Figure 4.2. Solid-state FTIR spectra of (A) Peptide A (i.e., Ac-(A₄K)₃A-NH₂) and (B) Peptide B (i.e., Ac-KA₁₂K-NH₂) in lyophilized formulations show peaks characteristic of α -helix and β -sheet structures, respectively..... 124

Figure 4.3. PXRD spectra of (A) Peptide A (i.e., Ac-(A₄K)₃A-NH₂) and (B) Peptide B (i.e., Ac-KA₁₂K-NH₂) lyophilized formulations show characteristic amorphous bands for sucrose, trehalose, excipient free formulations and crystalline bands for mannitol, sodium chloride, and guanidine HCl formulations, respectively. 125

Figure 4.4. Solution HDX-MS of (A) Peptide A (i.e., Ac-(A₄K)₃A-NH₂) vs. PDLA (16 aa) and (B) Peptide B (i.e., Ac-KA₁₂K-NH₂) vs. PDLA (14 aa). The dotted line represents the maximum possible theoretical deuteration level, n=3, mean \pm SD, error bars are not shown when smaller than the symbol..... 127

Figure 4.5. Solid-state HDX-MS of amorphous formulations (A) Peptide A (i.e., Ac-(A₄K)₃A-NH₂) vs PDLA (16 aa) at 11% RH D₂O, (B) Peptide A (i.e., Ac-(A₄K)₃A-NH₂) vs PDLA (16 aa) at 23% RH D₂O, (C) Peptide B (i.e., Ac-KA₁₂K-NH₂) vs PDLA (14 aa) at 11% RH D₂O and (D) Peptide B (i.e., Ac-KA₁₂K-NH₂) vs PDLA (14 aa) at 23% RH D₂O. n=3, mean \pm SD, error bars are not shown when smaller than the symbol. 129

Figure 4.6. Comparison of ssHDX-MS kinetics of amorphous peptide formulations at 11% RH D₂O (open bar) and 23% RH D₂O (hatched bar). (A) D_{max} (Peptide A), (B) k (Peptide A), (C) D_{max} (Peptide B), and (D) k (Peptide B), n=3, mean ± SE; error bars not shown when less than the height of the symbol..... 131

Figure 4.7. Comparison of maximum deuterium incorporation (D_{max}) in ssHDX-MS for unstructured PDLA peptides (open bar) vs structured Peptide A (α-helical) or Peptide B (β-sheet) amorphous formulations (hatched bar). (A) 16aa PDLA vs Peptide A (D_{max} at 11% RH D₂O), (B) 16aa PDLA vs Peptide A (D_{max} at 23% RH D₂O), (C) 14aa PDLA vs Peptide B (D_{max} at 11% RH D₂O), and (D) 14aa PDLA vs Peptide B (D_{max} at 23% RH D₂O). n=3, mean ± SE; error bars not shown when less than the height of the symbol..... 133

Figure 4.8. Comparison of ssHDX-MS kinetics of unstructured PDLA (open bar) vs structured Peptide A or Peptide B amorphous formulations (hatched bar). (A) PDLA vs Peptide A (k at 11% RH D₂O), (B) PDLA vs Peptide A (k at 23% RH D₂O), (C) PDLA vs Peptide B (k at 11% RH D₂O), and (D) PDLA vs Peptide B (k at 23% RH D₂O), n=3, mean ± SE; error bars not shown when less than the height of the symbol. 135

APPENDIX FIGURES

Figure A1. ssHDX-MS kinetics of different formulations of a 22 amino-acid PDLA peptide, grouped by RH A) 6% RH, B) 11% RH, C) 23% RH and D) 43% RH. n=3, mean ± SD; error bars not shown when less than the height of the symbol..... 149

Figure A2. ssHDX-MS of different formulations of PDLA peptides of different chain length at 6% RH. Data are shown for eight PDLA peptides from the polydisperse mixture having different amino acid (AA) chain length: A) 12AA, B) 15 AA, C) 18 AA, D) 25 AA, E) 27 AA, F) 29 AA, G) 31 AA, H) 34 AA. Colors indicate different formulations: sucrose (blue), trehalose (red), excipient free (black), mannitol (green), sodium chloride (purple) and guanidine hydrochloride (orange). n=3, mean ± SD; error bars not shown when less than the height of the symbol. 150

Figure A3. ssHDX-MS of different formulations of PDLA peptides of different chain length at 11% RH. Data are shown for eight PDLA peptides from the polydisperse mixture having different amino acid (AA) chain length: A) 12AA, B) 15 AA, C) 18 AA, D) 25 AA, E) 27 AA, F) 29 AA, G) 31 AA, H) 34 AA. Colors indicate different formulations: sucrose (blue), trehalose (red), excipient free (black), mannitol (green), sodium chloride (purple) and guanidine hydrochloride (orange). n=3, mean ± SD; error bars not shown when less than the height of the symbol. 151

Figure A4. ssHDX-MS of different formulations of PDLA peptides of different chain length at 23% RH. Data are shown for eight PDLA peptides from the polydisperse mixture having different amino acid (AA) chain length: A) 12AA, B) 15 AA, C) 18 AA, D) 25 AA, E) 27 AA, F) 29 AA, G) 31 AA, H) 34 AA. Colors indicate different formulations: sucrose (blue), trehalose (red), excipient free (black), mannitol (green), sodium chloride (purple) and guanidine hydrochloride (orange). n=3, mean ± SD; error bars not shown when less than the height of the symbol. 152

Figure A5. ssHDX-MS of different formulations of PDLA peptides of different chain length at 43% RH. Data are shown for eight PDLA peptides from the polydisperse mixture having different

amino acid (AA) chain length: A) 12AA, B) 15 AA, C) 18 AA, D) 25 AA, E) 27 AA, F) 29 AA, G) 31 AA, H) 34 AA. Colors indicate different formulations: sucrose (blue), trehalose (red), excipient free (black), mannitol (green), sodium chloride (purple) and guanidine hydrochloride (orange). $n=3$, mean \pm SD; error bars not shown when less than the height of the symbol. 153

Figure A6. ssHDX-MS of different formulations of PDLA peptides of 22 amino acid chain length at RH values from 57% to 97% A) 57% RH, B) 75% RH, C) 97% RH. Colors indicate different formulations: sucrose (blue), trehalose (red), excipient free (black), mannitol (green), sodium chloride (purple) and guanidine hydrochloride (orange). Data shown for the 22 amino acid length peptide, $n=3$, mean \pm SD; error bars not shown when less than the height of the symbol. 154

Figure A7. Linear regression of D_{max} vs. a_D for PDLA peptides at RH < 50%, with each formulation plotted individually, (A) sucrose, (B) trehalose, (C) mannitol, (D) sodium chloride, (E) guanidine HCl or (F) no excipient (excipient-free). The D_{max} was calculated from the back exchange corrected percentage deuterium uptake mono-exponential fits. Data shown for a 22 amino acid peptide, $n=3$, error bars not shown if smaller than the symbol. 155

Figure A8. Linear regression of D_{max} vs. a_D for PDLA peptides at RH < 50%, with all formulations plotted together. Colors indicate different formulations: sucrose (blue), trehalose (red), excipient free (black), mannitol (green), sodium chloride (purple) and guanidine hydrochloride (orange). The D_{max} was calculated from the back exchange corrected percentage deuterium uptake mono-exponential fits. Data shown for a 22 amino acid peptide, $n=3$, error bars not shown if smaller than the symbol. 156

Figure A9. Linear regression of A_0/D_{max} vs. $1/a_D$, with all formulations plotted together at RH < 50%. Colors indicate different formulations: sucrose (blue), trehalose (red), excipient free (black), mannitol (green), sodium chloride (purple) and guanidine hydrochloride (orange). The D_{max} was calculated from the back exchange corrected percentage deuterium uptake mono-exponential fits. Data shown for a 22 amino acid peptide. 157

Figure A10. Apparent ssHDX-MS rate constants (k_{ap}) for various formulations, RH values and PDLA chain lengths. Data shown for 8 selected peptides, $n=3$, error bars not shown if smaller than the symbol. 158

Figure B1. Pre-hydration and ssHDX-MS study schematic diagram, Case-1: X=6 %, Case-2: X=11 %. 162

Figure B2. Reversibility of ssHDX-MS study schematic diagram, Case-3a: X=6 %, Y= 0 %, Case-3b: X=6 %, Y= 6 %, Case-3c: X=6 %, Y= 43 %, Case-4a: X=11 %, Y= 0 %, Case-4b: X=11 %, Y= 11 %, Case-4c: X=11 %, Y= 43 %. 162

Figure B3. Comparison of pre-hydrated vs non-pre-hydrated ssHDX-MS of different PDLA formulations at 6% RD (Case-1). A) sucrose, B) trehalose, C) mannitol, D) sodium chloride, E) guanidine HCl, and F) no excipient (“excipient free”). Colors indicate different conditions: Non-prehydrated (blue), pre-hydrated (red). Data shown for an 18 amino acid length PDLA peptide, $n=3$, mean \pm SD; error bars not shown when less than the height of the symbol. 163

Figure B4. Comparison of pre-hydrated vs non-pre-hydrated ssHDX-MS of different PDLA formulations at 11% RD (Case-2). A) sucrose, B) trehalose, C) mannitol, D) sodium chloride, E) guanidine HCl, and F) no excipient (“excipient free”). Colors indicate different conditions: Non-

prehydrated (blue), pre-hydrated (red). Data shown for an 18 amino acid length PDLA peptide, n=3, mean ± SD; error bars not shown when less than the height of the symbol..... 164

Figure B5. Reversibility of ssHDX-MS in PDLA formulations lyophilized with various excipients. Formulations were first deuterated by exposure to D₂O vapor at 6% (A, B, C) or 11% RD (D, E, F). Deuterium removal was then accomplished at a controlled RH: (A, D) 0% RH (desiccated), (B, E) 6% RH, (C, F) 43% RH. Data shown for an 18 amino acid length PDLA peptide, n=3, mean ± SD. error bars not shown when less than the height of the symbol..... 165

Figure B6. Comparison of the forward and reverse ssHDX-MS kinetics for PDLA formulations deuterated at 11% RD (forward) followed by deuterium removal at 0% RH (reverse) (Case-4a). Formulations contained (A) sucrose, (B) trehalose, (C) mannitol, (D) sodium chloride, (E) guanidine HCl, and (F) no excipient (“excipient free”). Blue line indicates fit of the forward ssHDX reaction to a mono-exponential association model, red line indicates fit of the reverse ssHDX reaction to a mono-exponential decay model; see text for details. Data shown for an 18 amino acid length PDLA peptide, n=3, mean ± SD. error bars not shown when less than the height of the symbol..... 166

Figure B7. Comparison of the forward and reverse ssHDX-MS kinetics for PDLA formulations deuterated at 11% RD (forward) followed by deuterium removal at 11% RH (reverse) (Case-4b). Formulations contained (A) sucrose, (B) trehalose, (C) mannitol, (D) sodium chloride, (E) guanidine HCl, and (F) no excipient (“excipient free”). Blue line indicates fit of the forward ssHDX reaction to a mono-exponential association model, red line indicates fit of the reverse ssHDX reaction to a mono-exponential decay model; see text for details. Data shown for an 18 amino acid length PDLA peptide, n=3, mean ± SD. error bars not shown when less than the height of the symbol..... 167

Figure B8. Comparison of the forward and reverse ssHDX-MS kinetics for PDLA formulations deuterated at 11% RD (forward) followed by deuterium removal at 43% RH (reverse) (Case-4c). Formulations contained (A) sucrose, (B) trehalose, (C) mannitol, (D) sodium chloride, (E) guanidine HCl, and (F) no excipient (“excipient free”). Blue line indicates fit of the forward ssHDX reaction to a mono-exponential association model, red line indicates fit of the reverse ssHDX reaction to a mono-exponential decay model; see text for details. Data shown for an 18 amino acid length PDLA peptide, n=3, mean ± SD. error bars not shown when less than the height of the symbol..... 168

Figure B9. Comparison of the reverse ssHDX reaction rate constant (k_b) and forward reaction rate constant (k_f^*) values of PDLA formulations estimated using a series of deuterium labeling studies conducted at (6%, 11%, 23%, and 43% RD), as the slope of the apparent deuterium incorporation rate constant (k_{ap}) as a function of a_D (given by % RD/100), as reported previously.¹ Data shown for an 18 amino acid length PDLA peptide; n=3, mean ± SE. 169

Figure B10. Comparison of the $k_b/k_f C_{ss}$ values of PDLA formulations deuterated at 6% RD (Case-3) or 11% RD (Case-4) followed by deuterium removal at 0% RH, 6% RH or 11% RH. Data shown for an 18 amino acid length PDLA peptide; n=3, mean ± SE. 170

Figure C1. Solution HDX-MS of A) Peptide-A (i.e., Ac-(A₄K)₃A-NH₂) vs PDLA (16 aa) and B) Peptide-B (i.e., Ac-KA₁₂K-NH₂) vs PDLA (14 aa). The dotted line represents the maximum

possible theoretical deuteration level, $n=3$, mean \pm SD, error bars are not shown when smaller than the symbol. 171

Figure C2. Solid-state HDX-MS of crystalline formulations A) Peptide-A (i.e., Ac-(A₄K)₃A-NH₂) vs PDLA (16 aa) at 11% RH D₂O, B) Peptide-A (i.e., Ac-(A₄K)₃A-NH₂) vs PDLA (16 aa) at 23% RH D₂O, C) Peptide-B (i.e., Ac-KA₁₂K-NH₂) vs PDLA (14 aa) at 11% RH D₂O and D) Peptide-B (i.e., Ac-KA₁₂K-NH₂) vs PDLA (14 aa) at 23% RH D₂O. $n=3$, mean \pm SD, error bars are not shown when smaller than the symbol. 172

Figure C3. Solid-state HDX-MS of A) Peptide-A (i.e., Ac-(A₄K)₃A-NH₂) at 11% RH D₂O, B) Peptide-A (i.e., Ac-(A₄K)₃A-NH₂) at 23% RH D₂O, C) Peptide-B (i.e., Ac-KA₁₂K-NH₂) at 11% RH D₂O and D) Peptide-B (i.e., Ac-KA₁₂K-NH₂) at 23% RH D₂O. $n=3$, mean \pm SD, error bars are not shown when smaller than the symbol. 173

Figure C4. Comparison of ssHDX-MS of Peptide A formulations at 11% RH D₂O and 23% RH D₂O. A) sucrose, B) trehalose, C) mannitol, D) sodium chloride, E) guanidine HCl, and F) excipient free. Colors indicate different RH conditions: 11% RH D₂O (blue), 23% RH D₂O (red). $n=3$, mean \pm SD; error bars not shown when less than the height of the symbol. 174

Figure C5. Comparison of ssHDX-MS of Peptide B formulations at 11% RH D₂O and 23% RH D₂O. A) sucrose, B) trehalose, C) mannitol, D) sodium chloride, E) guanidine HCl, and F) excipient free. Colors indicate different RH conditions: 11% RH D₂O (blue), 23% RH D₂O (red). $n=3$, mean \pm SD; error bars not shown when less than the height of the symbol. 175

Figure C6. Comparison of ssHDX-MS kinetics at 11% RH D₂O and 23% RH D₂O (crystalline formulations). A) D_{\max} (Peptide A), B) k (Peptide A), C) D_{\max} (Peptide A), and D) k (Peptide B), Colors indicate different RH conditions: 11% RH D₂O (blue), 23% RH D₂O (red). $n=3$, mean \pm SE; error bars not shown when less than the height of the symbol. 176

Figure C7. Comparison of ssHDX-MS of unstructured PDLA (16 aa) vs α -helical Peptide A at 11% RH. A) sucrose, B) trehalose, C) mannitol, D) sodium chloride, E) guanidine HCl, and F) excipient free, Colors indicate different peptides: PDLA (blue), Peptide-A (red). $n=3$, mean \pm SD; error bars not shown when less than the height of the symbol. 177

Figure C8. Comparison of ssHDX-MS of unstructured PDLA (16 aa) vs α -helical Peptide A at 23% RH. A) sucrose, B) trehalose, C) mannitol, D) sodium chloride, E) guanidine HCl, and F) excipient free, Colors indicate different peptides: PDLA (blue), Peptide-A (red). $n=3$, mean \pm SD; error bars not shown when less than the height of the symbol. 178

Figure C9. Comparison of ssHDX-MS of unstructured PDLA (14 aa) vs β -sheet Peptide B at 11% RH. A) sucrose, B) trehalose, C) mannitol, D) sodium chloride, E) guanidine HCl, and F) excipient free, Colors indicate different peptides: PDLA (blue), Peptide-B (red). $n=3$, mean \pm SD; error bars not shown when less than the height of the symbol. 179

Figure C10. Comparison of ssHDX-MS of unstructured PDLA (14 aa) vs β -sheet Peptide B at 23% RH. A) sucrose, B) trehalose, C) mannitol, D) sodium chloride, E) guanidine HCl, and F) excipient free, Colors indicate different peptides: PDLA (blue), Peptide-B (red). $n=3$, mean \pm SD; error bars not shown when less than the height of the symbol. 180

Figure C11. Comparison of maximum deuterium incorporation (D_{\max}) in ssHDX-MS for unstructured PDLA peptides vs structured Peptide A (α -helical) or Peptide B (β -sheet)

formulations (crystalline). A) 16aa PDLA vs Peptide A (D_{\max} at 11% RH D_2O), B) 16aa PDLA vs Peptide A (D_{\max} at 23% RH D_2O), C) 14aa PDLA vs Peptide B (D_{\max} at 11% RH D_2O), and D) 14aa PDLA vs Peptide-B (D_{\max} at 23% RH D_2O). Colors indicate different peptides: PDLA (blue), Peptide A or Peptide B (red). $n=3$, mean \pm SE; error bars not shown when less than the height of the symbol. 181

Figure C12. Comparison of ssHDX-MS kinetics of unstructured PDLA vs structured Peptide A or Peptide B formulations (crystalline). A) PDLA vs Peptide A (k at 11% RH D_2O), B) PDLA vs Peptide A (k at 23% RH D_2O), C) PDLA vs Peptide B (k at 11% RH D_2O), and D) PDLA vs Peptide B (k at 23% RH D_2O), Colors indicate different peptides: PDLA (blue), Peptide A or Peptide B (red). $n=3$, mean \pm SE; error bars not shown when less than the height of the symbol. 182

Figure C13. Possible structures and H-bond patterns of Peptides A and B. Peptide B may also form a β -hairpin with six hydrogen bonds (not shown)..... 183

LIST OF ABBREVIATIONS

AA, Amino acid
aFGF, Acidic fibroblast growth factor
Asn, Asparagine
bFGF, Basic fibroblast growth factor
bGH, Bovine growth hormone
BPTI, Bovine pancreatic trypsin inhibitor
BSA, Bovine serum albumin
CD, Circular dichroism
CH₃CO₂K, Potassium acetate
Cys, Cysteine
D₂O, Deuterium oxide
DSC, Differential scanning calorimetry
DTT, Dithiothreitol
DVS, Dynamic vapor sorption
ESI, Electrospray ionization
FDA, Food and drug administration
FTIR, Fourier transform infrared spectroscopy
Gln, Glutamine
HDX, Hydrogen-deuterium exchange
hGH, Human growth hormone
hIGF-I, Human insulin-like growth factor I
His, Histidine
IgE, Immunoglobulin E
IgG, Immunoglobulin G
IL-1ra, Interleukin-1 receptor antagonist
IL-2, Interleukin 2
IL-6, Interleukin 6
K₂CO₃, Potassium carbonate
K₂SO₄, Potassium sulfate

LiBr, Lithium bromide
LiCl, Lithium chloride
mAb, Monoclonal antibody
Mb, Myoglobin
MDSC, Modulated differential scanning calorimetry
Met, Methionine
MS, Mass spectrometry
MW, Molecular weight
MWCO, Molecular weight cutoff
NaBr, Sodium bromide
NaCl, Sodium chloride
NIR, Near-infrared spectroscopy
PDB, Protein data bank
PDLA, Poly-D, L-alanine
PDLL, Poly-D, L-lysine
PEG, Polyethylene glycol
PXRD, Powder X-ray diffraction
rbSt, Recombinant bovine somatotropin
RD, Relative humidity in D₂O
RH, relative humidity
rHA, Recombinant human albumin
rhuMAb, Recombinant humanized monoclonal antibody
ssHDX, Solid-state hydrogen-deuterium exchange
ssNMR, Solid-state nuclear magnetic resonance spectroscopy
TNF, Tumor necrosis factor
Trp, Tryptophan
Tyr, Tyrosine

ABSTRACT

Proteins are susceptible to physical and chemical degradation in solution, which can lead to the loss of therapeutic activity and increase the potential for immunogenic responses when administered. Many degradation reactions are mediated by water, and therefore the proteins are often formulated as solids in which degradation rates are slowed significantly. Lyophilization is the most common method for producing solid protein formulations, which removes the water by sublimation and desorption under vacuum from the frozen protein solutions. Lyophilization requires excipients to protect the protein from the inherent stresses involved in the process. Degradation can still occur during lyophilization and storage, and needs to be characterized in order to develop a successful formulation with desired storage stability. The analytical techniques to characterize solid-state proteins are limited, however, and many do not provide site-specific information and lack the ability to predict stability beforehand.

Recently, solid-state hydrogen-deuterium exchange mass spectrometry (ssHDX-MS) has been developed to characterize proteins in solid powders with peptide level resolution. The technique was found to be sensitive to formulation and process changes. The ssHDX-MS metrics are highly correlated to the long-term storage stability, suggesting that the method can serve as a formulation screening tool. This dissertation aims to evaluate the factors affecting ssHDX kinetics and to develop a mechanistic understanding of the exchange process in solid samples, which in turn will support the solid-state protein development and enable it to be conducted in a more a cost and time-effective way. First, the contribution of peptide-matrix interactions to deuterium incorporation kinetics in the absence of higher-order structure was assessed using lyophilized poly-D, L-alanine peptides. Deuterium incorporation depended on excipient type and $D_2O_{(g)}$ activity in the solid samples. A reversible pseudo-first-order kinetic model was proposed and validated using the experimental data. Second, the reversibility of the hydrogen-deuterium exchange reaction in the solid-state was evaluated to support the ssHDX mechanistic model further. The reaction was found to be reversible irrespective of initial conditions and independent of the excipient type. Pre-hydration of the peptide samples prior to deuterium labeling did not affect deuterium incorporation in amorphous samples compared to the controls not subjected to pre-hydration. Third, the contribution of peptide secondary structure to deuterium uptake kinetics was quantified using

structured PDLA analogs. The deuterium incorporation in structured peptides was less than that of the PDLA peptides suggesting that both peptide structure and peptide-matrix interactions contribute to ssHDX-MS. Finally, a quantitative data analysis method was presented that allows the interpretation of ssHDX-MS data of a protein relative to controls. Altogether, the findings present a comprehensive mechanistic understanding of the ssHDX-MS of proteins that is relevant to the industry.

CHAPTER 1. INTRODUCTION

1.1 Therapeutic proteins

Proteins are an important class of therapeutic agents, which include hormones, enzymes, cytokines, growth factors, monoclonal antibodies, and various vaccines.¹ Proteins provide effective and unique therapy for a broad range of diseases including cancer, cardiovascular diseases, metabolic and autoimmune disorders.² Since 1993, more than 150 protein-based drugs have been approved by the Food and Drug Administration (FDA) for clinical use.³ In 2019 alone, approximately 21% of newly approved drugs in the United States are based on proteins, and many more are in development.³ Globally, the current market for protein therapeutics is approximately 150 billion USD and is expected to reach 240 billion USD by 2025.⁴ The growing interest in protein-based therapeutics can be attributed to their advantages over traditional small molecule drugs. Proteins exhibit highly specific functions to treat complex diseases that cannot be treated by simple chemical compounds.⁵ Proteins possess less potential for adverse effects as the interference with normal biological processes is minimized due to their high target specificity.⁵ In addition, proteins are less likely to induce immunogenic responses as many therapeutic proteins are naturally produced in humans, such as insulin and glucagon. In terms of the economic benefits, the clinical development and approval time frames are usually shorter by at least 1 year for proteins compared to small molecule drugs.⁵ The patent protection may also be far longer for proteins than for small molecules as they exhibit unique structural conformations and biologic functions.⁵

Proteins are complex molecules containing hundreds of amino acids with molecular masses in the range of ten to hundreds of kDa.⁶ Proteins form three dimensional structures comprising primary, secondary, tertiary, and quaternary levels, unlike the traditional low molecular weight drugs. Modifications in any of these structural levels can negatively impact the safety and efficacy, due to which the clinical development of these molecules is challenging.⁶ Protein modifications can arise due to physical (e.g., aggregation) and chemical instabilities (e.g., oxidation) in solution because of the presence of water which acts as a medium, reactant or catalyst for many degradation pathways. These reactions are drastically reduced if water is removed from the formulation. As a result, proteins are often freeze-dried (lyophilized) to remove water, to reduce the propensity for degradation and to achieve acceptable storage stability.⁷

Lyophilization is a two-step batch drying technique most widely used to produce solid-state protein pharmaceuticals to date. The first step is freezing of the protein solution under controlled conditions, and the second step is drying of the frozen formulation under vacuum. The drying step consists of two phases, including primary drying and secondary drying. The frozen bulk water is removed via sublimation in primary drying, and the non-frozen "bound" water is removed by desorption in secondary drying.⁷ The temperatures in the primary drying phase are typically less than the product critical collapse temperatures (-10°C to -35°C). In contrast, secondary drying is usually carried out at higher temperatures (25°C-35°C).

Even though lyophilization is a gentle drying process, it exerts various freezing and drying stresses on proteins. The freezing stresses include cold denaturation, the formation of ice crystals, solute concentration, pH changes, and the drying stresses include dehydration and removal of the hydration shell of the protein molecules.^{7, 8} Lyophilization cycle parameters such as cooling rates affect the size of the ice crystals formed during the freezing step. For example, rapid cooling results in the formation of large ice crystals, while slow cooling results in small ice crystals with an increased surface area, which in turn increases the adsorption of proteins on the ice interfaces. Together, the freezing and drying stresses can denature the proteins to various degrees and lead to the formation of aggregates. Therefore, to develop a successful formulation with desired storage stability, certain excipients are required to minimize the stresses and stabilize proteins during the freezing and drying processes. Since the stresses exerted by freezing and drying are different, the mechanisms of excipient stabilization are also different. For example, proteins in solution are stabilized by preferential interaction with water or by the preferential exclusion of excipients from the protein surface. Similarly, excipients which are preferentially excluded from the surface of a protein (e.g., sugars) are found to be effective during the freezing step.⁹ Some excipients (e.g., surfactants) stabilize the proteins by reducing the surface tension or by modifying ice crystal dimensions during the freezing process. During the drying process, the hydration layer of a protein is removed, so the preferential interaction mechanism is not applicable to explain the stabilizing effect of a lyoprotective excipient. In this case, the excipients stabilize proteins either by forming an amorphous glass or by replacing interactions with water. According to the vitrification hypothesis, proteins are stabilized by being trapped in a highly viscous amorphous glassy state, which drastically reduces the conformational interconversion, thereby increasing protein stability.¹⁰ In contrast, according to the water replacement hypothesis, stabilizing excipients

replace water and form hydrogen bonds with the proteins at the end of the drying process and preserve native structure by inhibiting interchain interactions.¹¹ However, a single excipient may not be sufficient to stabilize the protein adequately, and thus a combination of excipients in the appropriate proportion is required to produce a stable formulation. In addition, the storage stability of the formulations depends on the process parameters that are used, such as cooling or heating rates, and temperature set points in primary and secondary drying. Therefore, it is imperative to understand the degradation processes and characterize proteins in the solid-state to guide the development of protein pharmaceuticals.

1.2 Protein instability in the solid-state

Protein degradation rates usually are significantly slower in the solid-state compared to solution formulations. Nevertheless, degradation can still occur at rates sufficient to impact the safety and efficacy due to the residual moisture, storage temperature, lack of optimum proportion or combination of excipients or due to the lyophilization process parameters. Degradation in the solid-state can be categorized as physical and chemical instabilities. However, the physical and chemical instabilities are not mutually exclusive as physical instability can induce chemical instability and vice versa.¹²

1.2.1 Physical instability

Physical instability arises due to the changes in three-dimensional conformation and does not involve any covalent modifications. Protein denaturation, non-covalent aggregation, phase separation, and phase transition, are four types of physical degradation that occur in lyophilized protein formulations.

Denaturation: Denaturation refers to the perturbation of protein three-dimensional native structure. It can occur at both the secondary and tertiary structure levels and leads to the exposure of hydrophobic residues from the core of a protein. Denaturation arises due to the stresses involved in the lyophilization process such as low temperatures (i.e., cold denaturation), freeze concentration, adsorption onto ice-liquid interfaces during the freezing step or due to the dehydration in subsequent drying steps.¹³ The free energy of unfolding (ΔG_{unf}) has a parabolic relationship with temperature, suggesting that there is a specific temperature at which the protein

has maximum stability. Therefore, the protein has decreased stability at high or low temperatures. The lyophilization related stresses may also directly impact the ΔG_{unf} , and thereby cause perturbations in the three-dimensional protein structure.¹³ In addition to the process-related stresses, proteins can be denatured during storage due to elevated temperatures (i.e., thermal denaturation). The denaturation temperature (T_m) of a dried protein formulation is usually very high (i.e., $\sim 150^\circ\text{C}$), but the T_m can be lower ($\sim 65^\circ\text{C}$) for formulations with increased levels of moisture.¹⁴

Non-covalent aggregation: Non-covalent protein aggregation is a major physical instability in the lyophilized protein formulation, which arises due to the association of partially unfolded or misfolded proteins. These conformational changes are generally induced by lyophilization related stresses and expose portions of protein hydrophobic core, leading to aggregation during manufacturing, storage or upon reconstitution.¹² Proteins adsorbed at ice-liquid interfaces may also unfold to expose the hydrophobic groups leading to aggregation upon dissociation from the interfaces. Such aggregation is driven by intermolecular hydrophobic interactions, which reduce unfavorable interactions between water and hydrophobic amino acids. In addition, non-covalent aggregation is also promoted by hydrogen bonding, ionic interactions, and van der Waals forces. Several proteins such as bovine growth hormone (bGH), γ -interferon, ovalbumin, tetanus toxoid, and glucose oxidase are known to aggregate non-covalently.¹⁵⁻¹⁸

Phase separation: Protein formulations produced by lyophilization exist in an amorphous phase with a uniform distribution of the protein and excipients. The complete miscibility of proteins and excipients is desirable to obtain a formulation with optimum storage stability. However, phase separation can occur during manufacturing or storage due to the crystallization of buffer salts or excipients, leading to the formation of protein-rich or excipient rich local domains. For example, the dibasic form of the sodium phosphate buffer crystallizes during freezing, leaving only the mono-basic form resulting in extremely low pH (~ 3.6) in the remaining liquid.¹⁹ Similarly, bulking excipients such as mannitol or glycine also tend to crystallize during storage due to temperature and moisture effects. Polymeric excipients such as polyethylene glycol (PEG) and dextran also possess a tendency to phase separate conferring different levels of protection to proteins.^{20,21} Phase separation can exacerbate the destabilization of a protein and may also induce other physical or chemical degradations.

Phase transition: The amorphous solids produced by lyophilization present a dynamically constrained "glassy" state for proteins in which molecular mobility is limited. Amorphous solids have a glass transition temperature (T_g) above which the proteins exist in a dynamically relaxed viscoelastic state.²² The T_g depends on both the proportions of glass-forming components and residual moisture in the formulation. Increased moisture levels can reduce the T_g significantly by plasticizing effects. Phase transition occurs when the T_g is lowered below the storage temperature, so that the amorphous glassy state becomes a viscoelastic state leading to increased conformational flexibility of a protein.²³ Degradation reactions which require mobility of water or protein are then greatly enhanced in such phase transitioned systems.

1.2.2 Chemical instability

The chemical instability of a protein involves covalent modification of its residues via bond formation, cleavage, or rearrangement. It may also include substitution of certain residues leading to the formation of a new molecule. Protein hydrolysis, deamidation, oxidation, covalent aggregation, and the Maillard reaction are common chemical instabilities that occur in lyophilized protein formulations.

Hydrolysis: Lyophilized protein formulations are susceptible to hydrolytic reactions even though the residual moisture levels are usually less than 1%. Hydrolysis involves chemical reaction with water by which the covalent bonds connecting the amino acids (i.e., peptide bonds), or side chains are broken.²⁴ A low amount of residual moisture hinders the hydrolysis of peptide bonds. However, either the N-terminal or C-terminal amide bonds adjacent to Asp residues are susceptible to peptide bond hydrolysis. The mechanism of N-terminal peptide bond hydrolysis involves the formation of a six-membered ring intermediate. In contrast, the C-terminal peptide bond hydrolysis proceeds via a five-membered ring intermediate.²⁵ Hydrolysis involving the side chain groups (e.g., the hydroxyl group of Ser) has also been observed. The nucleophilic side chain group of an amino acid may react with excipients such as glucose followed by the peptide bond hydrolysis. For example, the loss of activity in lyophilized human relaxin was attributed to the glucose-induced elimination of the C-terminal Ser residue on the B chain.²⁶

Deamidation: Deamidation arises due to the hydrolysis of the side chain amide groups of asparagine (Asn) or glutamine (Gln) residues resulting in the formation of a free carboxylic acid.^{13,}

²⁷ Many proteins are susceptible to deamidation in the solid-state. For example, human insulin is known to deamidate at AsnA21 and AsnB3 positions in the solid-state.²⁸ The reaction proceeds with the formation of a cyclic intermediate, which further reacts with water to form desamidoA21 insulin. The cyclic intermediate is also known to react with other insulin molecules resulting in the formation of a covalent dimer. The deamidation mechanism in the solid-state was found to be dependent on the pH of the solution before lyophilization.^{29, 30} For example, the deamidation of an Asn-containing hexapeptide lyophilized from pH 3 solution proceeded via the direct hydrolysis of the side chain. In contrast, de-amidation of the peptide lyophilized from a pH 5 solution proceeded via the formation of a succinimidyl intermediate due to intramolecular reaction between the carbonyl carbon of Asn side chain and amide nitrogen anion of the succeeding amino acid.^{29, 30} Lyophilized proteins such as human growth hormone (hGH), basic fibroblast growth factor (bFGF), recombinant bovine somatotropin (rbSt) and interleukin-1 receptor antagonist (IL-1ra) have also been found to be susceptible to deamidation during storage.³¹⁻³⁴

Oxidation: The oxidation reaction in the solid-state can occur at the side chains of cysteine (Cys), methionine (Met), histidine (His), tryptophan (Trp) and tyrosine (Tyr).³⁵ Oxidation at cysteine residues yields sulfenic acid (-SOH), sulfinic acid (-SO₂H), sulfonic acid (-SO₃H), or disulfide (-SSH) depending on the conditions such as the thiol group spatial position. In contrast, oxidation at methionine residues leads to the formation of methionine sulfoxide.²⁴ Proteins such as human insulin-like growth factor I (hIGF-I) and interleukin 2 (IL-2) are known to oxidize at methionine residues in the solid-state.³⁶⁻³⁸ Methionine oxidation can occur at low levels of oxygen as in lyophilized human growth hormone (hGH), where the protein was oxidized at 0.4% of headspace oxygen during storage.^{33, 39} However, the presence of oxygen may not be the only cause for oxidation as molecular oxygen is not reactive. Other factors such as peroxide contamination in formulation excipients, photoactivation of molecular oxygen to reactive singlet oxygen (¹O₂), and the presence of trace metals which can generate hydroxyl ([•]OH) and superoxide radicals (O₂^{•-}) may make a significant contribution to the oxidation in the solid-state.^{13, 26} Methionine oxidation in lyophilized hIGF-I was accelerated upon light exposure by a factor of 30 suggesting the formation of photoactivated reactive oxygen species.³⁶ Oxidation was also found to be affected by the physical nature of the solid. Peptides in the crystalline phase showed no oxidation, while peptides in the amorphous phase degraded much faster than the corresponding crystalline counterparts, presumably due to increased mobility in the amorphous phase.¹³

Covalent aggregation: Covalent aggregation proceeds via intermolecular bond formation between protein molecules. Covalent aggregation can be categorized into two types as reducible and non-reducible aggregation.²⁷

Reducible covalent aggregation arises due to intermolecular disulfide exchange, which can be dissociated using denaturants such as dithiothreitol (DTT). Intermolecular thiol-disulfide exchange occurs when an ionized thiol on one protein molecule attacks the disulfide linkage on another protein molecule resulting in a new intermolecular disulfide bond.²⁷ Several lyophilized proteins such as bovine serum albumin (BSA),¹⁶ β -lactoglobulin,¹⁶ β -galactosidase,⁴⁰ recombinant human albumin (rHA),⁴¹ and humanized monoclonal antibodies (rhuMAb)⁴² are known to aggregate covalently via thiol-disulfide exchange. Temperature-induced protein denaturation also leads to reducible covalent aggregation as a result of disulfide bond formation between non-covalent aggregates.⁴³ Moisture may also induce covalent aggregation in lyophilized solids if the proteins contain free thiol groups and disulfide bonds. Covalent aggregation via disulfide exchange can also occur in proteins that do not contain a free thiol group. For example, insulin does not contain a free thiol group but possesses two interchain and one intrachain disulfide bonds. However, cleavage of the sulfur-carbon bond (i.e., β -elimination) yields a free thiol which leads to disulfide exchange followed by covalent reducible aggregation.⁴⁴

Non-reducible covalent aggregation does not involve disulfide exchange, and aggregates do not dissociate in the presence of denaturants. Non-reducible aggregation was observed in lyophilized tumor necrosis factor (TNF) and human insulin.^{29, 45} The first step in the insulin dimerization is the formation of a cyclic anhydride intermediate through the deamidation of AsnA21 residue at the C-terminal. The cyclic anhydride then reacts with the N-terminal free amine resulting in the formation of dimers such as AspA21-PheB1 and AspA21-GlyA1.²⁹ In contrast, the aggregation of TNF results in the formation of dimers, trimers, and oligomers.⁴⁵

Maillard reaction: Non-enzymatic browning occurs through the Maillard reaction in which the carbonyl group of a reducing sugar (e.g., glucose, maltose, lactose) reacts with the free amino group of a basic amino acid (e.g., lysine, arginine, asparagine, and glutamine) leading to the formation of an N-substituted glycosylamine. This carbohydrate adduct then converts to a Schiff base and a molecule of water.^{26, 27} Subsequent rearrangement of the reaction end products leads to the loss of protein activity and formation of derivatives that cause discoloration of the

formulation.^{26, 27} Several lyophilized proteins are known to be susceptible to the Maillard reaction, including human relaxin,²⁶ acidic fibroblast growth factor (aFGF),⁴⁶ basic fibroblast growth factor (bFGF),³² and porcine pancreatic elastase.⁴⁷ The Maillard reaction was also found to occur in monoclonal antibodies such as lyophilized IgG,⁴⁸ and spray-dried anti-IgE.⁴⁹ Formulations co-lyophilized with non-reducing sugars such as sucrose may also show the Maillard reaction as the sugar excipient can be hydrolyzed into reducing sugars, which can then react with the free amine groups.⁵⁰ Lueckel et al. demonstrated such chemical degradation for lyophilized interleukin 6 (IL-6) formulations containing sucrose.⁵¹

1.3 Solid-state protein characterization techniques

Proteins exhibit unique stability profiles due to their complex structures with chemical and physical instabilities, which make the development process challenging and expensive. Therefore, the characterization of the proteins in solid-state is essential to the development of a successful formulation with acceptable storage stability. The critical parameters such as amorphous glass dynamics, structural mobility, and conformational changes during storage are characterized using several techniques discussed below.

Fourier transform infrared (FTIR) spectroscopy: Fourier transform infrared spectroscopy is the most frequently used method to detect the secondary structural changes after lyophilization or during storage. FTIR measures the absorption of infrared (IR) light due to vibrational motions of protein molecules and produces characteristic absorption bands. Proteins possess several vibrational modes, but only the amide I and amide II regions are sensitive to structural changes. The signal is produced mainly by the stretching vibrations of the C=O groups of the peptide bond in the amide I region (1600-1700 cm^{-1}) and in-plane bending vibrations of the N-H groups in the amide II region (1500-1600 cm^{-1}).^{52, 53} Any changes in protein secondary structure due to process or storage-related stresses result in differences in the FTIR spectrum. For example, protein denaturation shifts amide I bands to higher wavenumbers and broadens the peaks.⁵⁴ Similarly, aggregation shows an increase in β -sheet content and is reflected in the FTIR signal.⁵⁵ However, the FTIR spectrum typically consists of several overlapping bands and requires mathematical manipulations. The amide I and amide II spectral readings provide global protein conformational information, but they do not provide information about local conformational changes, which are

critical for storage stability. Therefore, FTIR is considered to be a semi-quantitative and low-resolution technique. It is also insensitive to aggregation caused by tertiary structural changes. Moreover, FTIR measurements such as peak intensity, and peak position do not always correlate with storage stability or degradation rates.⁵⁶ This may be because there are several other factors, in addition to the native structure preservation, that are not detected by FTIR but govern the protein stability.

Near-infrared spectroscopy (NIR): Near-infrared spectroscopy is useful to assess the protein conformation in the solid-state and measures the absorption of IR light by C-H, N-H, and O-H bonds in the NIR region (i.e., 4000-13,000 cm^{-1}). The 4000-5000 cm^{-1} frequency range is considered as the combination spectral range, whereas the 5000-13000 cm^{-1} frequency range is known as the overtone spectral range.⁵³ Structural changes, such as unfolding, are usually associated with changes in intramolecular hydrogen bonding patterns. Any decrease in the intramolecular hydrogen bonding results in an increase in the frequency of the combination band in a typical NIR spectrum and vice versa.^{56, 57} The secondary structural elements such as α -helices or β -sheets possess specific band positions, and NIR can monitor any changes in those structures. For example, an increase in the β -sheet content of lyophilized bovine serum albumin (BSA) due to aggregation was monitored with band positional changes in NIR spectra.⁵⁸ NIR spectroscopy is also useful to measure moisture content, molecular interactions, and crystallinity of the lyophilized protein formulations.⁵⁹ However, the assignment of the bands to specific structural elements is challenging in NIR spectroscopy due to poor resolution and overlapping of the bands. Also, the signal intensity is weak compared to FTIR spectroscopy.^{53, 56}

Raman spectroscopy: Raman spectroscopy is useful to probe protein structural changes and side-chain environments. Raman spectroscopy is a complementary technique to IR spectroscopy as it measures the inelastic scattering (i.e., Raman scattering) of photons from the polarizable groups. The monochromatic incident light can be any type, such as visible, near UV, or near IR light because the Raman effect is independent of the incident light wavelength. Several groups in the proteins such as -CH, -CH₂, aromatic amino acids, and disulfide bonds produce Raman bands.⁶⁰ Therefore, side-chain environments such as tyrosine hydrogen bonding and disulfide bridge conformations can be probed with Raman spectroscopy.⁶¹ Raman spectroscopy can also be used to measure structural perturbations due to process-related stresses and to screen excipients for formulations. For example, the effects of lyophilization and spray drying on the structure of a

monoclonal antibody were quantified using Raman spectroscopy, and the secondary structure content was successfully correlated with storage stability.⁶² The disadvantages of this technique include weak Raman scattering and the requirement of a large quantity of sample to obtain a reliable spectrum. The heat generated during the analysis may also affect protein stability and the background fluorescence signal might interfere with the Raman signal of the protein sample.⁵⁶

Solid-state fluorescence spectroscopy: The secondary structure of the protein, either α -helix or β -sheet, comprises intramolecular hydrogen bonds. The secondary structural elements fold into a three-dimensional tertiary structure due to the interactions of the side chains of amino acid residues. Thus, minor changes in the secondary structure can lead to the loss of the tertiary structure of a protein. Therefore, it is crucial to characterize the tertiary structure of a protein in a solid sample, and solid-state fluorescence spectroscopy is an ideal technique for such purpose.⁶³ In this method, the fluorescence of aromatic amino acids, such as tryptophan, is measured. When the aromatic amino acids are exposed, as in unfolding, the emission maximum (i.e., λ_{max}) shifts to longer wavelengths (i.e., redshift). For example, unfolding in lyophilized β -lactoglobulin was identified with the redshift in λ_{max} of tryptophan fluorescence.⁶³ In another study, aggregation caused a decrease in the fluorescence intensity of a lyophilized monoclonal antibody.⁶⁴ The disadvantages of this technique include the interference of scattered light and the high optical density of solid protein samples.

Differential scanning calorimetry (DSC): Differential scanning calorimetry measures the heat capacity difference between a sample and a reference as a function of temperature. It is widely used to measure the glass transition temperatures of amorphous solids.⁶⁵ Since lyophilization usually produces amorphous protein samples, it is essential to obtain the T_g value of a formulation as it defines the storage conditions. Because the molecular mobility of the protein is limited at temperatures below the T_g , protein degradation rates are significantly reduced at these conditions. The measured T_g values of proteins often act as a supplement to the spectroscopic or chromatographic techniques. This technique has been used to evaluate the degradation of lyophilized proteins such as human growth hormone (hGH), monoclonal antibodies and to study phase separation during lyophilization and storage.^{66,67} Glass transition temperature measurements may not be sufficient to design a formulation as they merely suggest a safe storage condition. However, degradation still occurs temperatures below the T_g and the T_g values often correlate poorly with storage stability.⁵⁶

Solid-state nuclear magnetic resonance spectroscopy (ssNMR): Solid-state nuclear magnetic resonance spectroscopy is a high-resolution analytical technique that measures the absorbance of radiofrequency radiation by atomic nuclei (^1H , ^{13}C , ^{15}N) in a magnetic field. Solid-state NMR provides atomic-level information about protein structure and dynamics.⁶⁸ It is also useful to study the physical and chemical degradation of proteins in the solid-state. For example, ssNMR has been used to study the effects of excipients on asparagine deamidation rates in model peptides.⁶⁹ The ssNMR metrics such as the spin-lattice relaxation time (T_1), and rotating frame spin-lattice relaxation time ($T_{1\rho}$) have been used to study the protein miscibility with excipients in lyophilized solids.⁷⁰ The relaxation times have also been successfully correlated to long-term storage stability, demonstrating the advantages of ssNMR.⁶⁴ However, lyophilized solids are spatially heterogeneous, and the molecular orientation of the protein is random, which makes it challenging to obtain detailed structural information. Moreover, the ssNMR technique itself is complex, and the peak assignments to obtain site-specific information for large proteins like monoclonal antibodies may be challenging.

The techniques described in this section provide either global or local level structural information and often lack the ability to predict storage stability. Thus, there is an unmet need for a high-resolution analytical technique that can be used to characterize solid-state protein formulations with the capability to predict storage stability. Such a technique would significantly advance formulation development and enhance our understanding of the proteins in the solid-state. Solid-state hydrogen-deuterium exchange mass spectrometry (ssHDX-MS) has been promising in solid-state protein characterization, as discussed in the following section.

1.4 Solid-state hydrogen-deuterium exchange mass spectrometry (ssHDX-MS)

Solid-state hydrogen-deuterium exchange mass spectrometry is a novel analytical technique that measures protein structure and conformational dynamics in the solid-state. In ssHDX-MS, the solid protein samples are exposed to vapor phase D_2O under controlled relative humidity and temperature conditions.⁷¹ The solid samples absorb D_2O from the vapor phase due to their inherent hygroscopicity. The absorbed D_2O diffuses into the matrix leading to the interaction with amide groups. The unprotected amide groups exchange faster and to a greater extent than the protected amide groups. The deuterium uptake by the protein in the solid sample is measured by quenching

and reconstituting the protein sample in a low pH and ice-cold buffer (pH ~ 2.7) followed by mass spectrometric analysis. The deuterium uptake kinetics, such as the rate and extent, are obtained by fitting the mass spectrometric data to a mono-exponential or bi-exponential model.⁷¹ The method provides global (i.e., intact protein) and local (i.e., peptide/protein digest) structural information, and therefore it is considered as a high-resolution technique.^{72,73}

The extent of deuterium incorporation is related to the preservation of the native structure. Proteins with well-preserved native structures show lower deuterium incorporation, and proteins with poor structure preservation (e.g., partial unfolding) show increased levels of deuterium incorporation. The extent of deuterium incorporation has been found to be highly correlated with the storage stability of lyophilized proteins such as myoglobin, monoclonal antibodies, and antibody fragments.⁷³⁻⁷⁵ This suggests that ssHDX-MS can be used as an early read-out technique to screen formulations in the development stage, reducing cost and time significantly.

ssHDX-MS can also be used to study the spatial or conformational heterogeneity of a protein in solid samples by comparing the deconvoluted mass spectrum peak widths at the same deuteration levels. The peak width is related to the heterogeneity in the solid protein samples, so that broad peaks suggest higher heterogeneity than narrow peaks. For example, Wilson et al. recently compared the deconvoluted mass spectral peak widths of myoglobin or bovine serum albumin co-spray dried with or without excipients.⁷⁶ The formulations containing dextran showed broader peaks than the formulations with sucrose or trehalose, suggesting an increase in the heterogeneity in dextran containing formulations.⁷⁶ Similarly, Moorthy et al. quantified the formulation heterogeneity in myoglobin formulations by comparing the deconvoluted mass spectral peaks. The formulations containing sodium chloride or without excipient showed broader peaks than formulations containing sucrose, consistent with the increased spatial or conformational heterogeneity.⁷³

In the past ten-years, ssHDX-MS has been used extensively to study protein conformation and dynamics in solid powders produced by lyophilization or spray drying. The method has shown promising results and can act as a surrogate to the time consuming conventional long-term stability studies. However, to date, the fundamental mechanisms of ssHDX-MS are not clear. Current research addresses this knowledge gap and begins to develop a mechanistic understanding of the solid-state hydrogen-deuterium exchange mass spectrometry of proteins.

1.4.1 Fundamentals of hydrogen-deuterium exchange in solution

Proteins consist of several amino acids linked by amide bonds, each of which possesses an amide proton except proline. A typical protein molecule contains three types of hydrogens from hydrogen-deuterium exchange reaction perspective: (i) hydrogens attached to carbon (C), (ii) hydrogens attached to oxygen (O), nitrogen (N) or sulfur (S) groups on side chains and (iii) hydrogens attached to nitrogen (N) on amide groups.⁷⁷ The hydrogen atoms attached to carbon do not exchange and the hydrogens attached to O, N, or S groups on side chains exchange on the millisecond time scale, which is not measurable with any analytical technique. The hydrogens attached to the amide nitrogen group exchange on measurable time scales.^{77, 78}

The primary reaction in hydrogen-deuterium exchange is the transfer of deuteron from D₂O to protein amide and the subsequent transfer of amide proton from protein to D₂O. The hydrogen exchange between D₂O and the protein amide groups is either base-catalyzed (OD⁻) or acid-catalyzed (D₃O⁺) in pH-dependent reactions (Figure 1.1).⁷⁹ In the base-catalyzed reaction, the amide proton is abducted by the nucleophilic attack of OD⁻ resulting in the formation of an amidate anion. Next, this anion is deuterated by excess D₂O in the environment. On the other hand, the acid-catalyzed mechanism involves the deuteration of either the amide nitrogen group or the amide oxygen group by D₃O⁺. Given that an oxygen group is more basic than a nitrogen group, O-deuteration is a predominant acid-catalysis hydrogen exchange mechanism. The O-deuteration of amide groups by D₃O⁺ leads to the acidification of amide hydrogen, which is then abstracted by excess D₂O in the environment resulting in the formation of an imidic acid group. This group is then deuterated by D₃O⁺, leading to the formation of deuterated amide nitrogen. In contrast, N-deuteration is simpler where the amide nitrogen group is deuterated by D₃O⁺, and then the amide proton is abstracted by excess D₂O in the environment.⁸⁰

The hydrogen-deuterium exchange reaction is also catalyzed by water (i.e., D₂O). This reaction involves the deuteration of the amide carbonyl group by water (D₂O) followed by the NH group proton removal by OD⁻. Thus, for an unstructured peptide, the chemical exchange rate (k_{ch}) in a D₂O solution can be defined as:⁷⁹

$$k_{ch} = k_{int,D}[D_3O^+] + k_{int,OD}[OD^-] + k_{int,D_2O}[D_2O] \quad (1.1)$$

where k_{ch} is the chemical exchange rate and $k_{int,D}$, $k_{int,OD}$, k_{int,D_2O} are acid-catalyzed, base-catalyzed, and water catalyzed intrinsic exchange rate constants, respectively.

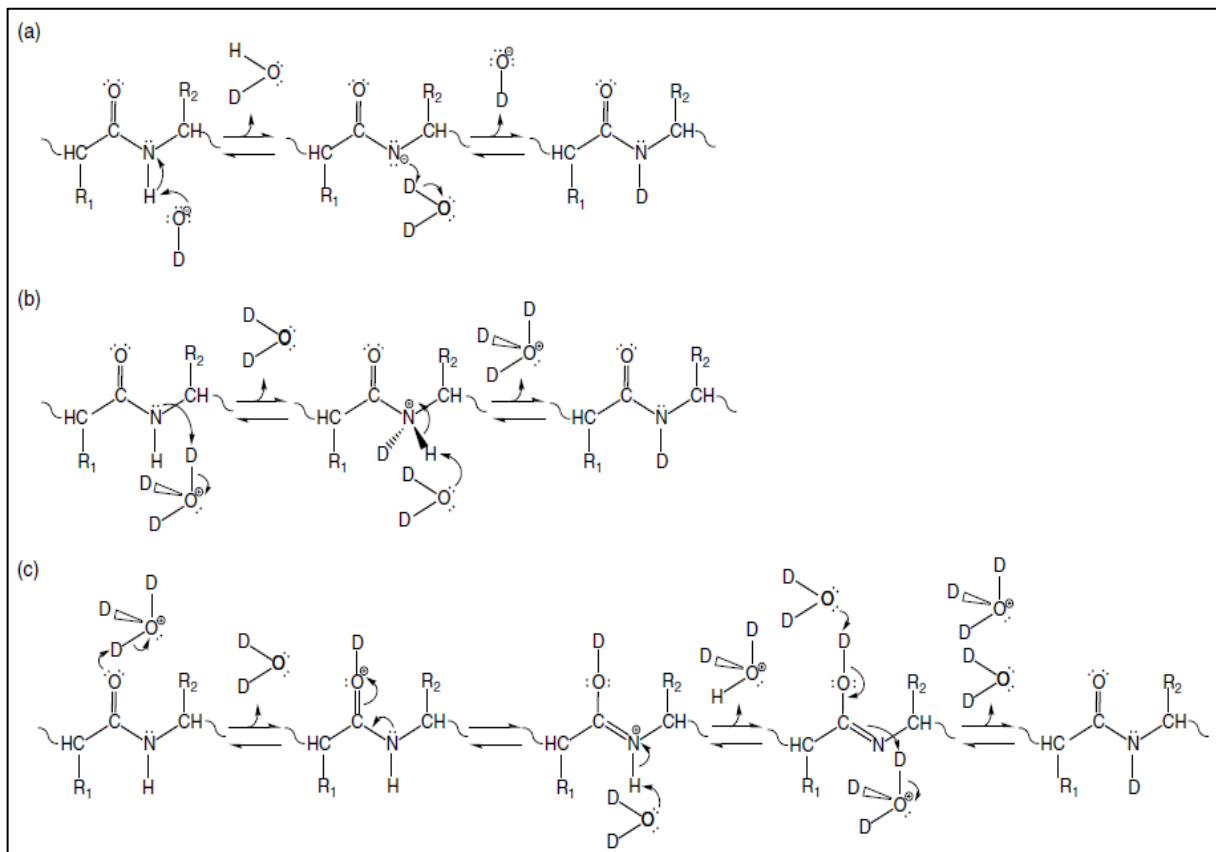


Figure 1.1. Hydrogen-deuterium exchange reaction mechanisms in solution. (a) base catalysis, (b) acid catalysis by N-protonation, and (c) acid catalysis by O-protonation (adapted from ⁸¹).

1.4.2 Hydrogen-deuterium exchange in proteins with higher-order structure

The hydrogen-deuterium exchange reaction in proteins with higher-order structure is complicated since the amide hydrogens are not easily accessible to exchange catalysts. Some amide hydrogens are distributed on the surface, and some are buried inside the hydrophobic core. Therefore, the structural environment is non-homogeneous. Several factors, such as steric inaccessibility, internal hydrogen bonding, and local charge distributions, affect hydrogen exchange rates. There are multiple mechanistic models available to explain hydrogen-deuterium exchange in folded proteins (stable state), as discussed below.

Local unfolding model: According to the local unfolding model,⁸² proteins in solution show local conformational fluctuations. These fluctuations can be small scale, such as the breakage of a single hydrogen bond or as large as the unfolding of a local segment in a structured protein. The fluctuations lead to an "open" state of a protein in which the amide hydrogen groups are accessible to the deuterium donor. One assumption in this model is that in the opened state, a protein is considered to be an unstructured segment, so the hydrogen-deuterium exchange is thought to occur outside the protein native state. The local fluctuations can occur in small segments (approximately ten amino acid residues) of a protein due to the transient breakage of internal hydrogen bonds. Since a segment is assumed to be unfolding, the exchange rates of all amide hydrogens in that region are expected to be of the same order of magnitude. This is known as cooperative exchange behavior. The local fluctuation model does not consider the depth of the burial of amide hydrogens that can hinder the exchange rates by several folds.

Solvent penetration model: According to the solvent penetration model,⁸³ the hydrogen exchange catalyst penetrates the core of a protein through channels formed by non-cooperative motions. The exchange rate of a proton depends on the depth of burial and accessibility to the hydrogen exchange catalyst. The amide hydrogens exposed on the surface and in channels exchange rapidly due to high solvent accessibility. In contrast, the amide hydrogens in the core of a protein exchange slowly because the solvent or catalyst has to diffuse through transient channels and cavities. The protein motions which are assumed to create channels for solvent penetration occur on a small scale. Unlike the local fluctuation model, the exchange rates of adjacent protons differ, and thus the exchange is highly localized. As shown in Figure 1.2, the protein is in its native state, and the deuteration catalyst (c) is in the bulk solution. In step II, the formation of a channel leads to the penetration of the catalyst into the protein where the internal diffusion of the catalyst leads to its collision with amide protons resulting in hydrogen-deuterium exchange.⁸⁴

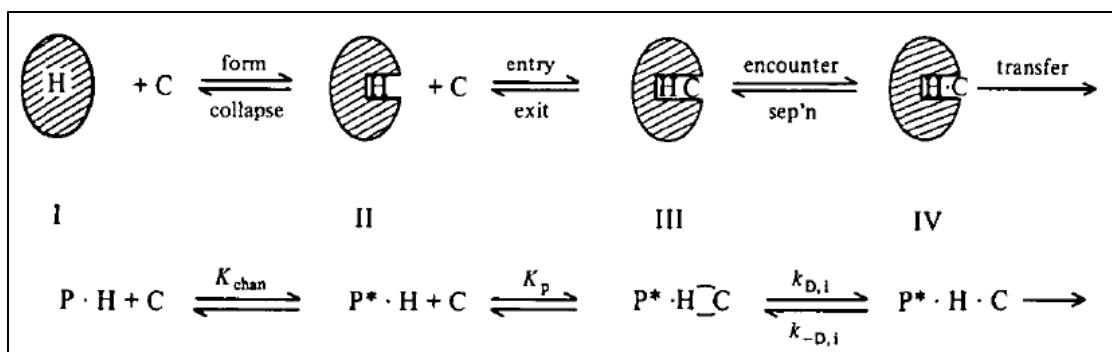


Figure 1.2. Schematic representation of the solvent penetration model (adapted from ⁸⁴).

Two notable differences with the local unfolding model are, i) hydrogen exchange occurs in the protein interior, and ii) the exchange rates are non-cooperative, i.e., the neighboring residues exchange independently.

Regional melting model: Kossiakoff proposed a variant of the local unfolding model in 1982.⁸⁵ According to this model, the local unfolding does not lead to the extrusion of the protein backbone into solution. In contrast, cooperative intramolecular hydrogen bond breakage leads to localized structural disruption of protein and forms small clefts on the surface. These clefts are then filled with solvent molecules or deuteration catalysts, leading to hydrogen-deuterium exchange inside the clefts.

Relayed imidic acid model: Tuchsien et al. proposed a variant of the solvent penetration model in 1985.⁸⁶ This model addresses the critical issues of the solvent penetration model where the catalyst ions must penetrate channels either in large-sized hydrated states or in energetically costly ionized state. The relayed imidic acid model suggests that the hydronium ions need not pass through the channels, but the charge delocalization through the hydrogen bond network can initiate exchange in buried sites where water molecules are available. According to this model, hydrogen-deuterium exchange occurs at the surface, and the charge delocalization results in the formation of imidic acid intermediates, as shown in Figure 1.3.

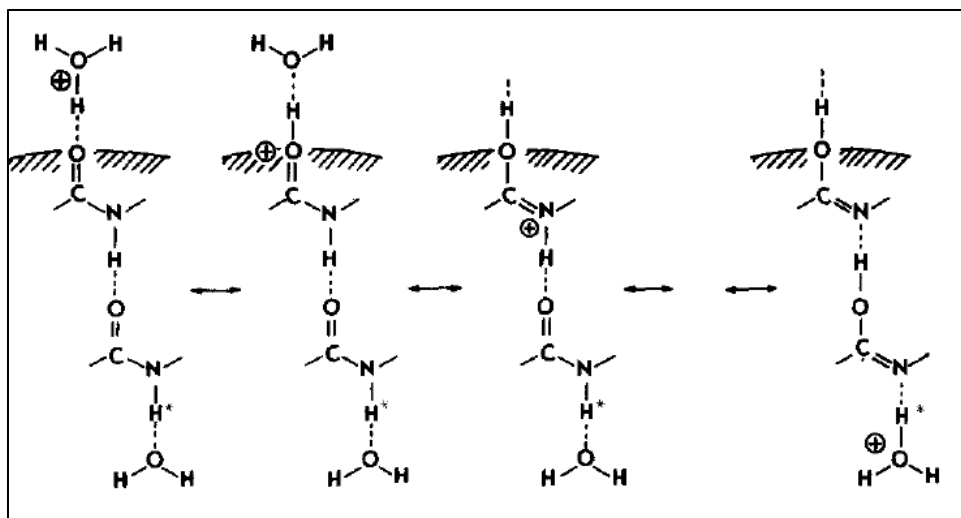


Figure 1.3. Schematic representation of the relayed imidic acid model (adapted from ⁸⁶).

Linderstrom-Lang model: The Linderstrom-Lang model of protein hydrogen-deuterium exchange is widely accepted and is based on the unfolding model described earlier. This model explains hydrogen-deuterium exchange as a two-step process in which the protein undergoes breathing motions, i.e., transient opening and closing events in solution as a result of internal hydrogen bond breakage and reformation (Figure 1.4). Deuteration catalysts such as hydroxyl and hydronium ions then access amide groups in the opened state leading to hydrogen-deuterium exchange.

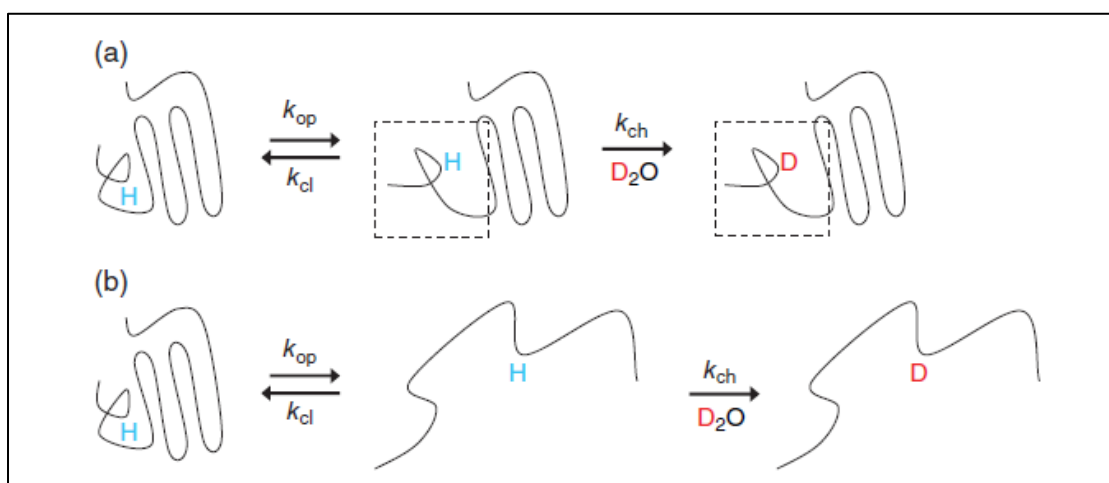


Figure 1.4. Schematic representation of the Linderstrom-Lang model. (a) local unfolding events, or (b) global unfolding events (adapted from ⁸¹).

This model favors local fluctuations rather than the rare global unfolding events. Since it includes opening and closing events in a protein, there are several kinetic processes in addition to the rate of chemical hydrogen exchange (k_{ch}) such as the rate of opening (k_{op}) and the rate of reclosing (k_{cl}).

Thus, the hydrogen-deuterium exchange rate in a folded protein can be described by the following equation:

$$k_{HDX} = \frac{k_{op} \times k_{ch}}{k_{op} + k_{cl} + k_{ch}}$$

In the native state of a protein $k_{cl} \gg k_{op}$ so that the above equation can be re-arranged as:

$$k_{HDX} = \frac{k_{op} \times k_{ch}}{k_{cl} + k_{ch}}$$

In the Ex1 limit, where $k_{cl} \ll k_{ch}$, the hydrogen exchange rate depends only on the rate of opening events, i.e., $k_{HDX} = k_{op}$.

In the Ex2 limit, where $k_{cl} \gg k_{op}$, the hydrogen exchange rate depends on both the opening and closing rates as shown below:

$$k_{HDX} = \frac{k_{op} \times k_{ch}}{k_{cl}}$$

1.4.3 Factors affecting hydrogen-deuterium exchange in solution

The hydrogen-deuterium exchange of a peptide or protein depends on several factors in addition to the structural and conformational changes, as discussed below.

pH and temperature: The chemical hydrogen-deuterium exchange rate is pH dependent with a minimum value in the range of 2.5-3.0 (pH_{min}). The pH vs. chemical hydrogen exchange rate profile shows a V-shaped curve, as shown in Figure 1.5.

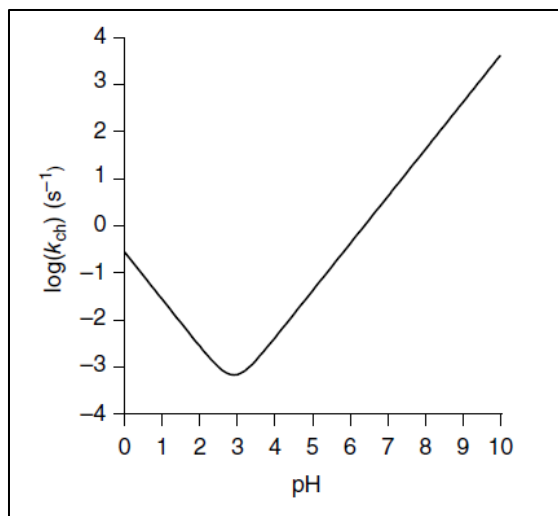


Figure 1.5. Chemical hydrogen exchange rate vs. pH profile in a poly-D, L-alanine peptide (adapted from ^{81,87}).

The reaction is base-catalyzed above pH_{min} and is acid-catalyzed below pH_{min} . The water catalyzed reaction rates are often omitted from equation (1.1) because those values are much smaller than the acid and base catalysis reaction rates. The water catalysis is predominant only in the pH range of 2.5 -3.0, where both acid and base catalysis are equal.^{79, 87}

The chemical exchange rates are also temperature-dependent because the water ionization constant (k_D for D_2O) increases with temperature, which results in increased hydrogen exchange catalysis. The exchange rates vary exponentially with temperature and decrease by 14- fold when the temperature is decreased from 25°C to 0°C .⁷⁹ Thus, the hydrogen exchange experiments typically are carried out at 25°C and at physiological pH 7.0 where the exchange rates are high. The reaction is then quenched by reducing the pH to pH_{min} , which is defined as the pH value where hydrogen exchange rates are lowest (i.e., 2.5-3.0), and the temperature to close to zero, prior to analysis.

Amino acid side chains: In 1972, Molday et al. studied the effect of nearest-neighbor amino acid side chains on adjacent amide hydrogen exchange rates in peptide derivatives.⁸⁸ The electron-withdrawing side chains increased the base-catalyzed reaction due to their inductive effects and decreased the acid-catalyzed reaction rates relative to a reference compound. Positively charged side chain groups increase the tendency of amide anion formation and thus increase the acidity of the amide proton in the base-catalyzed mechanism. On the other hand, such side chain groups inhibit the formation of cationic amide intermediate groups in acid-catalyzed hydrogen-deuterium

exchange reactions. The increase in base-catalyzed reaction rate and decrease in acid-catalyzed reaction rates are not equal, so the exchange rate at pH_{min} varies with the type of side-chain group. Charged amino acids, such as lysine and aspartic acid, were found to affect the acid-catalyzed reaction, and other amino acids such as histidine, asparagine were found to affect the base-catalyzed reaction. Amino acids with similar functional groups on their side chains (e.g., threonine, serine) have been found to affect neighboring amide exchange rates. Overall, the nearest neighbor amino acid groups affect adjacent amide hydrogen exchange rates.

In 1993, Bai et al. studied the effects of 20 amino acid side chains on neighboring alanine amide group hydrogen exchange rates in dipeptide models.⁷⁹ The adjacent group's inductive and steric blocking effects on amide exchange were evident in model peptides tested, and these effects were found to be additive. The polar side-chain groups, such as those in serine and cysteine, withdraw electron density from neighboring groups leading to the increased acidity of amide hydrogens. As a result, the base-catalyzed reaction rates increase, and the acid-catalyzed reaction rates decrease because the addition of a proton to the acidic amide group is non-favorable. Thus, the pH_{min} , in the V-shaped exchange rate vs. pH graph (Figure 1.5), shifts to lower pH values. Other side chains, such as in leucine, tend to decrease both acid and base catalyzed exchange rates leading to a reduction of k_{min} in the V-shaped exchange rate vs. pH graph (Figure 1.5). This effect has been attributed to the side-chain steric blocking of neighboring amide groups and is predominant for amino acids with beta-branched side chains. The steric blocking effect of an amino acid on its neighboring amide group is position-dependent, meaning that the N-terminal amide group tends to have a greater blocking effect than the one on C-terminal side of an amino acid which has polar or bulky side chains.⁷⁹

Solvent composition: Solvent composition influences peptide amide hydrogen exchange. For example, the hydrogen exchange of PDLA in 50% CH_3CN or 50% dioxane showed lower base-catalyzed rates than the corresponding rates in pure aqueous solutions.⁸⁴ This effect has been attributed to the decrease in water ionization constant (K_w) and subsequent decrease in the concentration of hydroxyl ions due to the presence of organic solvents. In addition, the denaturation effects of organic solvent on protein may contribute to changes in hydrogen exchange parameters.

Pressure: The effect of pressure on hydrogen exchange rates was studied by Carter et al. using folded proteins (i.e., lysozyme and ribonuclease), and random coil peptides (i.e., poly-D, L-lysine and oxidized ribonuclease-A).⁸⁹ Pressure enhanced base-catalyzed hydrogen exchange in folded proteins, but similar effects were not observed for random coil peptides. The effect of pressure on hydrogen exchange was attributed to pressure-induced unfolding and increased solvent penetration into folded proteins. In another study, hydrogen exchange rates of chymotrypsinogen-A increased proportionally with an increase in pressure at room temperature.⁹⁰ This effect was attributed to the denaturing effects of pressure since the exchange rates were larger at high pressure where the protein structure is completely perturbed.⁹⁰

Ionic strength: The effect of ionic strength on amide hydrogen exchange was studied by Baldwin et al. using a neutrally charged poly-D, L-alanine, and positively charged poly-D, L-lysine (PDLL) peptides in solutions varying in sodium chloride concentration.⁹¹ The effect of salt concentration on PDLA hydrogen exchange was negligible, but the acid-catalyzed PDLL hydrogen exchange was increased by three-fold when salt concentration was increased from 60 mM to 1 M. On the other hand, the base-catalyzed PDLL hydrogen exchange was decreased by fifty-fold when the salt concentration increased from 2 mM to 1 M. The concentration of salt was also found to affect the pH_{min} value. The changes in acid and base-catalyzed hydrogen exchange rates of PDLL are associated with a shift in pH_{min} from 1.3 to 2.6 when the sodium chloride concentration increased from 0 M to 2M. In another study, Tuchsén et al. found similar ionic strength effects on hydrogen exchange rates of bovine pancreatic trypsin inhibitor (BPTI) in potassium chloride solutions varying in concentration from 0.02 M to 0.43 M. However, the effect of ionic strength on hydrogen exchange was dependent on the location of amino acids in BTPI due to varying local electrostatic field.⁹²

1.4.4 Mechanistic models for solid-state hydrogen-deuterium exchange

To date, there are no mechanistic models to explain the hydrogen-deuterium exchange kinetics in the solid-state. The solution hydrogen-deuterium exchange models cannot be applied to the solid-state as there are several fundamental differences between these methods, as described below.

- The rate and extent of hydrogen exchange in the solid-state are affected by stabilizing excipients. Unlike solution HDX, protein matrix interactions play a vital role in solid-state HDX kinetics in addition to protein structure.⁹³
- Protein mobility in the solid-state is limited, so the transient folding and unfolding events which govern HDX in solution are very slow in solids.⁹⁴ This suggests that rate processes that are much slower than the k_{cl} , k_{op} , and k_{ch} dominate in solid-state HDX.
- HDX in the solid-state involves additional mass transport processes such as vapor sorption and diffusion. The Linderstrom-Lang model does not describe the effect of these processes on HDX kinetics.
- The rate and extent of hydrogen-deuterium exchange are affected by the activity of sorbed $D_2O_{(g)}$, which is not included in the Linderstrom-Lang model.⁷²
- The Linderstrom-Lang model assumes that the chemical exchange process (k_{ch}) is irreversible.⁹⁵ Since HDX in the solid-state is slower than HDX in solution, this assumption may be violated on the longer timescales of ssHDX.
- Chemical exchange in solution is affected by both pH and temperature. However, pH is not defined in the solid-state, and the interpretation of temperature effects is complicated by glass transitions of amorphous solids.
- The physical nature of solids (amorphous or crystalline) and the spatial heterogeneity of protein may affect hydrogen-deuterium exchange in the solid state. These parameters are not included in the Linderstrom-Lang model.
- According to the Linderstrom-Lang model, HDX in solution is a sequential process, meaning that the protein must unfold by the transient disruption of intramolecular hydrogen bonds before exchange can occur. It is not clear if this assumption holds for ssHDX.

For these reasons, the mechanistic interpretation of the ssHDX is complicated. The current research aims to evaluate the factors that influence the rate and extent of solid-state hydrogen-deuterium exchange. The studies also present a reversible pseudo-first-order kinetic model and a quantitative data analysis method that can be used to interpret the ssHDX-MS of therapeutic proteins.

1.5 Specific aims and hypotheses

The main objective of this research is to evaluate the factors affecting the kinetics of solid-state hydrogen-deuterium exchange and to develop a mechanistic model to interpret the deuterium incorporation kinetic data of proteins in ssHDX. The studies reported here test the central hypothesis that solid-state hydrogen-deuterium exchange is affected by protein structure, protein-matrix interactions and by $D_2O_{(g)}$ activity, and that the hydrogen-deuterium exchange reaction is reversible on the experimental time scale. The following specific aims were proposed to test the central hypothesis.

Specific Aim 1: To demonstrate that the rate and extent of deuteration in ssHDX-MS depend on excipient type and $D_2O_{(g)}$ activity in the absence of higher-order protein structure, using unstructured poly-D, L- alanine (PDLA) peptides, and to develop a model that describes ssHDX-MS kinetics in this system.

Protein amide hydrogen exchange rates are affected by intramolecular hydrogen bonds (i.e., structure) and by the extent of solvent shielding in solution. However, in the solid-state, protein-matrix interactions may contribute to ssHDX kinetics in addition to protein structure, as described earlier. To demonstrate that protein-matrix interactions play a role in ssHDX-MS, the ssHDX kinetics must be evaluated in the absence of significant secondary structure. The unstructured poly-D, L-alanine model peptides were selected for this reason. The PDLA peptides were co-lyophilized with stabilizing or destabilizing excipients, and the deuterium incorporation was evaluated at varying $D_2O_{(g)}$ relative humidities to quantify the effects of excipient type and $D_2O_{(g)}$ activity on the ssHDX-MS kinetics. The studies test the hypothesis that the rate and extent of deuterium incorporation will be affected by excipient type and $D_2O_{(g)}$ activity in ssHDX-MS studies of PDLA, effects that will not be observed in solution HDX controls.

Specific Aim 2: To evaluate the reversibility of deuterium incorporation in ssHDX-MS using fully deuterated PDLA peptides transferred from a fixed RH in $D_2O_{(g)}$ to fixed RH in $H_2O_{(g)}$, to develop a model that describes ssHDX-MS kinetics in this system, and to evaluate the effect of prehydration on deuterium incorporation in ssHDX-MS using PDLA peptides prehydrated at a fixed RH in $H_2O_{(g)}$ and transferred to a fixed RH in $D_2O_{(g)}$.

The chemical hydrogen-deuterium exchange reaction in the solution state is irreversible due to the high deuterium activity (i.e., $a_D \approx 1$), dilution of the protons that are exchanged with deuterium,

and short experimental time scales (milliseconds to minutes). However, this assumption may not be valid on the longer time scales (hours to days) of ssHDX-MS as the $D_2O_{(g)}$ activity in the solids is usually less than 0.5. To demonstrate that the chemical exchange reaction is reversible in the solid-state, the PDLA peptides were co-lyophilized with various excipients and maximally deuterated at controlled $D_2O_{(g)}$ relative humidity conditions. The deuterated samples were then transferred to corresponding H_2O relative humidities, and the deuterium loss monitored over time. The effects of pre-hydration on the rate and extent of deuterium incorporation was also evaluated by pre-hydrating the PDLA formulations in controlled H_2O RH followed by deuterium labeling in the corresponding D_2O RH conditions. The studies test the hypothesis that the hydrogen-deuterium exchange reaction in the solid-state is reversible, that the reverse rate constants are independent of excipient type and % RH D_2O on the experimental time scale and that deuteration kinetics are not affected by pre-hydration prior to deuterium labeling.

Specific Aim 3: To demonstrate the effects of peptide secondary structure and peptide-matrix interactions on the kinetics of deuteration in ssHDX-MS of lyophilized peptide formulations using analogs of PDLA with alpha-helical and beta-sheet structure, and to develop a quantitative data analysis and interpretation method for the ssHDX-MS of proteins.

Two model peptides were chosen to determine the contribution of peptide secondary structure to deuterium uptake kinetics in addition to peptide-matrix interactions: one peptide containing an α -helix secondary structure and the second peptide with a β -sheet secondary structure. These peptides were selected, ensuring that the comparisons between unstructured and structured peptides can be made. The PDLA and the PDLA analog peptides were co-lyophilized with stabilizing or destabilizing excipients, and deuterium incorporation was measured at two $D_2O_{(g)}$ relative humidities (i.e., 11% and 23% RH) to quantify the effects of secondary structure, excipient type and $D_2O_{(g)}$ activity on the ssHDX-MS kinetics. The studies test the hypothesis that the rate and extent of deuterium incorporation are affected by secondary structure, excipient type, and $D_2O_{(g)}$ activity in ssHDX-MS studies of analogs of PDLA with alpha-helical and beta-sheet structures, effects that will not be observed in solution HDX controls.

1.6 Overall approach

Model peptides: The poly-D, L-alanine peptides were chosen as a model for unstructured peptides as they lack higher-order structure in solution and solid-state due to the random arrangement of D- and L-alanine residues. The PDLA peptides also possess adequate solubility and are commercially readily available. The PDLA peptides do not contain bulky side chains, which may complicate the HDX analysis due to steric hindrance effects. In addition, PDLA is a mixture of peptides ranging from 6 amino acids to 44 amino acids in length, making it possible to monitor deuteration kinetics for peptides of varying length. The PDLA analogs, Peptide A and Peptide B, were chosen as they contain α -helix and β -sheet secondary structures, respectively. Peptide A consists of 16 amino acids (Ac-(A₄K)₃A-NH₂), and Peptide B consists of 14 amino acids (Ac-KA₁₂K-NH₂). Both are comprised mainly of alanine residues, allowing comparison of the ssHDX-MS kinetic data with the corresponding length PDLA peptides. Peptide A and Peptide B also contain a few lysine residues which impart the required aqueous solubility. The structured peptides were acetylated at N-terminus and amidated at the C-terminus based on previous reports.⁹⁶⁻⁹⁸

Excipients for lyophilization: Several stabilizing and destabilizing excipients were selected for lyophilization. Two sugar excipients (sucrose and trehalose) were chosen since they are known to protect proteins during lyophilization either by water replacement or vitrification.^{11,99} Sucrose and trehalose are similar in molecular size but have different glass transition temperatures. Since sucrose has a lower glass transition temperature (T_g) than trehalose, the extent of interaction between the peptide and sucrose is expected to be greater than the interaction between the peptide and trehalose.¹⁰⁰ Another sugar, mannitol, was chosen because of its tendency to crystallize during lyophilization and possess reduced interaction with the peptide. A common tonicity modifying agent, sodium chloride, was used as a negative control since it is not capable of interacting with the peptides through hydrogen bonding. A chaotropic agent, guanidine HCl, was selected as a control since it does not protect the peptides. A control peptide-only formulation lyophilized without any excipients was also used in the study.

Methods: A conservative lyophilization cycle was used to produce six different formulations of PDLA, Peptide A and Peptide B. The peptide and the excipient ratio were 1:7 % w/w for all formulations except the excipient-free formulation. The peptide structures were confirmed with circular dichroism (CD) in solution, and Fourier transform infrared spectroscopy (FTIR) in the

solid-state. The physical nature of the solid samples was characterized by powder X-ray diffraction (PXRD). The glass transition temperatures of the peptide formulations were determined using modulated differential scanning calorimetry (MDSC). Solution HDX-MS was carried out on pre-lyophilization solution samples as a control. ssHDX-MS was carried out at varying D₂O relative humidities ranging from 6% RH to 97 % RH D₂O (Specific Aim 1). The pre-hydration and the reversibility ssHDX-MS experiments were carried out at 6% RH and 11% RH D₂O (Specific Aim 2). Similarly, the ssHDX-MS experiments of structured PDLA analogs were carried out at 11% RH and 23% RH D₂O (Specific Aim 3).

Data analysis: The deuterium incorporation in each peptide formulation was determined using the Mass Hunter-Bioconfirm software package (B.03.01, Agilent Technologies) and the HDExaminer software (Version 2.0, Sierra Analytics). Deuteration data from the ssHDX-MS experiments were fitted to a mono-exponential model, and the deuterium incorporation kinetic parameters were calculated and statistically analyzed using GraphPad Prism software (Version 8.4.0).

$$D = D_{max}(1 - e^{-kt})$$

where D is the percent deuterium uptake at labeling time t, D_{max} is the deuterium uptake at infinite time, and k is an apparent first-order rate constant for deuterium incorporation. The deuterium removal data in the reversibility ssHDX-MS experiments (Specific Aim 2) were fitted to a mono-exponential decay equation, and the kinetic parameters were calculated and statistically analyzed using GraphPad Prism software (Version 8.4.0).

$$D = D_{min} + (D_{max} - D_{min})e^{-kt}$$

where D is the percent deuterium (%) remaining at time t, D_{min} is the minimum deuterium incorporation (%) at infinite time, D_{max} is the initial deuteration (t₀), and k is an apparent first-order rate constant for deuterium loss.

1.7 References

- (1) Wang, W. Instability, stabilization, and formulation of liquid protein pharmaceuticals. *Int. J. Pharm.* **1999**, *185* (2), 129-188.
- (2) Krejsa, C.; Rogge, M.; Sadee, W. Protein therapeutics: New applications for pharmacogenetics. *Nat. Rev. Drug Discovery.* **2006**, *5* (6), 507-521.
- (3) Mullard, A. 2019 FDA drug approvals. *Nat. Rev. Drug Discovery.* **2020**, *19*, 79-84.
- (4) Research and Markets, Protein therapeutics market 2020 global analysis, opportunities and forecast to 2025. *Medgadget*, **2019**.
- (5) Leader, B.; Baca, Q. J.; Golan, D. E. Protein therapeutics: A summary and pharmacological classification. *Nat. Rev. Drug Discovery.* **2008**, *7* (1), 21-39.
- (6) Leurs, U.; Mistarz, U. H.; Rand, K. D. Getting to the core of protein pharmaceuticals—comprehensive structure analysis by mass spectrometry. *Eur. J. Pharm. Biopharm.* **2015**, *93*, 95-109.
- (7) Wang, W. Lyophilization and development of solid protein pharmaceuticals. *Int. J. Pharm.* **2000**, *203* (1), 1-60.
- (8) Maltesen, M. J.; Van De Weert, M. Drying methods for protein pharmaceuticals. *Drug Discovery Today: Technol.* **2008**, *5* (2-3), e81-e88.
- (9) Carpenter, J.; Arakawa, T.; Crowe, J. Interactions of stabilizing additives with proteins during freeze-thawing and freeze-drying. *Dev. Biol. Stand.* **1992**, *74*, 225-238.
- (10) Mensink, M. A.; Frijlink, H. W.; van der Voort Maarschalk, K., *et al.* How sugars protect proteins in the solid state and during drying (review): Mechanisms of stabilization in relation to stress conditions. *Eur. J. Pharm. Biopharm.* **2017**, *114*, 288-295.
- (11) Allison, S. D.; Chang, B.; Randolph, T. W., *et al.* Hydrogen bonding between sugar and protein is responsible for inhibition of dehydration-induced protein unfolding. *Arch. Biochem. Biophys.* **1999**, *365*, 289-298.
- (12) Stotz, C. E.; Winslow, S. L.; Houchin, M. L., *et al.*, Degradation pathways for lyophilized peptides and proteins. In *Lyophilization of biopharmaceuticals*, Costantino, H. R.; Pikal, M. J., Eds. AAPS Press: **2004**; Vol. 2, pp 443-480.
- (13) Chang, L.; Pikal, M. J. Mechanisms of protein stabilization in the solid state. *J. Pharm. Sci.* **2009**, *98* (9), 2886-2908.

- (14) Manning, M. C.; Chou, D. K.; Murphy, B. M., *et al.* Stability of protein pharmaceuticals: An update. *Pharm. Res.* **2010**, *27* (4), 544-575.
- (15) Costantino, H. R.; Langer, R.; Klibanov, A. M. Solid-phase aggregation of proteins under pharmaceutically relevant conditions. *J. Pharm. Sci.* **1994**, *83* (12), 1662-1669.
- (16) Liu, W. R.; Langer, R.; Klibanov, A. M. Moisture-induced aggregation of lyophilized proteins in the solid state. *Biotechnol. Bioeng.* **1991**, *37* (2), 177-184.
- (17) Brems, D. N.; Plaisted, S. M.; Havel, H. A., *et al.* Stabilization of an associated folding intermediate of bovine growth hormone by site-directed mutagenesis. *Proc. Natl. Acad. Sci.* **1988**, *85* (10), 3367-3371.
- (18) Arakawa, T.; Hsu, Y. R.; Yphantis, D. A. Acid unfolding and self-association of recombinant *Escherichia coli* derived human interferon γ . *Biochemistry.* **1987**, *26* (17), 5428-5432.
- (19) Van den Berg, L.; Rose, D. Effect of freezing on the pH and composition of sodium and potassium phosphate solutions: The reciprocal system $\text{KH}_2\text{PO}_4 \cdot \text{Na}_2\text{HPO}_4 \cdot \text{H}_2\text{O}$. *Arch. Biochem. Biophys.* **1959**, *81* (2), 319-329.
- (20) Randolph, T. W. Phase separation of excipients during lyophilization: Effects on protein stability. *J. Pharm. Sci.* **1997**, *86* (11), 1198-1203.
- (21) Heller, M. C.; Carpenter, J. F.; Randolph, T. W. Manipulation of lyophilization-induced phase separation: Implications for pharmaceutical proteins. *Biotechnol. Prog.* **1997**, *13* (5), 590-596.
- (22) Towns, J. K. Moisture content in proteins: Its effects and measurement. *J. Chromatogr. A.* **1995**, *705* (1), 115-127.
- (23) Carpenter, J. F.; Chang, B. S.; Garzon-Rodriguez, W., *et al.*, Rational design of stable lyophilized protein formulations: Theory and practice. In *Rational design of stable protein formulations*, Carpenter, J. F.; Manning, M. C., Eds. Springer: **2002**; Vol. 13, pp 109-133.
- (24) Zhang, L.; Sinha, S.; Topp, E. M., Protein conformation and reactivity in amorphous solids. In *Formulation and process development strategies for manufacturing biopharmaceuticals*, Jameel, F.; Hershenson, S., Eds. John Wiley & Sons, Inc.: **2010**; pp 493-506.
- (25) Inglis, A. Cleavage at aspartic acid. *Meth. Enzymol.* **1983**, *91*, 324-332.
- (26) Li, S.; Patapoff, T. W.; Overcashier, D., *et al.* Effects of reducing sugars on the chemical stability of human relaxin in the lyophilized state. *J. Pharm. Sci.* **1996**, *85* (8), 873-877.

- (27) Lai, M.; Topp, E. Solid-state chemical stability of proteins and peptides. *J. Pharm. Sci.* **1999**, *88* (5), 489-500.
- (28) Pikal, M. J.; Rigsbee, D. R. The stability of insulin in crystalline and amorphous solids: Observation of greater stability for the amorphous form. *Pharm. Res.* **1997**, *14* (10), 1379-1387.
- (29) Strickley, R. G.; Anderson, B. D. Solid-state stability of human insulin. I. Mechanism and the effect of water on the kinetics of degradation in lyophiles from pH 2–5 solutions. *Pharm. Res.* **1996**, *13* (8), 1142-1153.
- (30) Strickley, R. G.; Anderson, B. D. Solid-state stability of human insulin II. Effect of water on reactive intermediate partitioning in lyophiles from pH 2–5 solutions: Stabilization against covalent dimer formation. *J. Pharm. Sci.* **1997**, *86* (6), 645-653.
- (31) Chang, B. S.; Beauvais, R. M.; Dong, A., *et al.* Physical factors affecting the storage stability of freeze-dried interleukin-1 receptor antagonist: Glass transition and protein conformation. *Arch. Biochem. Biophys.* **1996**, *331* (2), 249-258.
- (32) Wu, S.; Leung, D.; Vemuri, S., *et al.* Degradation mechanism of lyophilized basic fibroblast growth factor (BFGF) protein in sugar formulation. *Pharm. Sci.* **1998**, *1*, S-539.
- (33) Pikal, M. J.; Dellerman, K. M.; Roy, M. L., *et al.* The effects of formulation variables on the stability of freeze-dried human growth hormone. *Pharm. Res.* **1991**, *8* (4), 427-436.
- (34) Hageman, M. J.; Bauer, J. M.; Possert, P. L., *et al.* Preformulation studies oriented toward sustained delivery of recombinant somatotropins. *J. Agric. Food Chem.* **1992**, *40* (2), 348-355.
- (35) Manning, M. C.; Patel, K.; Borchardt, R. T. Stability of protein pharmaceuticals. *Pharm. Res.* **1989**, *6* (11), 903-918.
- (36) Fransson, J.; Florin-Robertsson, E.; Axelsson, K., *et al.* Oxidation of human insulin-like growth factor I in formulation studies: Kinetics of methionine oxidation in aqueous solution and in solid state. *Pharm. Res.* **1996**, *13* (8), 1252-1257.
- (37) Kenney, W.; Watson, E.; Bartley, T., *et al.* Parameters for the evaluation of IL-2 stability. *Lymphokine Res.* **1986**, *5*, S23-7.
- (38) Hora, M.; Rana, R.; Wilcox, C. L., *et al.* Development of a lyophilized formulation of interleukin-2. *Dev. Biol. Stand.* **1992**, *74*, 295-303.

- (39) Pikal, M.; Dellerman, K.; Roy, M. Formulation and stability of freeze-dried proteins: effects of moisture and oxygen on the stability of freeze-dried formulations of human growth hormone. *Dev. Biol. Stand.* **1992**, *74*, 21-37.
- (40) Yoshioka, S.; Aso, Y.; Izutsu, K.-i., *et al.* Aggregates formed during storage of β -galactosidase in solution and in the freeze-dried state. *Pharm. Res.* **1993**, *10* (5), 687-691.
- (41) Costantino, H. R.; Langer, R.; Klibanov, A. M. Aggregation of a lyophilized pharmaceutical protein, recombinant human albumin: Effect of moisture and stabilization by excipients. *Biotechnology.* **1995**, *13* (5), 493-496.
- (42) Andya, J. D.; Hsu, C. C.; Shire, S. J. Mechanisms of aggregate formation and carbohydrate excipient stabilization of lyophilized humanized monoclonal antibody formulations. *AAPS PharmSci.* **2003**, *5* (2), 21-31.
- (43) Chen, B.-I.; Arakawa, T.; Morris, C. F., *et al.* Aggregation pathway of recombinant human keratinocyte growth factor and its stabilization. *Pharm. Res.* **1994**, *11* (11), 1581-1587.
- (44) Costantino, H. R.; Langer, R.; Klibanov, A. M. Moisture-induced aggregation of lyophilized insulin. *Pharm. Res.* **1994**, *11* (1), 21-29.
- (45) Hora, M. S.; Rana, R. K.; Smith, F. W. Lyophilized formulations of recombinant tumor necrosis factor. *Pharm. Res.* **1992**, *9* (1), 33-36.
- (46) Volkin, D. B.; Middaugh, C. R., The characterization, stabilization, and formulation of acidic fibroblast growth factor. In *Formulation, characterization, and stability of protein drugs: case histories*, Pearlman, R.; Wang, J. Y., Eds. Springer: **2002**; Vol. 9, pp 181-217.
- (47) Chang, B. S.; Randall, C. S.; Lee, Y. S. Stabilization of lyophilized porcine pancreatic elastase. *Pharm. Res.* **1993**, *10* (10), 1478-1483.
- (48) Hekmana, C.; Park, S.; Teng, W.-Y., *et al.* Degradation of lyophilized and reconstituted MACROSCINT® (DTPA-IgG): Precipitation vs. glycosylation. *J. Pharm. Biomed. Anal.* **1995**, *13* (10), 1249-1261.
- (49) Andya, J. D.; Maa, Y.-F.; Costantino, H. R., *et al.* The effect of formulation excipients on protein stability and aerosol performance of spray-dried powders of a recombinant humanized anti-IgE monoclonal antibody. *Pharm. Res.* **1999**, *16* (3), 350-358.
- (50) te Booy, M. P.; de Ruiter, R. A.; de Meere, A. L. Evaluation of the physical stability of freeze-dried sucrose-containing formulations by differential scanning calorimetry. *Pharm. Res.* **1992**, *9* (1), 109-114.

- (51) Lueckel, B.; Helk, B.; Bodmer, D., *et al.* Effects of formulation and process variables on the aggregation of freeze-dried interleukin-6 (IL-6) after lyophilization and on storage. *Pharm. Dev. Technol.* **1998**, *3* (3), 337-346.
- (52) van de Weert, M.; Hering, J. A.; Haris, P. I., Fourier transform infrared spectroscopy. In *Methods for structural analysis of protein pharmaceuticals*, Jiskoot, W.; Crommelin, D. J. A., Eds. AAPS Press: **2005**; Vol. 3, pp 131-166.
- (53) Hawe, A.; Sinha, S.; Friess, W., *et al.*, Structural analysis of proteins in dried matrices. In *Formulation and process development strategies for manufacturing biopharmaceuticals*, Jameel, F.; Hershenson, S., Eds. John Wiley & Sons, Inc.: **2010**; pp 549-563.
- (54) Prestrelski, S. J.; Tedeschi, N.; Arakawa, T., *et al.* Dehydration-induced conformational transitions in proteins and their inhibition by stabilizers. *Biophys. J.* **1993**, *65* (2), 661-671.
- (55) Yeo, S. D.; Debenedetti, P. G.; Patro, S. Y., *et al.* Secondary structure characterization of microparticulate insulin powders. *J. Pharm. Sci.* **1994**, *83* (12), 1651-1656.
- (56) S Moorthy, B.; K Iyer, L.; M Topp, E. Characterizing protein structure, dynamics and conformation in lyophilized solids. *Curr. Pharm. Des.* **2015**, *21* (40), 5845-5853.
- (57) Liu, Y.; Cho, R.-K.; Sakurai, K., *et al.* Studies on spectra/structure correlations in near-infrared spectra of proteins and polypeptides. Part I: A marker band for hydrogen bonds. *Appl. Spectrosc.* **1994**, *48* (10), 1249-1254.
- (58) Izutsu, K.-i.; Fujimaki, Y.; Kuwabara, A., *et al.* Near-infrared analysis of protein secondary structure in aqueous solutions and freeze-dried solids. *J. Pharm. Sci.* **2006**, *95* (4), 781-789.
- (59) Reich, G. Near-infrared spectroscopy and imaging: Basic principles and pharmaceutical applications. *Adv. Drug Delivery Rev.* **2005**, *57* (8), 1109-1143.
- (60) Wen, Z. Q. Raman spectroscopy of protein pharmaceuticals. *J. Pharm. Sci.* **2007**, *96* (11), 2861-2878.
- (61) Nielsen, O. F., Raman spectroscopy. In *Methods for structural analysis of protein pharmaceuticals*, Jiskoot, W.; Crommelin, D. J. A., Eds. AAPS Press: Arlington, VA, **2005**; pp 167-198.
- (62) Sane, S. U.; Wong, R.; Hsu, C. C. Raman spectroscopic characterization of drying-induced structural changes in a therapeutic antibody: Correlating structural changes with long-term stability. *J. Pharm. Sci.* **2004**, *93* (4), 1005-1018.

- (63) Sharma, V. K.; Kalonia, D. S. Steady-state tryptophan fluorescence spectroscopy study to probe tertiary structure of proteins in solid powders. *J. Pharm. Sci.* **2003**, *92* (4), 890-899.
- (64) Park, J.; Nagapudi, K.; Vergara, C., *et al.* Effect of pH and excipients on structure, dynamics, and long-term stability of a model IgG1 monoclonal antibody upon freeze-drying. *Pharm. Res.* **2013**, *30* (4), 968-984.
- (65) Crowe, J. H.; Carpenter, J. F.; Crowe, L. M. The role of vitrification in anhydrobiosis. *Annu. Rev. Physiol.* **1998**, *60* (1), 73-103.
- (66) Pikal, M. J.; Rigsbee, D.; Roy, M. L. Solid state stability of proteins III: calorimetric (DSC) and spectroscopic (FTIR) characterization of thermal denaturation in freeze dried human growth hormone (hGH). *J. Pharm. Sci.* **2008**, *97* (12), 5122-5131.
- (67) Breen, E.; Curley, J.; Overcashier, D., *et al.* Effect of moisture on the stability of a lyophilized humanized monoclonal antibody formulation. *Pharm. Res.* **2001**, *18* (9), 1345-1353.
- (68) McDermott, A. E. Structural and dynamic studies of proteins by solid-state NMR spectroscopy: rapid movement forward. *Curr. Opin. Struct. Biol.* **2004**, *14* (5), 554-561.
- (69) Li, B.; O'Meara, M. H.; Lubach, J. W., *et al.* Effects of sucrose and mannitol on asparagine deamidation rates of model peptides in solution and in the solid state. *J. Pharm. Sci.* **2005**, *94* (8), 1723-1735.
- (70) Mensink, M. A.; Nethercott, M. J.; Hinrichs, W. L., *et al.* Influence of miscibility of protein-sugar lyophilizates on their storage stability. *AAPS J.* **2016**, *18* (5), 1225-1232.
- (71) Moorthy, B. S.; Iyer, L. K.; Topp, E. M. Mass spectrometric approaches to study protein structure and interactions in lyophilized powders. *J. Vis. Exp.* **2015**, (98), No. e52503.
- (72) Sophocleous, A. M.; Zhang, J.; Topp, E. M. Localized hydration in lyophilized myoglobin by hydrogen–deuterium exchange mass spectrometry. 1. Exchange mapping. *Mol. Pharmaceutics.* **2012**, *9* (4), 718-726.
- (73) Moorthy, B. S.; Schultz, S. G.; Kim, S. G., *et al.* Predicting protein aggregation during storage in lyophilized solids using solid state amide hydrogen/deuterium exchange with mass spectrometric analysis (ssHDX-MS). *Mol. Pharmaceutics.* **2014**, *11* (6), 1869-1879.
- (74) Moorthy, B. S.; Zarraga, I. E.; Kumar, L., *et al.* Solid-state hydrogen–deuterium exchange mass spectrometry: correlation of deuterium uptake and long-term stability of lyophilized monoclonal antibody formulations. *Mol. Pharmaceutics.* **2018**, *15* (1), 1-11.

- (75) Kumar, L.; Chandrababu, K. B.; Balakrishnan, S. M., *et al.* Optimizing the formulation and lyophilization process for a fragment antigen binding (Fab) protein using solid-state hydrogen–deuterium exchange mass spectrometry (ssHDX-MS). *Mol. Pharmaceutics*. **2019**, *16* (11), 4485-4495.
- (76) Wilson, N. E.; Mutukuri, T. T.; Zemlyanov, D. Y., *et al.* Surface composition and formulation heterogeneity of protein solids produced by spray drying. *Pharm. Res.* **2019**, *37* (1), 14.
- (77) Morgan, C. R.; Engen, J. R. Investigating solution-phase protein structure and dynamics by hydrogen exchange mass spectrometry. *Curr. Protoc. Protein Sci.* **2009**, *58* (1), 17.6. 1-17.6. 17.
- (78) Marcsisin, S. R.; Engen, J. R. Hydrogen exchange mass spectrometry: What is it and what can it tell us? *Anal. Bioanal. Chem.* **2010**, *397* (3), 967-972.
- (79) Bai, Y.; Milne, J. S.; Mayne, L., *et al.* Primary structure effects on peptide group hydrogen exchange. *Proteins: Struct., Funct., Bioinf.* **1993**, *17* (1), 75-86.
- (80) Perrin, C. L. Proton exchange in amides: Surprises from simple systems. *Acc. Chem. Res.* **1989**, *22* (8), 268-275.
- (81) Jensen, P. F.; Rand, K. D., Hydrogen exchange: a sensitive analytical window into protein conformation and dynamics. In *Hydrogen exchange mass spectrometry of proteins: fundamentals, methods, and applications*, Weis, D. D., Ed. John Wiley & Sons: **2015**; pp 1-17.
- (82) Hvidt, A.; Nielsen, S. O. Hydrogen exchange in proteins. *Adv. Protein Chem.* **1966**, *21*, 287-386.
- (83) Woodward, C.; Simon, I.; Tüchsen, E. Hydrogen exchange and the dynamic structure of proteins. *Mol. Cell. Biochem.* **1982**, *48* (3), 135-160.
- (84) Englander, S. W.; Kallenbach, N. R. Hydrogen exchange and structural dynamics of proteins and nucleic acids. *Q. Rev. Biophys.* **1983**, *16* (4), 521-655.
- (85) Kossiakoff, A. Protein dynamics investigated by the neutron diffraction–hydrogen exchange technique. *Nature*. **1982**, *296* (5859), 713-721.
- (86) Tüchsen, E.; Woodward, C. Mechanism of surface peptide proton exchange in bovine pancreatic trypsin inhibitor salt effects and O-protonation. *J. Mol. Biol.* **1985**, *185* (2), 421-430.

- (87) Smith, D. L.; Deng, Y.; Zhang, Z. Probing the non-covalent structure of proteins by amide hydrogen exchange and mass spectrometry. *J. Mass Spectrom.* **1997**, *32* (2), 135-146.
- (88) Molday, R.; Englander, S.; Kallen, R. Primary structure effects on peptide group hydrogen exchange. *Biochemistry.* **1972**, *11* (2), 150-158.
- (89) Carter, J. V.; Knox, D.; Rosenberg, A. Pressure effects on folded proteins in solution: Hydrogen exchange at elevated pressures. *J. Biol. Chem.* **1978**, *253* (6), 1947-1953.
- (90) Wong, P.; Heremans, K. Pressure effects on protein secondary structure and hydrogen deuterium exchange in chymotrypsinogen: A Fourier transform infrared spectroscopic study. *Biochim. Biophys. Acta, Protein Struct. Mol. Enzymol.* **1988**, *956* (1), 1-9.
- (91) Kim, P. S.; Baldwin, R. L. Influence of charge on the rate of amide proton exchange. *Biochemistry.* **1982**, *21* (1), 1-5.
- (92) Christoffersen, M.; Bolvig, S.; Tüchsen, E. Salt effects on the amide hydrogen exchange of bovine pancreatic trypsin inhibitor. *Biochemistry.* **1996**, *35* (7), 2309-2315.
- (93) Li, Y.; Williams, T. D.; Topp, E. M. Effects of excipients on protein conformation in lyophilized solids by hydrogen/deuterium exchange mass spectrometry. *Pharm. Res.* **2008**, *25* (2), 259-267.
- (94) Lam, Y.-H.; Bustami, R.; Phan, T., *et al.* A solid-state NMR study of protein mobility in lyophilized protein–sugar powders. *J. Pharm. Sci.* **2002**, *91* (4), 943-951.
- (95) Wales, T. E.; Engen, J. R. Hydrogen exchange mass spectrometry for the analysis of protein dynamics. *Mass Spectrom. Rev.* **2006**, *25* (1), 158-170.
- (96) Marqusee, S.; Robbins, V. H.; Baldwin, R. L. Unusually stable helix formation in short alanine-based peptides. *Proc. Natl. Acad. Sci.* **1989**, *86* (14), 5286-5290.
- (97) Blondelle, S. E.; Forood, B.; Houghten, R. A., *et al.* Polyalanine-based peptides as models for self-associated β -pleated-sheet complexes. *Biochemistry.* **1997**, *36* (27), 8393-8400.
- (98) Chakrabarty, A.; Kortemme, T.; Baldwin, R. L. Helix propensities of the amino acids measured in alanine-based peptides without helix-stabilizing side-chain interactions. *Protein Sci.* **1994**, *3* (5), 843-852.
- (99) Duddu, S. P.; Zhang, G.; Dal Monte, P. R. The relationship between protein aggregation and molecular mobility below the glass transition temperature of lyophilized formulations containing a monoclonal antibody. *Pharm. Res.* **1997**, *14* (5), 596-600.

- (100) Taylor, L. S.; Zografi, G. Sugar-polymer hydrogen bond interactions in lyophilized amorphous mixtures. *J. Pharm. Sci.* **1998**, 87 (12), 1615-1621.

CHAPTER 2. SOLID-STATE HYDROGEN-DEUTERIUM EXCHANGE MASS SPECTROMETRY (ssHDX-MS) OF LYOPHILIZED POLY-D, L-ALANINE

This chapter was published as a research article in *Molecular Pharmaceutics* (2019, 16 (7), 2935-2946) and reproduced with permission. Copyright (2019) American Chemical Society.

DOI: 10.1021/acs.molpharmaceut.9b00162

2.1 Abstract

Solid-state hydrogen deuterium exchange mass spectrometry (ssHDX-MS) has been developed to study proteins in amorphous solids, but the relative contributions of protein structure and protein-matrix interactions to exchange are not known. In this work, short unstructured poly-D,L-alanine (PDLA) peptides were co-lyophilized with sucrose, trehalose, mannitol, sodium chloride or guanidine hydrochloride to quantify the contributions of protein-matrix interactions to deuterium uptake in ssHDX-MS in the absence of higher order structure. Deuterium incorporation differed with excipient type and relative humidity (RH) in $D_2O_{(g)}$, effects that were not observed in solution controls and are not described by the Linderstrom-Lang model for solution HDX. A reversible pseudo first-order kinetic model for deuterium uptake ssHDX-MS is proposed. The model agrees with the experimentally observed dependences of apparent deuteration rate and plateau value on RH in ssHDX-MS of PDLA, and reduces to the Linderstrom-Lang limit when the forward rate of exchange is much greater than the reverse rate.

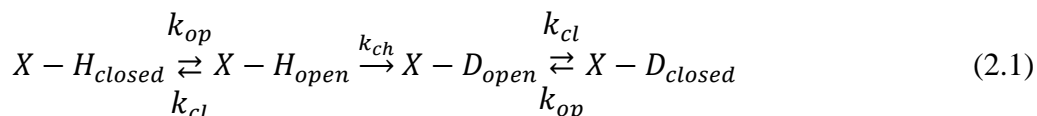
2.2 Introduction

Many protein drugs are marketed as lyophilized solid powders to preserve their structure and prolong shelf-life. Of the 107 protein drugs approved by the FDA in the last ten years, 46 (43%) are marketed in solid forms. Excipients such as sucrose or trehalose are usually included in these products, and are thought to stabilize proteins by forming hydrogen bonds with the protein¹ or by producing a glassy solid of low molecular mobility.² To select excipients and develop the final product, candidate excipients are evaluated in stability studies, which can take months or years to complete. In principle, detailed physicochemical analysis of the lyophilized powders could be used as an alternative to stability studies, reducing the time needed for product development. Stability data are in fact supplemented with various physicochemical properties of the powders, including the glass transition temperature (T_g), moisture content and protein secondary structure in the solid state (e.g., by Fourier Transform Infrared Spectroscopy, FTIR). While these measurements provide information about the solid-state properties of the drug product, they are usually poorly correlated with storage stability, and stability studies therefore remain the benchmark. In order to accelerate formulation development and improve our understanding of protein stability in amorphous solids, there is an unmet need for a stability-indicating analytical method for proteins in the amorphous solid state.

Over the past ten years, our group has developed solid-state hydrogen deuterium exchange with mass spectrometric analysis (ssHDX-MS) as a novel analytical method for proteins in lyophilized solids, providing high resolution information on protein structure and matrix interactions in the amorphous solid state.³⁻¹³ In an ssHDX-MS experiment, vials containing a lyophilized protein are placed uncapped in a sealed desiccator and exposed to $D_2O_{(g)}$ at constant temperature and D_2O activity (i.e., relative humidity (RH) in D_2O). Vials are removed at various times, flash frozen in liquid nitrogen and stored at -80°C prior to analysis. For analysis, vials are reconstituted under quench conditions (pH 2.5, $\sim 0^\circ\text{C}$) and quickly injected into a tandem liquid chromatography / mass spectrometry system (e.g., ESI-MS). The number of deuterium atoms incorporated is calculated from the deconvoluted m/z spectra by subtracting the native (non-deuterated) mass of the protein from the mass value at each time point. Samples can also be subjected to proteolytic digestion (e.g., using an in-line immobilized pepsin column) to enable the sites of deuterium incorporation to be identified. The kinetics of exchange for the intact protein and each digest peptide are fitted to mono-exponential or bi-exponential equations, as warranted by the data.

Deuterium incorporation for the fragments can be mapped onto a three-dimensional structure or a homology model to provide a visual representation of the sites of deuterium incorporation. Our group has shown that ssHDX-MS is sensitive to changes in formulation,^{5,6,10,12,13} moisture content^{8,9} and processing method.^{4,11} More recently, ssHDX-MS has also been shown to be highly correlated with the storage stability of various formulations of myoglobin (Mb) and of a monoclonal antibody (mAb),^{6,10} and thus shows promise as a stability-indicating analytical method. To date, however, there is no mechanistic model that describes the ssHDX-MS and the factors influencing the rate and extent of exchange. A mechanistic model would allow data to be better analyzed and interpreted, and would advance our understanding of the amorphous solid state. The studies presented here begin to address this gap.

HDX studies for proteins in solution are analyzed and interpreted using the model first introduced by Lindstrom-Lang.¹⁴⁻¹⁸ According to the Lindstrom-Lang model, HDX in solution is the result of reversible protein unfolding (i.e., “opening” and “closing” events, with rate constants k_{op} and k_{cl}), which may be global or local, followed by an irreversible chemical exchange reaction at free amide groups (k_{ch}):



The observed rate of hydrogen-deuterium exchange (k_{HDX}) for a native state folded protein, subject to the assumptions that the open form ($X-H_{open}$) is in steady-state and $k_{cl} \gg k_{op}$, is related to the rates of opening, closing and chemical exchange by following equation:¹⁹

$$k_{HDX} = \frac{k_{op} \times k_{ch}}{k_{cl} + k_{ch}} \quad (2.2)$$

When $k_{cl} \gg k_{ch}$, the observed rate of exchange (k_{HDX}) reduces to the “EX2” limiting case, and is given by:

$$EX2 \text{ limit: } k_{HDX} = \frac{k_{op} \times k_{ch}}{k_{cl}} \quad (2.3)$$

In the EX2 limit, k_{HDX} is related to the chemical exchange rate and the equilibrium constant for protein opening and closing events (i.e., k_{op}/k_{cl}), and the observed rate of exchange can be used to estimate the equilibrium constant if k_{ch} is known. EX2 kinetics are generally observed in solution HDX studies of native state proteins. In contrast, EX1 kinetics are relatively rare and are observed when chemical exchange rates are much faster than the rate of structural closing ($k_{cl} \ll k_{ch}$). In the EX1 limit:

$$EX1 \text{ limit: } k_{HDX} = k_{op} \quad (2.4)$$

and the observed rate of exchange is a measure of the rate of opening.

The effects of pH and temperature on k_{ch} are well established for solution HDX. Below pH 2.5, exchange is acid catalyzed (H_3O^+/D_3O^+) and is base catalyzed above pH 3.0 (OH^-/OD^-), with a minimum in the range of 2.5 – 3.0.^{20,21} Slower exchange rates are observed at lower temperatures; the rate of exchange decreases approximately 14-fold from 25 °C to 0 °C.^{21,22} In a typical HDX experiment, labelling is carried out at ambient temperature and pH ~7 followed by quenching at low temperature and low pH.

Protein amide hydrogen exchange rates in solution are affected by intramolecular hydrogen bonds and by the extent of solvent shielding, which are directly related to protein structure. The exchange rates are quantified by fitting deuterium incorporation as a function of time to exponential models (one-, two- or three component), in which the total number of exchangeable amide hydrogens is divided into different pools based on their relative exchange rates.^{13,20,23–25} In general, amide hydrogens in the core of a protein exchange much more slowly than those on the surface,^{26,27} although intramolecular hydrogen bonding of surface amide groups may slow their exchange.²⁸

While it is reasonable to expect that hydrogen-bonding interactions are important in ssHDX-MS as well as in solution HDX, a number of observations indicate that the Linderstrom-Lang model does not adequately describe ssHDX-MS. For example, while both the rate and extent of ssHDX-MS are strongly affected by stabilizing excipients,^{5,8} protein-excipient interactions are not described by the Linderstrom-Lang model. Similarly, ssHDX-MS is affected by $D_2O_{(g)}$ activity (i.e., by the relative humidity in D_2O), a parameter that is not relevant in most solution HDX studies and is not included in the Linderstrom-Lang model. An ssHDX-MS experiment takes days to

weeks to complete, far longer than solution HDX experiments. This suggests that rate processes much slower than those identified by Linderstrom-Lang (i.e., k_{ct} , k_{op} , k_{ch}) dominate ssHDX-MS, or at the very least that the rate constants are greatly reduced in solids. The Linderstrom-Lang assumption that chemical exchange (k_{ch}) is irreversible may also be violated on this time scale. Finally, applying the Linderstrom-Lang model requires an independent measure of k_{ch} , which depends on pH and temperature; pH is not defined in the solid state and glass transitions may complicate the interpretation of any observed temperature dependences.

It is reasonable to expect that ssHDX-MS is affected not only by the *intramolecular* hydrogen bonds that contribute to protein structure and are interrogated in solution HDX, but also by *intermolecular* hydrogen bonds between the protein and the matrix. The amorphous solid matrix can be viewed as an extended, hydrogen-bonded network of protein and excipient. Because amorphous solids are spatially and dynamically heterogeneous,²⁹⁻³¹ “the protein” in a solid sample is likely to be an ensemble in different environments and having different conformations and dynamics. When the solid is exposed to D₂O vapor in an ssHDX-MS experiment, D₂O is first sorbed into the solid, and hydrogen atoms are then exchanged for deuterium atoms at exchangeable sites on both protein and excipient. In the exchange reaction, sorbed D₂O competes with hydrogen bonds of various strengths in this extended hydrogen-bond network. As in solution HDX, only deuteration of the peptide bonds in the protein can be measured, however, since the reverse reaction (“back exchange”) occurs rapidly at other exchangeable sites and usually cannot be measured.^{17,21} Currently, the relative contributions of intra- and intermolecular hydrogen bonds to the rate and extent of exchange in ssHDX-MS are not known. This limits our ability to interpret ssHDX-MS data or to assign features of ssHDX-MS kinetics to protein structure (i.e., to intramolecular hydrogen bonds) or interactions with excipients (i.e., to intermolecular hydrogen bonds).

The aim of the current study is to determine the contributions of peptide-matrix interactions to ssHDX-MS in the absence of higher order protein structure. Unstructured poly-D,L-alanine peptides were co-lyophilized with several excipients, exposed to D₂O_(g) at various RH conditions, and the extent of deuteration monitored over time. Deuterium incorporation in solid samples differed with excipient type and relative humidity (RH) in D₂O_(g), effects that were not observed in solution controls and are not described by the Linderstrom-Lang model. A reversible pseudo first-order kinetic model for deuterium uptake ssHDX-MS is proposed that describes the ssHDX-

MS results and reduces to the Linderstrom-Lang limit when the forward rate of exchange is much greater than the reverse rate. To our knowledge, this is the first reported kinetic model for ssHDX-MS.

2.3 Materials and methods

Deuterium oxide (D₂O; 99.9 %) was purchased from Cambridge Isotope Laboratories (Andover, MA) and poly-D,L-alanine peptides (PDLA; MW 1000-5000 Da, # P9003) were purchased from Sigma Aldrich (St. Louis, MO). The salts used to prepare saturated solutions for controlling relative humidity were purchased from Sigma Aldrich (LiBr, CH₃CO₂K), Fisher Scientific (LiCl, NaCl, K₂SO₄; Hampton, NH) and VWR International (K₂CO₃; Radnor, PA). The excipients were purchased from Sigma Aldrich (sucrose, mannitol, guanidine HCl) and Fisher Scientific (trehalose, NaCl). Dibasic and monobasic potassium phosphates were purchased from Sigma Aldrich. Lyophilization vials (Wheaton™ serum tubing vials) were purchased from Fisher Scientific. All LC-MS grade solvents (water, acetonitrile, formic acid) were purchased from Fisher Scientific (Hampton, NH). All buffers and solutions were filtered through 0.22 μm sterile membrane syringe filters (Millex GV, EMD Millipore, Burlington, MA) prior to use.

2.3.1 Sample preparation by lyophilization

Six lyophilized formulations of PDLA were prepared by dissolving the peptide (5 mg/mL) and each of the excipients (35 mg/mL) in 2.5 mM potassium phosphate buffer (pH 7.4). Equal volumes of the peptide and excipient solutions were then mixed to yield solutions of 2.5 mg/mL peptide, 17.5 mg/mL excipient and a total solids content of 20 mg/mL in buffer. Next, 250 μL of this solution was aliquoted into 2 mL lyophilization vials and lyophilized using a benchtop freeze dryer (Virtis Advantage Plus, SP Scientific, Warminster, PA). The lyophilization process was initiated by pre-cooling the shelf to 5°C followed by freezing at -40°C, primary drying at -35°C for 28 h under vacuum (80 mTorr), secondary drying at 25°C for 6 h under vacuum (80 mTorr), and additional secondary drying at 5°C for another 6 h under vacuum (80 mTorr).

2.3.2 Solution HDX-MS

The PDLA peptides were subjected to HDX-MS in solution, serving as controls for the ssHDX-MS studies described below. Solutions of the PDLA peptide and excipients (sucrose, trehalose, mannitol, NaCl and guanidine hydrochloride) were prepared as described above. The HDX labelling solution was prepared by reconstituting lyophilized 2.5 mM potassium phosphate buffer in D₂O. HDX labelling was carried out at room temperature by mixing the peptide-excipient solution with deuterium labelling buffer at a ratio of 1:9 v/v. At pre-determined time intervals, samples were quenched by diluting the samples with ice cold quench buffer (0.2 % formic acid, 5 % methanol in water, pH 2.5). Deuterium uptake in quenched samples was then measured by LC-MS (Agilent 6520 QTOF, Agilent Technologies, Santa Clara, CA). The instrument was equipped with a custom LC column refrigeration unit capable of maintaining the low temperatures required for minimizing deuterium back exchange. The quenched, diluted samples were injected and trapped onto a peptide micro trap (Michrom Biosources, Inc., Auburn, CA), de-salted for 1.7 min with 0.1 % formic acid in water at a flow rate of 0.2 mL/min (isocratic) and then eluted onto an analytical column (Zorbax 300SB-C18; Agilent Technologies, Santa Clara, CA) using gradient flow for 8.5 min (mobile phase A: 0.1 % formic acid in water, mobile phase B: 0.1 % formic acid in acetonitrile). The mass spectra were obtained over the 100-1700 m/z range.

An un-deuterated control was used to obtain the peptide list using Mass Hunter Workstation Software equipped with the Bioconfirm software package (B.03.01, Agilent Technologies). The peptide list from un-deuterated samples was used as a reference to calculate deuterium uptake in the labelled samples using HDExaminer software (Version 2.0, Sierra Analytics, Modesto, CA). Graphing, regression analysis to calculate HDX kinetic parameters and statistical analysis were performed using GraphPad Prism software (Version 7.03, La Jolla, CA).

2.3.3 Solid-state HDX-MS (ssHDX-MS)

In ssHDX-MS studies, deuterium labeling was initiated by placing lyophilized samples of the peptides, in open vials, into sealed desiccators containing saturated solutions of various salts in D₂O. Samples were labelled at several RH conditions (i.e., RH equivalent in D₂O): 6% (produced using a saturated solution of LiBr in D₂O), 11% (LiCl in D₂O), 23% (CH₃CO₂K in D₂O), 43% (K₂CO₃ in D₂O), 57% (NaBr in D₂O), 75% (NaCl in D₂O) and 97% (K₂SO₄ in D₂O) at room

temperature.³² Uncapped lyophilized samples containing the solid powders were placed into desiccators containing the saturated salt solutions and labeling was carried out for up to 10 days. The vials were removed at pre-determined time intervals (1 h, 3 h, 6 h, 9 h, 12 h, 24 h, 3 days, 5 days and 10 days) capped and quenched by flash freezing (dropping into liquid N₂). Labelled samples were stored at -80°C until they were analyzed by LC-MS as described above for solution state HDX-MS.

An undeuterated control sample for each formulation was used to obtain a peptide list using Mass Hunter Workstation Software equipped with the Bioconfirm software package (B.03.01, Agilent Technologies). The peptide list from the undeuterated control sample was then used to calculate the percentage deuterium uptake for selected peptides using HDExaminer software (Version 2.0, Sierra Analytics, Modesto, CA).

The percentage deuterium uptake data from ssHDX-MS experiments ($\leq 43\%$ RH) was fitted to a mono-exponential model and the kinetic parameters were calculated for the nine selected peptides using GraphPad Prism version 7.03 for Windows (GraphPad Software, La Jolla California USA).

$$D = D_{max}(1 - e^{-kt}) \quad (2.5)$$

Here D is the deuterium uptake at labelling time t, D_{max} is the deuterium uptake at infinite time, and k is an apparent first-order rate constant.

The percentage deuterium uptake data from high RH ($\geq 57\%$ RH) ssHDX-MS experiments was fitted to a horizontal line ($Y = \text{Mean} + 0 \cdot X$), a modified version of linear regression. Since the earlier time points, i.e. $\leq 12\text{h}$, showed inconsistent and variable deuteration levels at high RH, perhaps due to phase transformation from amorphous solid to viscous solution, deuteration data beginning at 24h of labelling time was used to obtain D_{max} values at high RH.

2.3.4 Dynamic vapor sorption

Dynamic vapor sorption (DVS Intrinsic, Surface Measurement Systems NA, Allentown, PA) was used to measure the rate of water sorption and the moisture content in lyophilized PDLA formulations under ssHDX-MS labelling conditions. Initially, approximately 5-7 mg of sample was placed in the sample pan and equilibrated at 0% RH, 25°C to remove loosely bound moisture.

The equilibration was carried out until the mass change was less than 0.002% for 10 min. After the initial equilibration, the RH was increased stepwise (6%, 11%, 23%, 43% and 57%) and finally reduced to 0% RH. At each RH condition, the sample was equilibrated until the signal was constant (i.e., mass change < 0.002 % for 10 min; dm/dt stability time of at least 10 min) or for a maximum time of 6 h (maximum dm/dt stability time of 360 min).

2.3.5 Powder X-ray diffraction (PXRD)

PXRD was used to characterize the physical state (amorphous or crystalline) of lyophilized peptide formulations immediately after lyophilization. The X-ray diffractograms were collected using a Rigaku SmartLab (XRD 6000) diffractometer (The Woodlands, TX) at 0.15405 nm wavelength. The diffraction patterns were collected from 5° - 40° 2 θ at a step size of 0.02°.

2.3.6 Solid state FT-IR

Solid state FT-IR was used to confirm the lack of secondary structure for PDLA after lyophilization. The FT-IR spectra were acquired using a Nexus FT-IR spectrometer (Thermo Nicolet Corp., Madison, WI) equipped with a smart iTR single bounce attenuated total reflectance (ATR) sampling accessory. Approximately 2 mg of solid sample was placed on the ATR crystal and the spectra collected at a resolution of 4 cm⁻¹ with 128 scans. To reduce atmospheric moisture interference, the instrument was continuously purged with nitrogen gas. For each sample, the amide-I region (1720 cm⁻¹ to 1580 cm⁻¹) was extracted, the background spectra (128 scans at 4 cm⁻¹ resolution) were subtracted, baseline corrected, and the area was normalized. Finally, the second derivative spectra were generated using Opus software (Version 6.5, Bruker Optics, Billerica, MA).

2.3.7 Modulated differential scanning calorimetry (MDSC)

Thermal analysis of lyophilized samples was performed using a differential scanning calorimeter (DSC 25, TA Instruments, New Castle, DE) and the resulting data were analyzed using Trios software (Version 4.2.1, TA Instruments). Approximately 5 mg of lyophilized solid sample was placed in a Tzero pan and hermetically sealed using the Tzero hermetic lid. The samples were then cooled to -5°C and equilibrated for 5 min isothermally. The temperature modulation was set to an

amplitude of $\pm 1^\circ\text{C}$ for every 60 s and the samples were then heated from -5°C to 150°C at a ramp rate of $2^\circ\text{C}/\text{min}$ under nitrogen gas flow. In all experiments, an empty aluminum pan, crimped in the same way as the sample pans, was used as a reference.

2.4 Results

2.4.1 Physical characterization of lyophilized solids by PXRD

The crystallinity of lyophilized PDLA samples was characterized immediately following lyophilization ($t=0$) using PXRD (Figure 2.1). The diffractograms of the sucrose, trehalose and excipient free formulations showed smooth, broad and featureless spectra consistent with an amorphous solid. In contrast, the diffractograms of the mannitol, sodium chloride and guanidine HCl formulations showed sharp peaks of varying magnitudes, indicating the presence of crystalline material. The compositions of the crystalline phases in the mannitol, sodium chloride and guanidine hydrochloride samples cannot be determined from PXRD, and the presence of peptide in these phases cannot be ruled out. It is reasonable to assume that excipient crystallization produces a “peptide-rich” amorphous phase and a “peptide-poor” crystalline phase in each case.

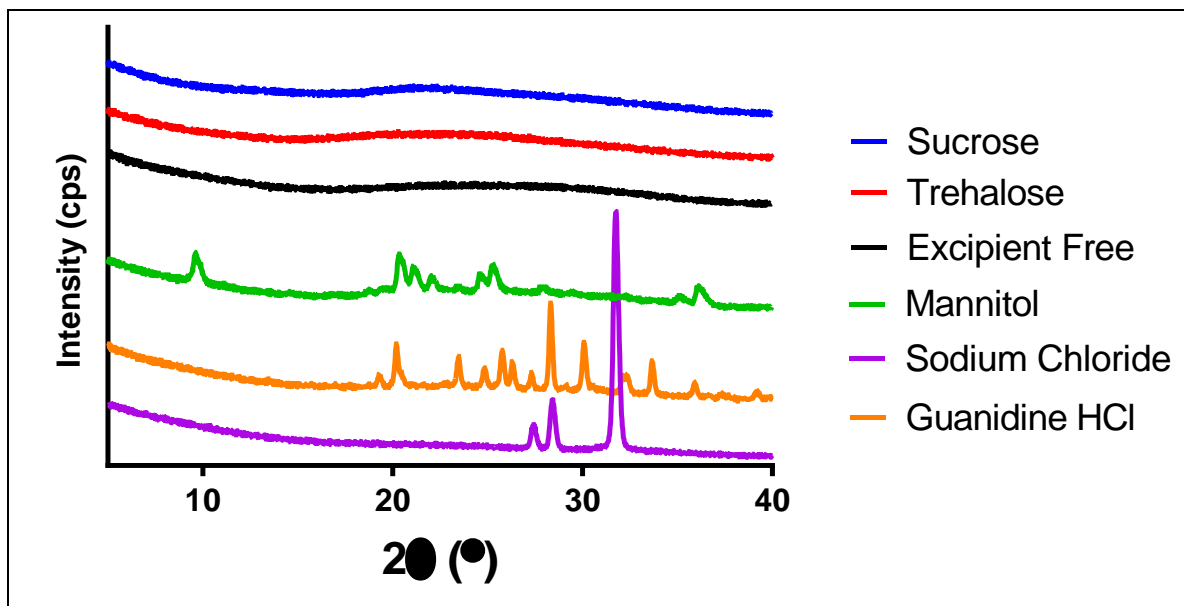


Figure 2.1. Powder X-ray diffraction profiles of lyophilized PDLA formulations show amorphous characteristics for sucrose, trehalose and excipient-free formulations and crystalline characteristics for mannitol, sodium chloride and guanidine HCl formulations.

2.4.2 Thermal analysis of lyophilized samples by MDSC

Glass transition temperatures (T_g) were measured for the three amorphous formulations using MDSC (Figure 2.2). The initial ($t=0$) T_g values for the sucrose, trehalose and excipient free samples were ~ 68 °C, ~ 101 °C and ~ 107 °C, respectively. When stored at RH values of 43% or greater in D₂O (i.e., for ssHDX-MS), sucrose and trehalose containing samples showed deliquescence consistent with a significant decrease in T_g due to plasticization by sorbed moisture. The excipient free formulation had a T_g of approximately 55°C after 24 h at 43% RH. This T_g value is greater than the room temperature deuterium labelling conditions. Other than melting transitions, thermal transitions were not detected in the crystalline formulations.

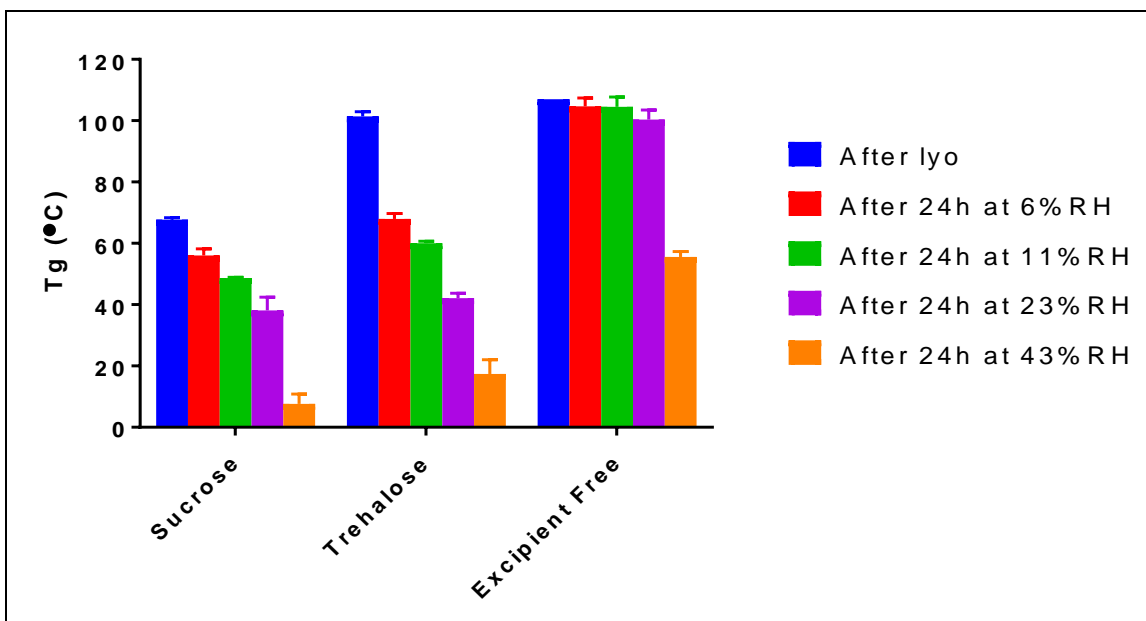


Figure 2.2. T_g values of amorphous lyophilized PDLA formulations as a function of RH. Samples showed deliquescence for $T_g < 20$ °C ($n=3$, mean \pm SD).

2.4.3 Secondary structure of peptides after lyophilization by FT-IR

Solid-state FT-IR spectra were generated for PDLA samples following lyophilization (Figure 2.3) to confirm that the peptides have no appreciable secondary structure. The second derivative spectra in the amide-I region (1720 cm^{-1} to 1580 cm^{-1}) showed a band at 1645 cm^{-1} for the excipient free formulation consistent with the absence of higher order structure and a random coil/disordered conformation.³³ With the exception of the guanidine HCl formulation, this peak was slightly broadened for the other formulations. The similarity of the FT-IR spectra among the formulations

suggests similar random coil structures in the various lyophilized samples and indicates the absence of significant structural differences. However, the FT-IR spectra of the guanidine HCl formulation showed peaks at 1639 cm^{-1} and 1673 cm^{-1} . While the peak at 1639 cm^{-1} is consistent with disordered structure, the peak at 1673 cm^{-1} may suggest the presence of a beta-turn in this formulation, or may indicate contributions to the spectrum by guanidine HCl despite background correction (see Materials and Methods). With this exception, FT-IR spectra confirm the lack of structure in the lyophilized peptide formulations.

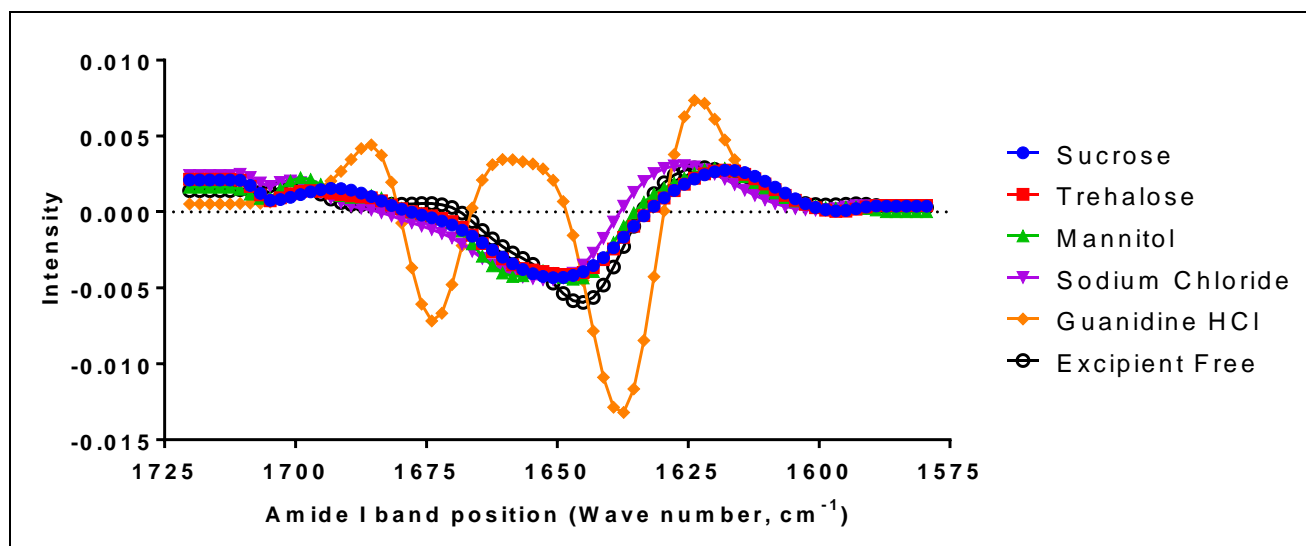


Figure 2.3. Solid state FT-IR spectra of PDLA peptides after lyophilization.

2.4.4 Residual moisture content by DVS

The residual moisture content in the lyophilized PDLA formulations was measured by DVS. The sucrose, trehalose, mannitol, sodium chloride and guanidine HCl formulations showed comparable residual moisture content (<4 % or <40 mg of water per 1 g of dry solid) (Figure 2.4). Low residual moisture may be desirable, since over-drying is known to be detrimental to lyophilized proteins.^{34,35} The excipient free formulation showed the highest residual moisture content (~10 %) of the formulations studied.

2.4.5 Vapor sorption by DVS

The vapor sorption behavior of the various formulations was evaluated by DVS (Figure 2.4). The sucrose and trehalose formulations sorbed more moisture than the mannitol and sodium chloride

formulations at each RH. Both the sucrose and trehalose formulations are amorphous and possess high surface free energy and surface area, which may lead to greater moisture sorption than in crystalline formulations such as mannitol and sodium chloride.³⁶⁻³⁸ The guanidine HCl formulation sorbed less moisture than the sucrose and trehalose formulations except at high RH, i.e., 57 % RH. At high RH, the guanidine HCl formulation showed deliquescence and the condensation of adsorbed moisture, which may be reflected in the mass change. The excipient free formulation sorbed more moisture than all other formulations at each RH. Vapor sorption at higher RH (>57 % RH) was not evaluated because all samples showed deliquescence and could not be considered solids.

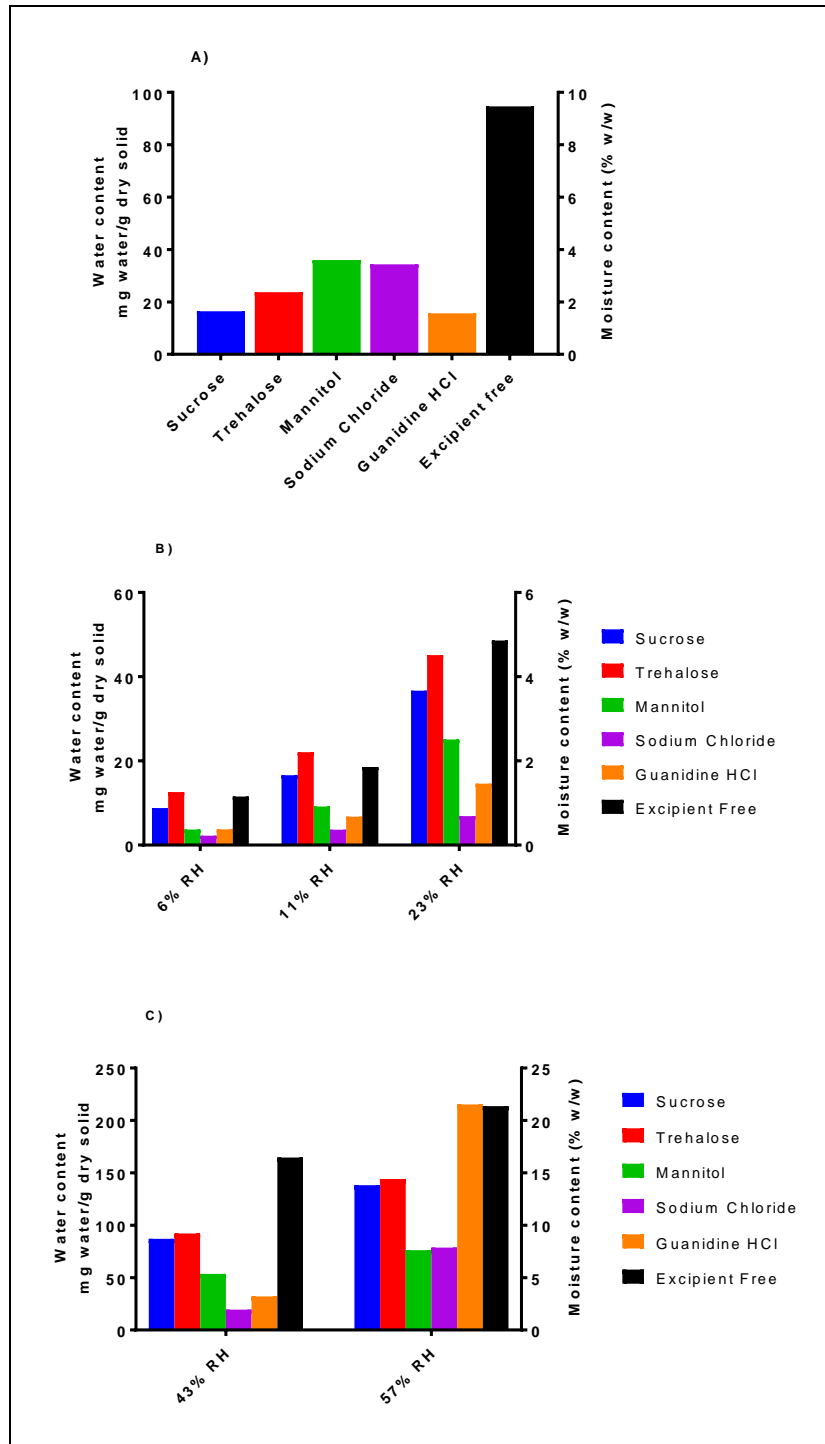


Figure 2.4. Moisture content in lyophilized PDLA formulations measured with dynamic vapor sorption (DVS): A) Residual moisture content in lyophilized poly-DL-alanine formulations at $t=0$, B) Equilibrium moisture content at 6 % RH, 11 % RH and 23 % RH and C) Equilibrium moisture content at 43 % RH, 57 % RH ($n=1$).

2.4.6 Mass spectrometric characterization of PDLA

Initial mass spectrometric (MS) analysis of PDLA revealed a mixture of peptides ranging from 6 to 44 amino acids in length. Since authentic standards were not available, it was not possible to quantify the amount of each peptide in the mixture and the oligomeric mixture was used as received in both solution and solid formulations. In solution and solid state HDX-MS studies, deuterium uptake was calculated for eight peptides from the mixture having the greatest signal intensity. Appendix A - Table A1 shows the list of peptides detected in the PDLA peptide mixture from initial MS analysis.

2.4.7 Solution state HDX-MS

Solution state HDX-MS of PDLA formulations was carried out as a control for solid state HDX-MS. Data were analyzed for eight peptides from the mixture and compared across formulations for deuterium uptake (Figure 2.5). All peptides in all solution formulations showed approximately 85% of the theoretical maximum deuterium uptake within 2 min of the initiation of labelling, consistent with a high degree of solvent accessibility of the amide hydrogens and a lack of higher order structure. The percentage deuterium uptake was constant for all formulations and there was no increase in deuterium uptake even at longer labelling times. Given that the peptides are unstructured, the constant 85% labeling in solution may be taken as a measure of the extent of back exchange (~15%) in these experiments. A back-exchange correction was not applied to the solution and solid state HDX results reported in Figures 2.5 and 2.6, and the reported deuterium incorporation values are those measured. However, a back exchange correction was applied when fitting the data to the reversible first-order kinetic model (Figures 2.7 and 2.8) by using solution HDX experiments as fully deuterated controls in HDExaminer software, as discussed below.

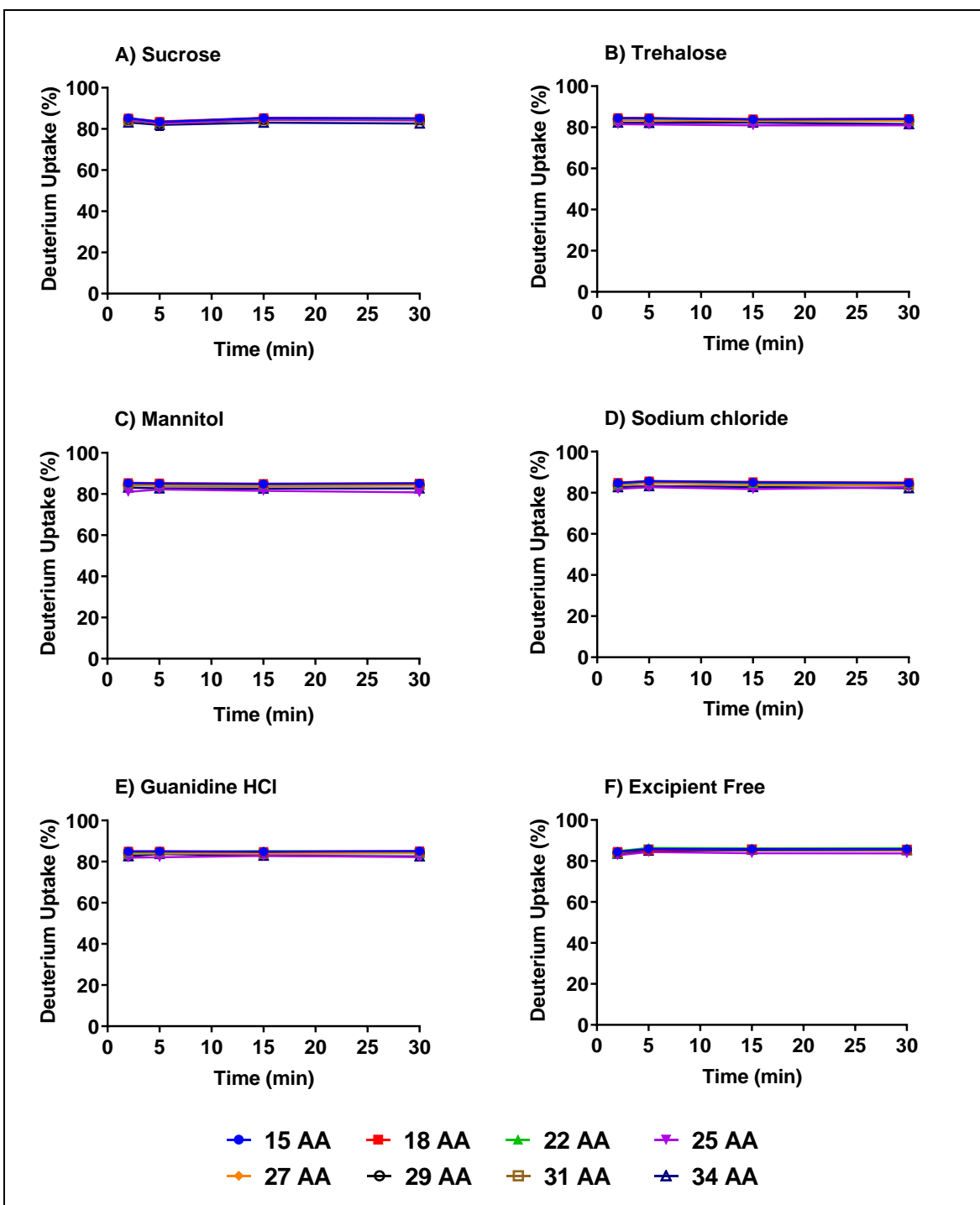


Figure 2.5. Solution state hydrogen deuterium exchange mass spectrometry (HDX-MS) of PDLA formulations containing: A) sucrose, B) trehalose, C) mannitol, D) sodium chloride, E) guanidine hydrochloride or F) no excipient (“excipient free”). Deuterium incorporation data are shown for eight PDLA peptides from the polydisperse mixture having different amino acid (AA) chain length: 15 AA (blue), 18 AA (red), 22 AA (green), 25 AA (purple), 27 AA (orange), 29 AA (black), 31 AA (brown) and 34 AA (dark blue). n=3, mean \pm SD; error bars not shown when less than the height of the symbol.

2.4.8 Solid-state HDX-MS

Solid-state HDX-MS kinetic data for the various formulations and RH conditions for the 22-amino acid (22 AA) PDLA peptide are presented in Figure 2.6, grouped according to excipient type. Supplemental figures show the data grouped by RH (Appendix A - Figure A1), and present data for other PDLA chain lengths (12 AA, 15AA, 18AA, 25AA, 27AA, 29AA, 31AA, 34AA) for comparison (6% RH, Appendix A - Figure A2; 11% RH, Appendix A - Figure A3; 23% RH, Appendix A - Figure A4; 43% RH, Appendix A - Figure A5; high RH, Appendix A - Figure A6).

On exposure to $D_2O_{(g)}$ at 6% RH, deuterium incorporation for solid samples of the PDLA peptides increased mono-exponentially with time (Figure 2.6, Appendix A - Figure A1 and A2). Unlike solution samples, deuterium incorporation in the solid samples depended on both formulation type and time (Figure 2.6, Appendix A - Figure A1 and A2). With the exception of the sodium chloride and excipient-free formulations, deuterium incorporation values for solid samples were significantly different from one another ($p < 0.0001$, one-way ANOVA with Tukey's multiple comparison). Since the PDLA peptides are unstructured, these results suggest that the peptides were protected from exchange in the solid state by their interactions with the solid matrix, and that the degree of protection depended on solid composition.

The deuterium uptake curves at 6% RH show the same rank order for all peptides, regardless of amino acid chain length (Appendix A - Figure A2). The guanidine HCl formulation showed the greatest deuterium uptake ($D_{max} \sim 60\%$) for all peptides (Appendix A - Figure A2). Though D_{max} values were slightly lower for peptides longer than 30 amino acids, the difference was not significant. In contrast, the sucrose and trehalose formulations showed the lowest deuterium uptake, with D_{max} values of approximately 20% and 24%, respectively (Appendix A - Figure A2). The low deuterium incorporation for the sucrose and trehalose formulations suggests that interactions between the peptide and the sugars in the solid state inhibit exchange. It is likely that these interactions involve hydrogen bonds between the peptide bonds of PDLA and the hydroxyl groups on the sugars. Deuterium incorporation values for the sucrose and trehalose formulations were significantly different from one another ($p < 0.0001$) (Figure 2.6 A, B, Appendix A - Figure A2), suggesting that there are differences in the extent and/or strength of the hydrogen bonding interactions in the two solids. Mannitol formulations showed greater deuteration than the trehalose and sucrose formulations ($D_{max}=45\%$) (Figure 2.6A, B, D, Appendix A - Figure A2), consistent

with crystallization of mannitol (Figure 2.1) and limited interaction with the peptides. The sodium chloride and excipient-free formulations showed identical deuterium uptake at 6% RH ($p=0.8339$) with a D_{\max} of approximately 30% (Appendix A - Figure A2), a value greater than in the sugar formulations and less than in the mannitol formulations. Weak peptide-peptide interactions in the excipient free formulation and ionic interactions with sodium chloride may provide some protection from exchange.

The extent of deuterium incorporation (D_{\max}) for the various excipients (Figure 2.6) is not simply related to the moisture content of the solid (Figure 2.4). For example, the sucrose and trehalose formulations have the greatest moisture content among all the formulations at 6% RH (Figure 2.4) and the lowest deuterium uptake (Figure 2.6, Appendix A - Figure A2). Similarly, vapor sorption at each RH in DVS reached equilibrium in 6 h or less (see Materials and methods), while deuterium incorporation in ssHDX-MS studies required more than 100 h to plateau for some formulations at 6% RH (Appendix A - Figure A1). These results indicate that the rate and extent of D_2O sorption do not dominate deuterium incorporation in ssHDX-MS studies of these peptides when compared across excipients, an observation made previously in ssHDX-MS studies of larger proteins.⁹

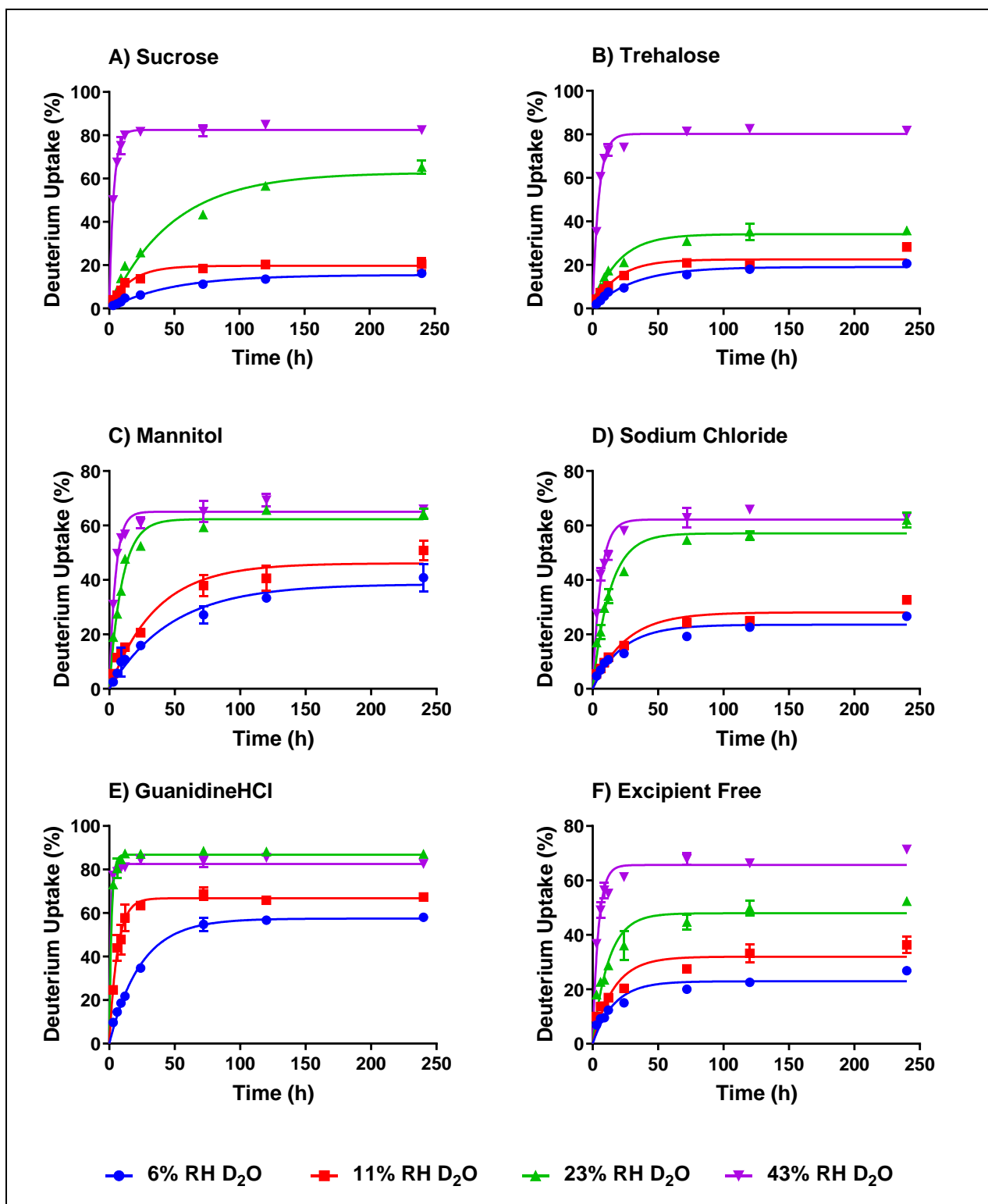


Figure 2.6. Solid state hydrogen deuterium exchange mass spectrometry (ssHDX-MS) of PDLA formulations containing: A) sucrose, B) trehalose, C) mannitol, D) sodium chloride, E) guanidine HCl or F) no excipient (“excipient-free”). Data shown for 22 amino acid peptide. n=3, mean \pm SD; error bars not shown when less than the height of the symbol.

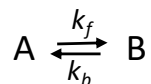
2.4.9 Effect of RH on ssHDX-MS

ssHDX-MS analysis of the peptide formulations was conducted at higher RH (11-97%) to assess the effects of $D_2O_{(g)}$ activity on exchange. At 11% RH, the rate and extent of deuterium incorporation were greater for all formulations than at 6% RH, though the shapes of the curves and the rank order of D_{max} values remained unchanged (Figure 2.6, Appendix A - Figure A3). At 23% RH, the rate and extent of deuterium incorporation again increased, with disproportionate increases for the sucrose formulation, so that the rank order of D_{max} values differed at 6% and 11% RH (Figure 2.6, Appendix A - Figure A4). At 43% RH, the sucrose, trehalose and guanidine HCl formulations showed D_{max} values of $\sim 80\%$, approaching the solution state HDX value of $\sim 85\%$ (Figure 2.6, Appendix A - Figure A5), and were greater than D_{max} values of the sodium chloride, mannitol and excipient-free formulations. This suggests that the sucrose, trehalose and guanidine HCl formulations are in a solution-like environment at 43% RH, though deliquescence was not observed visually. At the highest RH conditions ($\geq 57\%$ RH), deuterium incorporation was variable and the rank order was often inconsistent from one time point to another (Appendix A - Figure A6). Because formulations stored at $\geq 57\%$ RH exist in a highly concentrated viscous phase and were not solid-like, they have been excluded from analysis of ssHDX-MS kinetics.

2.5 Discussion

In the studies presented here, unstructured PDLA peptides were co-lyophilized with various excipients and subjected to ssHDX-MS by exposing the solids to D_2O vapor at different RH conditions (i.e., different activity of $D_2O_{(g)}$). Lyophilized PDLA samples showed protection from exchange in ssHDX-MS that depended on excipient type (Appendix A - Figure A1), an effect that was not observed in solution controls (Figure 2.5). ssHDX in lyophilized PDLA samples also depended on RH (Figure 2.6), a parameter that is not relevant in solution. Since PDLA is unstructured (Figure 2.3), protection in ssHDX-MS cannot be attributed to protein structure or to dynamic opening and closing events, as asserted by the Linderstrom-Lang model routinely used to interpret solution HDX.¹⁴⁻¹⁸ Instead, the results indicate that the solid matrix protects the peptide from deuterium exchange, to different degrees under different conditions.

We propose that, at $\text{RH} \leq 43\%$, ssHDX-MS kinetics in the PDLA solids can be described by a reversible pseudo first-order model:



where A is the number (or percentage) of exchangeable amide groups (i.e., still in protonated form), B is the number (or percentage) of deuterated amide groups, and k_f and k_b are the forward and reverse rate constants for deuterium incorporation, respectively. We describe the reaction as “pseudo first-order” to indicate that, at a fixed $\text{D}_2\text{O}_{(\text{g})}$ activity (a_D), the forward rate is proportional to A and the reverse rate is proportional to B. We further assume that the forward reaction is first-order in $\text{D}_2\text{O}_{(\text{g})}$ activity (a_D), measured experimentally as the relative humidity in D_2O (RH), so that:

$$k_f = k_f^* \times (a_D) \quad (2.6)$$

where k_f^* is the forward rate constant in the absence of RH effects. We assume that a_D in D_2O solution is unaffected by solutes and is equal to 1, and that a_D in solid samples is given by $\% \text{RH}/100$. In an ssHDX-MS experiment at fixed RH, a_D , k_f and k_f^* are constant; the dependence of k_f on a_D only becomes important when comparing results at different RH. We further assume that the rate constant for loss of deuterium label, k_b , is independent of RH. We define A_0 as the total number (or percentage) of exchangeable amide groups in the PDLA peptide, a value equal to the number (or percentage) still in protonated form at $t = 0$. With this model, and subject to the initial conditions that $A = A_0$ and $B = 0$ at $t = 0$, the extent of deuteration as a function of time is given by:³⁹⁻⁴¹

$$B = \frac{k_f^*(a_D) A_0}{k_f^*(a_D) + k_b} \left\{ 1 - e^{-(k_f^*(a_D) + k_b)t} \right\} = D_{max} \left\{ 1 - e^{-(k_f^*(a_D) + k_b)t} \right\} \quad (2.7)$$

where (D_{max}) is the maximum deuterium incorporation at large t . In the limit $k_f^* \times (a_D) \gg k_b$, $D_{max} = A_0$ and the observed rate of deuteration is governed by the forward rate. This corresponds to the Linderstrom-Lang model and describes the solution HDX results (Figure 2.5). Conversely,

in the limit $k_f^* \times (a_D) \ll k_b$, $D_{max} = K (a_D) A_0$, where K is a pseudo-equilibrium constant equal to the ratio of the forward and reverse rate constants (i.e., $K = k_f^* / k_b$). In this limit, D_{max} is linearly related to a_D . In the more general case, when neither the forward nor reverse rate dominates, D_{max} is related to a_D by:

$$\frac{A_0}{D_{max}} = 1 + \frac{1}{K} \left(\frac{1}{a_D} \right) \quad (2.8)$$

where (D_{max} / A_0) is the fraction of the total number of exchangeable amide groups deuterated at large t . The reversible pseudo first-order kinetic model predicts that plots of (A_0 / D_{max}) vs. $(1/a_D)$ will be linear and provide the value of K as the inverse of the slope. Similarly, the apparent rate constant for deuterium incorporation measured in an ssHDX-MS experiment (k_{ap}) is related to the forward and reverse rate constants by:

$$k_{ap} = (k_f^* \times (a_D)) + k_b \quad (2.9)$$

A linear relationship between k_{ap} and a_D is predicted by the reversible first-order kinetic model, and serves as a second test for the consistency of the model with experimental data.

Figure 2.7 shows linear regression of (A_0 / D_{max}) as a function of $(1/a_D)$ for ssHDX-MS data at RH $\leq 43\%$ for the 22 amino acid PDLA peptide. Here, a_D is taken as equal to the %RH in D_2O . Deuterium incorporation values were treated as percentages. The solution HDX data (Figure 2.5) were used as fully deuterated controls in the HDExaminer software to apply a back exchange correction to each deuterium uptake value of a particular formulation. A_0 is taken as 100%. Linearity is confirmed for all formulations tested, with R^2 values greater than 0.85, in agreement with Equation 2.8 and the reversible pseudo first-order kinetic model. Linear regression of D_{max} vs. a_D was also evaluated, as suggested by the $k_f^* \times (a_D) \ll k_b$ limit of the reversible pseudo first-order model (Appendix A - Figure A7). The resulting R^2 values are less than those in Figure 2.7, suggesting that the $k_f^* \times (a_D) \ll k_b$ limit is not valid here. Slopes of the lines range from 0.04 for the guanidine HCl formulation to 0.33 for the sucrose formulation (Figure 2.7), indicating that inverse of the equilibrium constant (i.e., $1/K$) is less than one and the forward rate constant (k_f^*) is somewhat greater than the reverse rate constant (k_b) in all formulations studied. Slopes are greater

for the sucrose and trehalose formulations than for the other four formulations; the sucrose and trehalose formulations are also amorphous (Figure 2.1) and generally thought to provide good stabilization for lyophilized proteins. With the exception of the sucrose formulation, intercepts of the regression lines are nearly equal to one, as predicted by the reversible first-order kinetic model (Eqn. 2.8).

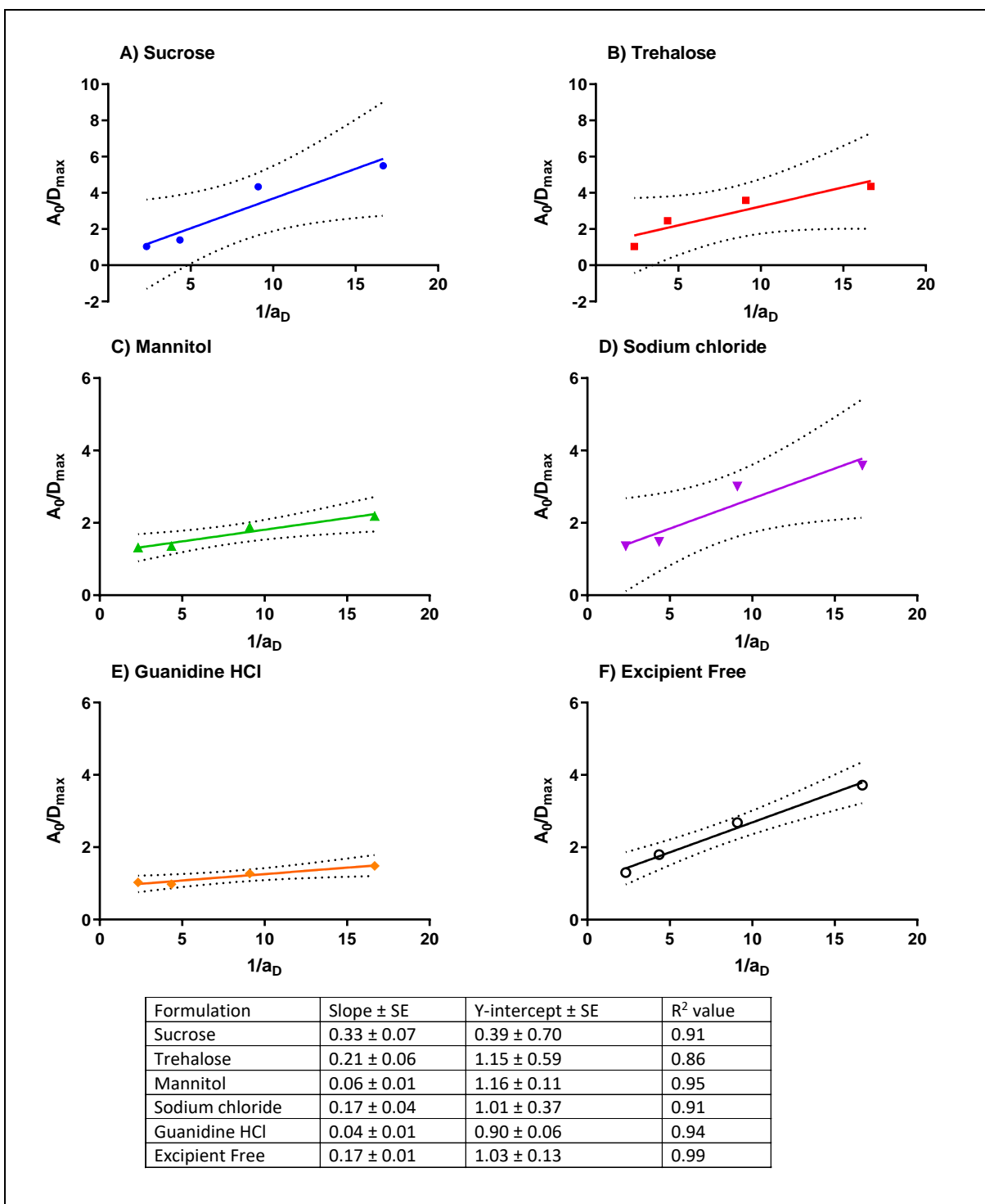


Figure 2.7. A_0/D_{\max} as a function of $1/a_D$ for lyophilized PDLA peptides at RH < 50% in formulations containing: A) sucrose, B) trehalose, C) mannitol, D) sodium chloride, E) guanidine HCl or F) no excipient (excipient-free), where $a_D = (\%RH/100)$ at equilibrium. D_{\max} was calculated from the back exchange corrected percentage deuterium uptake mono-exponential fits and A_0 is theoretical percentage of exchangeable amide groups (=100). Data shown for a 22 amino acid peptide, $n=3$; dotted lines represent 95% CI of the best fit line.

Figure 2.8 shows linear regression of k_{ap} as a function of a_D for ssHDX-MS data at $RH \leq 43\%$. Again, linearity is confirmed for most formulations, in agreement with Equation 2.9 and the reversible pseudo first-order kinetic model. Slopes of the lines are equal to k_f^* and range from 0.33 to 2.4 h^{-1} (Eqn. 2.9, Figure 2.8). Samples with greater values of k_f^* show stronger dependence of the apparent forward exchange rate constant (i.e., $k_f^* \times (a_D)$) on a_D than those with smaller values; here, the guanidine hydrochloride sample has the largest k_f^* value while the sodium chloride sample has the smallest k_f^* value. In principle, the y-intercepts of the regressions in Figure 2.8 are equal to the reverse rate constants, k_b , but the intercepts are not significantly different from zero for any of the samples studied here (Figure 2.8). k_b values can also be estimated as the product of the slopes of the lines in Figures 2.7 and 2.8 (i.e., $k_b = (1/K) k_f^*$), giving values in the range 0.03 to 0.23 h^{-1} (sucrose: $k_b = 0.23 h^{-1}$; trehalose: $k_b = 0.10 h^{-1}$; mannitol: $k_b = 0.03 h^{-1}$; sodium chloride: $k_b = 0.06 h^{-1}$; guanidine HCl: $k_b = 0.09 h^{-1}$; excipient-free: $k_b = 0.08 h^{-1}$) corresponding to half-lives for the reverse reaction between 3 and 23 hours. Since deuterium incorporation takes more than 100 hours to plateau for some formulations and RH values (Figure 2.6), the estimated half-lives for the reverse reaction suggest that it usually cannot be ignored on the typical ssHDX-MS time scale.

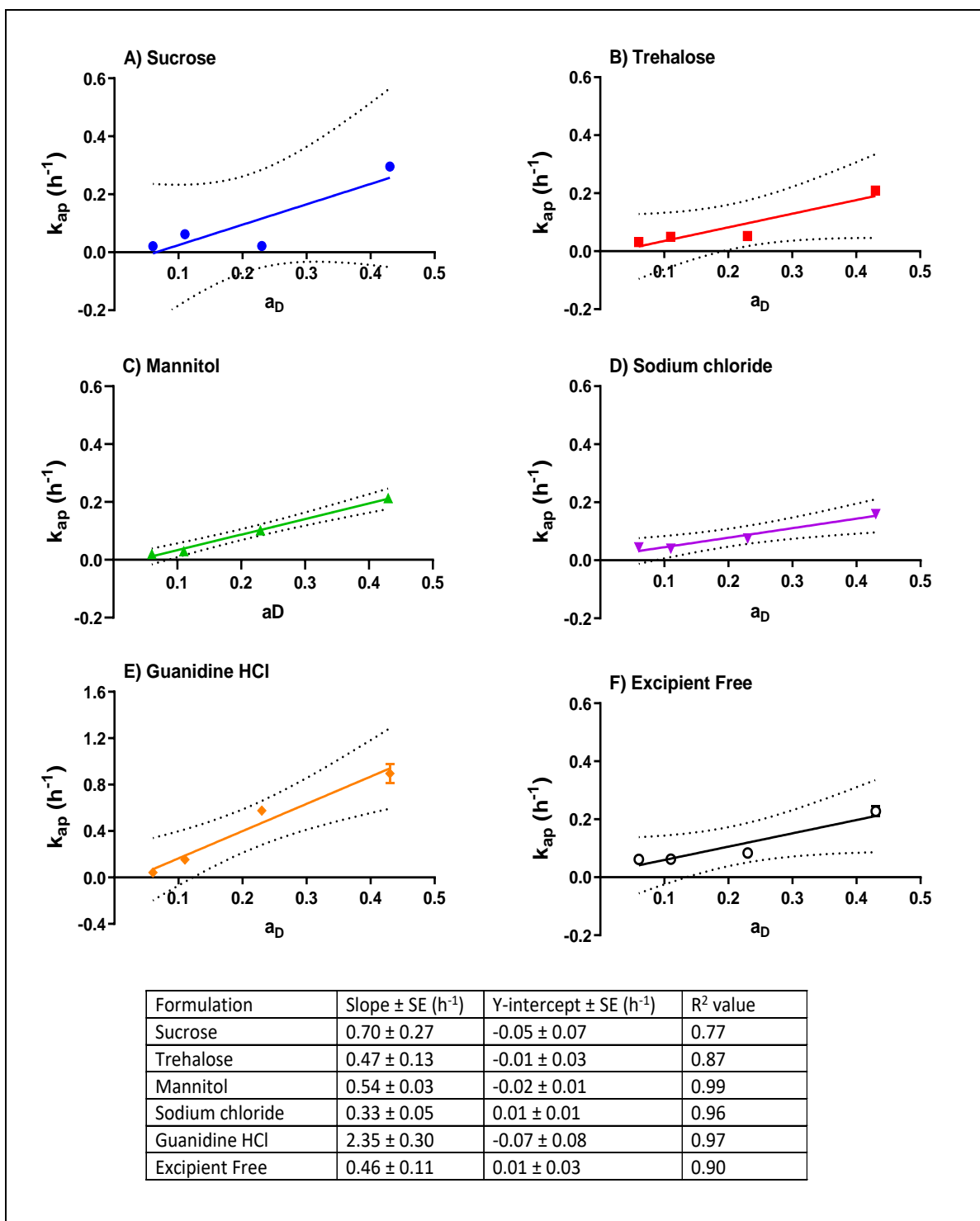


Figure 2.8. Apparent exchange rate constant (k_{ap}) as a function of a_D for lyophilized PDLA peptides at RH < 50% in formulations containing: A) sucrose, B) trehalose, C) mannitol, D) sodium chloride, E) guanidine HCl or F) no excipient (“excipient-free”), where $a_D = (\%RH/100)$ at equilibrium. Data shown for a back exchange corrected 22 amino acid peptide, $n=3$, dotted lines represent 95% CI of the best fit line.

Figures 2.7 and 2.8 demonstrate that, for unstructured PDLA peptides in various formulations and exposed to different a_D environments, ssHDX-MS kinetics is consistent with a reversible first-order model. While agreement with the model does not “prove” a mechanism for ssHDX-MS, it does suggest possible physicochemical interpretations. We envision that D_2O is first sorbed from the vapor phase into the solid, rapidly (i.e., in 1-2 h) reaching an equilibrium in which the activity of sorbed D_2O is equal to that in the vapor phase. Because amorphous solids are spatially heterogeneous²⁹⁻³¹ and proteins in the amorphous state undergo hydration non-uniformly at the molecular scale,⁴²⁻⁴⁴ we anticipate that sorbed D_2O is preferentially distributed to more hydrophilic regions of the solid, including more hydrophilic domains of the protein. We expect that unprotected peptide bonds and other exchangeable functional groups in these hydrated regions (i.e., those not involved in intra- or intermolecular hydrogen bonds) undergo exchange first, and then can serve as deuterium donors to nearby undeuterated groups that might be more protected. In serving as deuterium donors, they undergo the reverse exchange reaction described by the rate constant k_b . Excipients, buffer species and residual water in the matrix can also become deuterated and serve as deuterium donors. In this way, deuterons penetrate the H-bond network in the solid state, moving from unprotected functional groups to weakly protected groups, and finally (if ever) to those involved in the strongest hydrogen bonds. Note that the structural “opening” and “closing” events of the Linderstrom-Lang model need not be invoked to describe ssHDX-MS for unstructured PDLA peptides, though neither are they precluded for structured peptides and proteins by the PDLA results.

In the Linderstrom-Lang model of solution HDX, exchange is assumed to be irreversible, which is reasonable given the high D_2O activity in most solution HDX experiments ($a_D \approx 1$), the short duration of the experiments and the relatively dilute sources of proton for the reverse reaction (e.g., protein, excipients). In contrast, in ssHDX-MS, D_2O activity is lower, the experiment is longer and there are abundant sources of proton for the reverse reaction. These include not only HOD generated by the forward reaction, but also exchangeable hydrogen atoms on excipients (e.g., sucrose, trehalose, mannitol), on components of the buffer, in residual water remaining in the matrix, and on the peptide or protein itself. These species contribute to a pool of hydrogen atoms that can be shuttled through the solid matrix as the forward and reverse exchange reactions occur. The maximum deuterium incorporation in ssHDX-MS is usually much less than that achieved in

solution HDX (see Figure 2.4 vs. Figure 2.5), which indicates that, even at the end of an ssHDX-MS experiment, exchangeable hydrogen atoms are still present on the protein itself.

At the phenomenological level, ssHDX-MS kinetic data can be fitted to the exponential models used for solution HDX (Figure 2.6). At the mechanistic level, however, the results presented here demonstrate that the Linderstrom-Lang model for solution HDX does not adequately describe ssHDX-MS and a different interpretation is required. Ongoing studies in our laboratories are continuing to develop a mechanistic model for ssHDX-MS by examining the reverse exchange reaction directly, by exploring the effects of pre-hydration of the solid prior to ssHDX-MS, and by studying structured analogs of PDLA.

2.6 Conclusions

In ssHDX-MS of lyophilized unstructured PDLA peptides, solid samples showed protection from exchange that depended on both RH and excipient type, effects that were not observed in solution controls and cannot be described by the Linderstrom-Lang model. A reversible pseudo first-order kinetic model for deuterium uptake ssHDX-MS is proposed, in which the apparent forward rate constant (k_f) depends linearly on the relative humidity (RH) in $D_2O_{(g)}$ (i.e., $k_f = k_f^* \times (a_D)$). The model is in agreement with the experimentally observed dependences of apparent deuteration rate and plateau value on RH in ssHDX-MS studies of PDLA peptides and reduces to the Linderstrom-Lang limit when the forward rate of exchange is much greater than the reverse rate (i.e., $k_f^* \times (a_D) \gg k_b$).

2.7 Supporting information

Additional supporting information for this chapter is available in Appendix A: (i) ssHDX-MS kinetics of different formulations of a 22 amino-acid PDLA peptide, grouped by RH (Figure A1), (ii) ssHDX-MS of different formulations of PDLA peptides of different chain length at RH values from 6% to 43% (Figures A2-A5), (iii) ssHDX-MS of different formulations of PDLA peptides of 22 amino acid chain length at RH values from 57% to 97% (Figure A6), (iv) linear regression of D_{\max} vs. a_D for PDLA peptides at RH < 50%, with each formulation plotted individually (Figure A7), (v) linear regression of D_{\max} vs. a_D for PDLA peptides at RH < 50%, with all formulations plotted together (Figure A8), (vi) linear regression of A_0/D_{\max} vs. $1/a_D$, with all formulations

plotted together (Figure A9), (vii) apparent ssHDX-MS rate constants (k_{ap}) for various formulations, RH values and PDLA chain lengths (Figure A10), (viii) a list of PDLA peptides detected on MS analysis (Table A1), and (ix) tables of statistical analysis (Tables A2-A3).

2.8 References

1. Allison, S.D.; Chang, B.; Randolph T.W.; Carpenter J.F. Hydrogen bonding between sugar and protein is responsible for inhibition of dehydration-induced protein unfolding. *Arch. Biochem. Biophys.* **1999**, 365(2), 289–298.
2. Duddu, S.P.; Zhang, G.; Dal Monte, P.R. The relationship between protein aggregation and molecular mobility below the glass transition temperature of lyophilized formulations containing a monoclonal antibody. *Pharm. Res.* **1997**, 14(5), 596–600.
3. Moussa, E.M.; Singh, S.K.; Kimmel, M.; Nema, S.; Topp, E.M. Probing the conformation of an IgG1 monoclonal antibody in lyophilized solids using solid-state hydrogen–deuterium exchange with mass spectrometric analysis (ssHDX-MS). *Mol. Pharmaceutics.* **2018**, 15(2), 356-368.
4. Moussa, E.M.; Wilson, N.E.; Zhou, Q.T.; Singh, S.K.; Nema, S; Topp, E.M. Effects of drying process on an IgG1 monoclonal antibody using solid-state hydrogen deuterium exchange with mass spectrometric analysis (ssHDX-MS). *Pharm. Res.* **2018**, 35(1), 12.
5. Li, Y.; Williams, T.D.; Topp, E.M. Effects of excipients on protein conformation in lyophilized solids by hydrogen/deuterium exchange mass spectrometry. *Pharm. Res.* **2008**, 25(2), 259–267.
6. Moorthy, B.S.; Zarraga, I.E.; Kumar, L.; Walters, B.T.; Goldbach, P.; Topp, E.M. Solid-state hydrogen–deuterium exchange mass spectrometry: correlation of deuterium uptake and long-term stability of lyophilized monoclonal antibody formulations. *Mol. Pharmaceutics.* **2018**, 15(1), 1–11.
7. Moorthy, B.S.; Iyer, L.K.; Topp, E.M. Mass spectrometric approaches to study protein structure and interactions in lyophilized powders. *J. Visualized Exp.* **2015**, (98), 52503.
8. Sophocleous, A.M.; Zhang, J.; Topp, E.M. Localized hydration in lyophilized myoglobin by hydrogen–deuterium exchange mass spectrometry. 1. Exchange mapping. *Mol. Pharmaceutics.* **2012**, 9(4), 718–726.
9. Sophocleous, A.M.; Topp, E.M. Localized hydration in lyophilized myoglobin by

- hydrogen-deuterium exchange mass spectrometry. 2. Exchange kinetics. *Mol. Pharmaceutics*. **2012**, 9(4), 727–733.
10. Moorthy, B.S.; Schultz, S.G.; Kim, S.G.; Topp, E.M. Predicting protein aggregation during storage in lyophilized solids using solid state amide hydrogen/deuterium exchange with mass spectrometric analysis (ssHDX-MS). *Mol. Pharmaceutics*. **2014**, 11(6), 1869–1879.
 11. Iyer, L.K.; Sacha, G.A.; Moorthy, B.S.; Nail, S.L.; Topp, E.M. Process and formulation effects on protein structure in lyophilized solids using mass spectrometric methods. *J. Pharm. Sci.* **2016**, 105(5), 1684–1692.
 12. Sinha, S.; Li, Y.; Williams, T.D.; Topp, E.M. Protein conformation in amorphous solids by FTIR and by hydrogen/deuterium exchange with mass spectrometry. *Biophys. J.* **2008**, 95(12), 5951–5961.
 13. Li, Y.; Williams, T.D.; Schowen, R.L.; Topp, E.M.; Characterizing protein structure in amorphous solids using hydrogen/deuterium exchange with mass spectrometry. *Anal. Biochem.* **2007**, 366(1), 18–28.
 14. Hvidt, A.; Nielsen, S.O. Hydrogen exchange in proteins. *Adv. Protein Chem.* **1966**, 21, 287–386.
 15. Englander, S.W.; Downer, N.W.; Teitelbaum, H. Hydrogen exchange. *Annu. Rev. Biochem.* **1972**, 41(1), 903–924.
 16. Englander, S.W.; Kallenbach, N.R. Hydrogen exchange and structural dynamics of proteins and nucleic acids. *Q. Rev. Biophys.* **1983**, 16(4), 521–655.
 17. Wales, T.E.; Engen, J.R. Hydrogen exchange mass spectrometry for the analysis of protein dynamics. *Mass Spectrom. Rev.* **2006**, 25(1), 158–170.
 18. Majumdar, R.; Middaugh, C.R.; Weis, D.D.; Volkin, D.B. Hydrogen-deuterium exchange mass spectrometry as an emerging analytical tool for stabilization and formulation development of therapeutic monoclonal antibodies. *J. Pharm. Sci.* **2015**, 104(2), 327–345.
 19. Weis, D.D. Analysis of disordered proteins by hydrogen exchange mass spectrometry. In *Hydrogen Exchange Mass Spectrometry of Proteins: Fundamentals, Methods, and Applications*. Weis D.D., Eds; John Wiley & Sons, **2015**; pp 295–321.
 20. Smith, D.L.; Deng, Y.; Zhang, Z. Probing the non-covalent structure of proteins by amide hydrogen exchange and mass spectrometry. *J. Mass Spectrom.* **1997**, 32(2), 135–146.

21. Jensen, P. F.; Rand, K.D. Hydrogen exchange: A sensitive analytical window into protein conformation and dynamics. In *Hydrogen Exchange Mass Spectrometry of Proteins: Fundamentals, Methods, and Applications*. Weis D.D., Eds; John Wiley & Sons, **2015**; pp 1–17.
22. Bai, Y.; Milne, J.S.; Mayne, L.; Englander, S.W. Primary structure effects on peptide group hydrogen exchange. *Proteins: Struct., Funct., Bioinf.* **1993**, 17(1), 75–86.
23. Zhang, Z.; Smith, D.L. Determination of amide hydrogen exchange by mass spectrometry: A new tool for protein structure elucidation. *Protein Sci.* **1993**, 2(4), 522–531.
24. Nguyen, D.; Mayne, L.; Phillips, M.C.; Englander, S.W. Reference parameters for protein hydrogen exchange rates. *J. Am. Soc. Mass Spectrom.* **2018**, 29(9), 1936–1939.
25. Zhang, Z.; Zhang, A.; Xiao, G. Improved protein hydrogen/deuterium exchange mass spectrometry platform with fully automated data processing. *Anal. Chem.* **2012**, 84(11), 4942–4949.
26. Katta, V.; Chait, B.T. Hydrogen / deuterium exchange electrospray ionization mass spectrometry: A method for probing protein conformational changes in solution. *J. Am. Chem. Soc.* **1993**, 115(14), 6317–6321.
27. Truhlar, S.M.E.; Croy, C.H.; Torpey, J.W.; Koeppe, J.R.; Komives, E.A. Solvent accessibility of protein surfaces by amide H²H exchange MALDI-TOF mass spectrometry. *J. Am. Soc. Mass Spectrom.* **2006**, 17(11), 1490–1497.
28. Skinner, J.J.; Lim, W.K.; Bédard, S.; Black, B.E.; Englander, S.W. Protein hydrogen exchange: Testing current models. *Protein Sci.* **2012**, 21(7), 987–995.
29. Berthier, L. Dynamic heterogeneity in amorphous materials. *Physics*. **2011**, 4 (42).
30. Zografu, G.; Newman, A. Interrelationships between structure and the properties of amorphous solids of pharmaceutical interest. *J. Pharm. Sci.* **2017**, 106 (1), 5–27.
31. Ediger, M. D. Spatially heterogeneous dynamics in supercooled liquids. *Annu. Rev. Phys. Chem.* **2000**, 51 (1), 99–128.
32. Greenspan, L. Humidity fixed points of binary saturated aqueous solutions. *J. Res. NBS A Phys. Ch.* **1977**, 81(1), 89–96.
33. Bakshi, K.; Liyanage, M.R.; Volkin, D.B.; Middaugh, C.R. Fourier transform infrared spectroscopy of peptides. In *Therapeutic Peptides. Methods in Molecular Biology (Methods and Protocols)*, Nixon A., Eds.; vol. 1088. Humana Press, **2014**; pp 255–269.

34. Breen, E.D.; Curley, J.G.; Overcashier, D.E.; Hsu, C.C.; Shire, S.J. Effect of moisture on the stability of a lyophilized humanized monoclonal antibody formulation. *Pharm. Res.* **2001**, 18(9), 1345–1353.
35. Mensink, M.A.; Frijlink, H.W.; van der Voort Maarschalk, K.; Hinrichs, W.L.J. How sugars protect proteins in the solid state and during drying (review): Mechanisms of stabilization in relation to stress conditions. *Eur. J. Pharm. Biopharm.* **2017**, 114, 288–295.
36. Hancock, B.C.; Zografi, G. Characteristics and significance of the amorphous state in pharmaceutical systems. *J. Pharm. Sci.* **1997**, 86(1), 1–12.
37. Hancock, B.C.; Dalton, C.R. The effect of temperature on water vapor sorption by some amorphous pharmaceutical sugars. *Pharm. Dev. Technol.* **1999**, 4(1), 125–131.
38. Shamblin, S.L.; Hancock, B.C.; Zografi, G. Water vapor sorption by peptides, proteins and their formulations. *Eur. J. Pharm. Biopharm.* **1998**, 45(3), 239-247.
39. Atkins, P.; De Paula, J. The rates of chemical reactions. In *Atkins' Physical Chemistry*, 8th ed.; Oxford University Press, **2006**; pp 791-829.
40. Espenson, J.H. Reversible and concurrent reactions. In *Chemical Kinetics and Reaction Mechanisms*, 2nd ed.; McGraw-Hill, **2002**; pp 46-69.
41. Laidler, K.J. Analysis of kinetic results. In *Chemical Kinetics*. 3rd ed.; Harper & Row, **1987**; pp 18-53.
42. Rupley, J. A.; Careri, G. Protein hydration and function. In *Advances in Protein Chemistry*, Anfinsen, C.B.; Richards, F.M.; Edsall, J.T.; Eisenberg, D.S., Eds.; vol. 41. Academic Press, **1991**; pp 37–172.
43. Careri, G. Cooperative charge fluctuations by migrating protons in globular proteins. *Prog. Biophys. Mol. Biol.* **1998**, 70 (3), 223–249.
44. Köhler, M. H.; Barbosa, R. C.; Da Silva, L. B.; Barbosa, M. C. Role of the hydrophobic and hydrophilic sites in the dynamic crossover of the protein-hydration water. *Physica A.* **2017**, 468, 733–739.

CHAPTER 3. PRE-HYDRATION AND THE REVERSIBILITY OF SOLID-STATE HYDROGEN-DEUTERIUM EXCHANGE

This chapter was published as a research article in *Molecular Pharmaceutics* (2020, 17 (9), 3541–3552) and reproduced with permission. Copyright (2020) American Chemical Society.

DOI: 10.1021/acs.molpharmaceut.0c00571

3.1 Abstract

The reversibility of solid-state hydrogen-deuterium exchange (ssHDX) and the effects of pre-hydration on the rate and extent of deuterium incorporation were evaluated using poly-D, L-alanine (PDLA) peptides co-lyophilized with various excipients. In pre-hydration studies, samples were equilibrated at controlled relative humidity (6% or 11% RH) for 12 h and then transferred to corresponding D₂O humidity conditions (6% or 11% RD) for deuterium labeling. In amorphous samples, the rate and extent of deuterium incorporation were similar in pre-hydrated samples and controls not subjected to pre-hydration. In reversibility studies, PDLA samples were maximally deuterated in controlled D₂O humidity conditions (6% or 11% RD) and then transferred to corresponding H₂O relative humidity (0%, 6%, 11% or 43% RH). A hysteresis in deuterium removal was observed when compared with the deuterium incorporation kinetics for all formulations and conditions, confirming that the reaction is reversible in the solid state and that the forward and reverse processes differ. The extent of deuterium loss reached a plateau that depended on the de-labeling relative humidity. Reverse reaction rate constants were quantified using a first-order kinetic model, a limiting case of the reversible first-order model applicable under sink conditions. For other conditions, plateau (steady-state) deuteration levels were related to forward and reverse rate constants in a reversible first-order kinetic model. The results support a mechanistic interpretation of ssHDX kinetics as a reversible first-order process, in which the forward (deuteration) rate depends on the activity of the deuterium donor.

3.2 Introduction

Protein biologics are known to degrade physically (e.g., aggregation) and chemically (e.g., hydrolysis) in solution, which may lead to the loss of biological activity and increase the potential for immunogenic responses in patients.^{1,2} Maintaining the chemical and physical integrity of the drug throughout its shelf-life is essential, and an ideal formulation should protect the protein drug from the stresses related to processing, shipping and storage.² This can be challenging for solution formulations since water is an active participant in many degradation processes. Moreover, solution formulations may lack sufficient robustness to withstand temperature variations and vibrational stresses associated with shipping. As a result, protein therapeutics are often marketed in lyophilized (freeze-dried) forms to preserve their native conformation, to minimize exposure to water, and to produce a robust formulation that can withstand various stresses the product may experience before it is administered to the patient.³

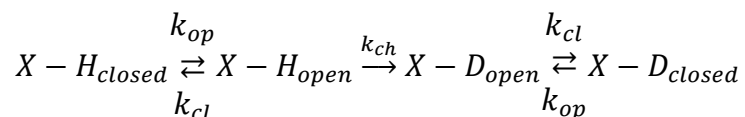
While lyophilization is often an effective formulation strategy, the lyophilization process itself imposes stresses on the protein, and proteins are susceptible to degradation in the solid-state as well. Maintaining the protein's native structure in the lyophilized powder has long been considered critical to ensuring stability.⁴ Thus, characterizing protein structure in solid samples is essential in developing a stable lyophilized protein drug formulation. Analytical methods to detect and quantify protein structure in the solid state are limited, however.⁵ For example, Fourier Transform Infrared Spectroscopy (FTIR) is routinely used to characterize proteins in amorphous solids, but the method can only provide global information about protein secondary structure. FTIR is semi-quantitative at best, and FTIR metrics are often poorly predictive of protein stability on storage.⁶ Thermal analysis techniques such as differential scanning calorimetry (DSC) are often used to characterize the physical and mechanical properties of the solid, and are valuable in developing lyophilization cycles. However, like FTIR metrics, the glass transition temperatures (T_g) measured by DSC are often poorly predictive of storage stability.⁶

Solid-state hydrogen-deuterium exchange mass spectrometry (ssHDX-MS) is a novel analytical method for proteins in the solid state that provides high-resolution information about the protein structure and matrix interactions. The method has been used to study local hydration,^{7,8} to probe protein conformation,⁹ to predict aggregation during storage,¹⁰ and to optimize formulations and processes for antibody-based modalities.¹¹ The lack of a mechanistic model for ssHDX-MS has

hindered data analysis and interpretation, however, and has limited insights into the properties of the solid that determine stability.

In solution, hydrogen-deuterium exchange refers to the process by which labile hydrogen atoms in a protein exchange with deuterium. On exposure to a deuterium donor, typically D₂O, hydrogen atoms in primary amine and side chain groups exchange rapidly. In contrast, backbone amide hydrogen atoms exchange more slowly, and at rates which depend on protein conformation and dynamics.¹² In pharmaceutical development, the conformational differences of a protein in different solution formulations can be monitored by studying backbone amide hydrogen-deuterium exchange, since exchange kinetics are affected by the structural changes associated with degradation in solution.¹³ Deuterium incorporation at side chain groups usually is rapidly reversible, and generally is not monitored.

Proteins in solution are structurally dynamic and undergo reversible “opening” and “closing” events. Labile amide hydrogen atoms, initially protected from the solvent by the protein structure, are exposed to the solution when the intra-chain hydrogen bonds are transiently disrupted due to the “opening events”. Such opening events are induced by local fluctuations or global unfolding. Exposed amide hydrogens in the “open” form of a protein spontaneously exchange with deuterium, as described by the Linderstrom-Lang model:¹⁴⁻¹⁶



where k_{op} , k_{cl} and k_{ch} are the rate constants for “opening” events, “closing” events and chemical hydrogen exchange, respectively. When the open form ($X-H_{open}$) can be assumed to be in steady-state and the rate of closing is much greater than the rate of opening (i.e., $k_{cl} \gg k_{op}$), the observed hydrogen exchange rate constant (k_{HDX}) is related to the individual rate constants by:¹⁷

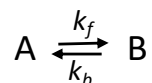
$$k_{HDX} = \frac{k_{op} \times k_{ch}}{k_{cl} + k_{ch}}$$

The observed rate of exchange can thus be related to protein folding if the intrinsic chemical rate of exchange (k_{ch}) is known.

The Linderstrom-Lang model assumes that the chemical hydrogen exchange reaction is irreversible, an assumption that is justified due to the high activity of D_2O in solution ($a_D \approx 1$) and the abundance of deuterium sources from the labeling solution. Hydrogen atoms exchanged for deuterium during the labeling process are diluted in the bulk solution, minimizing the activity of proton for the reverse HDX reaction, particularly in the short duration of solution exchange experiments (typically milliseconds to minutes).

The assumption that the chemical exchange reaction is irreversible may be violated in ssHDX-MS. In ssHDX-MS, dried protein samples are exposed to D_2O vapor in a controlled relative humidity and temperature environment. The solid samples are hydrated by D_2O and the amide groups then undergo exchange. The excipients, buffer species and residual water in the matrix can also become deuterated and can serve as deuterium donors. At equilibrium, the activity of sorbed D_2O in the solid is equal to that in the vapor phase. Because a typical ssHDX-MS experiment is conducted at less than 50% RH in $D_2O_{(g)}$, the D_2O activity in the solid is less than 1. Due to relatively low D_2O activity and the lower molecular mobility of the solid state, the local activity of hydrogen atoms near a protein amide group that has undergone exchange is likely to be greater than in solution. Additional sources of hydrogen atoms for back exchange include exchangeable hydrogen atoms on the buffer components, on excipient molecules (e.g., sugars), in residual water remaining in the solid matrix, and on the protein itself. In addition, an ssHDX-MS experiment is typically conducted on a longer time scale than solution HDX, typically lasting days to weeks, which enhances the likelihood of the reverse reaction.

To provide a description of ssHDX-MS that incorporates these factors and other experimental observations, a pseudo first order reversible model for ssHDX-MS has been proposed:¹⁸



Here A is the number or percentage of exchangeable amide groups, B is the number or percentage of deuterated amide groups, and k_f and k_b are the forward and reverse reaction rate constants, respectively. The forward and reverse reaction rates are assumed to be proportional to the reactant

concentrations, i.e., to be first-order in A and B, respectively. The forward reaction rate is also assumed to be linearly related to the $D_2O_{(g)}$ activity (a_D), which can be held constant in a given experiment, so that:

$$k_f = k_f^* \times (a_D)$$

With this model, for studies at constant a_D , the apparent deuterium incorporation rate constant (k_{ap}) depends on a_D and on the forward and reverse reaction rate constants:

$$k_{ap} = k_f^* (a_D) + k_b \quad (3.1)$$

where the k_f^* is the forward reaction rate in the absence of RH effects.

The model was tested using ssHDX-MS kinetic data for unstructured poly-D, L-alanine peptides (PDLA) in lyophilized formulations containing various excipients. The model showed good agreement with the data and estimates of k_f^* were obtained from the relationship of apparent deuterium incorporation rate constants to a_D . However, while the model predicted that k_b could also be determined from this relationship, the k_b values were not significantly different from zero for any of the formulations studied, and k_b values had to be estimated indirectly. This indirect estimate of k_b provided only weak support for the model assertion that the exchange reaction is reversible in ssHDX.

The reverse reaction in ssHDX-MS has been studied in greater detail in the studies reported here. In the reversibility experiments, lyophilized samples containing the PDLA peptides were first maximally deuterated (i.e., by exposure to D_2O vapor for up to 15 days). The samples were then removed from the D_2O vapor environment and transferred to a comparable H_2O vapor environment, and the loss of deuterium label monitored over time. ssHDX-MS experiments typically are conducted on samples with low residual moisture. While previous studies have shown that ssHDX-MS kinetics are much slower than the rate of water vapor sorption^{8, 10, 19}, the concurrence of water vapor sorption and exchange may complicate data interpretation and analysis, especially at early time points. Accordingly, the effects of pre-hydration (i.e., equilibration of samples in a controlled RH environment in H_2O) prior to initiation of an ssHDX-MS experiment were also investigated. Because solid samples were exposed to both D_2O vapor and H_2O vapor environments, for clarity we use the abbreviation “RH” to refer to the relative humidity of water vapor (i.e., its activity, a_w) and “RD” to refer to the relative humidity of D_2O vapor (i.e., its activity, a_D) hereinafter. The

results demonstrate that pre-hydration has little effect on ssHDX kinetics and confirm that the reverse reaction occurs at a rate that cannot be neglected on the time scale of an ssHDX-MS experiment.

3.3 Materials and methods

3.3.1 Materials

Poly-DL-alanine (PDLA) peptides (P9003, MW 1000-5000 Da), lyophilization excipients (sucrose, trehalose, mannitol, sodium chloride, guanidine hydrochloride), and dibasic and monobasic potassium phosphates were purchased from Sigma-Aldrich (St. Louis, MO). Lyophilization vials (Wheaton™ Type I Clear Glass 2 mL Serum Vials), stoppers (Wheaton™ Rubber Stoppers) and all liquid chromatography-mass spectrometry (LC-MS) grade solvents (water, acetonitrile, formic acid, and methanol) were purchased from Fisher Scientific (Hanover Park, IL). Deuterium oxide (D₂O, 99.9%) was purchased from Cambridge Isotope Laboratories (Andover, MA). Sterile membrane filters (0.22 μm, Millex-GV) were purchased from EMD Millipore (Burlington, MA). The salts used to prepare saturated solutions of D₂O to control relative humidity in sealed desiccators (LiBr, LiCl, and K₂CO₃) and Drierite (8 mesh) were purchased from Fisher Scientific (Hanover Park, IL).

3.3.2 Lyophilization

The solid peptide formulations were produced by lyophilization as described previously¹⁸. Briefly, a solution containing a 1:7 % w/w ratio of peptide and excipient was prepared by mixing equal volumes of peptide (5 mg/mL) and excipient (35 mg/mL) in 2.5 mM potassium phosphate buffer (pH 7.4). Then, 250 μL of this solution was aliquoted into 2 mL lyophilization vials and lyophilized using a pilot-scale lyophilizer (LyoStar3, SP Scientific, Warminster, PA). A conservative lyophilization cycle was used, with freezing at -40° C for 3 h followed by primary drying at -35° C for 28 h (80 mTorr) and secondary drying at 25° C for 8 h (80 mTorr). Finally, samples were backfilled with nitrogen gas under vacuum, stoppered, crimped, and stored at -80° C until further use.

3.3.3 Powder X-ray diffraction (PXRD)

PXRD studies were carried out on PDLA formulations immediately after lyophilization and after pre-hydration (12 h at 6% RH or 11% RH) to monitor the pre-hydration-induced changes in the physical nature of solid formulations. Diffractograms were collected from 5° to 40° 2 θ with a step size of 0.02° at a wavelength of 0.15405 nm using Rigaku SmartLab (XRD 600) diffractometer (The Woodlands, TX).

3.3.4 Pre-hydration and ssHDX-MS

The pre-hydration ssHDX-MS study was carried out in two steps: (i) pre-hydration of PDLA formulations in an H₂O desiccator followed by (ii) deuterium labeling of pre-hydrated samples in a D₂O desiccator. The pre-hydration of lyophilized PDLA formulations was initiated by placing open vials in sealed desiccators containing saturated salt solutions in H₂O to produce a controlled constant RH. Pre-hydration was carried out for 12 h at room temperature. The vials were transferred to a sealed desiccator containing saturated salt solutions in D₂O, equilibrated to maintain the desired RD. The study was carried out at two conditions, pre-hydration at 6% RH followed by deuterium labeling at 6% RD (Case-1) and pre-hydration at 11% RH followed by deuterium labeling at 11% RD (Case-2) (see Appendix B, Figure B1). Deuterium labeling was carried out for up to 10 days and the vials were removed at pre-determined time intervals (i.e., 3 h, 6 h, 9 h, 12 h, 1 day, 3 days, 5 days, and 10 days). The samples were quenched by flash freezing in liquid nitrogen and stored at -80° C until analyzed. To measure deuteration levels, the samples were reconstituted in ice-cold quench buffer (0.2% formic acid, 5% methanol in water, pH 2.5) and analyzed by LC-MS (Agilent 6520 TOF, Agilent Technologies, Santa Clara, CA). The system was equipped with a custom made refrigerated-box capable of maintaining low temperatures to minimize back exchange. The peptides were trapped onto a micro peptide trap (Michrom Biosources, Inc., Auburn, CA) and desalted for 1.7 min using a 0.2 mL/min isocratic flow of 0.1 % formic acid in water. The peptides were then eluted on to an LC column (Zorbax 300-SB-C18, Agilent Technologies, Santa Clara, CA) using a gradient flow of 0.1 % formic acid in acetonitrile. The mass spectra were collected over 100-1700 m/z range. An undeuterated control was analyzed in a similar manner to obtain a peptide list using the Mass Hunter workstation equipped with Bioconfirm software (B.03.01, Agilent Technologies). The peptide list was used as a reference to

calculate the percentage deuterium uptake for selected peptides using the following formula in the HDExaminer software (Version 2.0, Sierra Analytics, Modesto, CA).

$$\text{Deuterium uptake (\%)} = \frac{M_t - M_{UND}}{N} \times 100 \quad (3.2)$$

$$N = L_{peptide} - n_{Pro} - 2$$

where M_t is the mass of a deuterated peptide after a labeling time “t”, M_{UND} is the mass of the undeuterated peptide, N is the theoretical number of exchangeable amide hydrogens, $L_{peptide}$ is the length of the peptide which is equal to the number of amino acids and n_{pro} is the number of proline residues. The subtraction of 2 includes the N-terminal primary amine and the following amide hydrogen, which undergo rapid back-exchange.^{20, 21}

Deuterium uptake was recorded for five peptides selected from the polydisperse mixture of PDLA. The percentage deuterium uptake as a function of time as measured in prehydration ssHDX-MS experiments was fitted to a mono-exponential equation and the kinetic parameters calculated using GraphPad Prism software (Version 8.4.0, La Zolla, CA).

$$D = D_{max}(1 - e^{-kt}) \quad (3.3)$$

where D is the percent deuterium uptake at labeling time t , D_{max} is the percent deuterium uptake at infinite time, and k is an apparent first-order rate constant.

3.3.5 Reversibility of ssHDX-MS

The reversibility study was conducted in two steps, which essentially reverse the steps of the pre-hydration study. In the reversibility study, the two steps were: (i) labeling of lyophilized PDLA formulations with deuterium in a sealed D_2O desiccator for up to 15 days followed by (ii) deuterium removal in an H_2O desiccator containing saturated salt solutions in H_2O . Six sets of reversibility experiments were carried out using various combinations of RD values for labeling (6% or 11% RD) and de-labeling (0%, 6%, 11% or 43% RH) (see Appendix B, Figure B2). For example, Case-3a involved deuterium labeling at 6% RD followed by de-labeling at 0% RH, while

Case-4b involved deuterium labeling at 11% RD followed by de-labeling at 11 % RH. Samples were collected at pre-determined time intervals and quenched by flash freezing in liquid nitrogen, then analyzed by mass spectrometry to measure deuteration levels, as described above.

Deuterium uptake was recorded for five peptides selected from the polydisperse mixture of PDLA. The percentage deuterium uptake as a function of time in the reversibility ssHDX-MS experiments was fitted to a mono-exponential decay equation and the kinetic parameters calculated using GraphPad Prism software (Version 8.4.0, La Zolla, CA).

$$D = D_{min} + (D_{max} - D_{min})e^{-kt} \quad (3.4)$$

where D is the percent deuterium (%) remaining at time t, D_{min} is the minimum deuterium incorporation (%) at infinite time, D_{max} is the initial deuteration (t_0), and k is an apparent first-order rate constant for deuterium loss.

3.3.6 Statistical analysis

Deuteration kinetic data were analyzed using GraphPad Prism software (Version 8.4.0, La Zolla, CA). The unpaired t-test with Welch's correction was used to evaluate the statistical differences in the ssHDX-MS kinetic data of the pre-hydration study since two groups were compared independently with other groups in a data set. A two-way ANOVA followed by Tukey's multiple comparison test was used to evaluate differences in the ssHDX kinetic data of the reversibility studies by comparing the mean values (e.g., rate constant) of every peptide formulation with those of every other peptide formulation.

3.4 Results

3.4.1 Physical characterization by PXRD

PXRD diffractograms were collected for the PDLA formulations immediately after lyophilization (t_0), after 12 h of pre-hydration at 6% RH and after 12 h of pre-hydration at 11% RH. Immediately after lyophilization, the sucrose, trehalose, and excipient-free formulations showed broad, featureless spectra characteristic of amorphous material (Figure 3.1A, B, F). Similarly, the diffractograms of these formulations after pre-hydration for 12 h at 6% RH or 11% RH showed smooth spectra consistent with amorphous material and the lack of crystallinity after pre-hydration

(Figure 3.1A, B, F). The diffractograms of mannitol, sodium chloride and guanidine HCl formulations showed sharp peaks characteristic of crystalline material after lyophilization (t_0) and the intensity and/or area of the peaks increased upon pre-hydration, suggesting an increase in crystallinity (Figure 3.1C, D, E).

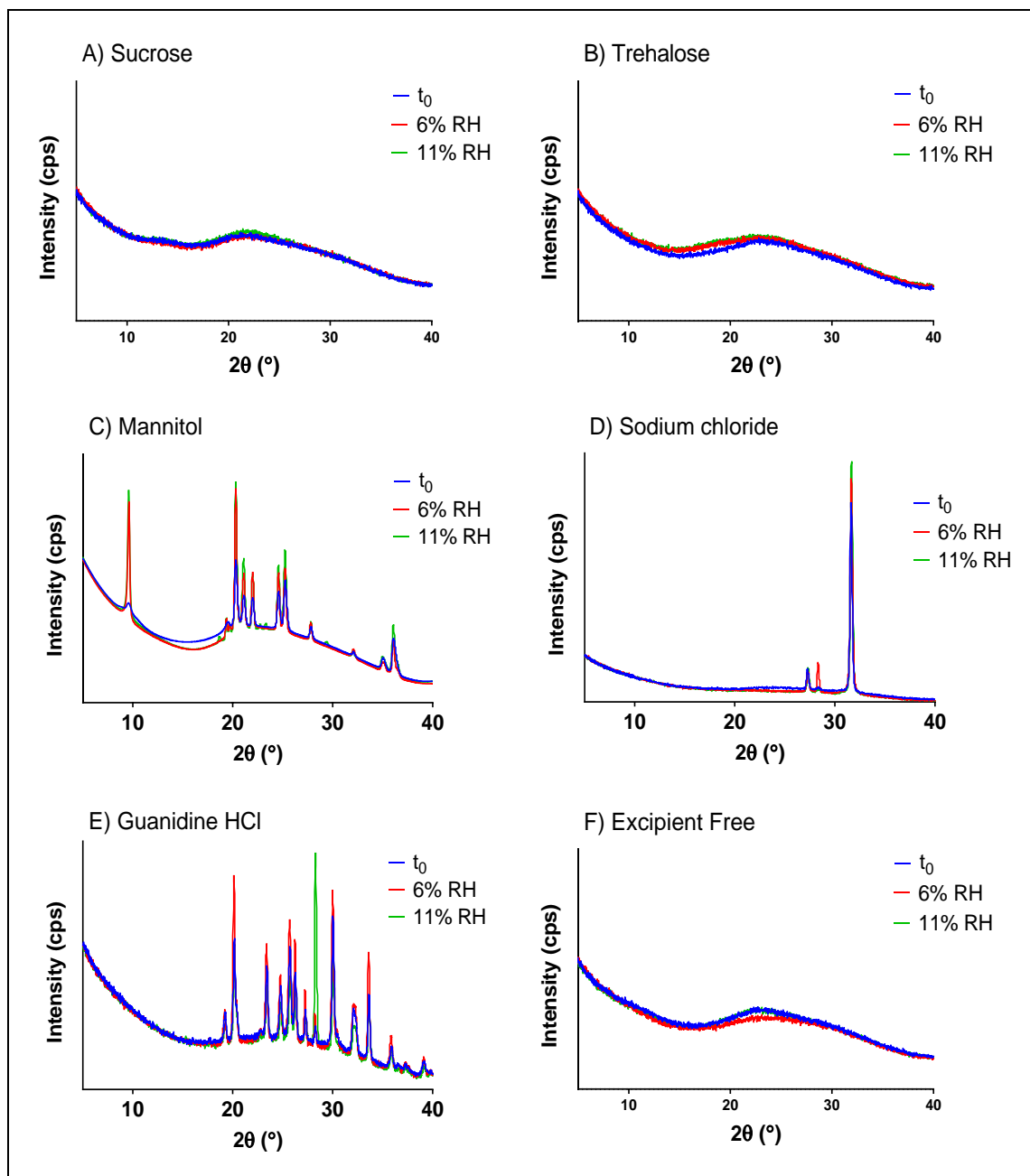


Figure 3.1. PXRD diffractograms of PDLA formulations immediately after lyophilization (t_0), after pre-hydration for 12 h at 6% RH or 11% RH: (A) sucrose, (B) trehalose, (C) mannitol, (D) sodium chloride, (E) guanidine HCl, and (F) no excipient (“excipient free”).

3.4.2 Effect of pre-hydration on ssHDX-MS kinetics

The kinetics of deuterium incorporation for an 18 amino acid PDLA peptide pre-hydrated at either 6% RH (Case-1) or 11% RH (Case-2) are shown in Figure 3.2, Appendix B - Figure B3, and Appendix B – Figure B4. For pre-hydration at 6% RH, the D_{\max} values obtained from the mono-exponential fit (Eqn. 3.3) of non-prehydrated amorphous PDLA formulations (i.e. sucrose, trehalose and excipient free) were approximately 17%, 22%, and 25% respectively (Figure 3.2A). With pre-hydration, the D_{\max} values were slightly less (i.e., 15%, 21% and 23%) than the non-prehydrated PDLA formulations, but the differences were not significant for the amorphous formulations (Figure 3.2A). The crystalline PDLA formulations (i.e. mannitol, sodium chloride and guanidine HCl) without pre-hydration showed D_{\max} values of approximately 42%, 26% and 56%, respectively under these conditions (Figure 3.2A). However, unlike the amorphous PDLA formulations, the D_{\max} values were significantly lower after pre-hydration (i.e. 26%, 22% and 41%, respectively) ($p < 0.05$, unpaired t-test with Welch's correction) (Figure 3.2A). For pre-hydration at 11% RH, the D_{\max} values for the pre-hydrated sucrose and trehalose formulations were not different than the non-prehydrated formulations (21% and 24%) (Figure 3.2B). The D_{\max} values of pre-hydrated crystalline formulations (i.e. mannitol, sodium chloride and guanidine HCl) and excipient-free formulation were significantly lower than non-prehydrated PDLA formulations under these conditions ($p < 0.05$, unpaired t-test with Welch's correction) (Figure 3.2B). The deuteration kinetic data before and after pre-hydration, in addition to PXRD results, suggest that prehydration-induced crystallization reduces the extent of deuteration, with the exception of the excipient-free formulation. The presence of moisture (i.e. H_2O) after pre-hydration may also contribute to the reduction in deuteration levels, perhaps by hydrating backbone amide groups thereby limiting hydrogen bonding with D_2O and subsequent exchange.

The hydrogen-deuterium exchange rate constants (k) of pre-hydrated PDLA formulations were also compared with rate constants for formulations that were not pre-hydrated. At 6% RH, the pre-hydrated mannitol and sodium chloride formulations showed greater k values than the non-pre-hydrated samples (Figure 3.2C). The excipient-free formulation showed a significantly lower k value after pre-hydration (Figure 3.2C). The remaining three formulations showed no significant differences in k values upon pre-hydration (Figure 3.2C). At 11% RH, the k values of pre-hydrated crystalline mannitol and sodium chloride formulations were significantly greater than those of non-pre-hydrated formulations (Figure 3.2D). The increased rate constants for crystalline formulations

upon pre-hydration suggest that deuteration is faster when the peptide is not protected by interactions with excipient in a relatively homogenous amorphous phase. The excipient-free formulation at 6% RH and sucrose formulation at 11% RH showed significantly smaller deuteration rate constant values for pre-hydrated samples than non-prehydrated samples, suggesting that deuteration may be slower due to the presence of additional residual moisture. At 11% RH, rate constants for the trehalose and excipient-free formulations were not affected by pre-hydration (Figure 3.2D).

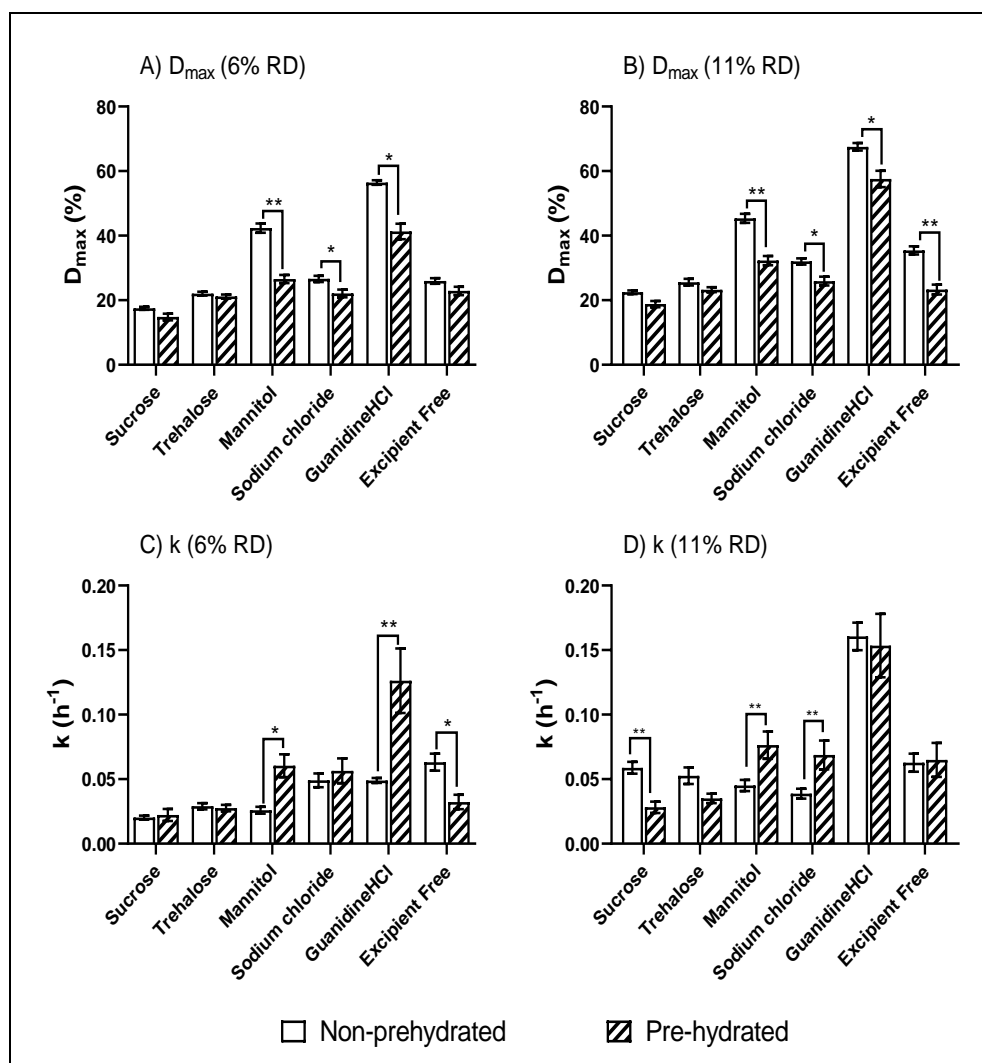


Figure 3.2. The maximum extent of deuterium (D_{max}) and deuteration rate constant (k) values of non-prehydrated (open bar) and pre-hydrated (hatched bar) PDLA formulations lyophilized with various excipients. (A) D_{max} at 6% RD (Case-1), (B) D_{max} at 11% RD (Case-2), (C) k at 6% RD (Case-1), (D) k at 11% RD (Case-2), Data shown for an 18 amino acid length PDLA peptide; $n=3$, mean \pm SE; error bars not shown when less than the height of the symbol.

3.4.3 Reversibility of ssHDX-MS

The kinetics of deuterium removal for an 18 amino acid (18 AA) PDLA peptide deuterated at either 6% RD (Case-3) or 11% RD (Case-4) are shown in Appendix B - Figure B5. The deuterium content of all the PDLA samples decreased rapidly (Appendix B -Figure B5). For samples deuterated at 6% RD (Case-3), the minimum extent of deuteration at long time (D_{\min}) decreased from ~12% to ~2% as the de-labelling RH increased from 0% to 43% (Appendix B - Figure B5A, B, C). The differences in D_{\min} values were not significantly different among the formulations ($p > 0.80$). Similarly, for samples deuterated at 11% RD (Case-4), the D_{\min} values decreased from ~17% to ~2% as the de-labelling RH increased from 0% to 43% with no significant differences among formulations ($p > 0.45$) (Appendix B - Figure B5C, D, E). These results suggest that the ssHDX reaction can be reversed rapidly, is independent of excipient type, and that the extent of deuterium removal and the plateau deuteration level depend on the de-labelling RH.

3.4.4 Comparison of the forward and reverse ssHDX-MS reactions

The deuterium labeling and de-labeling kinetics for the various formulations and RH conditions for an 18-amino acid (18 AA) PDLA peptide are shown in Figures 3.3-3.5 for samples deuterated at 6% RD. Similar results for samples deuterated at 11% RD are presented in Appendix B - Figures B6-B8.

Curves for the incorporation and loss of deuterium showed significant hysteresis for all formulations and conditions (Figures 3.3-3.5, Appendix B - Figures B6-B8). On exposure to 6% RD, deuterium incorporation for all PDLA solid samples increased mono-exponentially with time. Deuterium incorporation depended on RD, formulation type and time. Deuterium removal from the labeled PDLA samples followed a mono-exponential decay pattern showing hysteresis when both forward and reverse ssHDX kinetic data were compared. Unlike the forward ssHDX reaction, deuterium removal kinetics were generally independent of formulation, with ~12% deuterium incorporation at infinite time (D_{\min}). The guanidine HCl formulation is an exception (Figures 3.3, 3.4) and showed lower D_{\min} values. When the reverse reaction RH increased to 43%, the D_{\min} values were ~2% for all PDLA formulations (Figure 3.5). Similarly, for PDLA samples labeled at 11% RD, the deuterium incorporation levels were greater in the forward ssHDX reaction and the kinetics depended on the excipient type and time (Appendix B - Figure B6). In the reverse reaction,

the deuterium content in all PDLA samples decreased rapidly with a D_{\min} value of $\sim 15\%$ for all PDLA formulations (Appendix B - Figure B6, B7). When the reverse reaction RH was increased to 43%, the D_{\min} values decreased to $\sim 2\%$ (Appendix B - Figure B8).

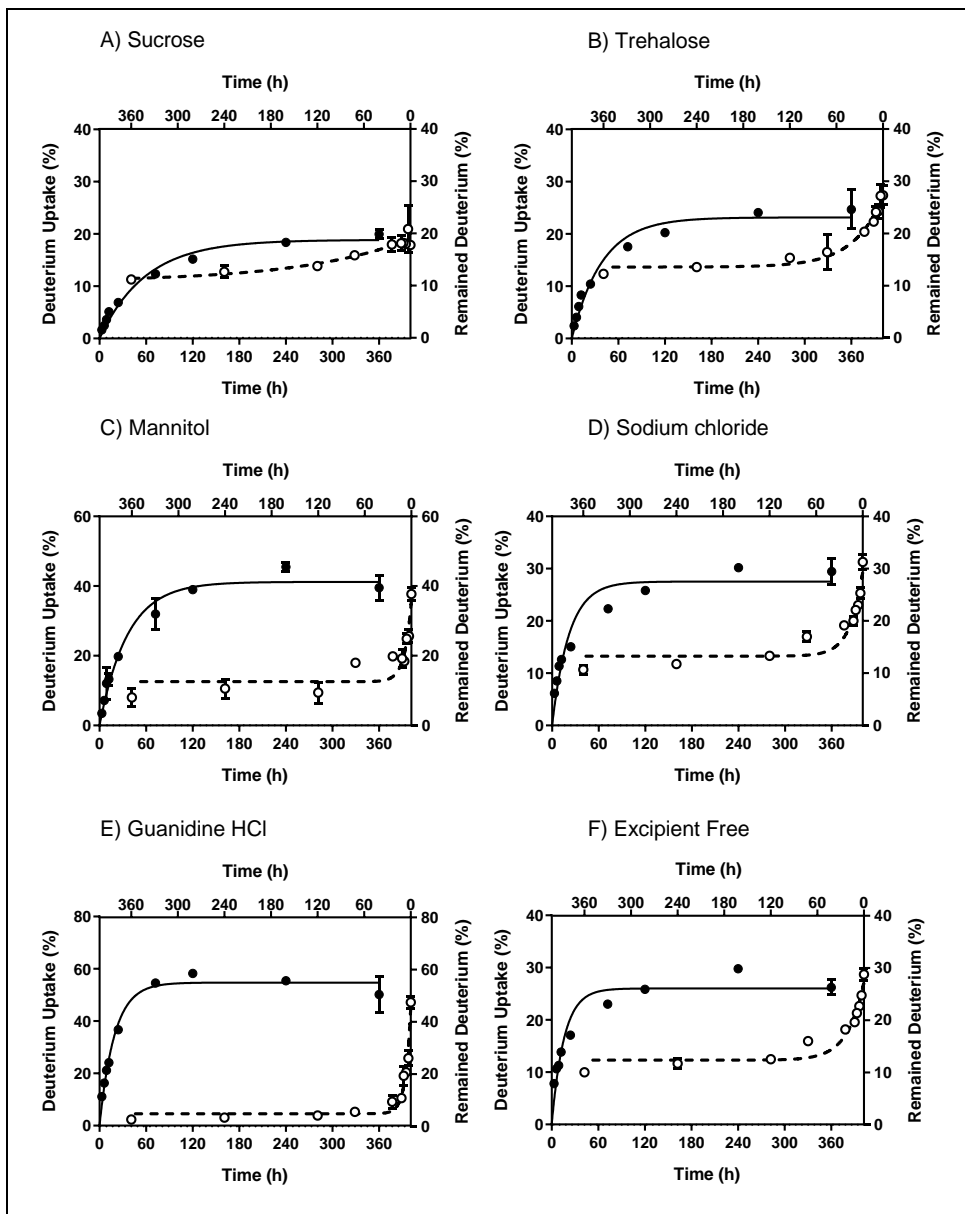


Figure 3.3. Comparison of the forward and reverse ssHDX-MS kinetics for PDLA formulations deuterated at 6% RD (forward) followed by deuterium removal at 0% RH (reverse) (Case-3a). Formulations contained (A) sucrose, (B) trehalose, (C) mannitol, (D) sodium chloride, (E) guanidine HCl, and (F) no excipient (“excipient free”). Solid line indicates fit of the forward ssHDX reaction to a mono-exponential association model, dotted line indicates fit of the reverse ssHDX reaction to a mono-exponential decay model; see text for details. Data shown for an 18 amino acid length PDLA peptide, $n=3$, mean \pm SD. error bars not shown when less than the height of the symbol.

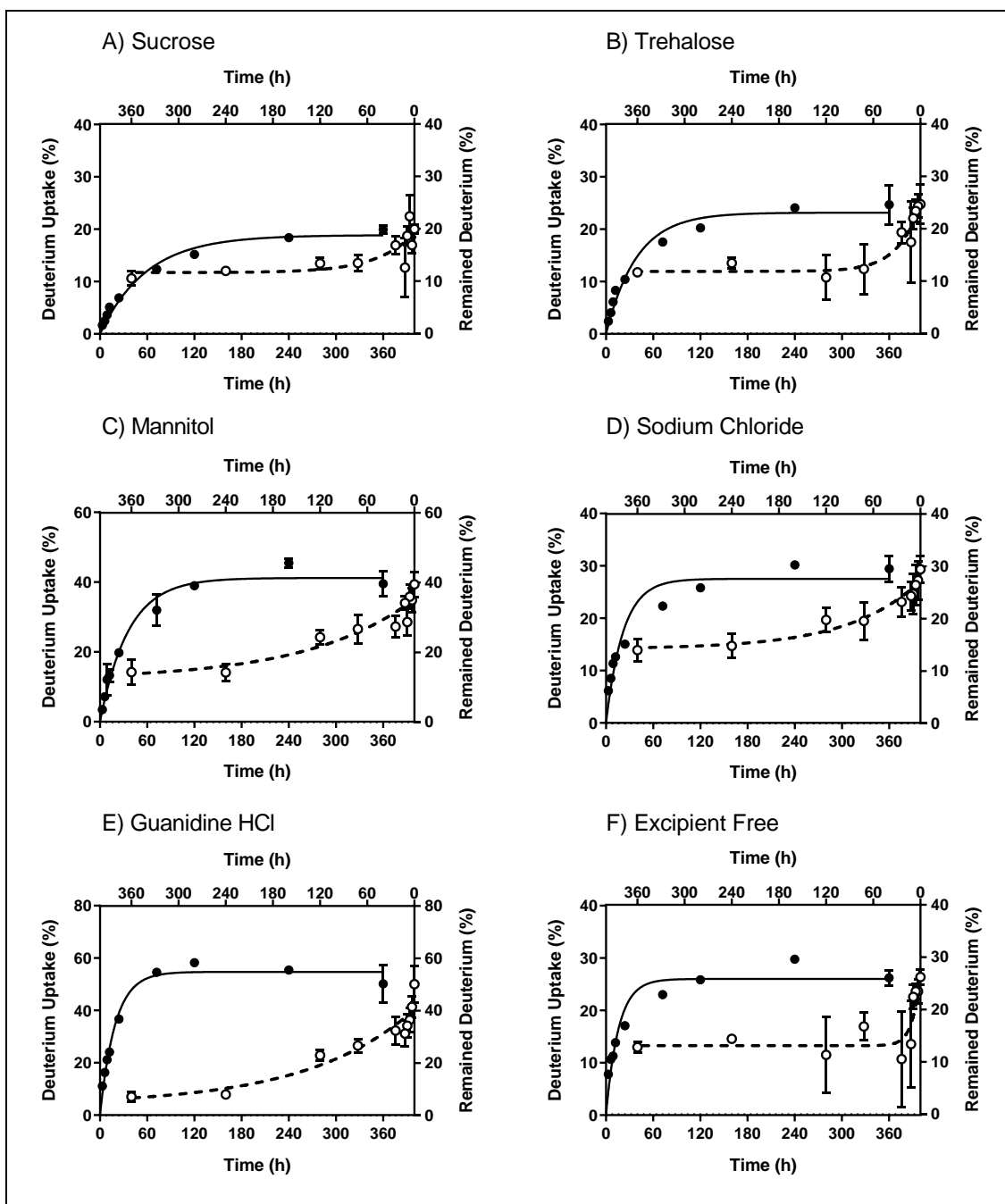


Figure 3.4. Comparison of the forward and reverse ssHDX-MS kinetics for PDLA formulations deuterated at 6% RD (forward) followed by deuterium removal at 6% RH (reverse) (Case-3b). Formulations contained (A) sucrose, (B) trehalose, (C) mannitol, (D) sodium chloride, (E) guanidine HCl, and (F) no excipient (“excipient free”). Solid line indicates fit of the forward ssHDX reaction to a mono-exponential association model, dotted line indicates fit of the reverse ssHDX reaction to a mono-exponential decay model; see text for details. Data shown for an 18 amino acid length PDLA peptide, $n=3$, mean \pm SD. error bars not shown when less than the height of the symbol.

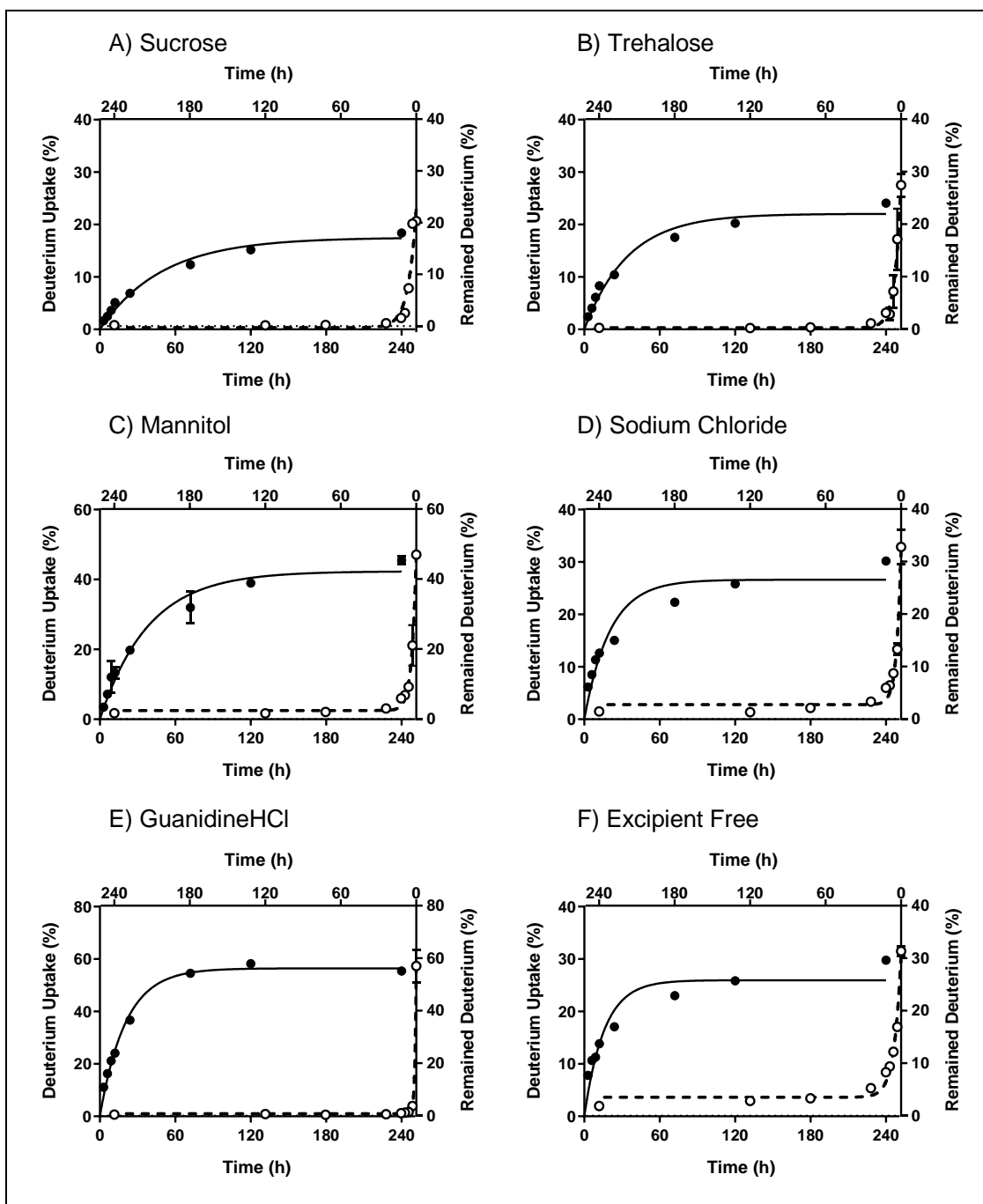


Figure 3.5. Comparison of the forward and reverse ssHDX-MS kinetics for PDLA formulations deuterated at 6% RD (forward) followed by deuterium removal at 43% RH (reverse) (Case-3c). Formulations contained (A) sucrose, (B) trehalose, (C) mannitol, (D) sodium chloride, (E) guanidine HCl, and (F) no excipient (“excipient free”). Solid line indicates fit of the forward ssHDX reaction to a mono-exponential association model, dotted line indicates fit of the reverse ssHDX reaction to a mono-exponential decay model; see text for details. Data shown for an 18 amino acid length PDLA peptide, $n=3$, mean \pm SD. error bars not shown when less than the height of the symbol.

3.5 Discussion

3.5.1 Pre-hydration and ssHDX-MS

Solid protein formulations typically contain low levels (<2%) of residual moisture. When an ssHDX experiment is conducted on these samples as received, deuterium incorporation at early time points may reflect the kinetics of mass transport and D₂O vapor sorption into the powder, as well as the exchange process itself. The pre-hydration studies reported here attempted to address these confounding effects by pre-equilibrating the powders in an H₂O vapor environment before exposing them to D₂O vapor at the same activity (i.e., pre-hydration RH = deuteration RD). At both 6% and 11% RH/RD, D_{max} values for the amorphous solids (i.e., sucrose, trehalose, excipient-free) were identical in pre-hydrated samples and in controls that were not pre-hydrated, with the exception of the excipient-free formulation at 11% RH/RD (Figure 3.2B). This indicates that total deuterium incorporation is generally unaffected by pre-hydration in the amorphous samples. Crystalline samples (mannitol, sodium chloride, guanidine hydrochloride) showed greater D_{max} values in samples that were not pre-hydrated (Figure 3.2A, B). Crystallization or partial crystallization of excipients during pre-hydration may promote peptide-peptide interactions that reduce deuterium incorporation in these samples. Similarly, with regard to deuterium incorporation rate constants, k values for the amorphous solids (i.e., sucrose, trehalose, excipient-free) were identical in pre-hydrated samples and their counterparts that were not pre-hydrated, with the exception of the excipient-free formulation at 6% RH/RD and sucrose formulation at 11% RH/RD (Figure 3.2C, D). In the crystalline solids (i.e., mannitol, sodium chloride, guanidine hydrochloride), differences in k values were observed between pre-hydrated samples and in controls that were not pre-hydrated (Figure 3.2C, D), which again can be attributed to crystallization or partial crystallization during the pre-hydration step. Thus, pre-hydration has little to no effect on the kinetics of deuterium incorporation for ssHDX-MS in the amorphous samples studied here.

3.5.2 Reversibility of ssHDX-MS

The reverse (3.5) and forward (3.6) deuterium exchange reactions in the solid powder can be written as:





where B is the concentration of deuterated backbone amide groups on the peptide in the solid state, A is the concentration of protonated backbone amide groups on the peptide in the solid state, X•H is the concentration of proton donor groups in the solid state, X• is the concentration of proton acceptor groups in the solid state, Z•D (= C) is the concentration of deuterium donor groups in the solid state, and Z• is the concentration of deuterium acceptor groups in the solid state.

These reactions are simply the reverse of one another. We assume that the concentrations of deuterium acceptor (Z•), proton acceptor (X•) and proton donor (X•H) groups in the solid powder are large and constant, and do not vary with time during the course of the ssHDX experiment. The rates of change of A and B then can be written as:

$$\frac{dB}{dt} = -k_b B + k_f AC \quad (3.7)$$

$$\frac{dA}{dt} = -k_f AC + k_b B \quad (3.8)$$

where k_b is the rate constant for the reverse reaction (i.e., for deuterium loss) and k_f is the rate constant for the forward reaction (i.e., for deuterium addition). The system is subject to the initial conditions that at $t = 0$, $A = A_0$ and $B = B_0$, and we make the additional observation that, for all times:

$$A + B = A_0 + B_0 \quad (3.9)$$

Using equation (3.9), equation (3.7) can be rewritten to eliminate A, giving:

$$\frac{dB}{dt} = -k_b B + k_f C [(A_0 + B_0) - B] \quad (3.10)$$

3.5.3 Limiting solution for deuterated peptide concentration, high RH

When the concentration of deuterium donors in the solid state is zero (i.e., when $C = Z\bullet D = 0$), equation (3.10) simplifies to:

$$\frac{dB}{dt} = -k_b B \quad (3.11)$$

with the solution:

$$B = B_0 e^{-k_b t} \quad (3.12)$$

Experimentally, this behavior was observed for the de-labeling study at 43% RH (Figures 3.5 and Appendix B - B8). The reverse rate constant values, k_b , were determined using equation (3.12) and deuterium loss data at 43% RH (Figure 3.6).

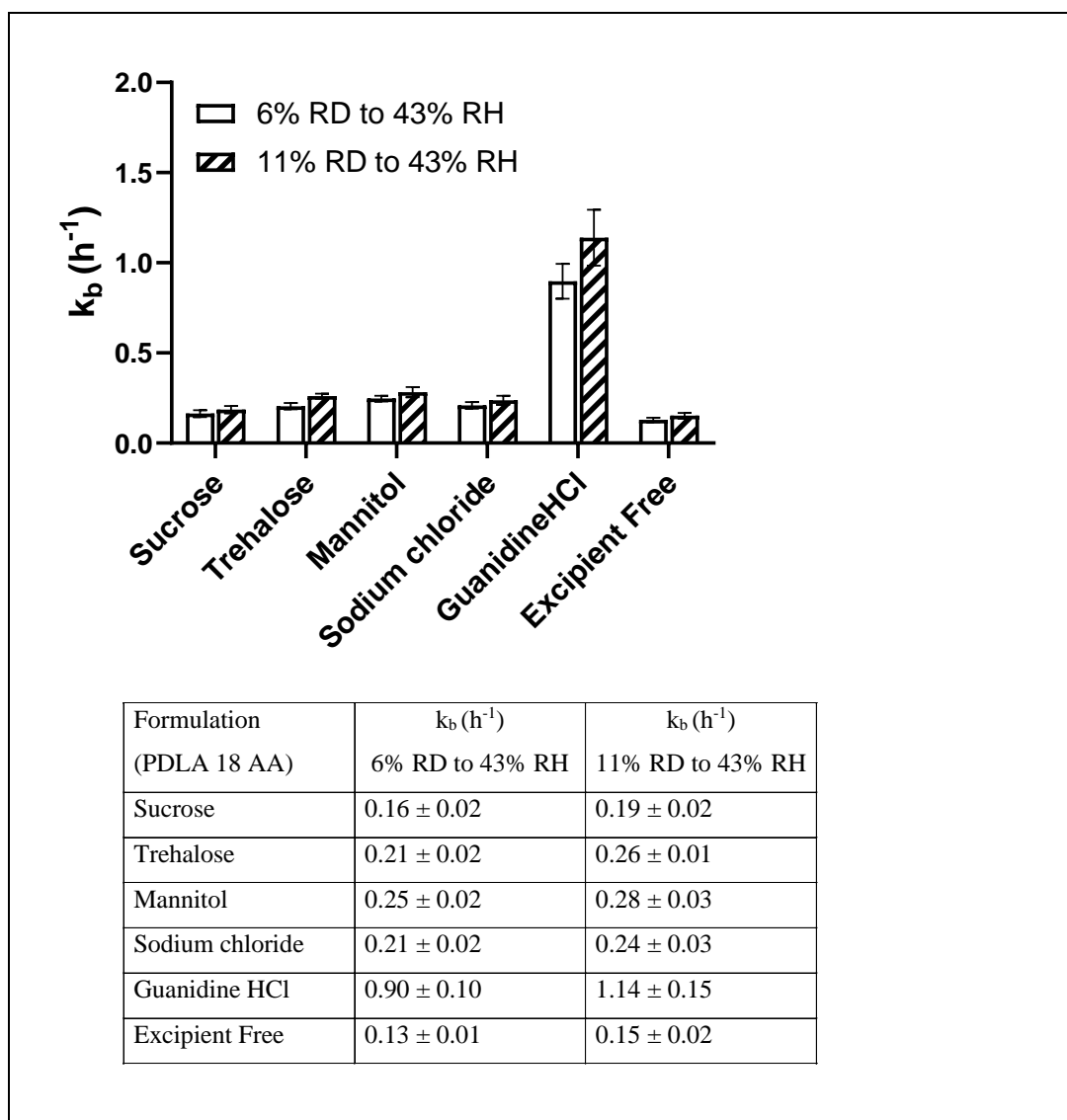


Figure 3.6. The reverse ssHDX reaction rate constant values, k_b , for PDLA formulations deuterated at 6% RD (open bar) or 11% RD (hatched bar) followed by deuterium removal at 43% RH (Case-3c, Case-4c). Data shown for an 18 amino acid length PDLA peptide; $n=3$, mean \pm SE.

The reverse reaction rate constant values (k_b) at 43% RH (de-labeling) range from 0.13 to 0.28 h⁻¹ for all formulations except guanidine HCl for samples deuterated at both 6% RD and 11% RD (Figure 3.6). For the guanidine HCl formulation, the k_b values were 0.90 h⁻¹ at 6% RD and 1.14 h⁻¹ at 11% RD, respectively, and were significantly greater than the k_b values of all other formulations ($p < 0.0001$, two-way ANOVA with Tukey's multiple comparisons). The greater k_b values for the guanidine HCl formulation may suggest weak interactions between the peptide and the excipient, so that the amide groups are readily available for exchange with either deuterons in the forward reaction or protons in the reverse reaction. The k_b values for the remaining formulations are not significantly different from one another ($p > 0.45$, two-way ANOVA with Tukey's multiple comparisons) suggesting that these values do not depend on the excipient type or initial deuterium content (i.e., labeling at either 6% RD or 11% RD).

The k_b values were also compared with the forward reaction rate constants (k_f^*) obtained in the forward ssHDX studies (Appendix B - Figure B9). The k_f^* values were estimated using a series of deuterium labeling studies conducted at different constant RD, as the slope of the apparent deuterium incorporation rate constant (k_{ap}) as a function of a_D (i.e., $a_D = \% \text{ RD}/100$; Eqn. 3.1), as reported previously.¹⁸ Note that k_f^* is a pseudo-first order rate constant valid in the absence of RD effects (i.e., at constant RD; Eqn. 3.1), and should not be confused with k_f , which is a second order rate constant (Eqns. 3.7, 3.8). The k_f^* values ranged from 0.3 to 2.3 h⁻¹ and were greater than the k_b values by a factor 1.4 to 6 in a given formulation (Appendix B - Figure B9). However, the differences between the k_b and k_f^* values were statistically significant only for the sucrose and guanidine HCl formulations. That the k_b and k_f^* values are of the same order of magnitude suggests that the rates of the forward and reverse ssHDX reactions can be comparable (Eqn. 3.7, 3.8), and further supports the importance of including the reverse reaction in the pseudo-first order kinetic model proposed previously.¹⁸ These estimates of k_b are strictly applicable only to de-labeling at 43% RH, and the relative values of k_f^* and k_b may depend on conditions.

3.5.4 Steady-state solution for plateau level of deuterated peptide

At de-labeling conditions other than 43% RH (i.e., at desiccated, 6% RH or 11% RH conditions), the concentration of deuterated peptide reaches a plateau at large time (Figures 3.3, 3.4, Appendix

B - B6 and B7). An algebraic equation for the steady-state value of B (i.e., B_{ss}) can be obtained by setting the time derivative equal to zero in equation (3.10) and rearranging to solve for B_{ss} :

$$\frac{B_{ss}}{A_0+B_0} = \frac{k_f C_{ss}}{k_b + k_f C_{ss}} \quad (3.13)$$

where C_{ss} is the steady-state concentration of deuterium donors in the solid state. The left-hand side of equation (3.13) is the fraction of total peptide (i.e., of $A_0 + B_0$) present in deuterated form at the plateau. The equation states that this fraction is related to the forward and reverse rate constants for exchange (k_f , k_b) and to C_{ss} . The pool of deuterium donors may include deuterated amide groups, excipients, and buffer species, as well as D_2O or DHO. The total concentration of these deuterium donors is unknown but is assumed to be constant at steady state. Equation (3.13) can be re-arranged to express the ratio, ($k_b/k_f C_{ss}$), in terms of the plateau value and initial conditions:

$$\frac{k_b}{k_f C_{ss}} = \frac{(A_0+B_0-B_{ss})}{B_{ss}} \quad (3.14)$$

The $k_b/k_f C_{ss}$ values were determined using equation (3.14) and plateau values for deuterium loss at low RH (i.e., 0%, 6% and 11%; Case-3 and Case-4) and are reported in Appendix B - Figure B10. The $k_b/k_f C_{ss}$ values were greater than 1, indicating that k_b is greater than $k_f C_{ss}$ (i.e., $k_b > k_f C_{ss}$). The $k_b/k_f C_{ss}$ values generally ranged from 3.5 to 8.4, with the exception of the guanidine HCl formulation, which showed values up to 23.5 (Appendix B - Figure B10). The values were similar for all formulations and conditions (no significant differences, $p > 0.05$, two-way ANOVA with Tukey's multiple comparisons) except for the guanidine HCl formulation. The forward and reverse rates are similar when D_2O vapor activity (a_D) is constant (Appendix B - Figure B9). That the reverse rate is greater here (i.e., $k_b > k_f C_{ss}$) suggests that the steady-state concentration of deuterium donors (C_{ss}) is low.

A general feature of the de-labeling experiments is that a higher RH in the vapor phase is associated with a lower plateau concentration of deuterated peptide (Figures 3.3-3.5 and Appendix B - Figures B6-B8). This can be attributed to the greater formation of volatile deuterated products at high RH, which can be removed from the solid (Figure 3.7). When the vapor phase RH is low, the concentration of H_2O in the solid powder is also low. Non-volatile species, such as excipient or

buffer molecules, then act as the predominant deuterium acceptors due to their greater concentration (Figure 3.7A). Deuterated excipient or buffer molecules, produced by the reverse reaction (Eqn. 3.5), cannot escape to the vapor phase, and remain trapped in the solid (Figure 3.7A). This allows the forward reaction (Eqn. 3.6) to occur. Conversely, when RH is high, the concentration of H₂O in the solid powder is also relatively high (Figure 3.7B). Under these conditions, water is the predominant deuterium acceptor in the solid state (Z• in equations (3.5), (3.6)). When the de-labeling reaction occurs (Eqn. 3.5), the deuterated peptide donates deuterium to H₂O as the most mobile and available acceptor, producing DHO and subsequently D₂O. Because DHO and D₂O are volatile, and because their vapor phase concentrations are essentially zero (sink conditions), these species can be removed from the solid. As a result, the solid phase concentration of deuterium donors is low and the forward (labeling) reaction (Eqn. 3.6) is hindered.

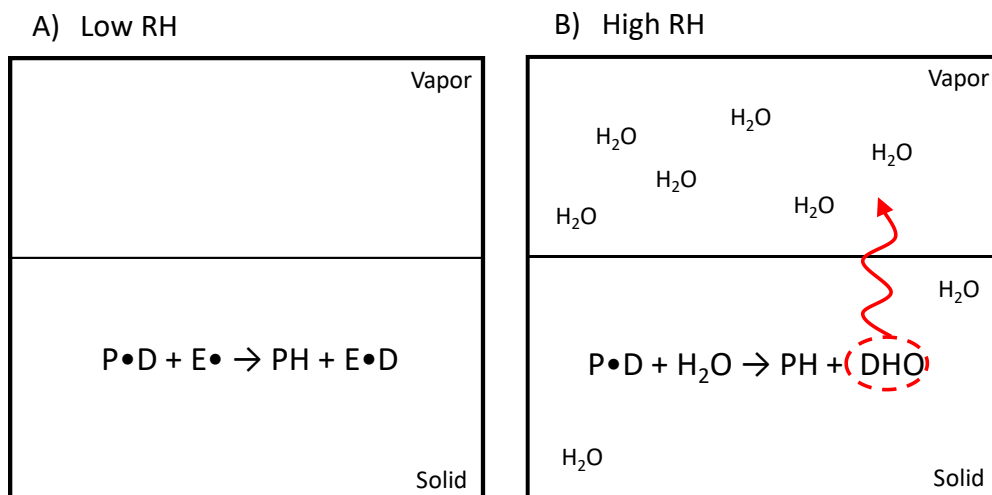


Figure 3.7. Effect of RH on the plateau level of deuterated peptide in de-labeling (reverse exchange) experiments conducted at (A) low RH (0%, 6% or 11%) or (B) high RH (43%). P•D represents deuterated peptide (B, Eqn. 3.5), E• represents a non-volatile excipient acting as a deuterium acceptor (Z•, Eqn. 3.5), PH represents protonated peptide (A, Eqn. 3.5) and E•D represents deuterated excipient (Z•D, Eqn. 3.5). At low RH (A), non-volatile excipients serve as deuterium acceptors during reverse exchange. These deuterated excipients remain in the solid and can serve as deuterium donors for the forward reaction (Eqn. 3.6; not shown). At high RH (B), sorbed H₂O serves as a deuterium acceptor and DHO (or D₂O, not shown) is generated as a reaction product. Volatile DHO and/or D₂O can be removed from the solid into the vapor phase, reducing the concentration of deuterium donors for the forward reaction (Eqn. 3.6).

3.6 Conclusions

The studies reported here have evaluated the reversibility of the ssHDX reaction and the effects of pre-hydration on deuterium incorporation kinetics in lyophilized formulations of unstructured PDLA peptides. In amorphous samples, pre-hydration had little to no effect on deuterium incorporation kinetics. In reversibility studies, the loss of deuterium label showed hysteresis when compared with deuterium incorporation in the forward ssHDX reaction. The rate and extent of deuterium removal depended on the de-labelling relative humidity but not on excipient type. The reverse ssHDX reaction rate constants were quantified, and an interpretation of plateau levels of deuterium incorporation was presented. The results support a mechanistic interpretation of ssHDX kinetics as a reversible first-order process, in which the forward (deuteration) rate depends on the activity of the deuterium donor.

3.7 Supporting information

Additional supporting information for this chapter is available in Appendix B: (i) pre-hydration and ssHDX-MS study schematic diagram (Figure B1), (ii) reversibility of ssHDX-MS study schematic diagram (Figure B2), (iii) comparison of pre-hydrated vs non-pre-hydrated ssHDX-MS of different PDLA formulations (Figures B3-B4), (iv) reversibility of ssHDX-MS in PDLA formulations lyophilized with various excipients (Figure B5), (v) comparison of the forward and reverse ssHDX-MS kinetics for PDLA formulations deuterated at 11% RD (Figure B6-B8), (vi) comparison of the reverse ssHDX reaction rate constant (k_b) and forward reaction rate constant (k_f^*) values of PDLA formulations (Figure B9), and (vii) comparison of the $k_b/k_f C_{ss}$ values of PDLA formulations (Figure B10).

3.8 References

- (1) Manning, M. C.; Patel, K.; Borchardt, R. T. Stability of protein pharmaceuticals. *Pharm. Res.* **1989**, *6* (11), 903-918.
- (2) Randolph, T. W. Phase separation of excipients during lyophilization: Effects on protein stability. *J. Pharm. Sci.* **1997**, *86* (11), 1198-1203.
- (3) Wang, W. Lyophilization and development of solid protein pharmaceuticals. *Int. J. Pharm.* **2000**, *203* (1), 1-60.

- (4) Chang, L.; Shepherd, D.; Sun, J., *et al.* Mechanism of protein stabilization by sugars during freeze-drying and storage: Native structure preservation, specific interaction, and/or immobilization in a glassy matrix? *J. Pharm. Sci.* **2005**, *94* (7), 1427-1444.
- (5) Li, Y.; Williams, T. D.; Schowen, R. L., *et al.* Characterizing protein structure in amorphous solids using hydrogen/deuterium exchange with mass spectrometry. *Anal. Biochem.* **2007**, *366* (1), 18-28.
- (6) S Moorthy, B.; K Iyer, L.; M Topp, E. Characterizing protein structure, dynamics and conformation in lyophilized solids. *Curr. Pharm. Des.* **2015**, *21* (40), 5845-5853.
- (7) Sophocleous, A. M.; Zhang, J.; Topp, E. M. Localized hydration in lyophilized myoglobin by hydrogen–deuterium exchange mass spectrometry. 1. Exchange mapping. *Mol. Pharmaceutics.* **2012**, *9* (4), 718-726.
- (8) Sophocleous, A. M.; Topp, E. M. Localized hydration in lyophilized myoglobin by hydrogen–deuterium exchange mass spectrometry. 2. Exchange kinetics. *Mol. Pharmaceutics.* **2012**, *9* (4), 727-733.
- (9) Moussa, E. M.; Singh, S. K.; Kimmel, M., *et al.* Probing the conformation of an IgG1 monoclonal antibody in lyophilized solids using solid-state hydrogen–deuterium exchange with mass spectrometric analysis (ssHDX-MS). *Mol. Pharmaceutics.* **2018**, *15* (2), 356-368.
- (10) Moorthy, B. S.; Schultz, S. G.; Kim, S. G., *et al.* Predicting protein aggregation during storage in lyophilized solids using solid state amide hydrogen/deuterium exchange with mass spectrometric analysis (ssHDX-MS). *Mol. Pharmaceutics.* **2014**, *11* (6), 1869-1879.
- (11) Kumar, L.; Chandrababu, K. B.; Balakrishnan, S. M., *et al.* Optimizing the formulation and lyophilization process for a fragment antigen binding (Fab) protein using solid-state hydrogen–deuterium exchange mass spectrometry (ssHDX-MS). *Mol. Pharmaceutics.* **2019**, *16* (11), 4485-4495.
- (12) Englander, S. W. Hydrogen exchange and mass spectrometry: A historical perspective. *J. Am. Soc. Mass Spectrom.* **2006**, *17* (11), 1481-1489.
- (13) Deng, B.; Lento, C.; Wilson, D. J. Hydrogen deuterium exchange mass spectrometry in biopharmaceutical discovery and development – A review. *Anal. Chim. Acta.* **2016**, *940*, 8-20.
- (14) Wales, T. E.; Engen, J. R. Hydrogen exchange mass spectrometry for the analysis of protein dynamics. *Mass Spectrom. Rev.* **2006**, *25* (1), 158-170.

- (15) Englander, S. W.; Kallenbach, N. R. Hydrogen exchange and structural dynamics of proteins and nucleic acids. *Q. Rev. Biophys.* **1983**, *16* (4), 521-655.
- (16) Hvidt, A.; Nielsen, S. O. Hydrogen exchange in proteins. *Adv. Protein Chem.* **1966**, *21*, 287-386.
- (17) Weis, D. D., Analysis of disordered proteins by hydrogen deuterium exchange mass spectrometry. In *Hydrogen Exchange Mass Spectrometry of Proteins: Fundamentals, Methods, and Applications*, Weis, D. D., Ed. John Wiley & Sons: **2015**; pp 295-321.
- (18) Kammari, R.; Topp, E. M. Solid-state hydrogen-deuterium exchange mass spectrometry (ssHDX-MS) of lyophilized poly-D, L-alanine. *Mol. Pharmaceutics.* **2019**, *16*, 2935-2946.
- (19) Moorthy, B. S.; Zarraga, I. E.; Kumar, L., *et al.* Solid-state hydrogen–deuterium exchange mass spectrometry: correlation of deuterium uptake and long-term stability of lyophilized monoclonal antibody formulations. *Mol. Pharmaceutics.* **2018**, *15* (1), 1-11.
- (20) Moorthy, B. S.; Iyer, L. K.; Topp, E. M. Mass spectrometric approaches to study protein structure and interactions in lyophilized powders. *J. Vis. Exp.* **2015**, (98), No. e52503.
- (21) Wales, T. E.; Eggertson, M. J.; Engen, J. R., Considerations in the analysis of hydrogen exchange mass spectrometry data. In *Mass Spectrometry Data Analysis in Proteomics: Methods and Protocols, Methods in Molecular Biology* Matthiesen, R., Ed. Humana Press: **2013**; Vol. 1007, pp 263-288.

CHAPTER 4. EFFECTS OF PEPTIDE SECONDARY STRUCTURE ON SOLID-STATE HYDROGEN-DEUTERIUM EXCHANGE

This chapter was published as a research article in *Molecular Pharmaceutics* (2020, 17 (9), 3501–3512) and reproduced with permission. Copyright (2020) American Chemical Society.

DOI: 10.1021/acs.molpharmaceut.0c00521

4.1 Abstract

The effects of peptide secondary structure on the rate and extent of deuterium incorporation in solid-state hydrogen deuterium exchange mass spectrometry (ssHDX-MS) were assessed. Unstructured PDLA peptides, an α -helical model peptide (Peptide A) and a β -sheet model peptide (Peptide B) were co-lyophilized with various excipients. Peptide structures were confirmed in solution using circular dichroism spectroscopy (CD) and in the solid state with Fourier transform infrared spectroscopy (FTIR). ssHDX-MS was conducted at two relative humidities (11% and 23% RH D₂O) and deuterium uptake kinetics were monitored over 10 days. The relative contributions of peptide secondary structure and matrix interactions to deuteration incorporation were evaluated by comparing the ssHDX-MS kinetic data of Peptide A and Peptide B with PDLA of similar molecular weight. The results demonstrate that both peptide secondary structure and interactions with the solid matrix contribute to the protection from exchange in ssHDX-MS. A quantitative data analysis and interpretation method is presented, in which the number of protected amide bonds is calculated as the difference between the maximum deuterium incorporation in solution and in solid samples.

4.2 Introduction

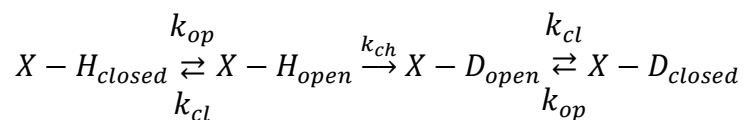
Since its introduction in the 1950's, hydrogen deuterium exchange (HDX) has become a widely used analytical tool for characterizing protein folding and dynamics in solution.^{1,2} When coupled with mass spectrometry (HDX-MS), the method measures the mass change of a protein upon isotopic exchange of backbone amide hydrogen atoms with deuterium.^{3,4} The method typically involves the dilution of a protein solution into high volumes of a deuterium labeling buffer (i.e., D₂O buffer, ~pH 7) at room temperature followed by isotopic labeling for pre-determined time intervals (milliseconds to hours). The reaction is then quenched by reducing the temperature and pH to ~ 0° C and ~ 2.5 respectively and the deuterium uptake is then measured by mass spectrometry.¹ HDX-MS has been used to evaluate protein folding mechanisms,^{5,6} to characterize protein structure,⁷ for epitope mapping,⁸ to probe protein-protein interactions,^{5,9} and in studies of conformational changes in protein complexes.¹⁰ The technique also relates protein structure and dynamics, and thus has been used in the discovery and development of protein biologics such as monoclonal antibodies and antibody drug conjugates.^{11,12}

Although solution formulations of protein drugs are usually preferred for ease of administration and the relatively low cost of manufacturing, the protein may be insufficiently stable in solution to provide an adequate shelf life. Water promotes many protein degradation pathways such as hydrolysis, oxidation, deamidation and aggregation by acting as a reactant, catalyst or solvent.¹³ To improve stability, it is often desirable to remove water and produce a solid formulation.¹³ Solid-state protein formulations are generally produced by lyophilization and require the addition of excipients, such as cryoprotectants (to protect from freezing stress) and lyoprotectants (to protect from drying stress).¹⁴ In addition, excipients such as mannitol and sodium chloride may be included to produce a formulation with acceptable physical appearance that maintains isotonicity upon reconstitution.¹⁴ The combination and amount of these excipients is usually optimized using long-term stability studies, aided by conventional biophysical characterization techniques such as differential scanning calorimetry (DSC) and Fourier transform infrared spectroscopy (FTIR). There is an unmet need for novel analytical methods that can reduce the dependence on time-consuming stability studies in formulation and process development.

Recently, the HDX-MS technique has been applied to proteins in the solid-state, providing higher resolution information on protein structure and interactions with the solid matrix. Termed solid-

state hydrogen deuterium exchange mass spectrometry (ssHDX-MS), the method involves isotopically labeling dried protein formulations by exposing them to D₂O in the vapor phase at controlled temperature and D₂O relative humidity. After labeling for pre-determined time intervals (hours to days), the samples are quenched by flash freezing and the deuterium content is analyzed by mass spectrometry after reconstituting in an ice-cold, low pH buffer (pH 2.5).¹⁵ In several recent studies, deuterium uptake during ssHDX-MS has been shown to be highly correlated with the stability of the protein during long-term storage, suggesting that the method may be a cost and time-effective alternative to stability studies. The correlation of deuterium uptake to long term storage stability of small proteins, therapeutic antibodies and antibody fragments has been demonstrated.¹⁶⁻¹⁸ More recently, ssHDX-MS has also been used to study the surface composition of protein formulations produced by spray drying,¹⁹ to optimize the lyophilization and formulation process of an antibody fragment,¹⁸ and to evaluate the effects of drying methods on storage stability of protein formulations.^{20, 21} Despite these advances, the fundamental mechanisms and the factors contributing to the kinetics of ssHDX-MS are not clear, limiting interpretation of ssHDX-MS kinetics.

The mechanism of hydrogen-deuterium exchange in solution is described by the Linderstrom-Lang model²²⁻²⁴ which considers that a protein in solution exhibits transient folding and unfolding events (i.e., protein dynamics) with the rate constants k_{op} and k_{cl} , respectively. The model asserts that, when a protein is exposed to a deuterium source such as D₂O, reversible protein folding is followed by an irreversible chemical exchange reaction (k_{ch}) at backbone amide groups.



For a protein in its native folded state, the observed hydrogen exchange rate (k_{HDX}) is given by the following equation (assuming that the $k_{cl} \gg k_{op}$):²⁵

$$k_{HDX} = \frac{k_{op} \times k_{ch}}{k_{cl} + k_{ch}}$$

According to this model, the kinetics of deuteration are governed by the protein structure (i.e., intramolecular hydrogen bonding), protein dynamics (i.e., transient folding and unfolding events) and solvent accessibility of amide hydrogen atoms. The folded regions of a protein exhibit slower

deuteration kinetics than the disordered regions due to intramolecular hydrogen bonding. Rapid deuteration rates indicate high solvent exposure or facile structural opening in that region of the protein molecule.¹

Despite its success and wide acceptance in describing solution HDX, the Linderstrom-Lang model fails to describe common experimental observations in ssHDX-MS, including the dependence of the rate and extent of exchange on D₂O activity and excipient type. In addition, the Linderstrom-Lang model does not account for the complexity of the spatially and dynamically heterogeneous amorphous matrix. These limitations have been described in our previous study.²⁶ At present, the extent to which ssHDX-MS is a measure of protein structural conformation vs. protein-matrix interactions is not clear, and the relative contributions of these two factors to ssHDX-MS kinetics are not known. The effects of the physical state of the solid matrix (i.e., amorphous or crystalline) on ssHDX-MS kinetics are also unknown.

To address these limitations and to begin to provide a mechanistic understanding of ssHDX-MS, we have developed a model for ssHDX-MS kinetics.²⁶ In the model, chemical exchange is treated as a reversible chemical reaction, in which the forward rate is proportional to D₂O activity. The model successfully described ssHDX-MS kinetics for unstructured poly-D,L-alanine (PDLA) peptides in various solid formulations. The applicability of the model to these peptides establishes that peptide-matrix interactions contribute to the rate and extent of ssHDX-MS in the absence of higher-order structure, an effect that was not observed (and would not be expected) in solution HDX of these unstructured peptides. The model does not account for the effects of higher order structure in ssHDX-MS, however, an attribute critical to the formulation and stability of lyophilized protein therapeutics. The solid-state forms of these molecules are affected both by intramolecular hydrogen bonds that contribute to their secondary structure and by intermolecular hydrogen bonds with stabilizing excipients in the surrounding solid matrix. The aim of the current study is to evaluate the relative contributions of secondary structure and matrix-interactions to deuteration kinetics in ssHDX-MS, and to provide a more comprehensive mechanistic description of ssHDX-MS relevant to the industry.

To achieve this goal, two model peptides were chosen, one containing an α -helical secondary structure and the second with β -sheet secondary structure. The peptides were selected to allow comparisons with the unstructured PDLA studied previously. A 16-amino acid length peptide

(“Peptide A”, Ac-(A₄K)₃A-NH₂) was selected as a model for the α -helix conformation and a 14-amino acid length peptide (“Peptide B”, Ac-(KA₁₂K)-NH₂) was selected as a model for the β -sheet conformation.²⁷⁻²⁹ Unlike the PDLA peptides, peptides that contain only L-alanine would be expected to be structured, but to have poor aqueous solubility and be difficult to synthesize and purify. To overcome this challenge, lysine residues were introduced at the two termini of Peptide B. The repeating alanine residues in the center of the sequence produce the β -sheet conformation by hydrophobic interactions of methyl groups.²⁸ Peptide A consists of three lysine residues separated by four alanine residues. This spacing is necessary to avoid charge interactions between the lysine side chains and to disrupt possible intermolecular interactions between peptides. The lysine side chains are external to the helix and help solubilize the peptide. Both peptides were acetylated at the N-terminus and amidated at the C-terminus.^{27, 28}

The peptides were co-lyophilized with various excipients, exposed to D₂O vapor under controlled conditions, and the deuteration kinetics monitored over a period of 10 days. The ssHDX-MS kinetics of the two structured peptides were then compared with those of unstructured PDLA peptides to assess the contributions of secondary structure to ssHDX-MS kinetics. The results demonstrate that both peptide secondary structure and matrix interactions contribute to the protection from exchange observed in ssHDX-MS. A data analysis and interpretation method is presented that quantifies protection from exchange relative to controls.

4.3 Materials and methods

4.3.1 Materials

The model α -helical peptide (“Peptide A”, Ac-(A₄K)₃A-NH₂, MW 1368.55 Da) and β -sheet peptide (“Peptide B”, Ac-(KA₁₂K)-NH₂, MW 1169.30 Da) were custom synthesized by ABclonal Science (Woburn, MA). Poly-D,L-alanine peptides (“PDLA”, P9003, MW 1000-5000 Da), lyophilization excipients (sucrose, trehalose, mannitol, sodium chloride, guanidine hydrochloride), dibasic and monobasic potassium phosphates were purchased from Sigma-Aldrich (St. Louis, MO). Lyophilization vials (Wheaton™ Type I Clear Glass 2 mL Serum Vials), stoppers (Wheaton™ Rubber Stoppers), and all liquid chromatography mass spectrometry (LC-MS) grade solvents (water, acetonitrile, formic acid, and methanol) were purchased from Fisher Scientific (Hanover Park, IL). Deuterium oxide (D₂O, 99.9%) was purchased from Cambridge Isotope Laboratories

(Andover, MA). Sterile membrane filters (0.22 μm , Millex-GV) were purchased from EMD Millipore (Burlington, MA). The salts used to prepare saturated solutions of D_2O to control relative humidity in sealed desiccators (LiCl and $\text{CH}_3\text{CO}_2\text{K}$) were purchased from Fisher Scientific (Hanover Park, IL). The Float-A-Lyzer™ G2 Dialysis Devices (molecular weight cut-off 0.1-0.5 kD) were purchased from Spectrum Laboratories, Inc. (Rancho Dominguez, CA).

4.3.2 Lyophilization

The lyophilized formulations were prepared as reported previously.²⁶ Briefly, the peptides were dissolved in 2.5 mM potassium phosphate buffer (pH 7.4) and exhaustively dialyzed using Float-A-Lyzer™ G2 dialysis devices overnight at 4° C to remove salts and impurities remaining from synthesis. After dialysis, peptides were diluted to 5 mg/mL concentration. The excipients were also dissolved in 2.5 mM potassium phosphate buffer (pH 7.4) at 35 mg/mL concentrations. Equal volumes of peptide and excipient solutions were then mixed to yield a final peptide concentration of 2.5 mg/mL and an excipient concentration of 17.5 mg/mL (1:7 % w/w). Finally, 250 μL of peptide-excipient solution was aliquoted into 2 mL lyophilization vials and lyophilized using a pilot-scale freeze drier (LyoStar3, SP Scientific, Warminster, PA). A conservative lyophilization cycle was used with freezing at -40° C for 3 h, followed by primary drying at -35° C for 28 h (80 mTorr) and secondary drying at 25° C for 8 h (80 mTorr). At the end of the lyophilization cycle, samples were backfilled with nitrogen gas under vacuum, stoppered, and crimped.

4.3.3 Circular dichroism spectroscopy (CD)

The secondary structure of the peptides in solution was confirmed by far UV CD spectroscopy using a JASCO J-815 spectrometer (JASCO Analytical Instruments, Easton, MD). The instrument was purged continuously with nitrogen gas at a flow rate of 15 L/min and approximately 200 μL of a 100 μM peptide sample in 2.5 mM potassium phosphate buffer was analyzed using a 1 mm path length cell at 20° C. The spectra were acquired from 190 nm to 260 nm using a 1 nm bandwidth at 50 nm/min scanning speed. An average of three scans was reported.

4.3.4 Fourier transform infrared spectroscopy (FTIR)

The secondary structure of the peptides in lyophilized formulations was confirmed by solid-state FTIR using a Nexus FTIR spectrometer (Thermo Nicolet Corp., Madison, WI) equipped with an attenuated total reflectance (ATR) crystal. The instrument was purged with nitrogen gas to reduce background moisture interference and 128 scans of the background spectra were acquired at a resolution of 4 cm^{-1} . Approximately 5 mg of solid was placed on the ATR crystal and 128 scans of the spectra were acquired at a resolution of 4 cm^{-1} . For each sample, the baseline was corrected, background spectra were subtracted, the area was normalized for the amide-I region ($1720\text{-}1580\text{ cm}^{-1}$) and the second derivative spectra were generated using the Opus software (Version 6.5, Bruker Optics, Billerica, MA).

4.3.5 Powder X-ray diffraction (PXRD)

The physical state of the formulations was characterized using a Rigaku SmartLab (XRD 600) diffractometer (The Woodlands, TX). The diffractograms were collected at a wavelength of 0.15405 nm between 5° to $40^\circ 2\theta$ with a step size of 0.02° .

4.3.6 Solution HDX-MS

The solution HDX-MS experiments were carried out on solution samples of unstructured PDLA, Peptide A and Peptide B formulations prior to lyophilization as a control for ssHDX-MS. The peptide formulations (i.e., 2.5 mg/mL peptide and 17.5 mg/mL excipient in 2.5 mM potassium phosphate buffer, pH 7.4) were diluted with deuterium labeling buffer (2.5 mM potassium phosphate buffer in D_2O) at 1:9 (v/v). The deuterium labeling experiments were carried out at room temperature and the samples were quenched at pre-determined time intervals by diluting with an excess volume of ice-cold quench buffer (0.2% formic acid, 5% methanol in water, pH 2.5). The quenched samples were analyzed for deuterium content by LC-MS (Agilent 6520 TOF, Agilent Technologies, Santa Clara, CA). The LC-MS system was equipped with a custom-made refrigerated box capable of maintaining low temperatures to reduce back exchange. The peptide was trapped onto a peptide trap (Michrom Biosources, Inc., Auburn, CA) and desalted for 1.7 min using an isocratic flow of 0.1% formic acid in water at 0.2 mL/min flow rate. The peptides were eluted using an LC column (Zorbax 300-SB-C18, Agilent Technologies, Santa Clara, CA) with a

gradient flow of 0.1 % formic acid in acetonitrile. The data were acquired from 100-1700 m/z and an undeuterated sample was used as a reference to calculate the deuterium content in labeled samples. A peptide list for the synthetic peptide consisting of an experimental mass, retention time and m/z was generated using Mass Hunter workstation software equipped with the Bioconfirm software package (B.03.01, Agilent Technologies). These reference parameters were then used to calculate deuteration levels in labeled samples using HDExaminer software (Version 2.0, Sierra Analytics, Modesto, CA).

4.3.7 Solid-state HDX-MS (ssHDX-MS)

The ssHDX-MS experiments for the PDLA, Peptide A and Peptide B formulations were carried out at two relative humidity conditions (i.e., 11% RH D₂O and 23% RH D₂O). Solid samples in open vials were placed in sealed desiccators containing saturated salt solutions in D₂O at room temperature (LiCl in D₂O for 11% RH and CH₃CO₂K in D₂O for 23% RH). Labeling was carried out for up to 10 days and the samples were withdrawn at pre-determined time intervals (i.e., 3 h, 6 h, 9 h, 12 h, 1 day, 3 days, 5 days and 10 days). The samples were quenched by flash freezing in liquid nitrogen and stored at -80° C until analyzed by LC-MS. The quenched samples were reconstituted in ice-cold buffer (0.2 % formic acid, 5 % methanol in water, pH 2.5) and analyzed on a mass spectrometer as described above.

The deuteration data were fitted to a mono-exponential equation:

$$D = D_{max}(1 - e^{-kt}) \quad (4.1)$$

where D is the deuterium uptake at labeling time t, D_{max} is the deuterium uptake at infinite time, and k is an apparent first-order rate constant. The calculation of deuteration kinetic parameters and statistical analysis were carried out using GraphPad Prism software (Version 8.3.0, La Zolla, CA).

4.3.8 Statistical analysis

Deuteration data were analyzed using GraphPad Prism software (Version 8.3.0, La Zolla, CA). A two-way ANOVA followed by Tukey's multiple comparison test was used to evaluate the differences in solution HDX-MS data by comparing the mean deuteration levels of every peptide formulation with those of every other peptide formulation. A two-way ANOVA followed by

Sidak's multiple comparisons was used to evaluate the ssHDX-MS data, since two groups were compared independently with other groups in a data set. Maximum deuteration values or rate constants for two different peptides in the same formulation at the same RH were compared similarly.

4.4 Results

4.4.1 Peptide secondary structure in solution by CD

The secondary structures of the model peptides were evaluated in solution using CD spectroscopy (Figure 4.1). Peptide A showed characteristic minima at 222 nm and 208 nm, as well as a maximum at 190 nm, consistent with an α -helical structure.³⁰ Peptide B showed a characteristic minimum at 218 nm and a maximum between 195 - 200 nm, consistent with β -sheet structure in solution.³⁰

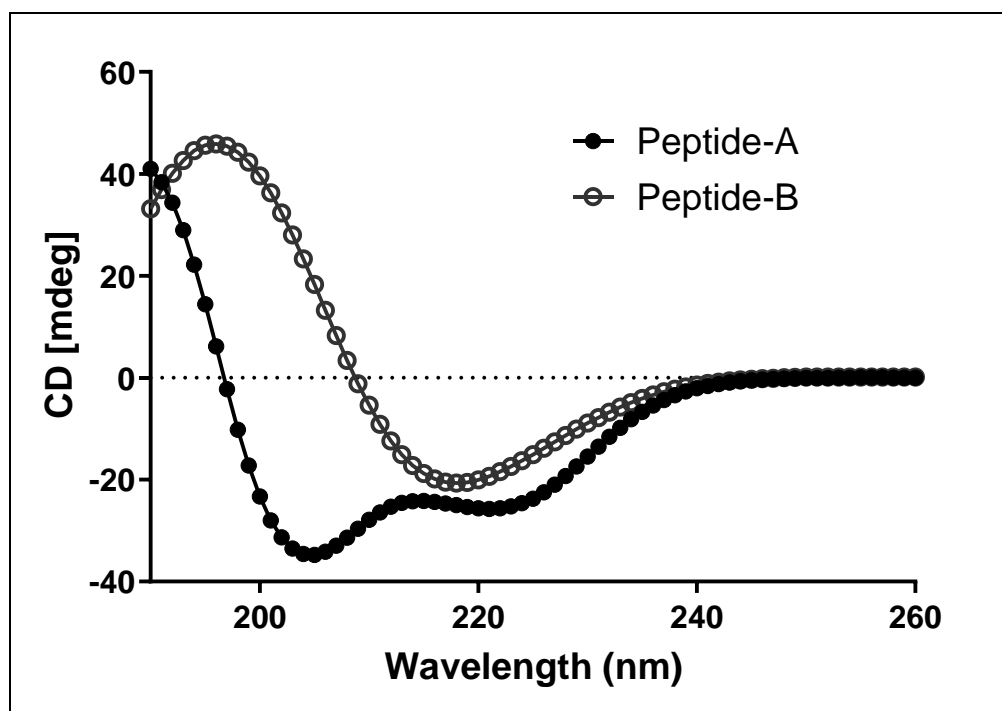


Figure 4.1. Circular dichroism (CD) spectra of Peptide A (i.e., Ac-(A₄K)₃A-NH₂) and Peptide B (i.e., Ac-KA₁₂K-NH₂) in solution show peaks characteristic of α -helix and β -sheet secondary structures, respectively.

4.4.2 Peptide secondary structure after lyophilization

Solid-state FTIR was used to assess the secondary structure of the model peptides in lyophilized formulations (Figure 4.2). The second derivative spectra in the amide-I region (1720-1580 cm^{-1}) were extracted for Peptide A and Peptide B for each formulation. The sucrose, trehalose and excipient-free formulations of Peptide A showed a band at 1652 cm^{-1} while the mannitol and sodium chloride formulations showed a band at 1658 cm^{-1} , consistent with retention of the peptide's α -helical structure in the solid-state (Figure 4.2). In contrast, the guanidine HCl formulation showed peaks consistent with a random coil, suggesting that the α -helical structure had been perturbed. The peak shifts of the mannitol and sodium chloride formulations, relative to the other formulations that retained structure, can be attributed to partial crystallinity of these excipients and reduced hydrogen bonding interactions between peptide and excipients.³¹ The small peak at 1630 cm^{-1} in the FTIR spectra of all formulations may be due to the signal produced by lysine residue side chains, while the peaks at 1675 cm^{-1} may suggest the presence of a β -turn like structure.³² The FTIR spectrum of Peptide A in the guanidine HCl formulation showed an additional broad peak between 1620-1630 cm^{-1} which can be attributed to interference from lysine side chains and guanidine HCl despite background correction.

The second derivative FTIR spectra in the amide-I region of Peptide B formulations showed a characteristic peak at 1625 cm^{-1} , consistent with the retention of β -sheet structure in all formulations.³² The guanidine HCl formulation peak in this region is broadened, which may indicate interference by the excipient and/or loss of secondary structure. With that exception, the solid-state FTIR spectra suggest that Peptide A exists in an α -helical conformation and Peptide B in a β -sheet conformation after lyophilization in all formulations except guanidine HCl.

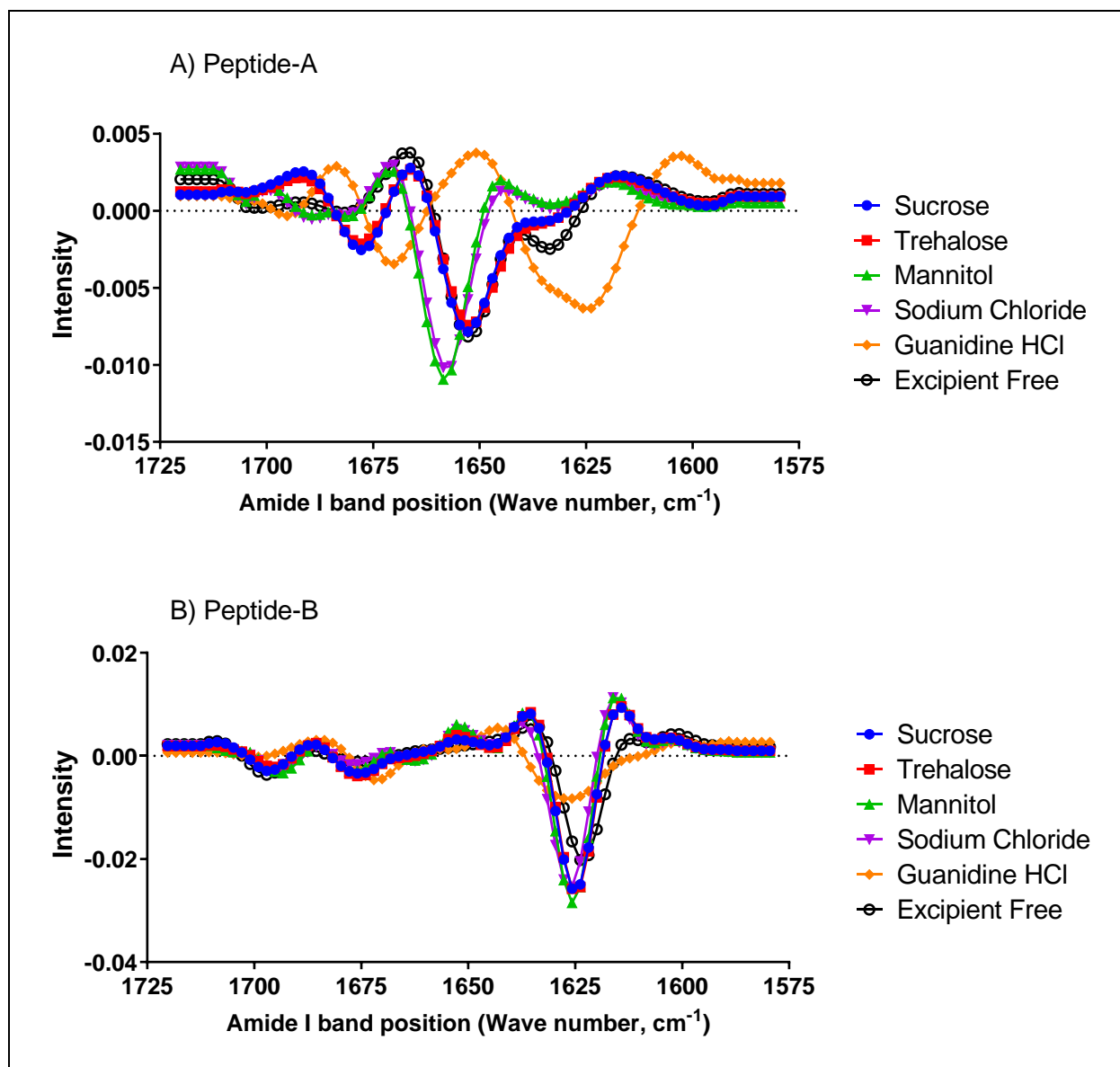


Figure 4.2. Solid-state FTIR spectra of (A) Peptide A (i.e., Ac-(A₄K)₃A-NH₂) and (B) Peptide B (i.e., Ac-KA₁₂K-NH₂) in lyophilized formulations show peaks characteristic of α -helix and β -sheet structures, respectively.

4.4.3 Solid physical form by PXRD

The PXRD diffractograms of sucrose, trehalose, and excipient free formulations of Peptide A and Peptide B showed featureless and broad spectra characteristic of amorphous material (Figure 4.3). In contrast, the diffractograms of the mannitol, sodium chloride and guanidine HCl formulations of the two peptides showed sharp peaks of varying magnitude, consistent with crystalline or partially crystalline solids (Figure 4.3). To ensure that mechanistic inferences are made for solid

materials of similar physical state, the remainder of this manuscript focuses on the amorphous formulations (i.e., sucrose, trehalose, excipient-free, Figure 4.3). Corresponding data for the crystalline or semi-crystalline formulations (i.e., mannitol, sodium chloride, guanidine HCl) are presented in Appendix C.

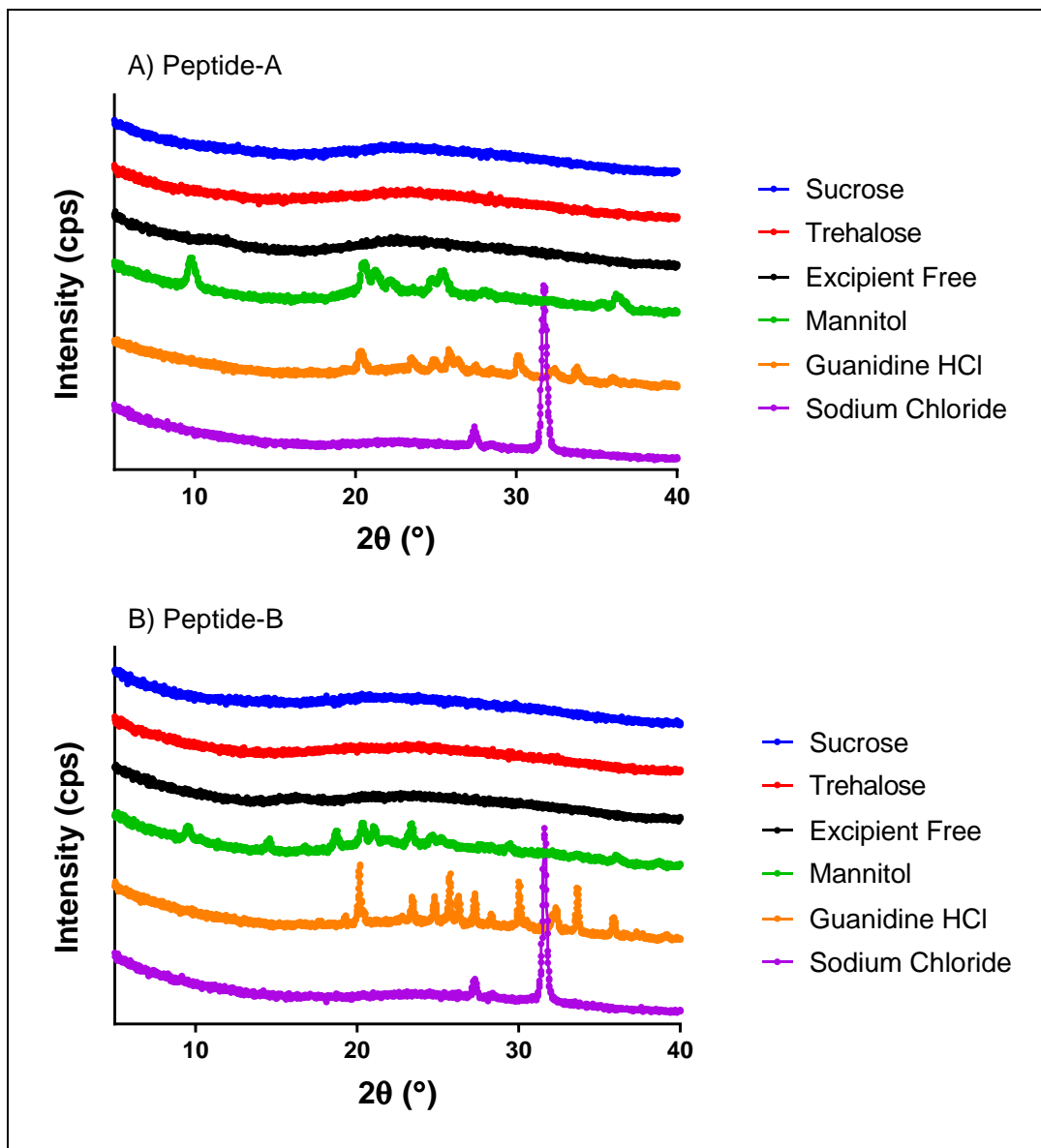


Figure 4.3. PXRD spectra of (A) Peptide A (i.e., Ac-(A₄K)₃A-NH₂) and (B) Peptide B (i.e., Ac-KA₁₂K-NH₂) lyophilized formulations show characteristic amorphous bands for sucrose, trehalose, excipient free formulations and crystalline bands for mannitol, sodium chloride, and guanidine HCl formulations, respectively.

4.4.4 Solution-state HDX-MS

Solution state HDX-MS of Peptide A formulations showed maximum deuteration (i.e., up to 14 Da, $\geq 95\%$ of theoretical maximum) within 2 min of the initiation of deuterium labeling (Figure 4.4A, Appendix C - Figure C1A). While minor differences in the extent of deuteration were observed among the formulations, the differences are not significant ($p > 0.10$, two-way ANOVA with Tukey's multiple comparison). When Peptide A formulations are compared with unstructured PDLA peptides of the same length, deuteration levels in Peptide A are significantly greater than those of the PDLA peptides for all formulations ($p < 0.0002$, two-way ANOVA with Tukey's multiple comparison). This may be due to the N-terminal modification in Peptide A, which may make the N-terminal amide hydrogen exchangeable and measurable. The result also suggests that, in solution, the deuteration of Peptide A is not hindered by its α -helical structure, consistent with facile unfolding and refolding.

In solution, Peptide B formulations showed lower deuteration than Peptide A (i.e., up to 8 Da, approx. 62% of theoretical maximum) even after 60 min of labeling, perhaps due to its more rigid β -sheet structure. The guanidine HCl and sodium chloride formulations of Peptide B showed significantly lower deuteration than the sucrose, trehalose and excipient-free formulations at 2 min of deuterium exposure; the differences were not significant at 60 min (Figure 4.4B, Appendix C - Figure C1B). When Peptide B formulations are compared with PDLA peptides of the same length, deuteration in Peptide B was significantly less than in the PDLA peptides ($p < 0.0001$, two-way ANOVA with Tukey's multiple comparison). This difference suggests that the β -sheet structure of Peptide B provides protection from exchange in solution, and that the extent of this protection is equivalent to approximately five hydrogen bonds (Figure 4.4B).

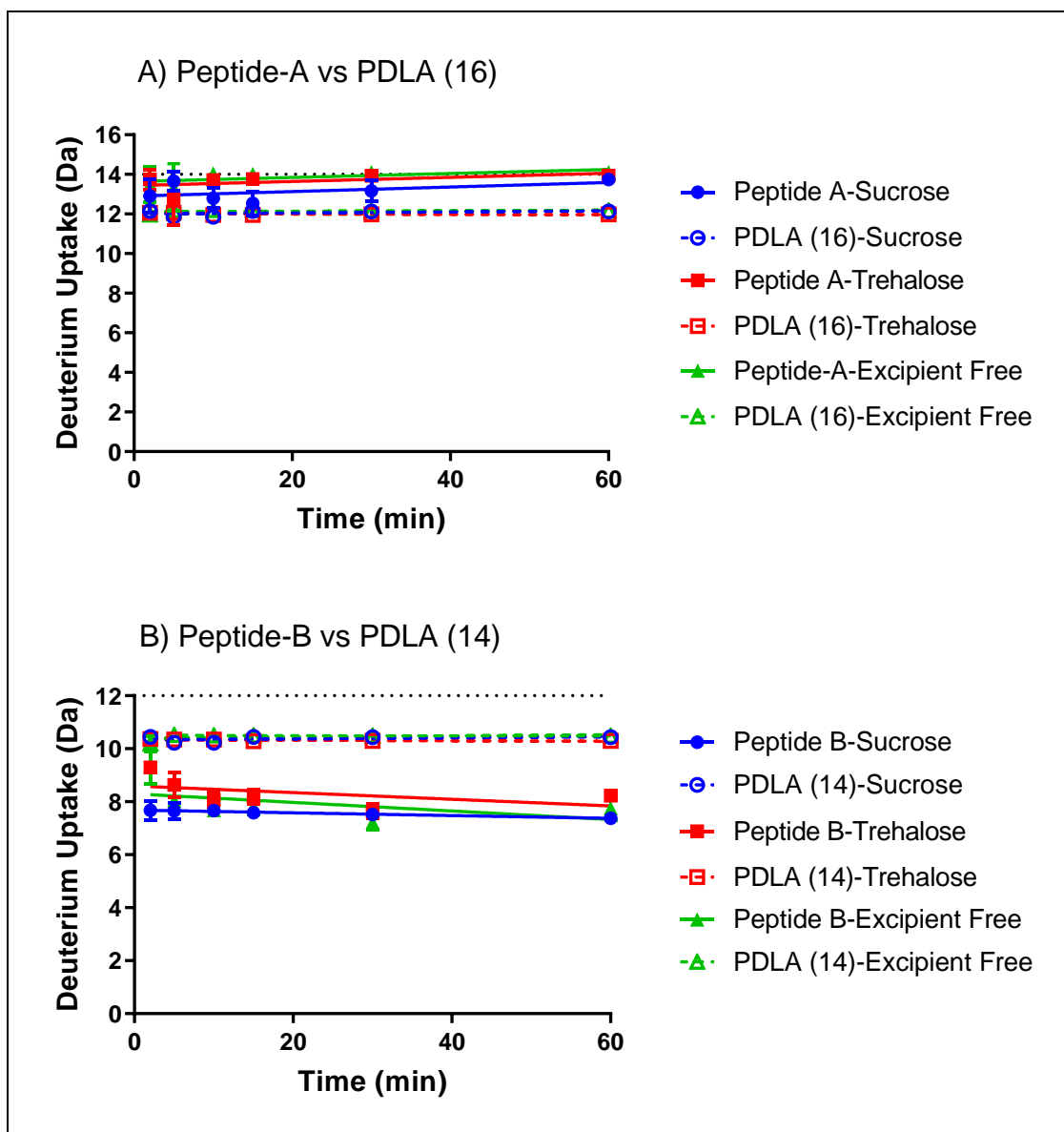


Figure 4.4. Solution HDX-MS of (A) Peptide A (i.e., Ac-(A₄K)₃A-NH₂) vs. PDLA (16 aa) and (B) Peptide B (i.e., Ac-KA₁₂K-NH₂) vs. PDLA (14 aa). The dotted line represents the maximum possible theoretical deuteration level, n=3, mean ± SD, error bars are not shown when smaller than the symbol.

4.4.5 Solid-state HDX-MS

Solid-state HDX-MS studies of Peptide A and Peptide B formulations were conducted at two RH conditions (i.e., 11% and 23% RH) (Figures 4.5, Appendix C - Figures C2 and C3). Deuterium incorporation in all amorphous Peptide A and Peptide B formulations increased monotonically with time (Figure 4.5). For a given formulation, deuterium incorporation for the

structured peptides (Peptides A, B) was less than or equal to that of the unstructured PLDA peptides for all formulations and both RH conditions (Figure 4.5). The differences between the structured and unstructured peptides were generally greater at the higher RH (23% vs. 11%, Figure 4.5A vs. 4.5B and Figure 4.5C vs. 4.5D). A detailed statistical comparison of the effects of RH and secondary structure on ssHDX-MS is presented below.

At 11% RH, the sucrose and trehalose formulations of Peptide A showed the lowest deuteration levels of the three amorphous formulations (D_{\max} = approximately 3.5 Da, Figure 4.5A). When compared to the corresponding formulations of PDLA peptides, the amorphous formulations of Peptide A showed somewhat lower deuteration (Figure 4.5A). Greater deuterium incorporation was observed for the excipient-free formulations of PDLA and Peptide A under these conditions, suggesting weaker intermolecular interactions than in the sucrose and trehalose formulations, and/or some loss of Peptide A structure. At 23% RH, deuterium incorporation for the trehalose formulation of Peptide A is approximately equal to that observed at 11% RH (Figure 4.5A, B), suggesting that the overall hydrogen bond environments are similar. In contrast, deuterium incorporation for both the sucrose and excipient-free formulations increases to ~ 6 Da at 23% RH (Figure 4.5B). That the excipient-free and sucrose formulations of Peptide A show similar deuteration at 23%RH suggests that the environments in the two formulations are similar, and may indicate that sucrose provides very little protection from exchange under these conditions, perhaps due to micro phase separation or partial crystallization. At 23% RH, both the sucrose and trehalose formulations of Peptide A show ~ 1.5 to 2 Da lower deuterium incorporation than their PDLA counterparts (Figure 4.5B). Interestingly, excipient-free formulations of Peptide A and PLDA show no differences in deuterium incorporation kinetics.

For Peptide B at 11% RH, the sucrose and trehalose formulations showed lower deuteration levels (~2.0 and 2.4 Da, respectively) than the excipient-free formulation (~ 4.8 Da) consistent with increased peptide-matrix interactions and/or more intact secondary structure (Figure 4.5C). At 23% RH, deuterium incorporation for Peptide B formulations and its PDLA controls was generally greater than at 11% RH, though the increase was less for the Peptide B formulations than for the PDLA controls (Figure 4.5C, D). Peptide B formulations also showed a smaller increase in deuterium incorporation with increasing RH than Peptide A formulations, suggesting that the hydrogen bonds in the β -sheet structure are more resistant to exchange than the α -helix hydrogen

bonds of Peptide A (Figure 4.5A-D). When compared to the deuteration levels in PDLA formulations, Peptide B formulations showed lower deuteration levels in all cases.

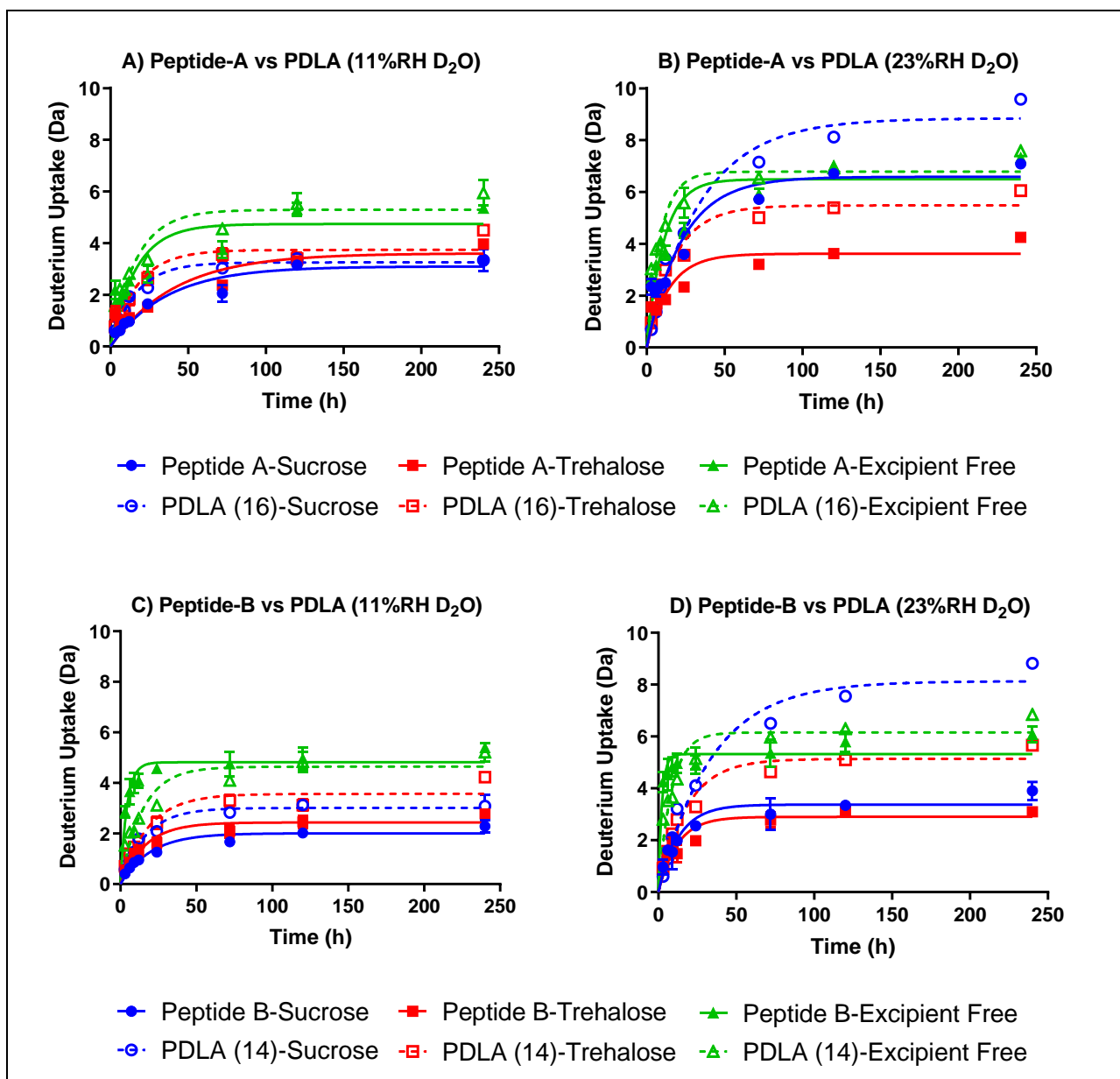


Figure 4.5. Solid-state HDX-MS of amorphous formulations (A) Peptide A (i.e., Ac-(A₄K)₃A-NH₂) vs PDLA (16 aa) at 11% RH D₂O, (B) Peptide A (i.e., Ac-(A₄K)₃A-NH₂) vs PDLA (16 aa) at 23% RH D₂O, (C) Peptide B (i.e., Ac-KA₁₂K-NH₂) vs PDLA (14 aa) at 11% RH D₂O and (D) Peptide B (i.e., Ac-KA₁₂K-NH₂) vs PDLA (14 aa) at 23% RH D₂O. n=3, mean ± SD, error bars are not shown when smaller than the symbol.

4.4.6 Effect of RH on ssHDX-MS

The kinetics of deuterium incorporation were fitted to the mono-exponential model (Eqn. 4.1) and the effects of RH on the regression parameters (D_{\max} , k) were evaluated statistically (Figure 4.6, Appendix C - Figure C4-C6; Appendix C - Tables C1, C2). D_{\max} values for all formulations of Peptide A increased when the RH was increased from 11% to 23% RH. The increase in D_{\max} was statistically significant for all formulations of Peptide A except the trehalose formulation ($p > 0.99$, two-way ANOVA with Sidak's multiple comparison test). Similarly, the D_{\max} values of Peptide B formulations increased when the RH was increased from 11% to 23%. However, this increase was smaller than for the Peptide A formulations. The increase in D_{\max} was statistically significant for all formulations of Peptide B except the trehalose and excipient-free formulations.

The exchange rate constants (k) also increased slightly with RH for the Peptide A formulations, but only the guanidine HCl formulation showed a statistically significant increase in the rate constant ($p=0.02$; Appendix C - Figure C6). For Peptide B, the rate constants increased with RH, but only the sodium chloride and guanidine HCl formulations showed a statistically significant increase ($p=0.03$; Appendix C - Figure C6). Increases in rate constants with RH were not significant for either Peptide A or Peptide B for any of the amorphous formulations except the excipient free formulation of Peptide B (Figures 4.5, 4.6).

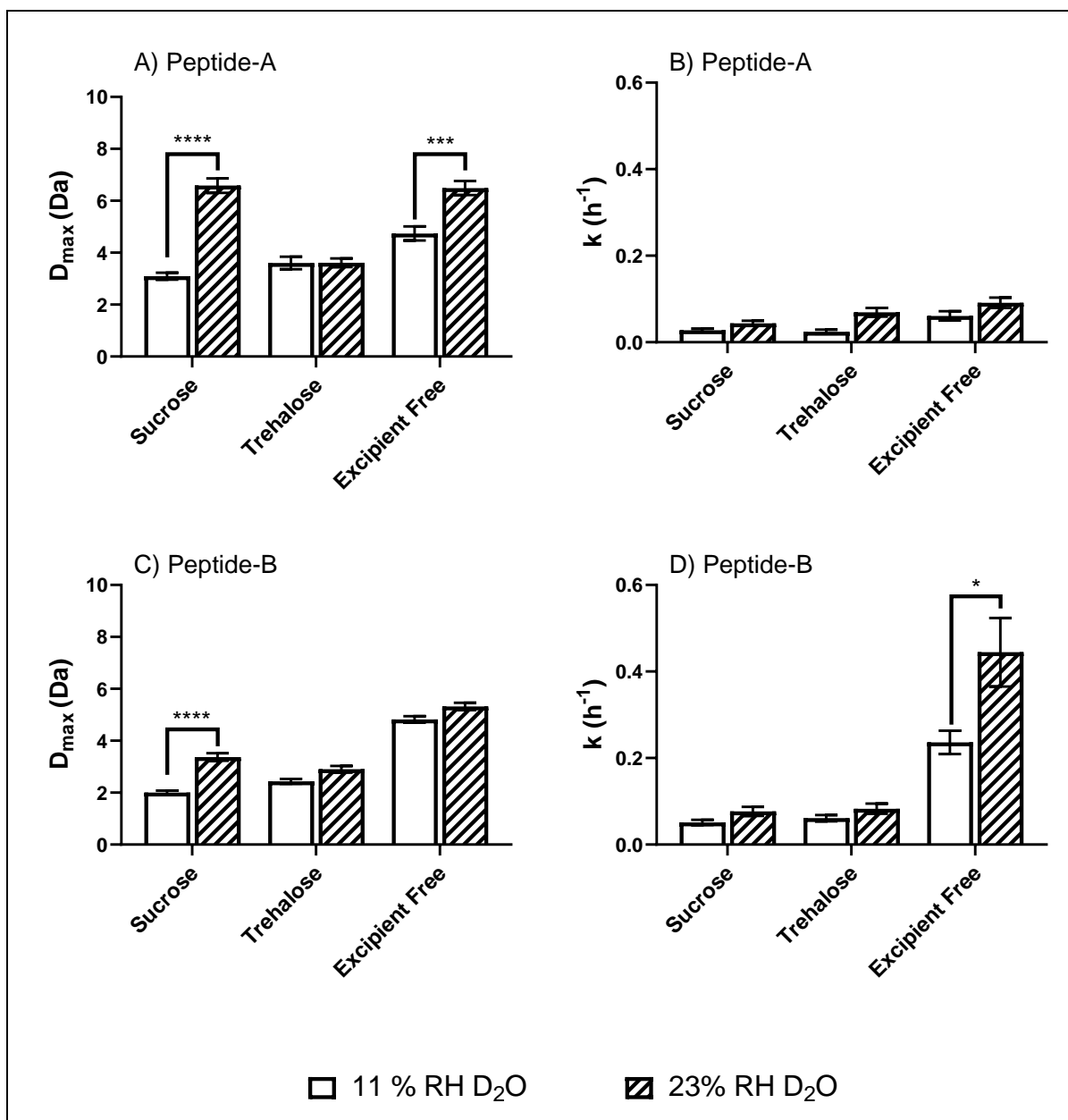


Figure 4.6. Comparison of ssHDX-MS kinetics of amorphous peptide formulations at 11% RH D₂O (open bar) and 23% RH D₂O (hatched bar). (A) D_{max} (Peptide A), (B) k (Peptide A), (C) D_{max} (Peptide B), and (D) k (Peptide B), n=3, mean ± SE; error bars not shown when less than the height of the symbol.

4.4.7 Effect of peptide secondary structure on ssHDX-MS

To quantify the effects of both structure and excipient type, the ssHDX-MS regression parameters for Peptide A and Peptide B were compared to those of unstructured PDLA peptides of similar length (Figures 4.7, 4.8 and Appendix C - Figures C7-C12). At 11% RH, Peptide A showed slightly

lower D_{\max} values than the 16aa PDLA peptide in the various formulations, but the difference was statistically significant only for the guanidine HCl formulation ($p < 0.0001$, two-way ANOVA with Sidak's multiple comparisons; Appendix C - Figure C11A, Appendix C - Table C3) and was not significant for any of the amorphous formulations (Figure 4.7A, Appendix C - Table C3). At 23% RH, D_{\max} values for Peptide A were less than those of the 16aa PDLA peptide in the same formulations, with the exception of the excipient free formulation (Figure 4.7B, Appendix C - Table C3). At 11% RH, D_{\max} values for the Peptide B formulations were significantly less than those of the corresponding 14aa PDLA formulations, except for the excipient-free formulation (Figure 4.7C, Appendix C - Table C4). The differences between the Peptide B and PDLA formulations were significant for all three formulations at 23% RH (Figure 4.7D, Appendix C - Table C4).

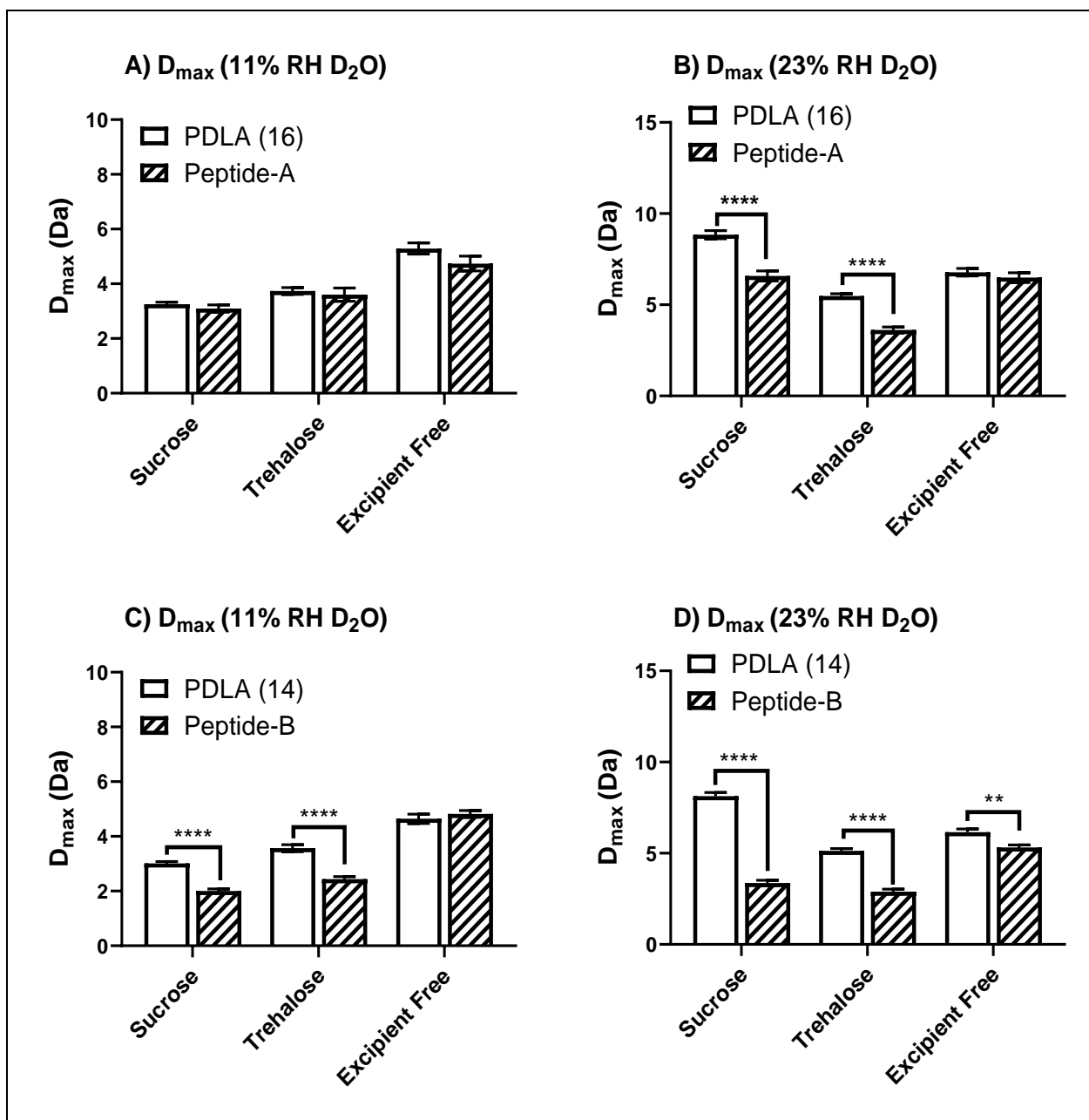


Figure 4.7. Comparison of maximum deuterium incorporation (D_{\max}) in ssHDX-MS for unstructured PDLA peptides (open bar) vs structured Peptide A (α -helical) or Peptide B (β -sheet) amorphous formulations (hatched bar). (A) 16aa PDLA vs Peptide A (D_{\max} at 11% RH D_2O), (B) 16aa PDLA vs Peptide A (D_{\max} at 23% RH D_2O), (C) 14aa PDLA vs Peptide B (D_{\max} at 11% RH D_2O), and (D) 14aa PDLA vs Peptide B (D_{\max} at 23% RH D_2O). $n=3$, mean \pm SE; error bars not shown when less than the height of the symbol.

The effect of peptide secondary structure on the exchange rate constants (k) was also evaluated (Figures 4.8, Appendix C - Figures C7-C10, C12; Appendix C - Tables C5, C6). At 11% RH, the

k values for Peptide A were slightly less than those of 16aa PDLA in the sucrose and trehalose formulations, though the differences were not significant (Figure 4.8A). At 23% RH, all Peptide A formulations had k values comparable to those of 16aa PDLA in the corresponding formulations (Figure 4.8B).

For Peptide B at 11% RH, the rate constants for the sucrose and trehalose formulations were comparable to those of 14aa PDLA in the corresponding formulations (Figure 4.8C). However, the value for the excipient-free formulation of Peptide B was significantly greater than in the corresponding 14aa PDLA formulations (Figure 4.8C). A similar trend was observed for the Peptide B formulations at 23% RH (Figure 4.8D).

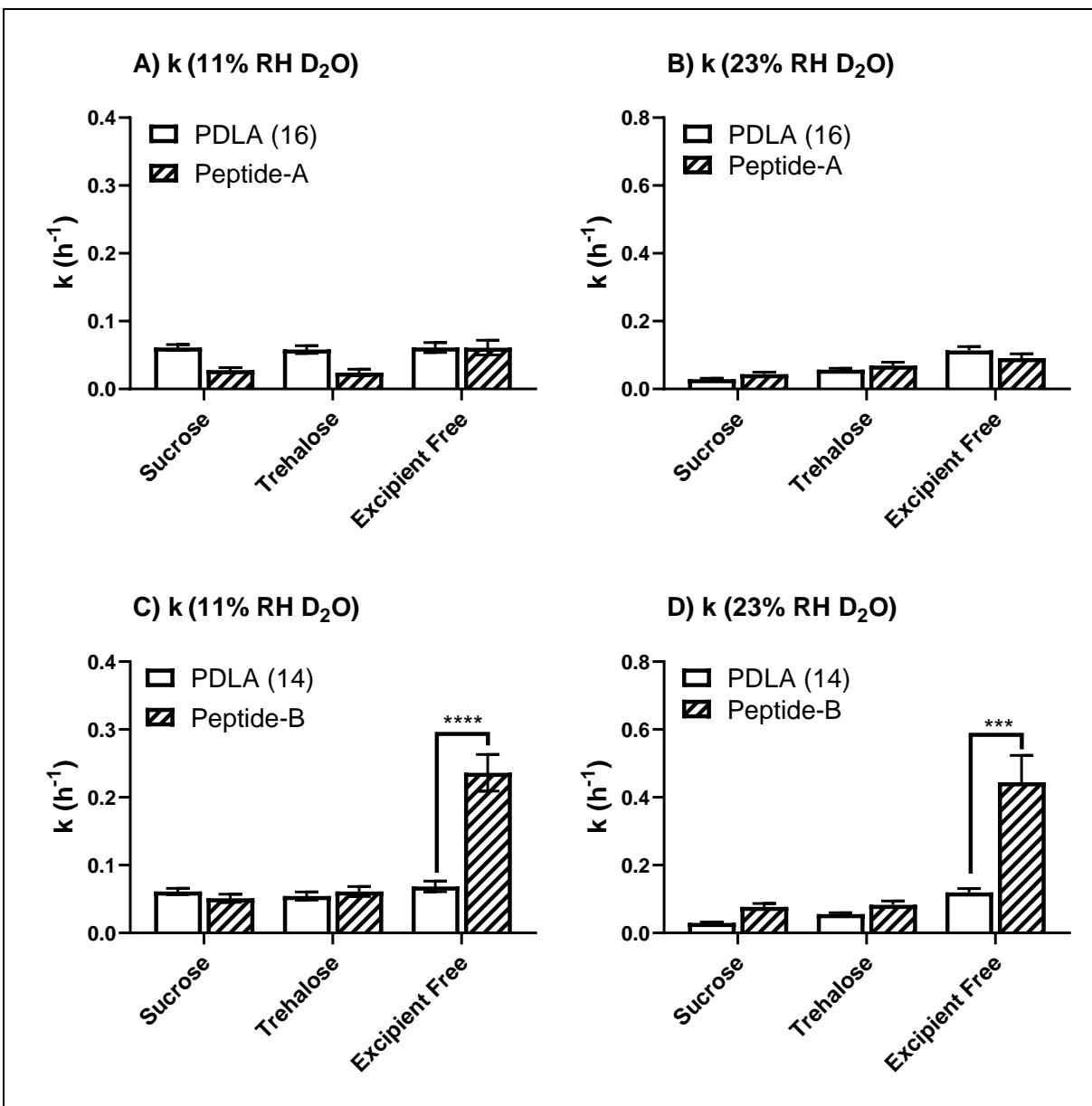


Figure 4.8. Comparison of ssHDX-MS kinetics of unstructured PDLA (open bar) vs structured Peptide A or Peptide B amorphous formulations (hatched bar). (A) PDLA vs Peptide A (k at 11% RH D₂O), (B) PDLA vs Peptide A (k at 23% RH D₂O), (C) PDLA vs Peptide B (k at 11% RH D₂O), and (D) PDLA vs Peptide B (k at 23% RH D₂O), $n=3$, mean \pm SE; error bars not shown when less than the height of the symbol.

4.5 Discussion

The studies presented here have explored the effects of secondary structure on ssHDX-MS using model peptides. The results demonstrate that both peptide structure and interactions between the peptide and the matrix provide protection from exchange in ssHDX-MS. Unstructured PDLA peptides were protected from exchange in ssHDX-MS to an extent that depended on solid composition and the relative humidity of D₂O vapor (RH) (Figure 4.5), as reported previously.²⁶ The Linderstrom-Lang model, widely used to describe solution HDX, predicts that such unstructured peptides would not be protected from exchange at all. In fact, the PDLA peptides are not protected from exchange in solution on the time scale of these experiments (Figure 4.4). The results further demonstrate that peptide secondary structure can provide additional protection from exchange in ssHDX-MS. Peptide A and Peptide B have α -helical and β -sheet secondary structure, respectively, both in solution and in lyophilized solids (Figures 4.1, 4.2). Peptides A and B showed greater protection from exchange in ssHDX than unstructured PDLA peptides of similar length in identical formulations (Figure 4.5). This finding demonstrates that higher order structure confers protection from exchange in ssHDX-MS, as asserted by the Linderstrom-Lang model for proteins in solution. At a broad qualitative level, then, the results demonstrate that both peptide structure and matrix interactions can contribute to the protection from exchange observed in ssHDX-MS.

The extent of deuterium incorporation can be used to quantify the protected amide bonds in each formulation, and to make comparisons. The total deuterium uptake for a given peptide in solution is a measure of the maximum number of amide groups that can be deuterated and quantified (Figure 4.4). Because the peptide undergoes back exchange during MS analysis, this value is somewhat less than total number of amide bonds. For example, the 16aa PDLA peptide showed a total deuterium uptake of 12 in solution (Figure 4.4A), suggesting that three of its amide bonds have undergone back exchange. We assume that the maximum deuterium uptake measured in solution is equal to the maximum number of amide groups that can be protected from exchange and subsequently detected in ssHDX-MS. The difference between this value and the plateau level of deuteration in ssHDX-MS is a measure of the number of amide groups that are protected under particular conditions. For example, in the ssHDX-MS experiment at 23% RH, the 16aa PDLA peptide had a plateau of 5.5 deuterons incorporated in the trehalose formulation (Figure 4.5B, Appendix C - Table C3). The 16aa PDLA peptide then has an average of 6.5 protected amide

groups (i.e., 12 – 5.5) under these conditions, corresponding to protection of ~58% of the total exchangeable amide groups.

Table 4.1 shows the number of protected amide bonds for the four model peptides in the various formulations, as measured in ssHDX-MS studies at 11% and 23% RH (Figure 4.5). Since the number of exchangeable amide hydrogens differed somewhat for Peptides A and B and the corresponding PDLA controls (Table 4.1, Row 1), the values are also reported as percentages.

Table 4.1. Number of protected amide bonds for model peptides in various formulations, as measured in ssHDX-MS studies at 11% and 23% RH

Row		Peptide A	PDLA 16	Peptide B	PDLA 14
1	Number of exchangeable amide hydrogens (Figure 4.4, Appendix C - Figure C1)	14	12	8	10
Protected amide groups, ssHDX-MS at 11% RH (Figure 4.5A, C)					
2	Sucrose formulation ^{a,b}	10.9 (78%)	8.7 (72%)	6.0 (75%)	7.0 (70%)
3	Trehalose formulation	10.4 (74%)	8.3 (69%)	5.6 (70%)	6.4 (64%)
4	Excipient-free formulation	9.3 (66%)	6.7 (56%)	3.2 (40%)	5.4 (54%)
Protected amide groups, ssHDX-MS at 23% RH (Figure 4.5B, D)					
5	Sucrose formulation	7.4 (53%)	3.2 (27%)	4.6 (58%)	1.9 (19%)
6	Trehalose formulation	10.4 (74%)	6.5 (54%)	5.1 (64%)	4.9 (49%)
7	Excipient-free formulation	7.5 (54%)	5.2 (43%)	2.7 (34%)	3.8 (38%)
^a Number of protected amide groups is the difference between maximum deuteration levels in solution (D_{max} , Figure 4.4) and in ssHDX-MS (Figure 4.5). Approximate error +/- (0.5) (see Figures. 4.4, 4.5, Appendix C - Tables C3, C4). ^b Protected amide groups as a percentage of number of exchangeable amide hydrogens (Row 1) shown in parentheses.					

In ssHDX-MS of Peptide A at 11% RH, approximately 10 of the 14 amide bonds are protected in all three formulations (Table 4.1, Rows 2-4). The value is somewhat lower for the excipient-free formulation than for the sucrose and trehalose formulations, suggesting greater structural perturbation and/or weaker interactions with the matrix. Peptide A is a 16aa α -helical peptide, and thus has 12 intramolecular hydrogen bonds if the helix is fully intact (see Appendix C - Figure C13). Approximately 10 amide bonds are protected at 11% RH, suggesting that at least two of the hydrogen bonds of the α -helix are not protected. Since some protection may be provided by intermolecular interactions with the matrix, it is possible that more than two α -helix hydrogen bonds are not protected, and the value thus is a minimum. The number of protected amide hydrogens in Peptide A is 5-10% greater than in the PDLA control at 11% RH, providing a measure of the extent of protection provided by the helical structure of Peptide A. This difference represents the net increase in protection, since some intermolecular hydrogen bonds that protect PDLA may be lost in forming the structural hydrogen bonds of Peptide A. At 23% RH, the number of protected hydrogen bonds in the sucrose and excipient-free formulations is less than at 11% RH (Table 4.1, Rows 5-7), as expected due to the increased D₂O activity in the solid samples. However, the trehalose formulation shows no such decrease, suggesting better retention of structure and/or stronger interactions with the matrix. Differences between Peptide A and its PDLA control with regard to the number of protected amide bonds are generally greater at 23% RH than at 11% RH (Table 4.1, Rows 2-4 vs. Rows 5-7). This may reflect greater disruption of intermolecular hydrogen bonds in PDLA.

In the carbohydrate-based formulations (i.e., sucrose and trehalose), amide-hydroxyl hydrogen bonds probably dominate the intermolecular interactions between the peptide and the matrix. These intermolecular hydrogen bonds can help protect the peptide from exchange. In contrast, the intramolecular hydrogen bonds that contribute to peptide structure are amide-amide hydrogen bonds; these, too, can help protect the peptide from exchange. Amide-amide hydrogen bonds are generally somewhat stronger than amide-hydroxyl hydrogen bonds,³³ though their strength can vary with the medium^{34,35} and within the secondary structure.³⁶ For example, in solution, amide-amide hydrogen bonds near the termini of an α -helix are generally weaker than those near its center.³⁶ It is reasonable to expect that, in the carbohydrate-based formulations, the increase in deuterium uptake with increasing RH is due to disruption of some of these weaker bonds. The excipient-free formulations lack the abundant excipient hydroxyl groups of the carbohydrate-based

formulations. Peptide A and Peptide B are comprised primarily of alanine, an amino acid that does not have hydrogen bond donor or acceptor groups in its side chain. In the excipient-free formulations then, intermolecular interactions probably involve amide groups on neighboring peptide molecules, though interactions involving the lysine groups cannot be ruled out. The lower number of protected amide groups in the excipient-free formulations of Peptide A (Table 4.1, Rows 4, 7) suggests that, while amide-amide hydrogen bonds are generally stronger than amide-hydroxyl hydrogen bonds, any such interactions in the excipient-free formulations provide less protection, perhaps because there are fewer of them.

Peptide B has 14 amide bonds, at least 13 of which are expected to be deuterated and measurable (i.e., resistant to back exchange) in solution (see Appendix C - Figure C13). Only 8 sites of deuteration are detected in solution (Figure 4.4, Table 4.1). This suggests that the amide bonds are not fully accessible, and that some residual β -sheet structure remains, or that Peptide B does not contain the expected number of amide bonds (e.g., due to non-amide linkages). Peptide B has CD and FTIR spectra consistent with β -sheet secondary structure (Figures 4.1, 4.2B). If the β -sheet structure is the result of intermolecular interactions, it may represent as many as 14 inter-strand hydrogen bonds. If instead the β -sheet structure is the result of intramolecular interactions (e.g., a β -hairpin), a maximum of 6 intra-strand hydrogen bonds could be formed (see Appendix C - Figure C13). Thus, unlike Peptide A, Peptide B presents some uncertainties in the number of amide bonds and in the theoretical number of hydrogen bonds in its secondary structure. Such uncertainty would also be expected for larger proteins, in which the theoretical number of structural hydrogen bonds may not be known precisely, though biophysical assays can give some indication of secondary structure. We assume that the maximum number of structural hydrogen bonds that can be formed and measured in Peptide B is equal to 8, the maximum deuteration measured in solution.

In Peptide B at 11% RH, the number of protected amide bonds ranges from 3.2 to 6.0, amounting to 40 to 75% of the experimentally observed maximum value of 8 (Table 4.1, Rows 2-4). The value is least for the excipient-free formulation, which suggests that secondary structure and/or matrix interactions are poorest in this formulation. For the sucrose formulation, the result suggests that at least two of the maximum of 8 structural hydrogen bonds have been disrupted. As with Peptide A, this should be regarded as a minimum. Similar inferences can be made for the trehalose and excipient-free formulations. As with Peptide A, the number of protected amide bonds is 5-10% greater for Peptide B than for its PDLA control at 11%RH in both the sucrose and trehalose

formulations, again providing a measure of the net protection from exchange provided by secondary structure. Interestingly, in the excipient-free formulation, the PDLA control shows greater protection from exchange than Peptide B (Table 4.1, Row 4). This suggests that structure provides no additional protection in this formulation, perhaps because both inter- and intramolecular hydrogen bonding interactions involve amide-amide interactions. At 23% RH, the number of protected amide bonds was less than at 11%RH for all three formulations (Table 4.1, Rows 2-6), as expected. For the sucrose and trehalose formulations, differences between Peptide B and its PDLA control are greater at 23% RH than at 11% RH (Table 4.1, Rows 2, 3, 5, 6), which may reflect disruption of intermolecular amide-hydroxyl hydrogen bonds with increasing D₂O activity.

A similar approach can be used to interpret ssHDX-MS data for large therapeutic proteins which can contain hundreds of amino acids. The maximum number of exchangeable amide hydrogens can be measured in solution HDX-MS experiments under denaturing conditions (Figure 4.4, Appendix C - Figure C1). This value also represents an upper bound on the number of intramolecular structural hydrogen bonds that can be formed and measured. The extent of deuterium incorporation then can be measured in ssHDX-MS experiments for solids of interest (D_{\max} , Figure 4.7). D_{\max} can be determined using non-linear regression of kinetic data, as reported here, or estimated using deuterium incorporation at a single time point of deuterium exposure, provided that measurement is made at sufficiently long time (e.g., 48-72 h). Solid formulations containing PDLA, at comparable weight percentage to the protein of interest, can be used as unstructured controls, allowing an estimate of the percentage protection provided by protein structure, as in Table 4.1. Polydisperse PDLA with MW 1000-5000 is inexpensive and readily available, and a single abundant chain length can be selected easily on MS analysis for use as a control. To allow meaningful comparisons of the number of protected amide bonds, replicate measurements of deuterium incorporation should be performed (Figure 4.7). For some proteins, it also may be possible to estimate the number of structural hydrogen bonds using the protein sequence structures in the Protein Data Bank (PDB). For example, myoglobin has eight α -helices connected by loops or turns. The number and sequence of amino acids in each of these helices are available from the protein sequence structures in the PDB. Combining this information with the hydrogen bonding pattern in helices, the maximum number of structural hydrogen bonds can be estimated (Appendix C - Table C7). Based on this information, a table quantifying the protected

amide bonds can be generated for a specific protein in various solids and compared to controls on a percentage basis. An example is presented for myoglobin in Appendix C - Table C8.

4.6 Conclusions

The studies reported here have evaluated the effects of peptide secondary structure on ssHDX-MS. An α -helical model (Peptide A) and a β -sheet model (Peptide B) were lyophilized in various solid formulations. Deuterium incorporation was measured in ssHDX-MS and compared with unstructured PDLA peptides in the same formulations. At a qualitative level, the results demonstrate that both peptide secondary structure and interactions with the solid matrix contribute to the protection from exchange observed in ssHDX-MS. A quantitative data analysis and interpretation method is presented, in which the number of protected amide bonds is calculated as the difference between the maximum deuterium incorporation in solution and in solid samples during ssHDX-MS. The method allows quantitative comparison among solid samples, and between samples and controls.

4.7 Supporting information

Additional supporting information for this chapter is available in Appendix C: (i) solution HDX-MS of Peptide-A (i.e., Ac-(A₄K)₃A-NH₂) vs PDLA (16 aa) and Peptide-B (i.e., Ac-KA₁₂K-NH₂) vs PDLA (14 aa) (Figure C1), (ii) solid-state HDX-MS of crystalline formulations of Peptide-A, Peptide-B vs PDLA at 11% RH D₂O, and 23% RH D₂O (Figure C2), (iii) solid-state HDX-MS of Peptide-A, and Peptide-B at 11% RH D₂O and 23% RH D₂O (Figure C3), (iv) comparison of ssHDX-MS of Peptide A formulations at 11% RH D₂O and 23% RH D₂O (Figure C4), (v) comparison of ssHDX-MS of Peptide B formulations at 11% RH D₂O and 23% RH D₂O (Figure C5), (vi) comparison of ssHDX-MS kinetics of Peptide A and Peptide B crystalline formulations at 11% RH D₂O and 23% RH D₂O (Figure C6), (vii) comparison of ssHDX-MS of unstructured PDLA (16 aa) vs α -helical Peptide A (Figures C7-C8), (viii) comparison of ssHDX-MS of unstructured PDLA (14 aa) vs β -sheet Peptide B (Figures C9-C10), (ix) comparison of ssHDX-MS kinetics of unstructured PDLA peptides vs structured Peptide A (α -helical) or Peptide B (β -sheet) crystalline formulations (Figures C11-C12), (x) Possible structures and H-bond patterns of Peptides A and B, (xi) effect of RH on the ssHDX-MS kinetics of Peptide A and Peptide B formulations

(Table C1-C2), xi) effect of secondary structure on the ssHDX-MS kinetics of Peptide A or Peptide B formulations in comparison with corresponding unstructured PDLA peptides (Table C3-C6), xii) calculation of approximate number of structural H-bonds in myoglobin using protein sequence structure information from PDB (Table C7), and xiii) number of protected amide bonds for myoglobin in various formulations, as measured in ssHDX-MS studies (Table C8).

4.8 References

- (1) Engen, J. R. Analysis of protein conformation and dynamics by hydrogen/deuterium exchange MS. *Anal. Chem.* **2009**, *81*, 7870-7875.
- (2) Masson, G. R.; Burke, J. E.; Ahn, N. G., *et al.* Recommendations for performing, interpreting and reporting hydrogen deuterium exchange mass spectrometry (HDX-MS) experiments. *Nat. Methods.* **2019**, *16* (7), 595-602.
- (3) Katta, V.; Chait, B. T.; Carr, S. Conformational changes in proteins probed by hydrogen-exchange electrospray-ionization mass spectrometry. *Rapid Commun. Mass Spectrom.* **1991**, *5* (4), 214-217.
- (4) Zhang, Z.; Smith, D. L. Determination of amide hydrogen exchange by mass spectrometry: A new tool for protein structure elucidation. *Protein Sci.* **1993**, *2* (4), 522-531.
- (5) Ramirez-Sarmiento, C. A.; Komives, E. A. Hydrogen-deuterium exchange mass spectrometry reveals folding and allostery in protein-protein interactions. *Methods.* **2018**, *144*, 43-52.
- (6) Khanal, A.; Pan, Y.; Brown, L. S., *et al.* Pulsed hydrogen/deuterium exchange mass spectrometry for time-resolved membrane protein folding studies. *J. Mass Spectrom.* **2012**, *47* (12), 1620-1626.
- (7) Huang, R. Y.-C.; Chen, G. Higher order structure characterization of protein therapeutics by hydrogen/deuterium exchange mass spectrometry. *Anal. Bioanal. Chem.* **2014**, *406* (26), 6541-6558.
- (8) Baerga-Ortiz, A.; Hughes, C. A.; Mandell, J. G., *et al.* Epitope mapping of a monoclonal antibody against human thrombin by H/D-exchange mass spectrometry reveals selection of a diverse sequence in a highly conserved protein. *Protein Sci.* **2002**, *11* (6), 1300-1308.
- (9) Tian, Y.; Huang, L.; Ruotolo, B. T., *et al.* Hydrogen/deuterium exchange-mass spectrometry analysis of high concentration biotherapeutics: Application to phase-separated antibody formulations. *MAbs.* **2019**, *11* (4), 779-788.

- (10) Harrison, R. A.; Engen, J. R. Conformational insight into multi-protein signaling assemblies by hydrogen–deuterium exchange mass spectrometry. *Curr. Opin. Struct. Biol.* **2016**, *41*, 187-193.
- (11) Deng, B.; Lento, C.; Wilson, D. J. Hydrogen deuterium exchange mass spectrometry in biopharmaceutical discovery and development– A review. *Anal. Chim. Acta.* **2016**, *940*, 8-20.
- (12) Masson, G. R.; Jenkins, M. L.; Burke, J. E. An overview of hydrogen deuterium exchange mass spectrometry (HDX-MS) in drug discovery. *Expert Opin. Drug Discovery.* **2017**, *12* (10), 981-994.
- (13) Mensink, M. A.; Frijlink, H. W.; van der Voort Maarschalk, K., *et al.* How sugars protect proteins in the solid state and during drying (review): Mechanisms of stabilization in relation to stress conditions. *Eur. J. Pharm. Biopharm.* **2017**, *114*, 288-295.
- (14) Wang, W. Lyophilization and development of solid protein pharmaceuticals. *Int. J. Pharm.* **2000**, *203* (1), 1-60.
- (15) Moorthy, B. S.; Iyer, L. K.; Topp, E. M. Mass spectrometric approaches to study protein structure and interactions in lyophilized powders. *J. Vis. Exp.* **2015**, (98), No. e52503.
- (16) Moorthy, B. S.; Zarraga, I. E.; Kumar, L., *et al.* Solid-state hydrogen–deuterium exchange mass spectrometry: correlation of deuterium uptake and long-term stability of lyophilized monoclonal antibody formulations. *Mol. Pharmaceutics.* **2018**, *15* (1), 1-11.
- (17) Moorthy, B. S.; Schultz, S. G.; Kim, S. G., *et al.* Predicting protein aggregation during storage in lyophilized solids using solid state amide hydrogen/deuterium exchange with mass spectrometric analysis (ssHDX-MS). *Mol. Pharmaceutics.* **2014**, *11* (6), 1869-1879.
- (18) Kumar, L.; Chandrababu, K. B.; Balakrishnan, S. M., *et al.* Optimizing the formulation and lyophilization process for a fragment antigen binding (Fab) protein using solid-state hydrogen–deuterium exchange mass spectrometry (ssHDX-MS). *Mol. Pharmaceutics.* **2019**, *16* (11), 4485-4495.
- (19) Wilson, N. E.; Mutukuri, T. T.; Zemlyanov, D. Y., *et al.* Surface composition and formulation heterogeneity of protein solids produced by spray drying. *Pharm. Res.* **2020**, *37* (1), 14.
- (20) Wilson, N. E.; Topp, E. M.; Zhou, Q. T. Effects of drying method and excipient on structure and stability of protein solids using solid-state hydrogen/deuterium exchange mass spectrometry (ssHDX-MS). *Int. J. Pharm.* **2019**, *567*, 118470.

- (21) Moussa, E. M.; Wilson, N. E.; Zhou, Q. T., *et al.* Effects of drying process on an IgG1 monoclonal antibody using solid-state hydrogen deuterium exchange with mass spectrometric analysis (ssHDX-MS). *Pharm. Res.* **2018**, *35* (1), 12.
- (22) Hvidt, A.; Nielsen, S. O. Hydrogen exchange in proteins. *Adv. Protein Chem.* **1966**, *21*, 287-386.
- (23) Wales, T. E.; Engen, J. R. Hydrogen exchange mass spectrometry for the analysis of protein dynamics. *Mass Spectrom. Rev.* **2006**, *25* (1), 158-170.
- (24) Englander, S. W.; Kallenbach, N. R. Hydrogen exchange and structural dynamics of proteins and nucleic acids. *Q. Rev. Biophys.* **1983**, *16* (4), 521-655.
- (25) Weis, D. D., Analysis of disordered proteins by hydrogen exchange mass spectrometry. In *Hydrogen Exchange Mass Spectrometry of Proteins: Fundamentals, Methods, and Applications*, Weis, D. D., Ed. John Wiley & Sons: **2015**; pp 295-321.
- (26) Kammari, R.; Topp, E. M. Solid-state hydrogen-deuterium exchange mass spectrometry (ssHDX-MS) of lyophilized poly-D, L-alanine. *Mol. Pharmaceutics.* **2019**, *16*, 2935-2946.
- (27) Marqusee, S.; Robbins, V. H.; Baldwin, R. L. Unusually stable helix formation in short alanine-based peptides. *Proc. Natl. Acad. Sci.* **1989**, *86* (14), 5286-5290.
- (28) Blondelle, S. E.; Forood, B.; Houghten, R. A., *et al.* Polyalanine-based peptides as models for self-associated β -pleated-sheet complexes. *Biochemistry.* **1997**, *36* (27), 8393-8400.
- (29) Chakrabartty, A.; Kortemme, T.; Baldwin, R. L. Helix propensities of the amino acids measured in alanine-based peptides without helix-stabilizing side-chain interactions. *Protein Sci.* **1994**, *3* (5), 843-852.
- (30) Bakshi, K.; Liyanage, M. R.; Volkin, D. B., *et al.*, Circular Dichroism of peptides. In *Therapeutic Peptides: Methods and Protocols, Methods in Molecular Biology*, Nixon, A. E., Ed. Humana Press: **2014**; Vol. 1088, pp 247-253.
- (31) Barth, A. Infrared spectroscopy of proteins. *Biochim. Biophys. Acta, Bioenerg.* **2007**, *1767* (9), 1073-1101.
- (32) Bakshi, K.; Liyanage, M. R.; Volkin, D. B., *et al.*, Fourier transform infrared spectroscopy of peptides. In *Therapeutic Peptides: Methods and Protocols, Methods in Molecular Biology*, Nixon, A. E., Ed. Humana Press: **2014**; Vol. 1088, pp 255-269.
- (33) Habermann, S. M.; Murphy, K. P. Energetics of hydrogen bonding in proteins: A model compound study. *Protein Sci.* **1996**, *5*, 1229-1239.

- (34) Sheu, S.-Y.; Yang, D.-Y.; Selzle, H., *et al.* Energetics of hydrogen bonds in peptides. *Proc. Natl. Acad. Sci.* **2003**, *100* (22), 12683-12687.
- (35) Pace, C. N. Energetics of protein hydrogen bonds. *Nat. Struct. Mol. Biol.* **2009**, *16* (7), 681-682.
- (36) Fierz, B.; Reiner, A.; Kiefhaber, T. Local conformational dynamics in α -helices measured by fast triplet transfer. *Proc. Natl. Acad. Sci.* **2009**, *106* (4), 1057-1062.

CHAPTER 5. CONCLUSIONS

There is an unmet need for a high-resolution analytical technique that can probe protein structure and conformation in solid powders to aid the pharmaceutical development process of solid-state proteins. Solid-state hydrogen-deuterium exchange mass spectrometry (ssHDX-MS) has the potential to fill this gap and has proven to be reliable in screening formulations according to their storage stability. Previously reported studies from our group demonstrated that ssHDX-MS kinetics correlate to long-term stability. However, the fundamental mechanisms and the factors contributing to ssHDX-MS kinetics are not clear to date. The research conducted in this dissertation has addressed these limitations and presented a mechanistic interpretation of ssHDX-MS of proteins.

Chapter 1 discussed the background information about therapeutic protein formulations, possible degradation pathways in the solid-state, and analytical techniques that are used to characterize proteins. It also discussed the theory and applications of hydrogen-deuterium exchange mass spectrometry in solution and the solid-state followed by the hydrogen-deuterium exchange models and their limitations.

Chapter 2 presented research aiming to quantify the contribution of peptide-matrix interactions to ssHDX-MS kinetics in the absence of higher-order structure. Poly-D, L-alanine (PDLA) peptides were used as a model for unstructured peptides. ssHDX-MS studies as a function of D_2O relative humidity revealed the dependence of deuterium incorporation on the excipient type and $D_2O_{(g)}$ activity. A reversible pseudo-first-order kinetic model was presented for the deuterium uptake in ssHDX-MS in which the forward reaction rate depended linearly on the activity of $D_2O_{(g)}$. The model was in agreement with the PDLA experimental data and provided a first in-depth insight into the mechanism of ssHDX-MS.

The research reported in Chapter 3 evaluated pre-hydration effects and the reversibility of chemical hydrogen-deuterium exchange reaction in the solid-state. Lyophilized PDLA peptides were used for these studies. The pre-hydration of PDLA samples prior to deuterium labeling did not affect the deuterium incorporation kinetics of the amorphous samples. However, according to the powder X-ray diffraction studies, an increase in crystallinity was observed for the samples containing crystallizing excipients after pre-hydration and the plateau level deuterium uptake reduced when

compared with controls not subjected to pre-hydration. The reversibility studies revealed hysteresis in the loss of deuterium label when compared with the forward reaction suggesting that the ssHDX is reversible for all formulations and conditions studied here and that the forward and reverse processes differ. Deuterium removal rate and extent depended on the de-labeling relative humidity, and the rate constants were quantified using a first-order kinetic model applicable under sink conditions. The steady-state plateau deuteration levels were also related to the forward and reverse reaction rate constants. These findings further support the mechanistic interpretation of ssHDX as a reversible first-order process, as presented in Chapter 2.

Therapeutic proteins often contain significant higher order structure that complicates the interpretation of ssHDX-MS kinetics. The mechanistic model proposed in Chapter 2 successfully explains the deuterium uptake kinetics of unstructured PDLA peptides. However, the model does not account for the effects of peptide structure on deuterium uptake kinetics. Therefore, the research presented in Chapter 4 evaluated the contribution of peptide secondary structure to ssHDX-MS kinetics using PDLA analog peptides with either α -helix or β -sheet structures. The findings suggest that both the secondary structure and peptide-matrix interactions contribute to deuterium incorporation kinetics. The relative contributions of peptide structure and peptide-matrix interactions were quantified, and a comprehensive data analysis method that can be applied to larger therapeutic proteins was presented.

ssHDX-MS is a promising technique for screening formulations and can give an indication of their relative storage stability. However, establishing ssHDX-MS as a surrogate for long-term stability studies require additional studies. For example, the effects of relative humidity on ssHDX-MS were studied extensively, but the effects of temperature were not evaluated to a similar extent in the work reported in this dissertation. The ssHDX-MS metrics have been shown to be highly correlated to the protein aggregation obtained in the stability studies. Similar correlations between the deuterium uptake and other types of degradation (e.g., deamidation or oxidation) must also be established. In addition, there is a need for the development of internal standards that can be used in solid protein samples while conducting ssHDX-MS. To date, the technique has been applied to lyophilized and spray dried protein formulations, but it should be evaluated for its applicability to solids produced by novel drying methods such as MicroglassificationTM and supercritical drying. Currently, the deuterium labeling in ssHDX-MS is carried out in sealed desiccators containing saturated salt solutions of D₂O. The salts that produce constant relative humidity are limited.

Moreover, the deuterated solid samples require reconstitution before the analysis, which makes it a manual process. Therefore, automation of the entire deuterium labeling and sample analysis process will be required to make ssHDX-MS an efficient technique from an industrial perspective.

APPENDIX A. SUPPORTING INFORMATION FOR CHAPTER 2

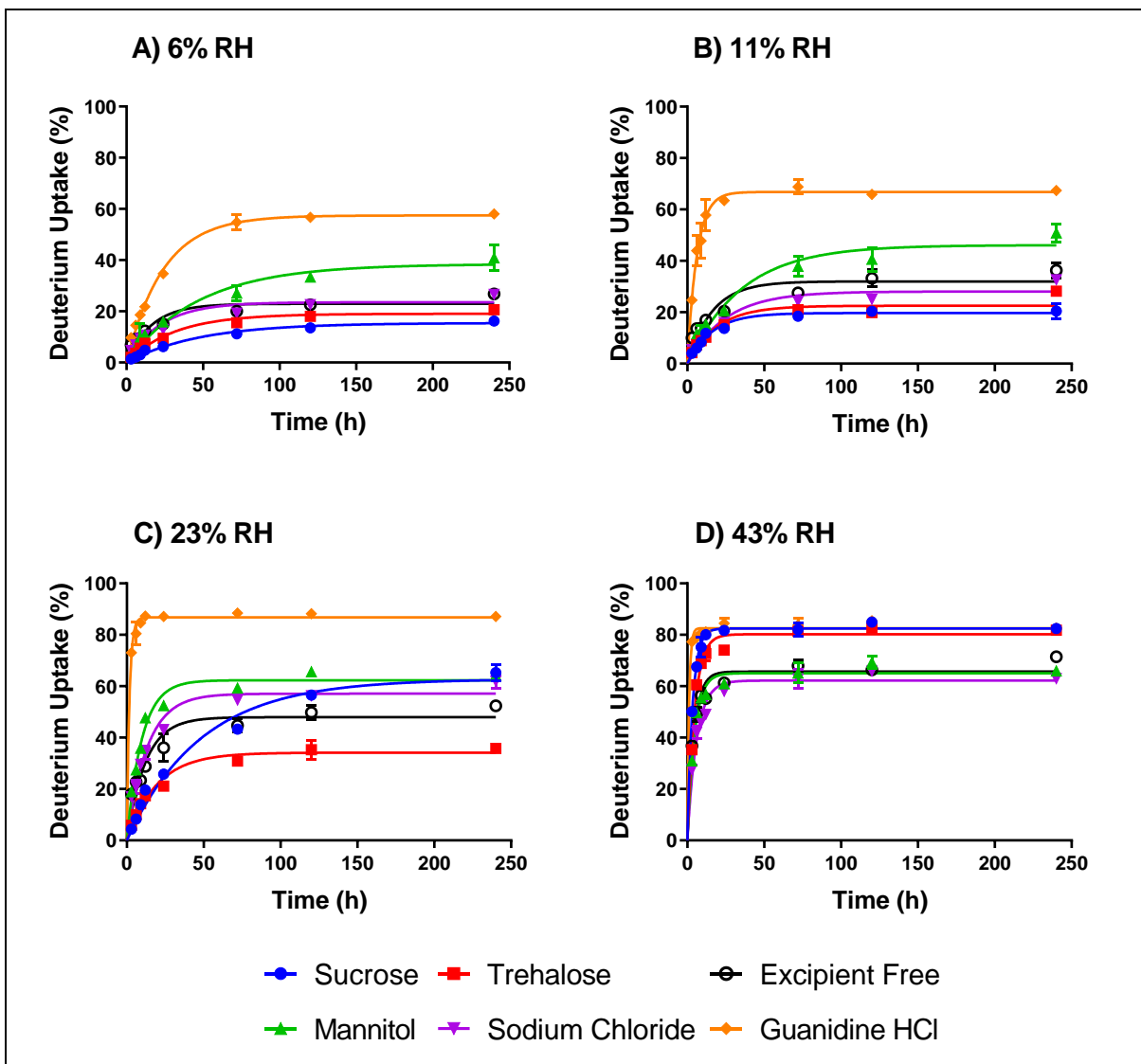


Figure A1. ssHDX-MS kinetics of different formulations of a 22 amino-acid PDLA peptide, grouped by RH A) 6% RH, B) 11% RH, C) 23% RH and D) 43% RH. $n=3$, mean \pm SD; error bars not shown when less than the height of the symbol.

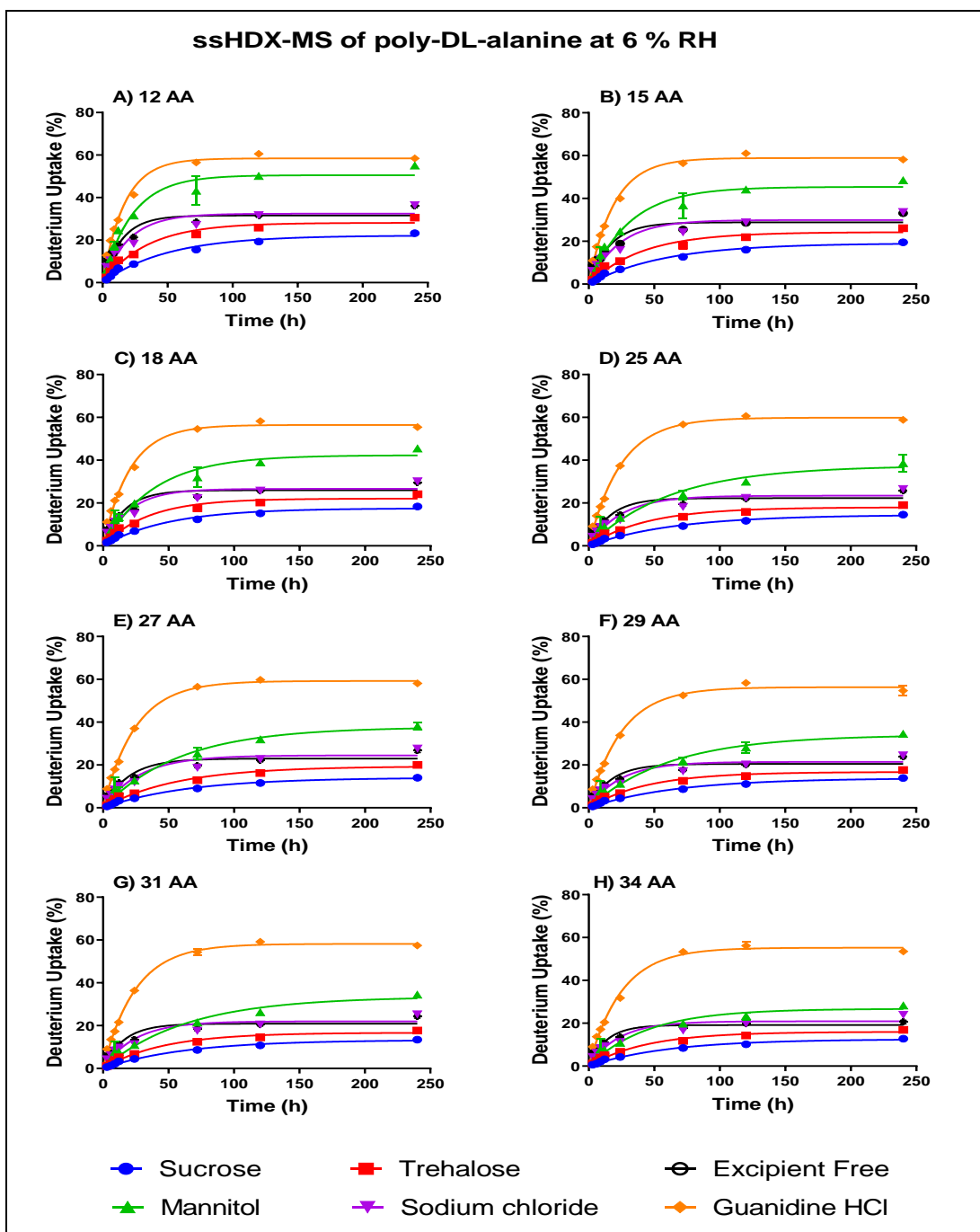


Figure A2. ssHDX-MS of different formulations of PDLA peptides of different chain length at 6% RH. Data are shown for eight PDLA peptides from the polydisperse mixture having different amino acid (AA) chain length: A) 12AA, B) 15 AA, C) 18 AA, D) 25 AA, E) 27 AA, F) 29 AA, G) 31 AA, H) 34 AA. Colors indicate different formulations: sucrose (blue), trehalose (red), excipient free (black), mannitol (green), sodium chloride (purple) and guanidine hydrochloride (orange). $n=3$, mean \pm SD; error bars not shown when less than the height of the symbol.

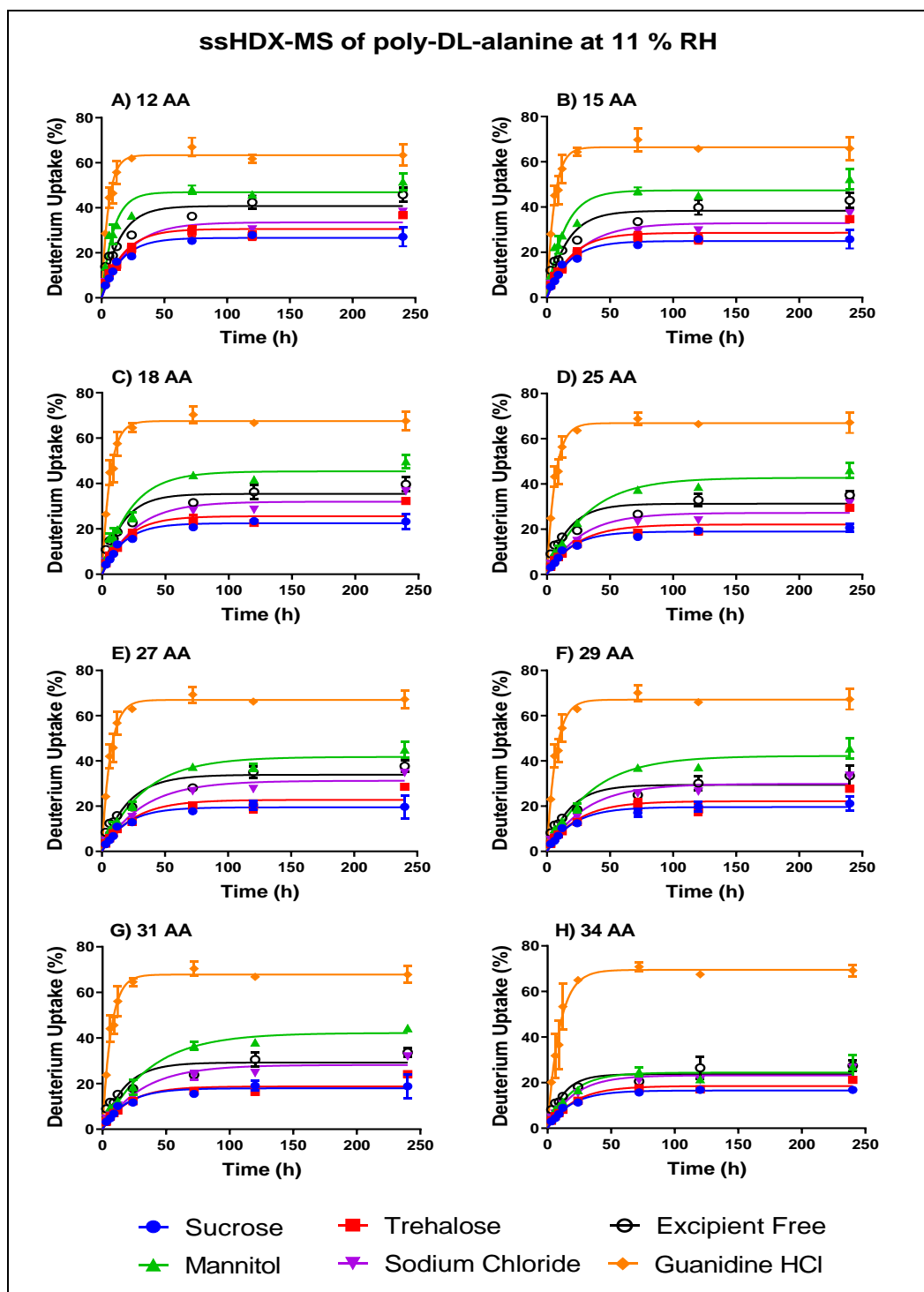


Figure A3. ssHDX-MS of different formulations of PDLA peptides of different chain length at 11% RH. Data are shown for eight PDLA peptides from the polydisperse mixture having different amino acid (AA) chain length: A) 12AA, B) 15 AA, C) 18 AA, D) 25 AA, E) 27 AA, F) 29 AA, G) 31 AA, H) 34 AA. Colors indicate different formulations: sucrose (blue), trehalose (red), excipient free (black), mannitol (green), sodium chloride (purple) and guanidine hydrochloride (orange). $n=3$, mean \pm SD; error bars not shown when less than the height of the symbol.

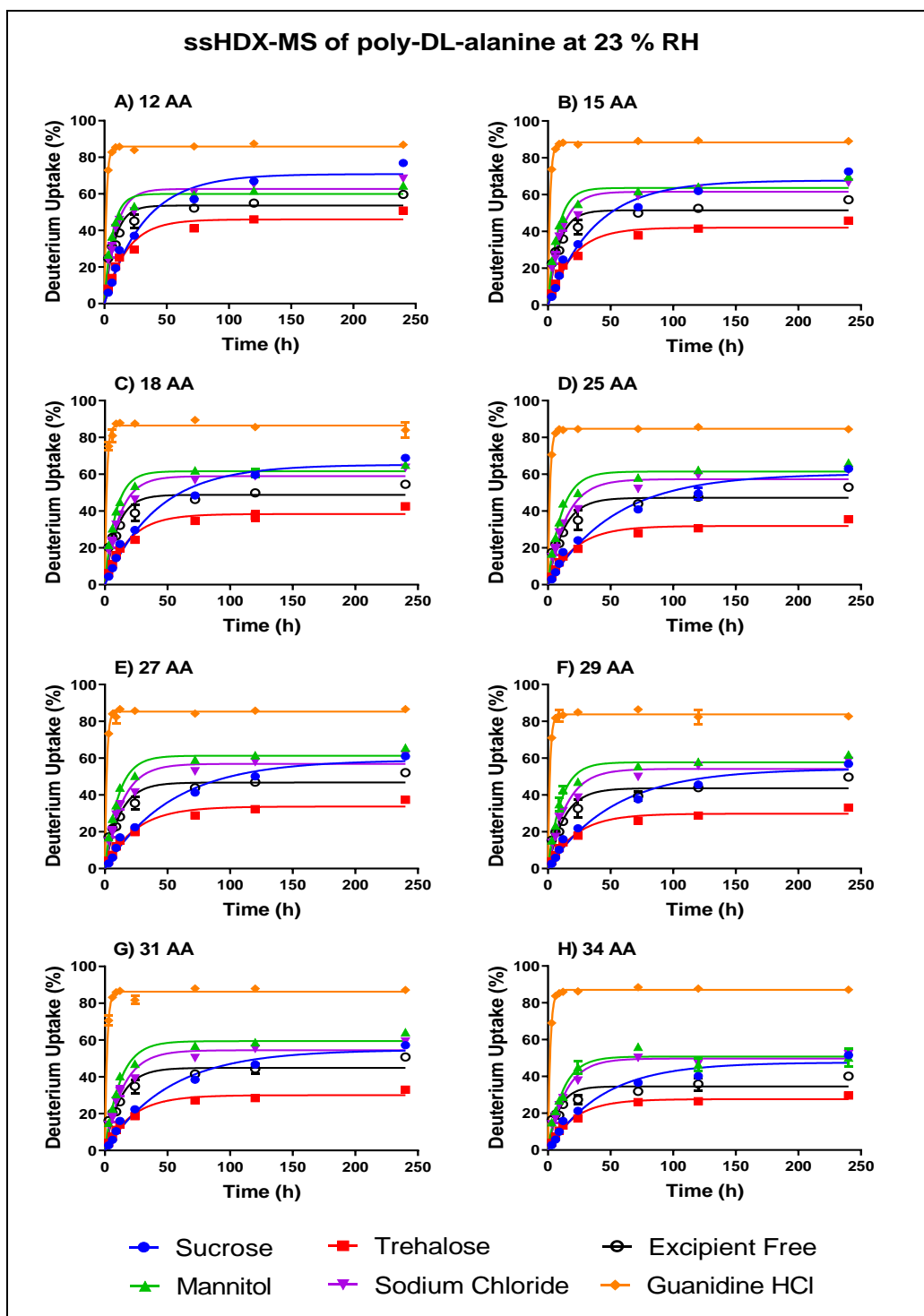


Figure A4. ssHDX-MS of different formulations of PDLA peptides of different chain length at 23% RH. Data are shown for eight PDLA peptides from the polydisperse mixture having different amino acid (AA) chain length: A) 12AA, B) 15 AA, C) 18 AA, D) 25 AA, E) 27 AA, F) 29 AA, G) 31 AA, H) 34 AA. Colors indicate different formulations: sucrose (blue), trehalose (red), excipient free (black), mannitol (green), sodium chloride (purple) and guanidine hydrochloride (orange). $n=3$, mean \pm SD; error bars not shown when less than the height of the symbol.

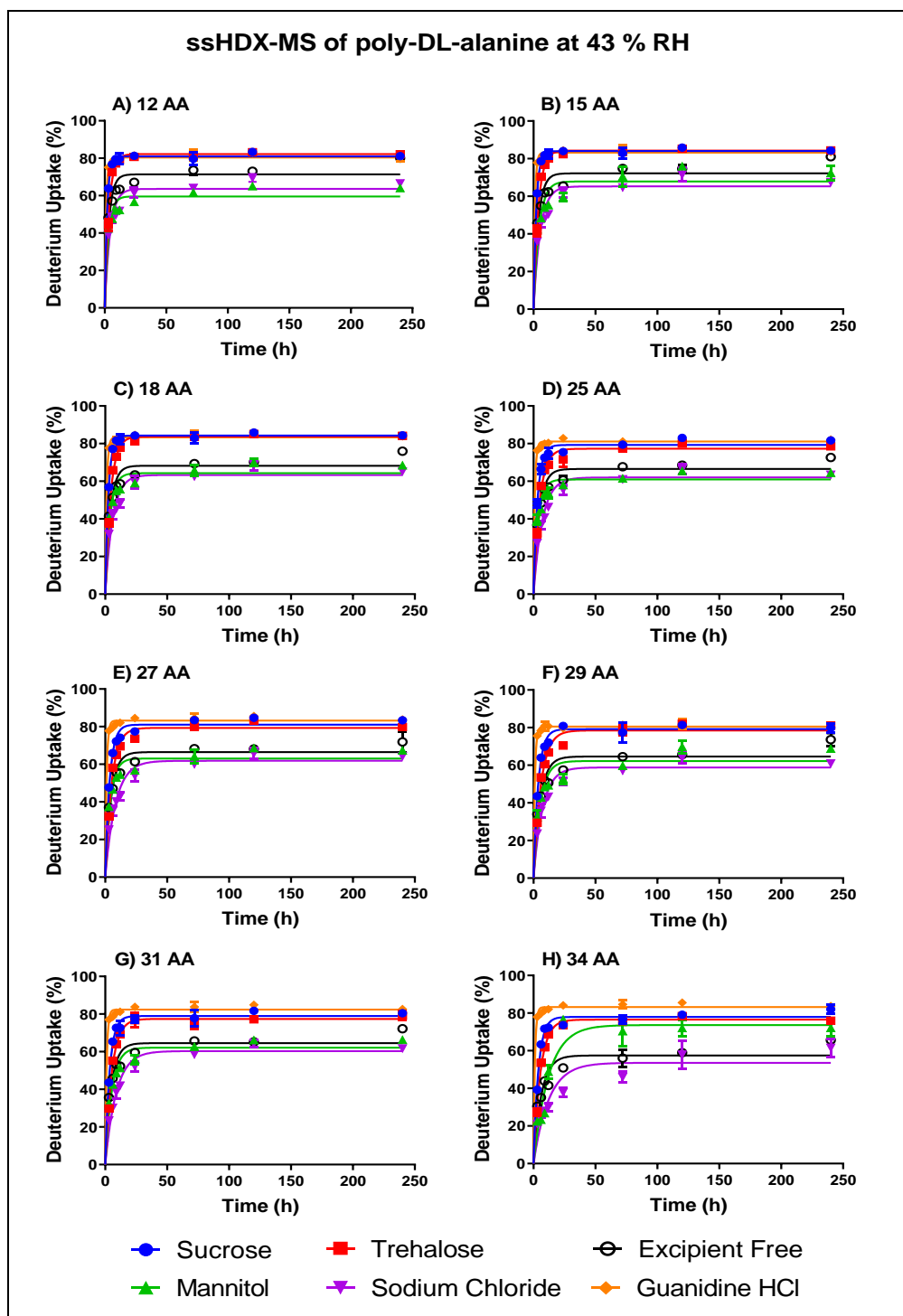


Figure A5. ssHDX-MS of different formulations of PDLA peptides of different chain length at 43% RH. Data are shown for eight PDLA peptides from the polydisperse mixture having different amino acid (AA) chain length: A) 12AA, B) 15 AA, C) 18 AA, D) 25 AA, E) 27 AA, F) 29 AA, G) 31 AA, H) 34 AA. Colors indicate different formulations: sucrose (blue), trehalose (red), excipient free (black), mannitol (green), sodium chloride (purple) and guanidine hydrochloride (orange). $n=3$, mean \pm SD; error bars not shown when less than the height of the symbol.

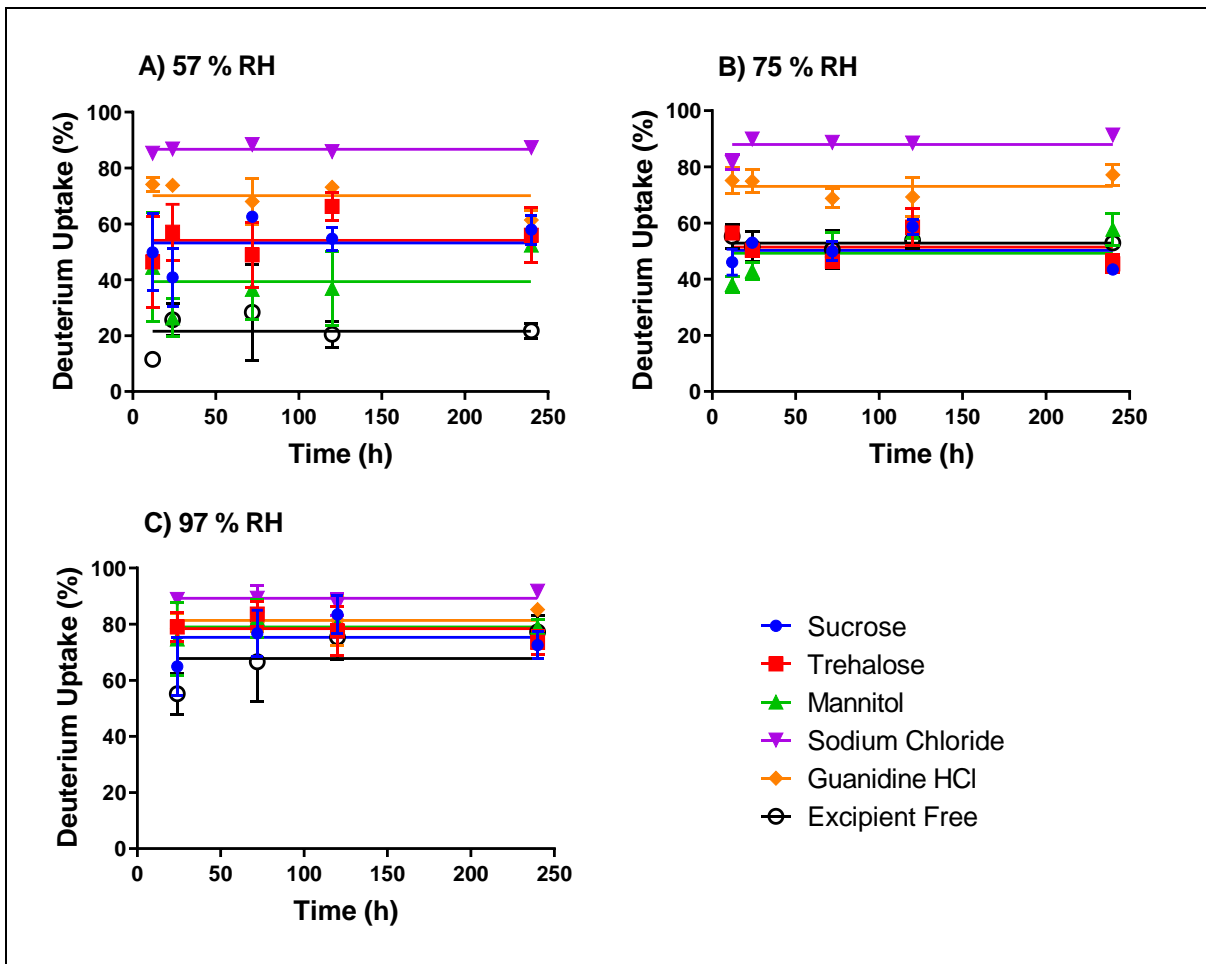


Figure A6. ssHDX-MS of different formulations of PDLA peptides of 22 amino acid chain length at RH values from 57% to 97% A) 57% RH, B) 75% RH, C) 97% RH. Colors indicate different formulations: sucrose (blue), trehalose (red), excipient free (black), mannitol (green), sodium chloride (purple) and guanidine hydrochloride (orange). Data shown for the 22 amino acid length peptide, n=3, mean \pm SD; error bars not shown when less than the height of the symbol.

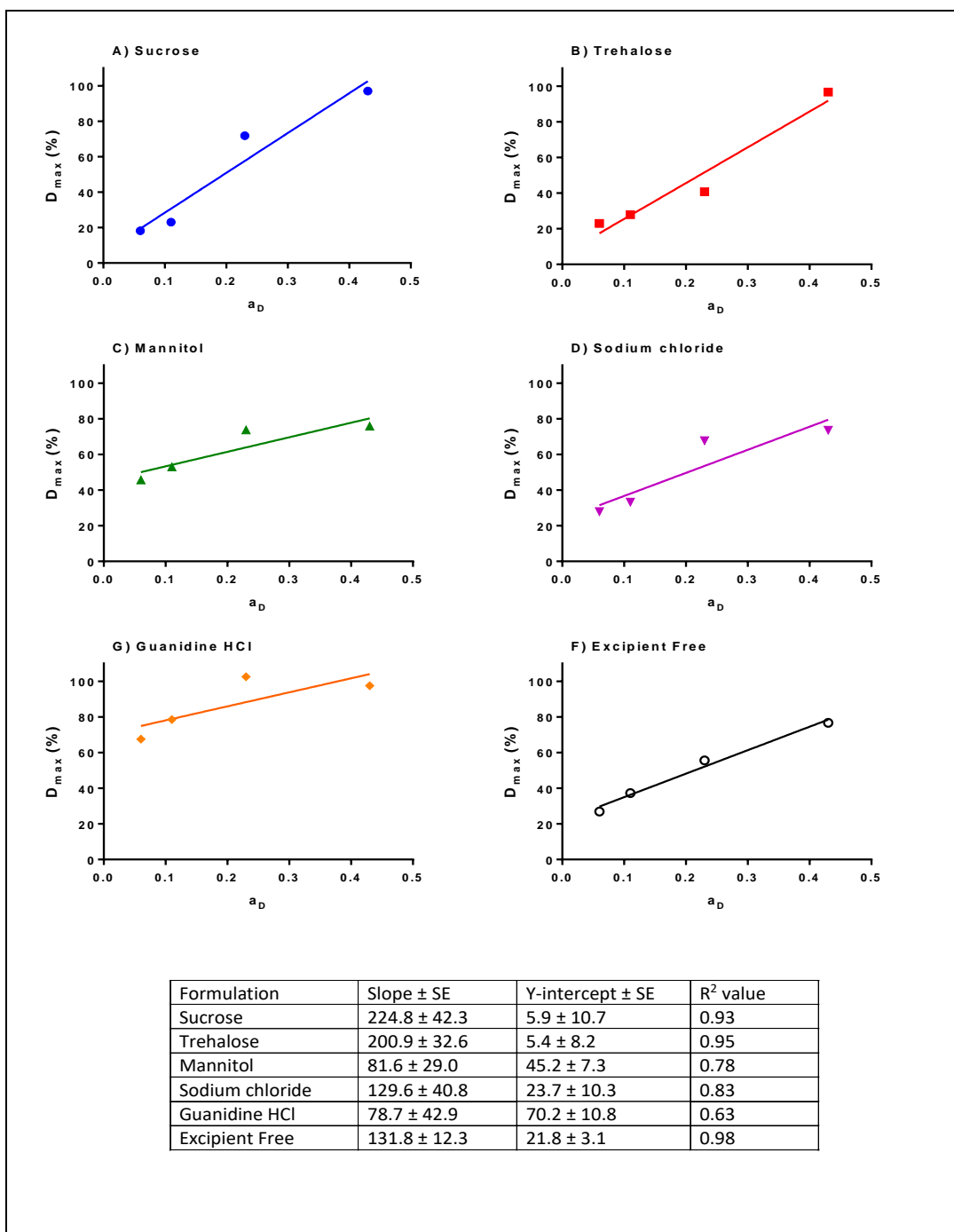


Figure A7. Linear regression of D_{\max} vs. a_D for PDLA peptides at RH < 50%, with each formulation plotted individually, (A) sucrose, (B) trehalose, (C) mannitol, (D) sodium chloride, (E) guanidine HCl or (F) no excipient (excipient-free). The D_{\max} was calculated from the back exchange corrected percentage deuterium uptake mono-exponential fits. Data shown for a 22 amino acid peptide, $n=3$, error bars not shown if smaller than the symbol.

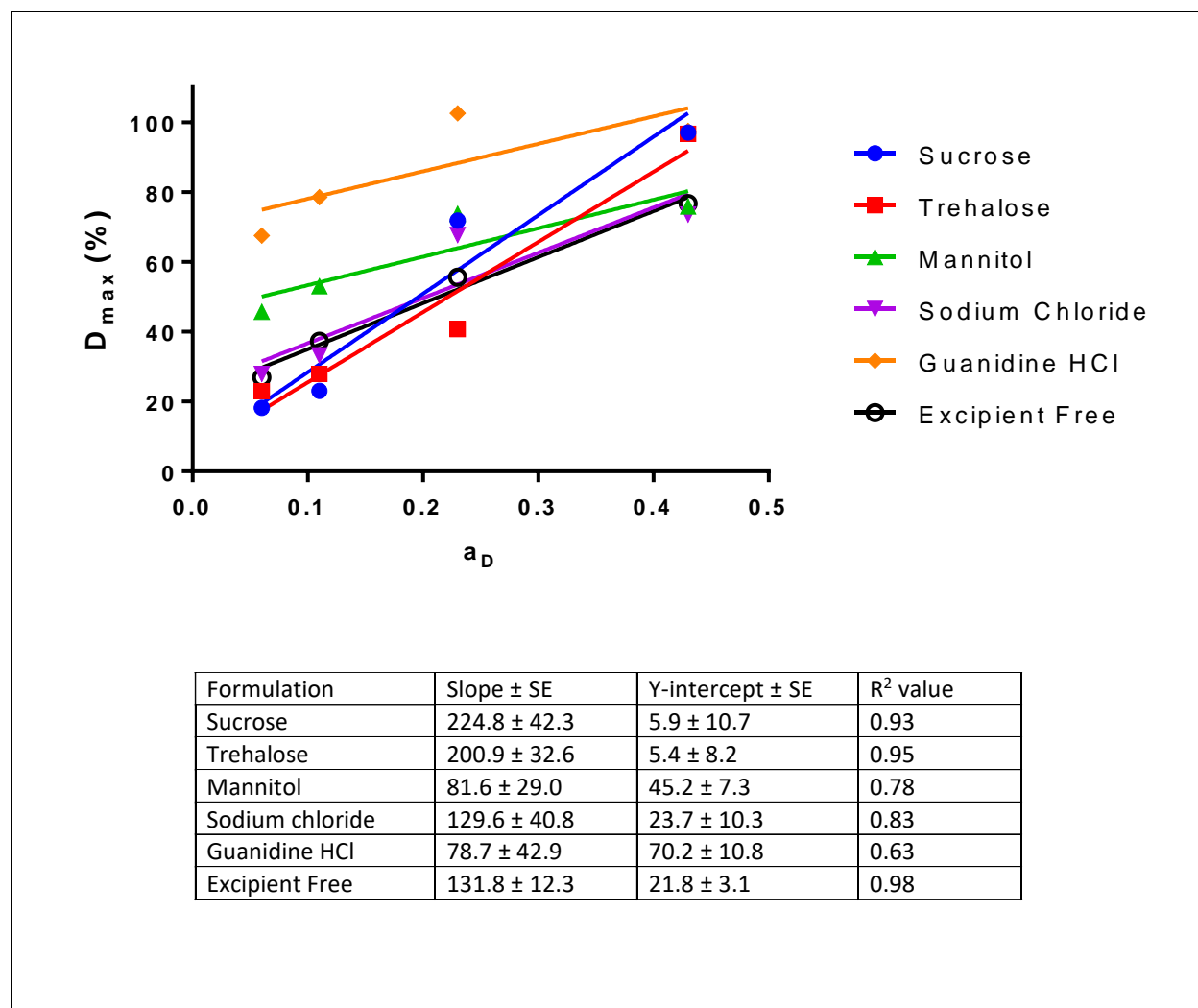


Figure A8. Linear regression of D_{\max} vs. a_D for PDLA peptides at $RH < 50\%$, with all formulations plotted together. Colors indicate different formulations: sucrose (blue), trehalose (red), excipient free (black), mannitol (green), sodium chloride (purple) and guanidine hydrochloride (orange). The D_{\max} was calculated from the back exchange corrected percentage deuterium uptake mono-exponential fits. Data shown for a 22 amino acid peptide, $n=3$, error bars not shown if smaller than the symbol.

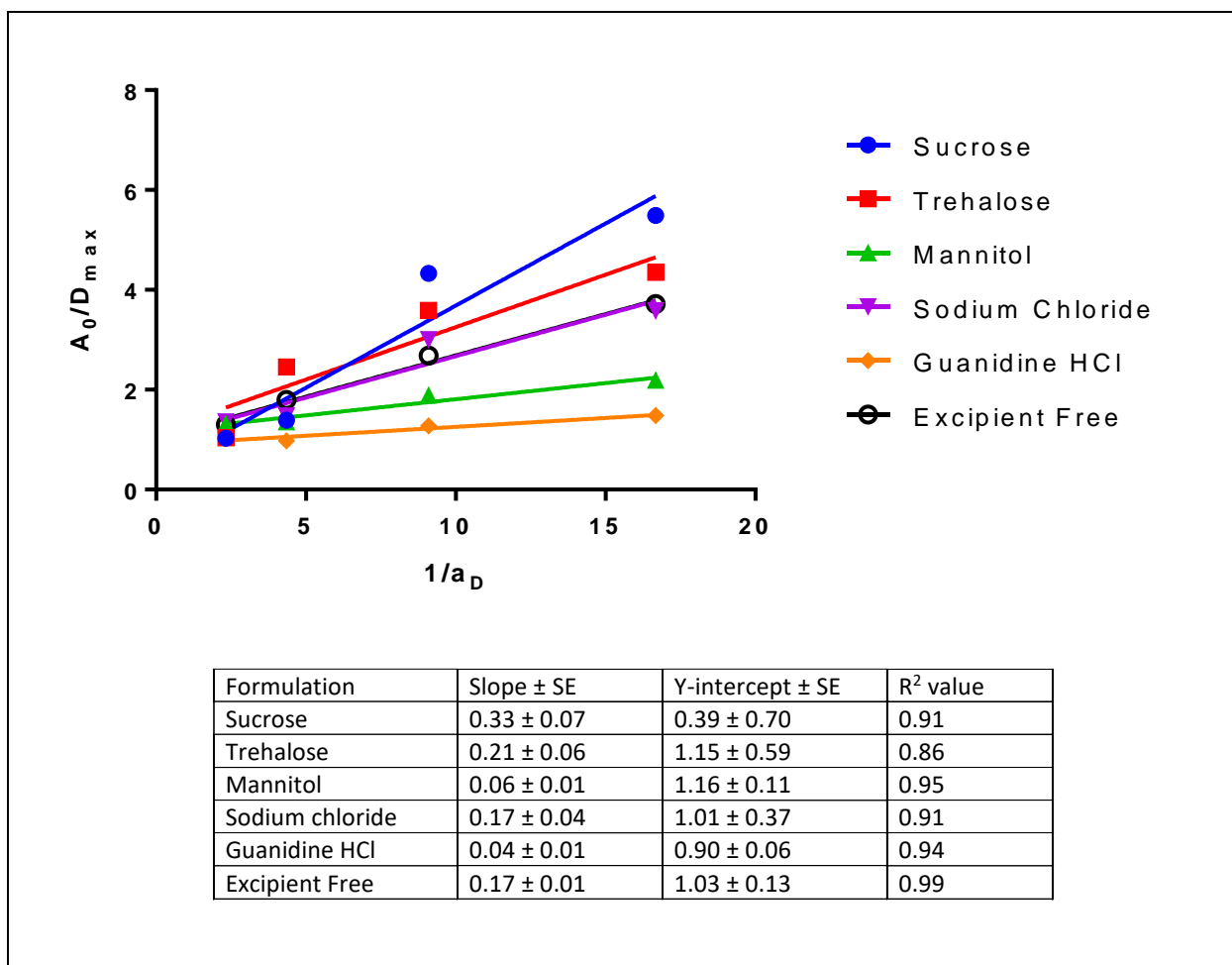


Figure A9. Linear regression of A_0/D_{\max} vs. $1/a_D$, with all formulations plotted together at $RH < 50\%$. Colors indicate different formulations: sucrose (blue), trehalose (red), excipient free (black), mannitol (green), sodium chloride (purple) and guanidine hydrochloride (orange). The D_{\max} was calculated from the back exchange corrected percentage deuterium uptake mono-exponential fits. Data shown for a 22 amino acid peptide.

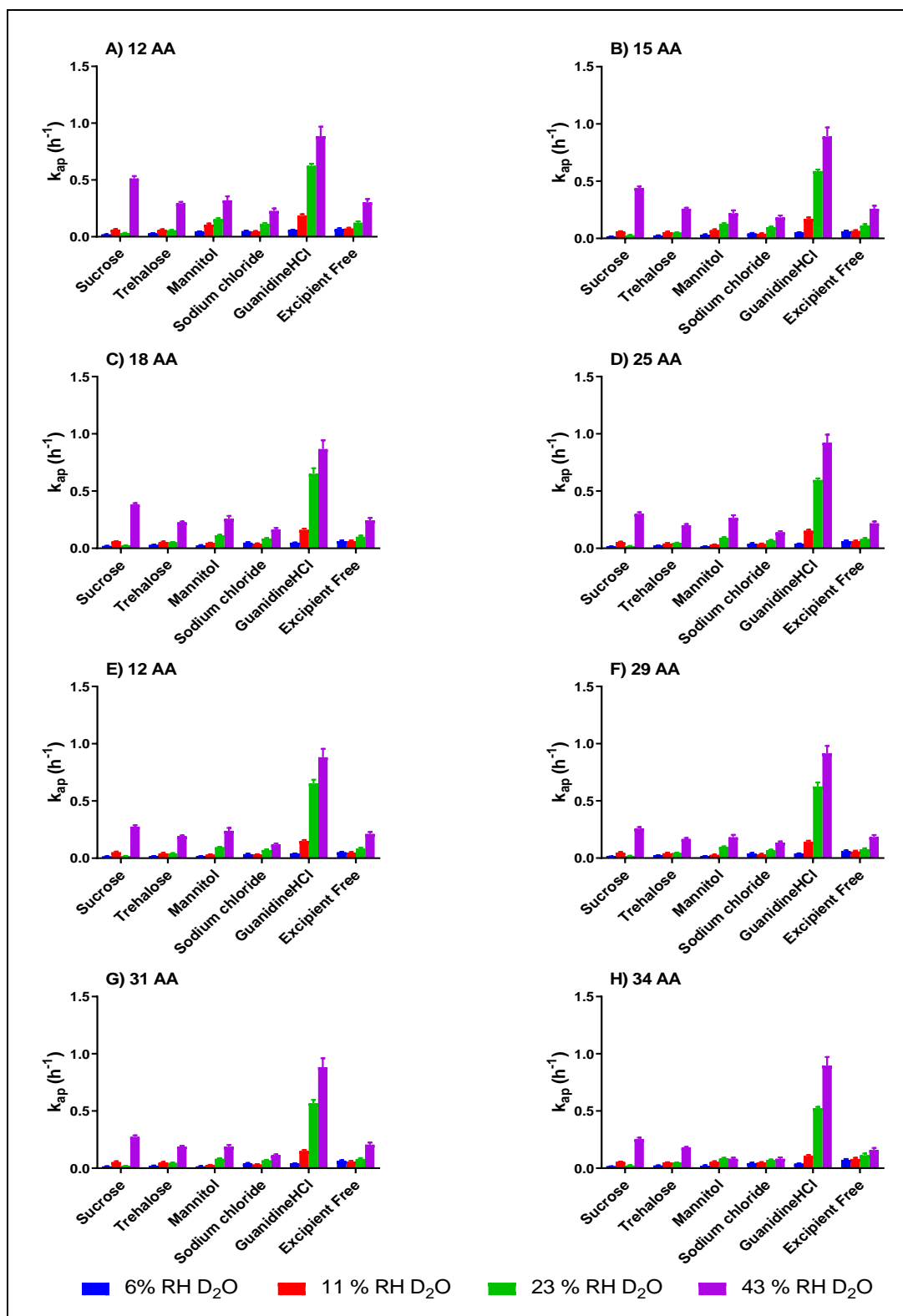


Figure A10. Apparent ssHDX-MS rate constants (k_{ap}) for various formulations, RH values and PDLA chain lengths. Data shown for 8 selected peptides, $n=3$, error bars not shown if smaller than the symbol.

Table A1. A list of PDLA peptides detected on MS analysis. Initial mass spec analysis data shows the presence of several peptides (6 amino acid length to 44 amino acid length) and their corresponding masses, m/z values and retention times are shown in below table-A1.

Compound	Sequence Location	Avg Mass	m/z	RT
Cpd 1: A(1-6)	A(1-6)	444.40	445.24	3.16
Cpd 2: A(1-7)	A(1-7)	515.58	516.27	3.16
Cpd 3: A(1-8)	A(1-8)	586.62	587.31	3.17
Cpd 4: A(1-9)	A(1-9)	657.71	658.35	3.18
Cpd 5: A(1-10)	A(1-10)	728.77	729.38	3.19
Cpd 6: A(1-11)	A(1-11)	799.86	800.42	3.20
Cpd 7: A(1-12)	A(1-12)	870.92	871.46	3.20
Cpd 8: A(1-13)	A(1-13)	942.00	942.50	3.21
Cpd 9: A(1-14)	A(1-14)	1013.07	1013.53	3.22
Cpd 10: A(1-15)	A(1-15)	1084.16	542.79	3.23
Cpd 11: A(1-16)	A(1-16)	1155.23	578.31	3.24
Cpd 12: A(1-17)	A(1-17)	1226.31	613.82	3.25
Cpd 13: A(1-18)	A(1-18)	1297.37	649.34	3.26
Cpd 14: A(1-19)	A(1-19)	1368.47	684.86	3.27
Cpd 15: A(1-20)	A(1-20)	1439.52	720.38	3.28
Cpd 16: A(1-21)	A(1-21)	1510.63	755.90	3.29
Cpd 17: A(1-22)	A(1-22)	1581.67	791.42	3.31
Cpd 18: A(1-23)	A(1-23)	1652.80	826.94	3.32
Cpd 19: A(1-24)	A(1-24)	1723.90	862.45	3.34
Cpd 20: A(1-25)	A(1-25)	1794.95	897.97	3.35
Cpd 21: A(1-26)	A(1-26)	1866.01	933.49	3.36
Cpd 22: A(1-27)	A(1-27)	1937.08	646.34	3.36
Cpd 23: A(1-28)	A(1-28)	2008.18	670.02	3.38
Cpd 24: A(1-29)	A(1-29)	2079.25	693.70	3.38

Table A1. Continued

Cpd 25: A(1-30)	A(1-30)	2150.31	717.38	3.39
Cpd 26: A(1-31)	A(1-31)	2221.43	741.06	3.41
Cpd 27: A(1-32)	A(1-32)	2292.47	764.74	3.40
Cpd 28: A(1-33)	A(1-33)	2363.51	788.42	3.41
Cpd 29: A(1-34)	A(1-34)	2434.56	812.09	3.43
Cpd 30: A(1-35)	A(1-35)	2505.55	1253.16	3.42
Cpd 31: A(1-36)	A(1-36)	2576.68	859.45	3.46
Cpd 32: A(1-37)	A(1-37)	2647.77	883.13	3.47
Cpd 33: A(1-38)	A(1-38)	2718.63	680.36	3.47
Cpd 34: A(1-39)	A(1-39)	2789.91	930.49	3.49
Cpd 35: A(1-40)	A(1-40)	2860.99	954.17	3.51
Cpd 36: A(1-41)	A(1-41)	2931.49	977.85	3.51
Cpd 37: A(1-42)	A(1-42)	3002.97	1001.53	3.53
Cpd 38: A(1-43)	A(1-43)	3073.68	1025.21	3.53
Cpd 39: A(1-44)	A(1-44)	3144.74	786.91	3.52

Table A2. Statistical analysis for a_D vs D_{max}

a. Is slope significantly non-zero?

Formulation	P value	Significantly Non-zero slope
Sucrose	0.0337	Significant
Trehalose	0.0253	Significant
Mannitol	0.1067	Non- significant
Sodium Chloride	0.0865	Non- significant
Guanidine HCl	0.2083	Non- significant
Excipient Free	0.0086	Significant

b. Are the slopes equal?

F=2.977, P=0.0564, Differences between the slopes are NOT significant.

c. Are the elevations or intercepts equal?

F=5.648, P=0.0030, Difference between the elevations or intercepts are very significant.

Table A3. Statistical analysis for $1/a_D$ vs A_0/D_{max}

a. Is slope significantly non-zero?

Formulation	P value	Significantly Non-zero slope
Sucrose	0.0443	Significant
Trehalose	0.0735	Non- significant
Mannitol	0.0273	Significant
Sodium Chloride	0.0471	Significant
Guanidine HCl	0.0329	Significant
Excipient Free	0.0061	Significant

b. Are the slopes equal?

F=6.364, P=0.0041, Differences between the slopes are significant.

c. Are the elevations or intercepts equal?

Because slopes differ so much, it is not possible to test whether the intercepts differ significantly.

APPENDIX B. SUPPORTING INFORMATION FOR CHAPTER 3

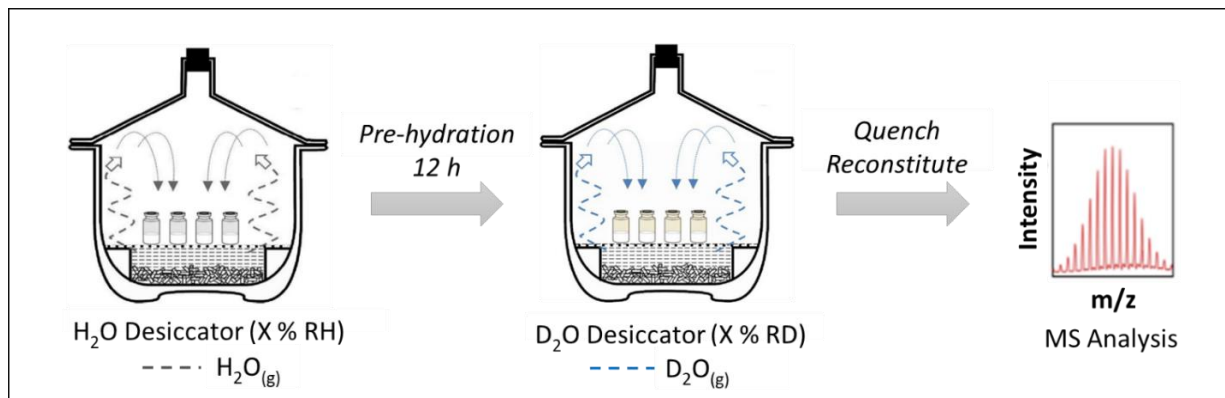


Figure B1. Pre-hydration and ssHDX-MS study schematic diagram, Case-1: X=6 %, Case-2: X=11 %.

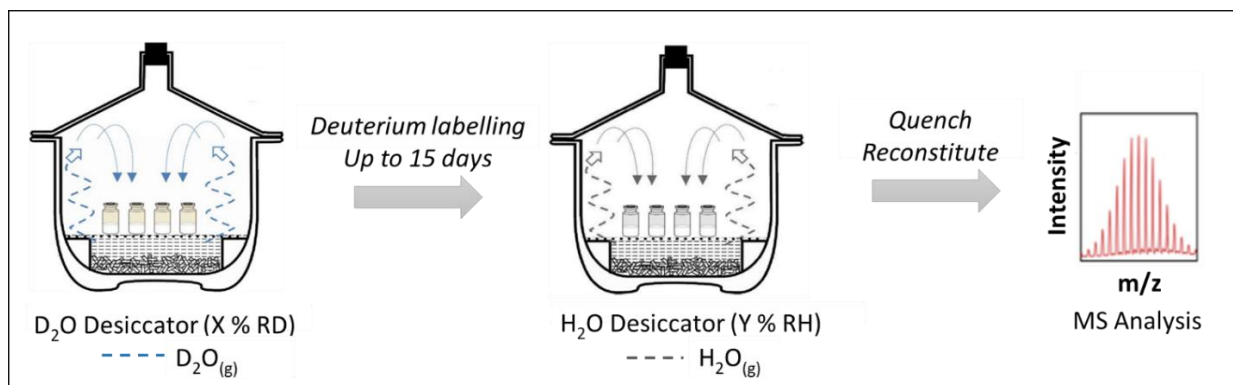


Figure B2. Reversibility of ssHDX-MS study schematic diagram, Case-3a: X=6 %, Y= 0 %, Case-3b: X=6 %, Y= 6 %, Case-3c: X=6 %, Y= 43 %, Case-4a: X=11 %, Y= 0 %, Case-4b: X=11 %, Y= 11 %, Case-4c: X=11 %, Y= 43 %.

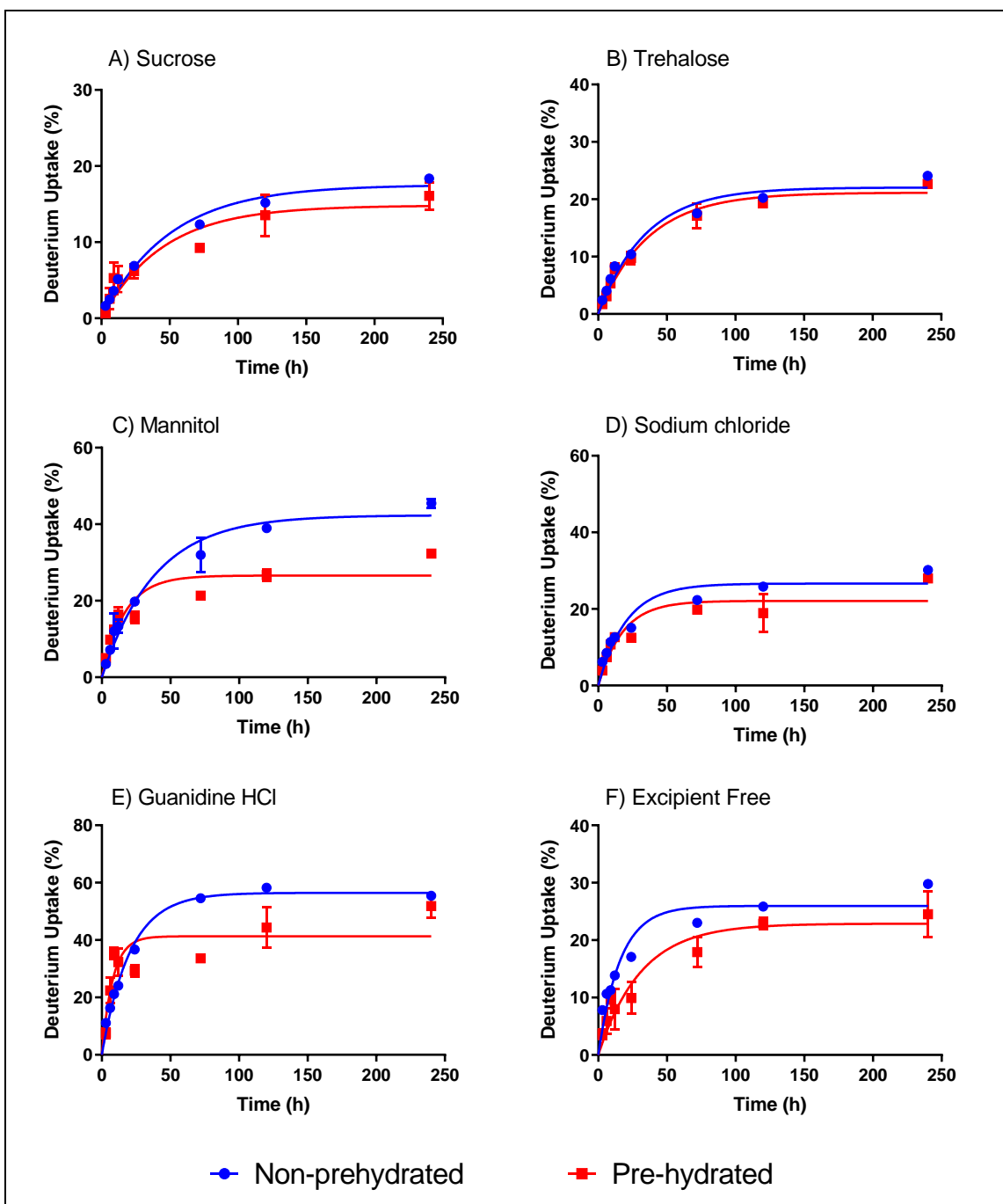


Figure B3. Comparison of pre-hydrated vs non-pre-hydrated ssHDX-MS of different PDLA formulations at 6% RD (Case-1). A) sucrose, B) trehalose, C) mannitol, D) sodium chloride, E) guanidine HCl, and F) no excipient (“excipient free”). Colors indicate different conditions: Non-prehydrated (blue), pre-hydrated (red). Data shown for an 18 amino acid length PDLA peptide, $n=3$, mean \pm SD; error bars not shown when less than the height of the symbol.

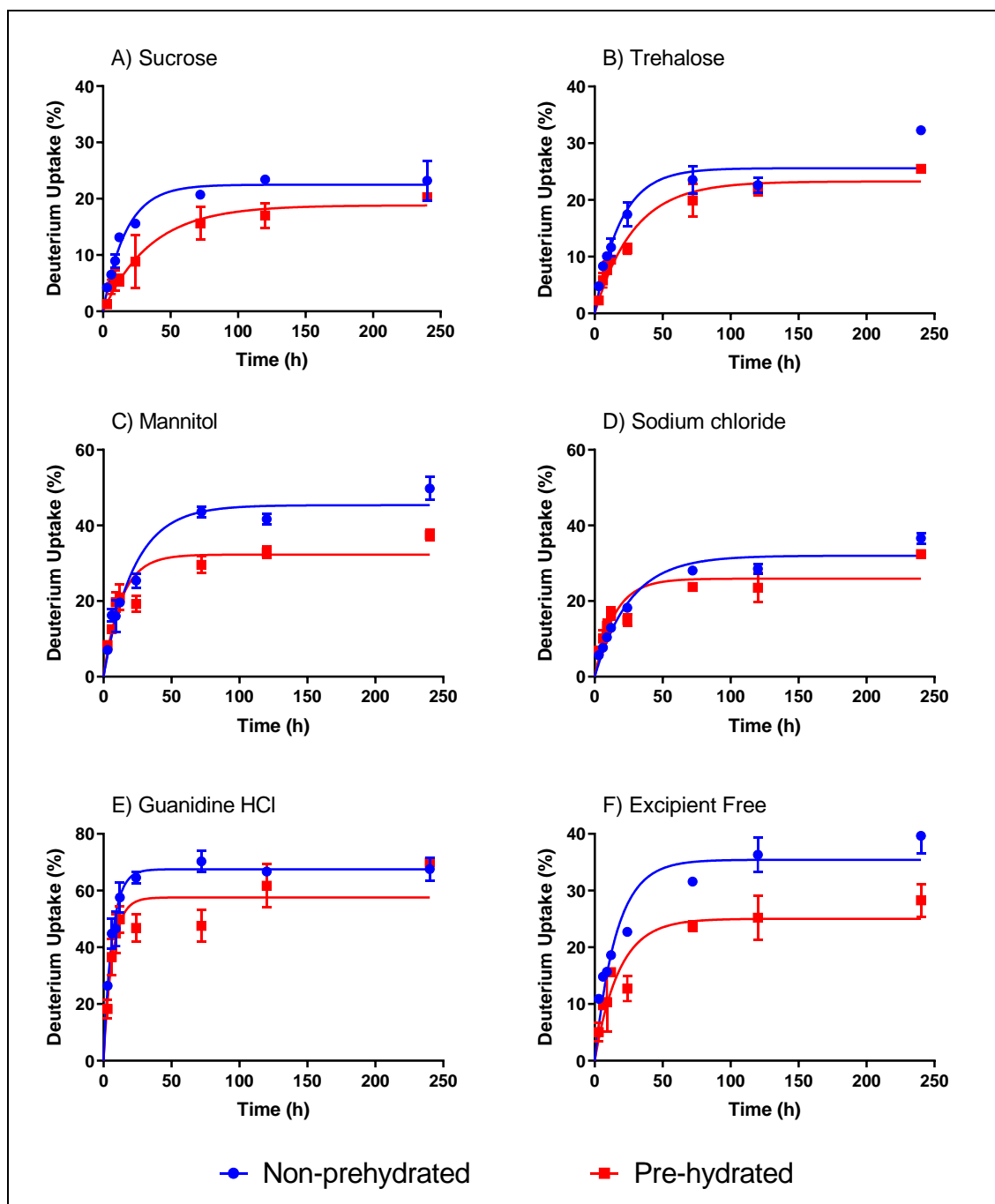


Figure B4. Comparison of pre-hydrated vs non-pre-hydrated ssHDX-MS of different PDLA formulations at 11% RD (Case-2). A) sucrose, B) trehalose, C) mannitol, D) sodium chloride, E) guanidine HCl, and F) no excipient (“excipient free”). Colors indicate different conditions: Non-prehydrated (blue), pre-hydrated (red). Data shown for an 18 amino acid length PDLA peptide, $n=3$, mean \pm SD; error bars not shown when less than the height of the symbol.

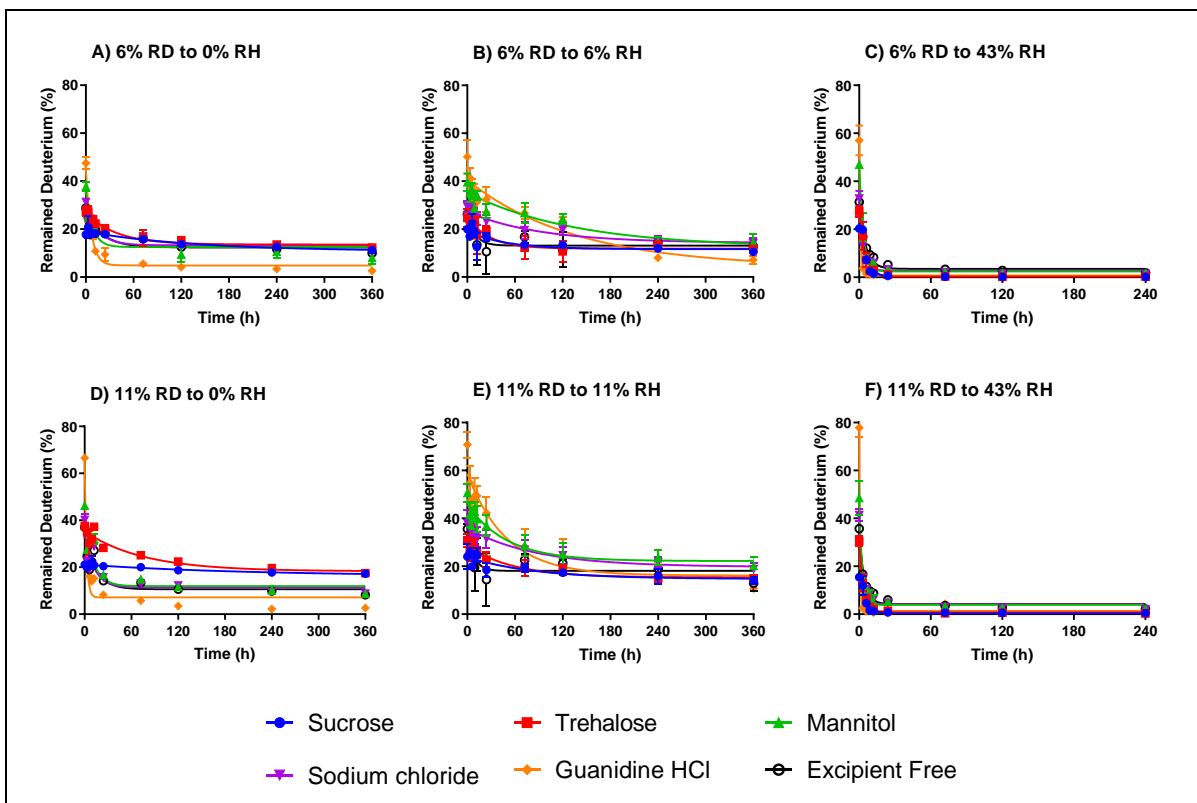


Figure B5. Reversibility of ssHDX-MS in PDLA formulations lyophilized with various excipients. Formulations were first deuterated by exposure to D₂O vapor at 6% (A, B, C) or 11% RD (D, E, F). Deuterium removal was then accomplished at a controlled RH: (A, D) 0% RH (desiccated), (B, E) 6% RH, (C, F) 43% RH. Data shown for an 18 amino acid length PDLA peptide, n=3, mean \pm SD. error bars not shown when less than the height of the symbol.

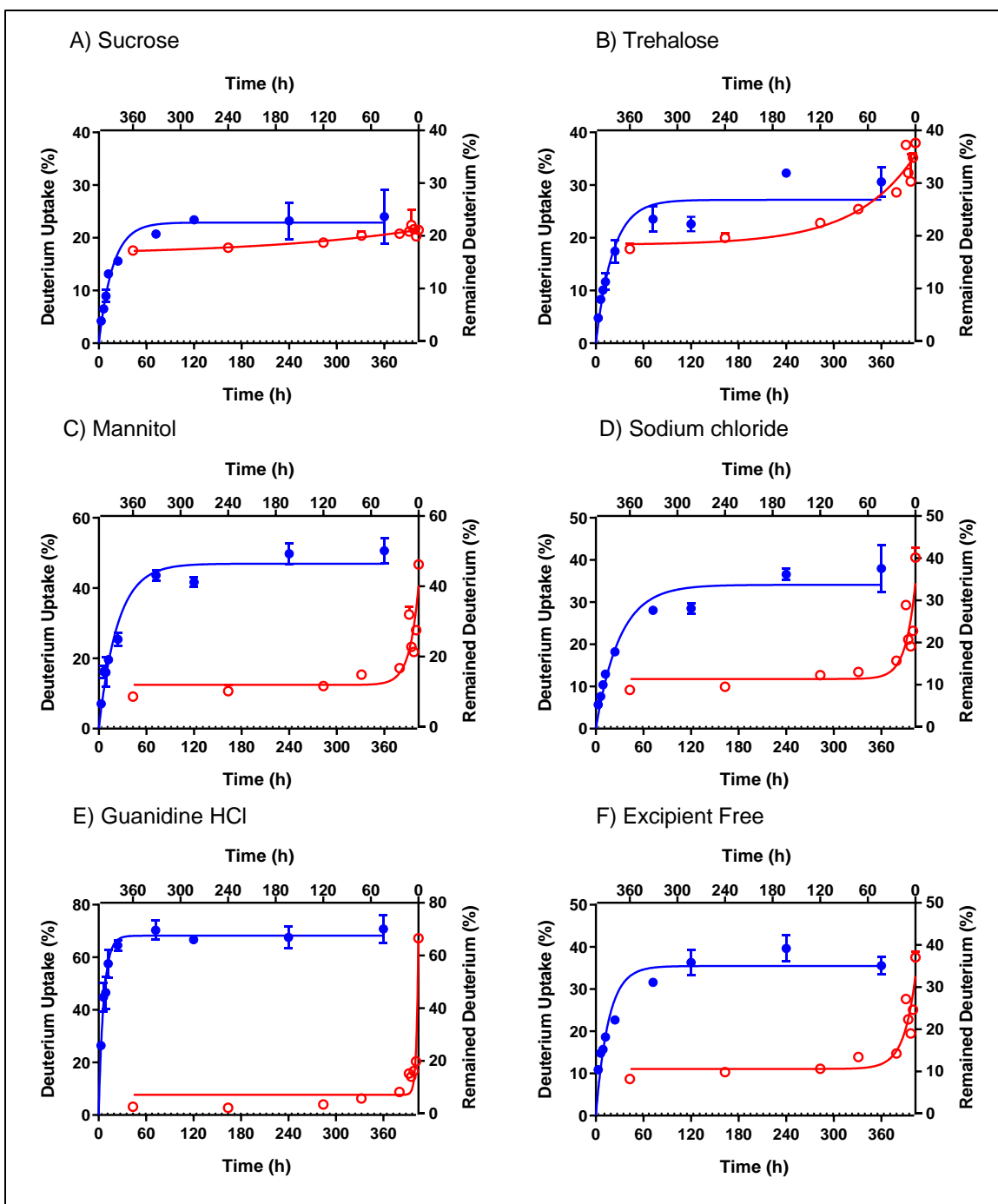


Figure B6. Comparison of the forward and reverse ssHDX-MS kinetics for PDLA formulations deuterated at 11% RD (forward) followed by deuterium removal at 0% RH (reverse) (Case-4a). Formulations contained (A) sucrose, (B) trehalose, (C) mannitol, (D) sodium chloride, (E) guanidine HCl, and (F) no excipient (“excipient free”). Blue line indicates fit of the forward ssHDX reaction to a mono-exponential association model, red line indicates fit of the reverse ssHDX reaction to a mono-exponential decay model; see text for details. Data shown for an 18 amino acid length PDLA peptide, $n=3$, mean \pm SD. error bars not shown when less than the height of the symbol.

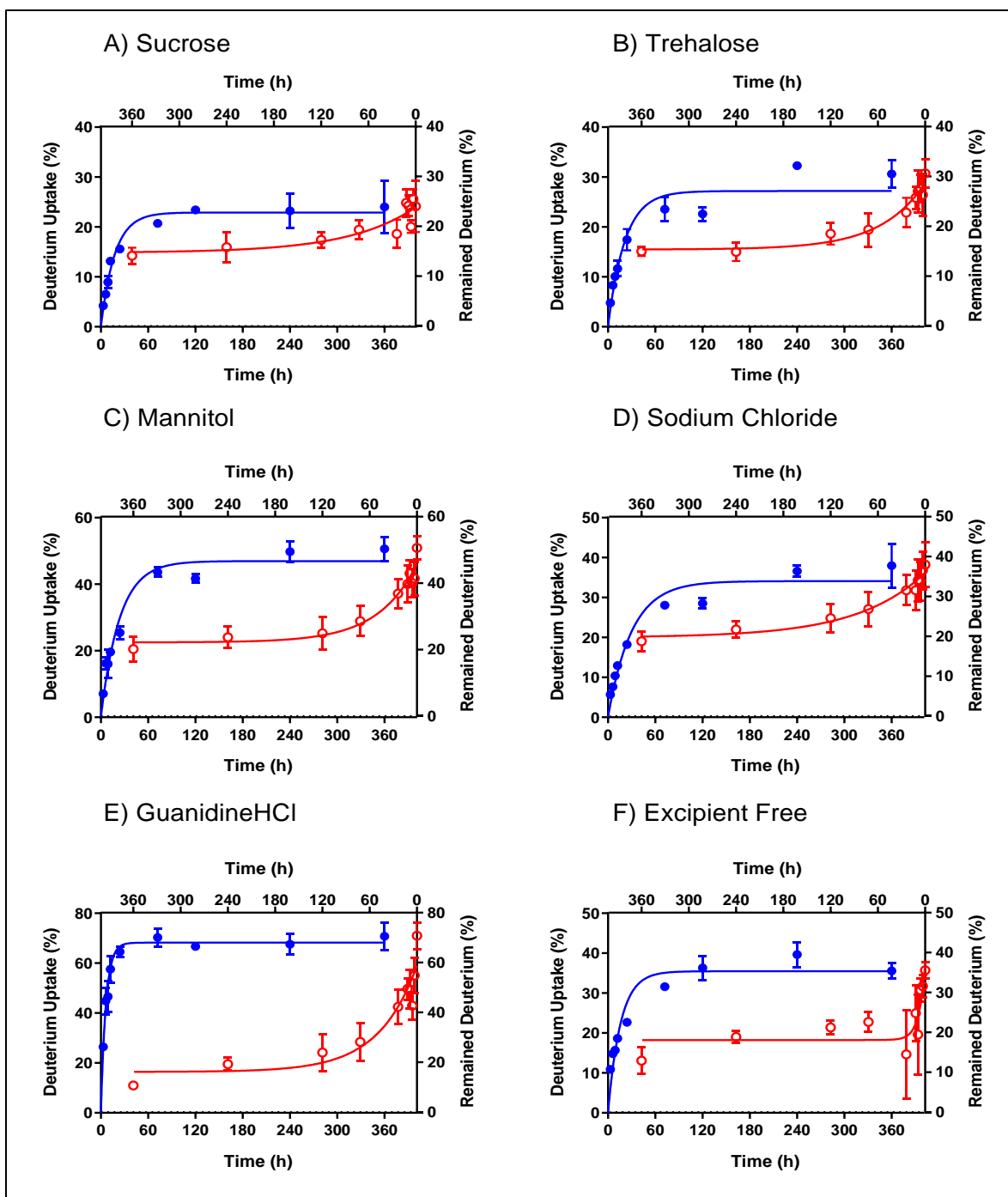


Figure B7. Comparison of the forward and reverse ssHDX-MS kinetics for PDLA formulations deuterated at 11% RD (forward) followed by deuterium removal at 11% RH (reverse) (Case-4b). Formulations contained (A) sucrose, (B) trehalose, (C) mannitol, (D) sodium chloride, (E) guanidine HCl, and (F) no excipient (“excipient free”). Blue line indicates fit of the forward ssHDX reaction to a mono-exponential association model, red line indicates fit of the reverse ssHDX reaction to a mono-exponential decay model; see text for details. Data shown for an 18 amino acid length PDLA peptide, $n=3$, mean \pm SD. error bars not shown when less than the height of the symbol.

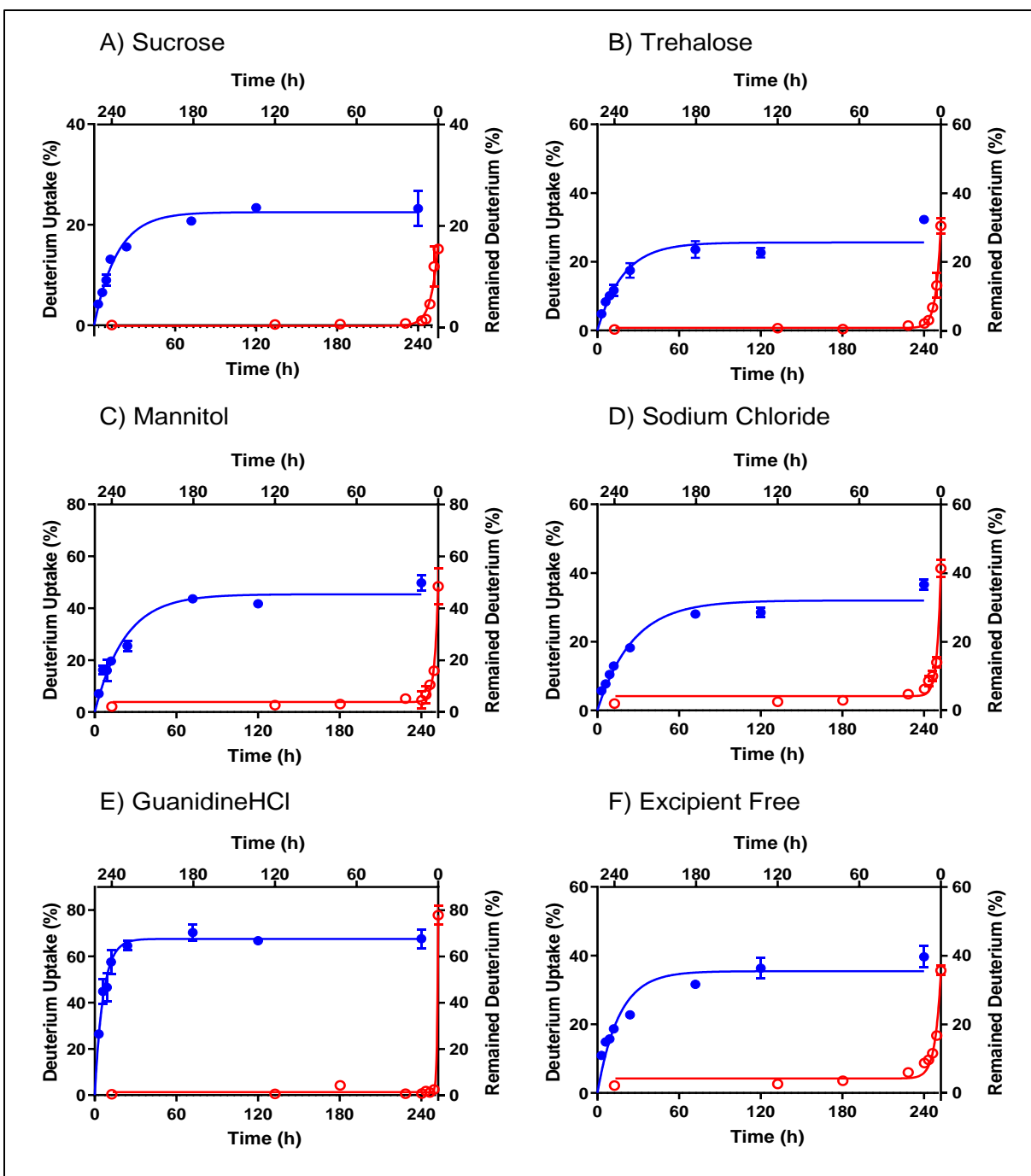


Figure B8. Comparison of the forward and reverse ssHDX-MS kinetics for PDLA formulations deuterated at 11% RD (forward) followed by deuterium removal at 43% RH (reverse) (Case-4c). Formulations contained (A) sucrose, (B) trehalose, (C) mannitol, (D) sodium chloride, (E) guanidine HCl, and (F) no excipient (“excipient free”). Blue line indicates fit of the forward ssHDX reaction to a mono-exponential association model, red line indicates fit of the reverse ssHDX reaction to a mono-exponential decay model; see text for details. Data shown for an 18 amino acid length PDLA peptide, $n=3$, mean \pm SD. error bars not shown when less than the height of the symbol.

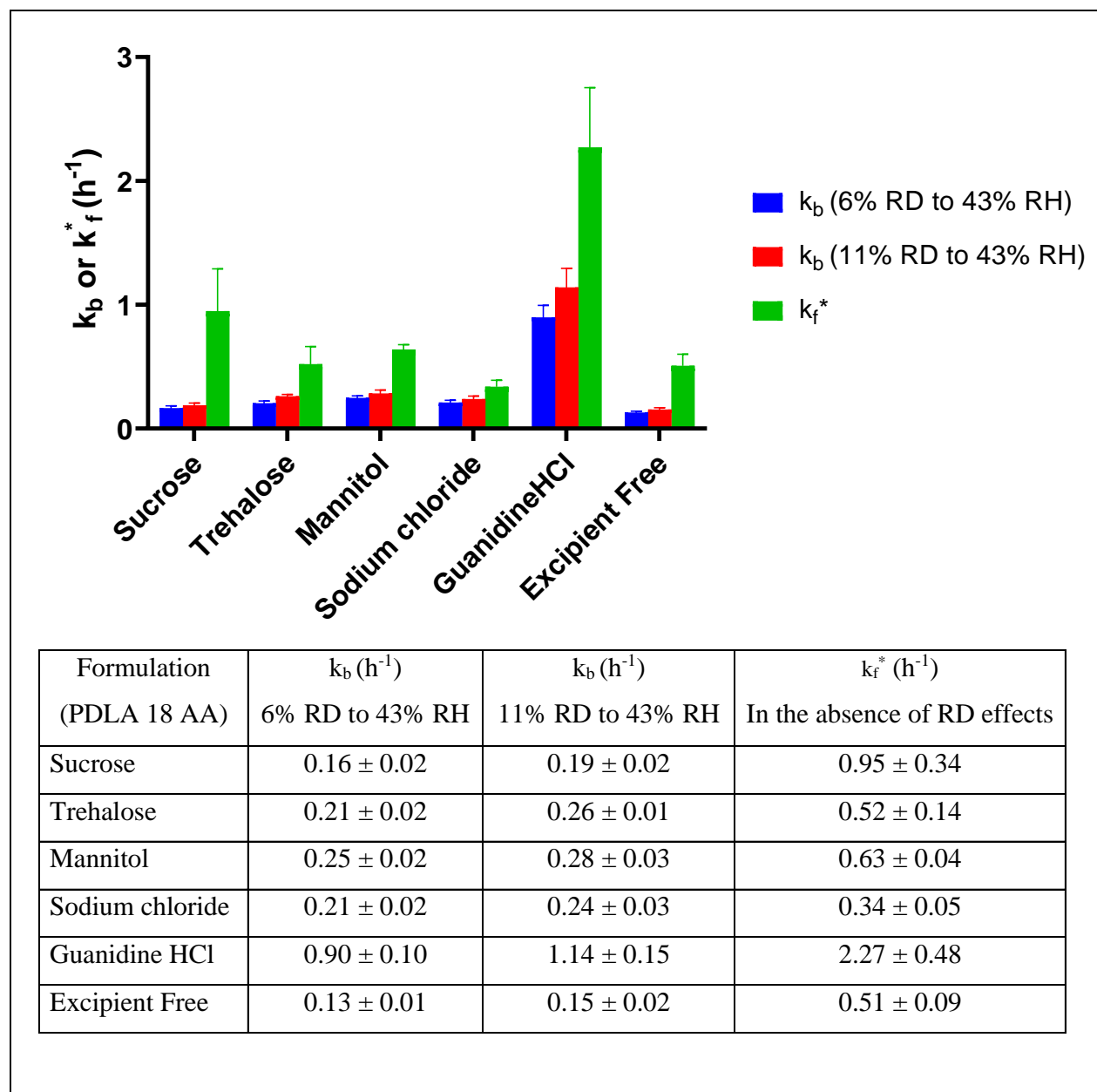


Figure B9. Comparison of the reverse ssHDX reaction rate constant (k_b) and forward reaction rate constant (k_f^*) values of PDLA formulations estimated using a series of deuterium labeling studies conducted at (6%, 11%, 23%, and 43% RD), as the slope of the apparent deuterium incorporation rate constant (k_{ap}) as a function of a_D (given by % RD/100), as reported previously.¹ Data shown for an 18 amino acid length PDLA peptide; $n=3$, mean \pm SE.

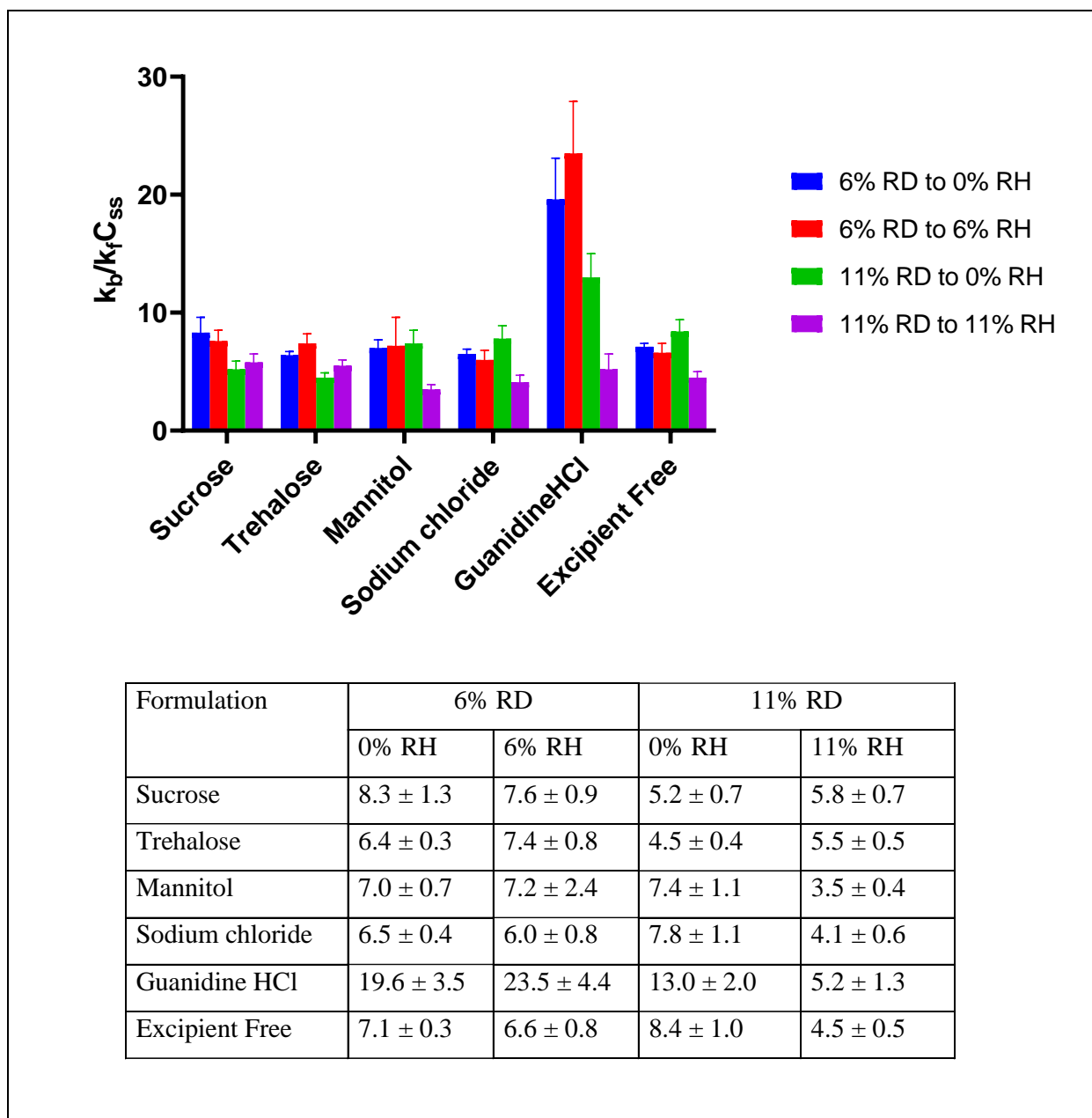


Figure B10. Comparison of the $k_b/k_f C_{ss}$ values of PDLA formulations deuterated at 6% RD (Case-3) or 11% RD (Case-4) followed by deuterium removal at 0% RH, 6% RH or 11% RH. Data shown for an 18 amino acid length PDLA peptide; $n=3$, mean \pm SE.

Reference:

1. Kammari, R.; Topp, E. M. Solid-state hydrogen-deuterium exchange mass spectrometry (ssHDX-MS) of lyophilized poly-D, L-alanine. *Mol. Pharmaceutics*. **2019**, *16*, 2935-2946.

APPENDIX C. SUPPORTING INFORMATION FOR CHAPTER 4

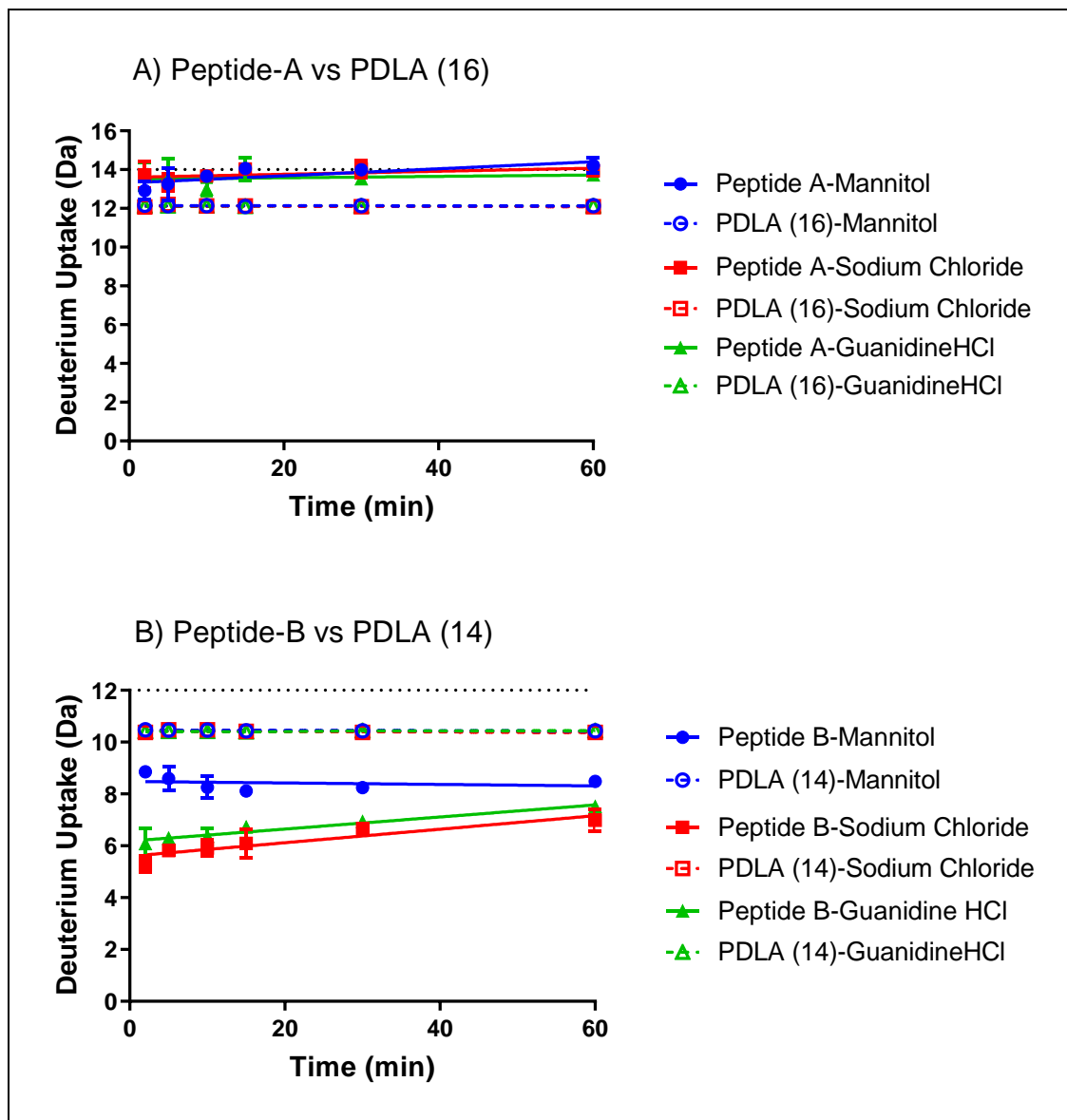


Figure C1. Solution HDX-MS of A) Peptide-A (i.e., Ac-(A₄K)₃A-NH₂) vs PDLA (16 aa) and B) Peptide-B (i.e., Ac-KA₁₂K-NH₂) vs PDLA (14 aa). The dotted line represents the maximum possible theoretical deuteration level, n=3, mean ± SD, error bars are not shown when smaller than the symbol.

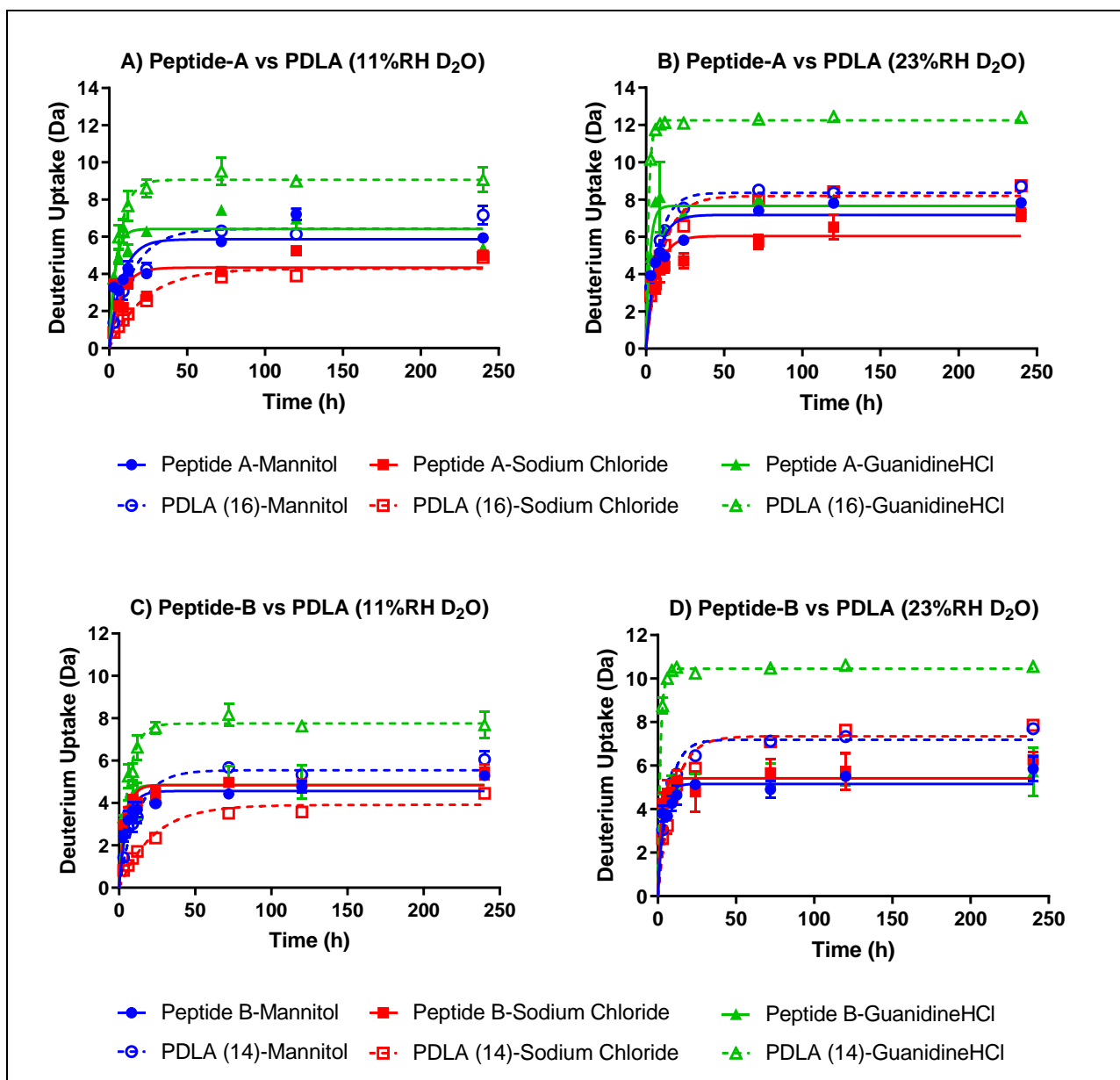


Figure C2. Solid-state HDX-MS of crystalline formulations A) Peptide-A (i.e., Ac-(A₄K)₃A-NH₂) vs PDLA (16 aa) at 11% RH D₂O, B) Peptide-A (i.e., Ac-(A₄K)₃A-NH₂) vs PDLA (16 aa) at 23% RH D₂O, C) Peptide-B (i.e., Ac-KA₁₂K-NH₂) vs PDLA (14 aa) at 11% RH D₂O and D) Peptide-B (i.e., Ac-KA₁₂K-NH₂) vs PDLA (14 aa) at 23% RH D₂O. n=3, mean ± SD, error bars are not shown when smaller than the symbol.

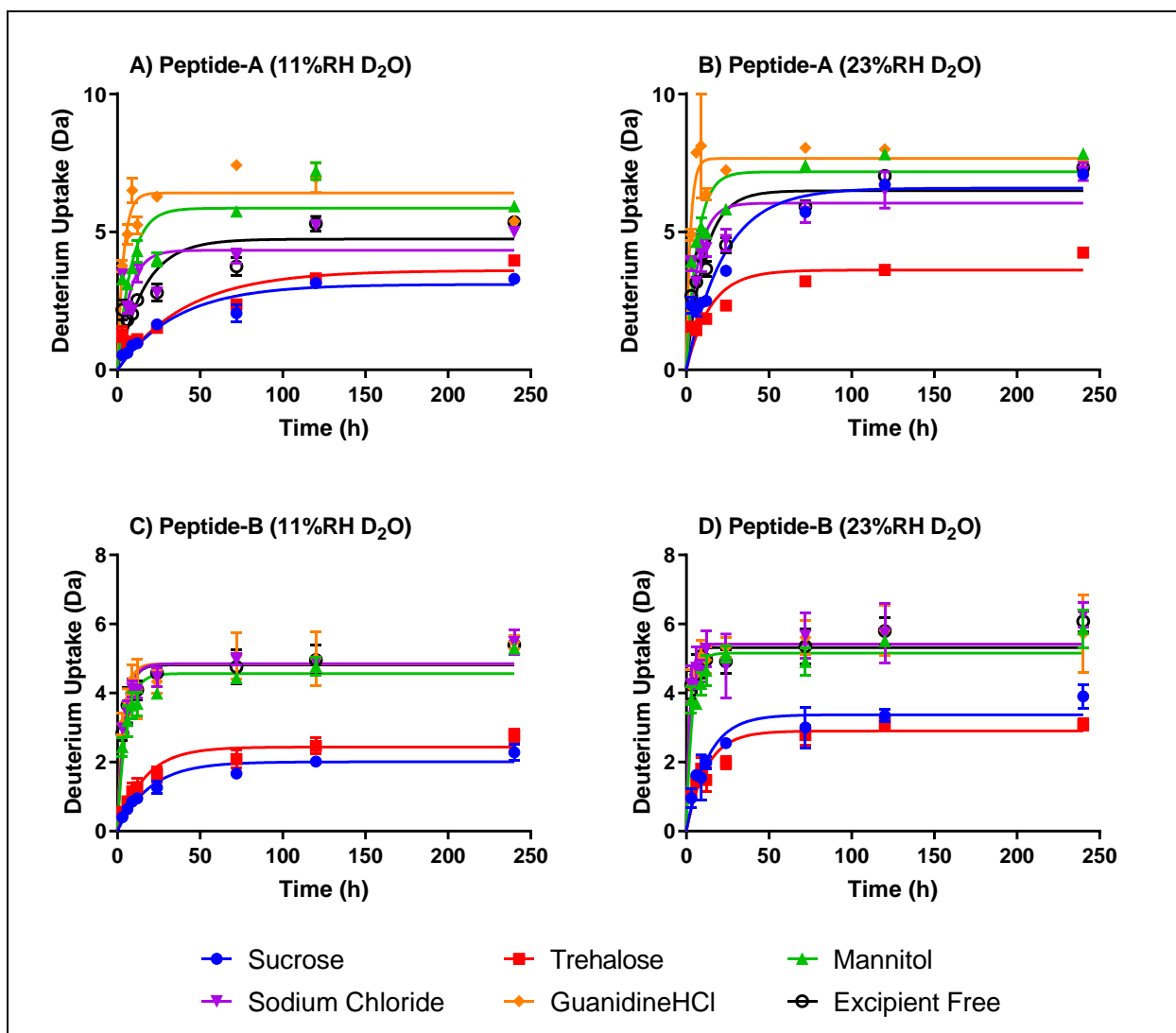


Figure C3. Solid-state HDX-MS of A) Peptide-A (i.e., Ac-(A₄K)₃A-NH₂) at 11% RH D₂O, B) Peptide-A (i.e., Ac-(A₄K)₃A-NH₂) at 23% RH D₂O, C) Peptide-B (i.e., Ac-KA₁₂K-NH₂) at 11% RH D₂O and D) Peptide-B (i.e., Ac-KA₁₂K-NH₂) at 23% RH D₂O. n=3, mean ± SD, error bars are not shown when smaller than the symbol.

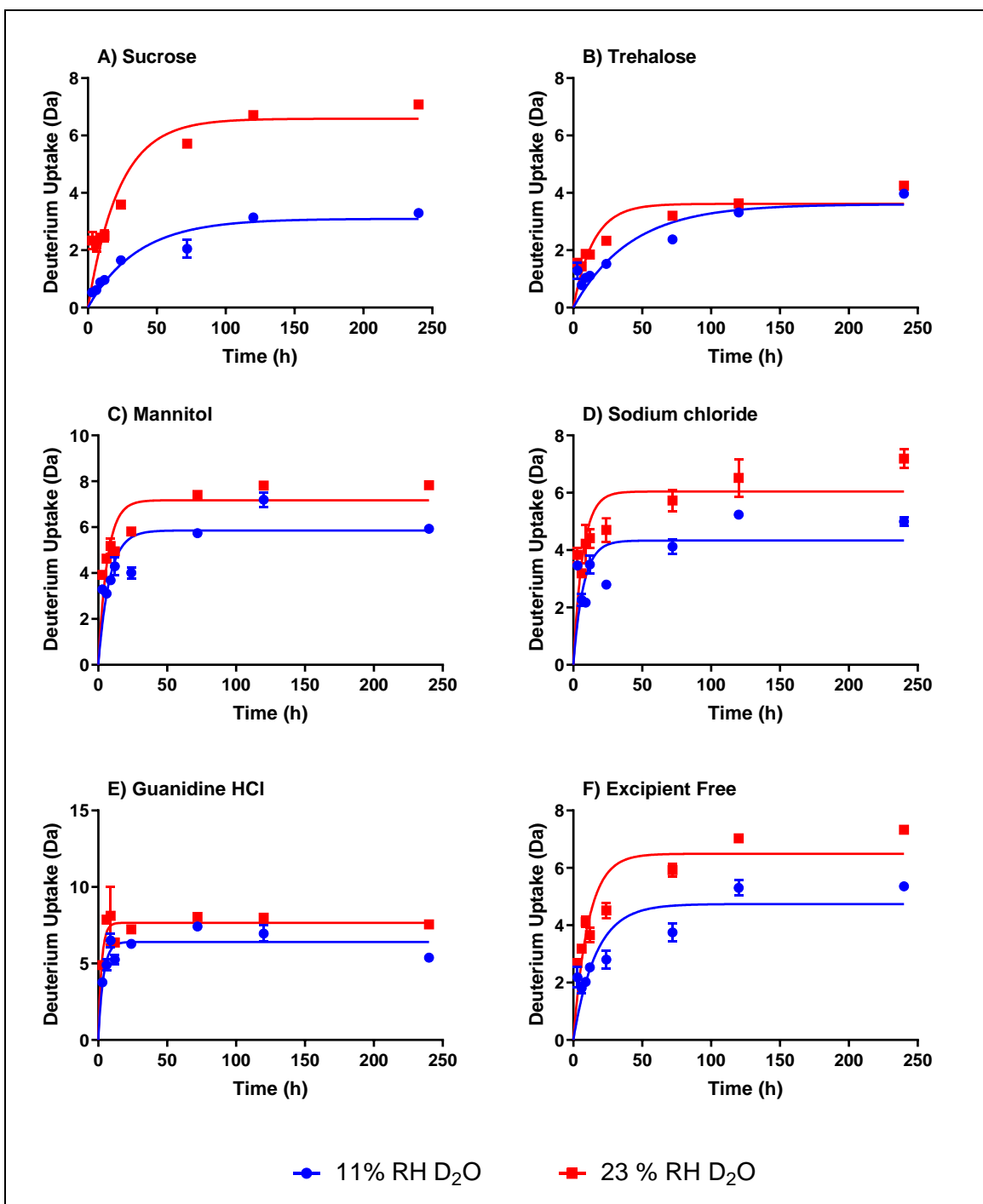


Figure C4. Comparison of ssHDX-MS of Peptide A formulations at 11% RH D₂O and 23% RH D₂O. A) sucrose, B) trehalose, C) mannitol, D) sodium chloride, E) guanidine HCl, and F) excipient free. Colors indicate different RH conditions: 11% RH D₂O (blue), 23% RH D₂O (red). n=3, mean ± SD; error bars not shown when less than the height of the symbol.

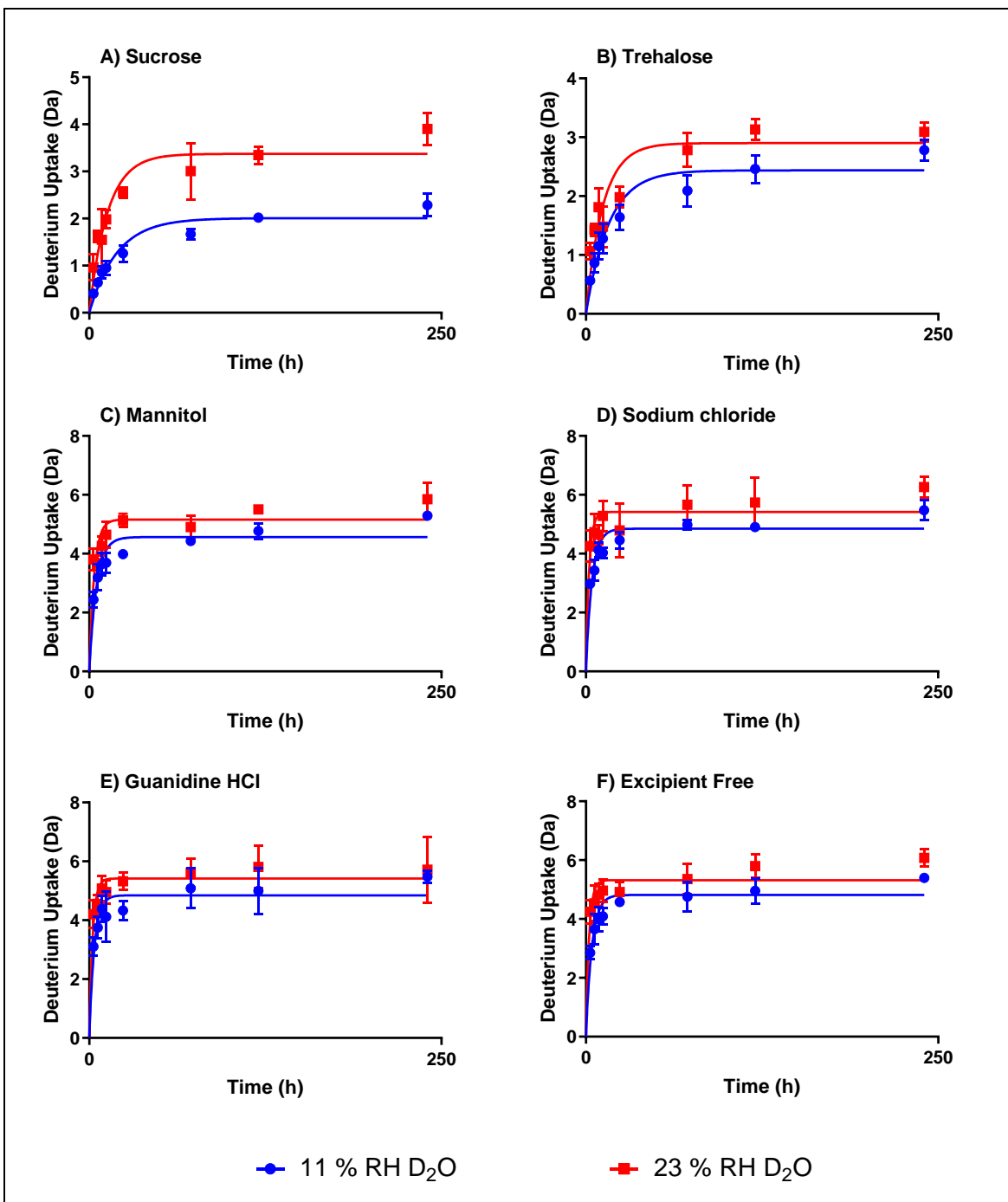


Figure C5. Comparison of ssHDX-MS of Peptide B formulations at 11% RH D₂O and 23% RH D₂O. A) sucrose, B) trehalose, C) mannitol, D) sodium chloride, E) guanidine HCl, and F) excipient free. Colors indicate different RH conditions: 11% RH D₂O (blue), 23% RH D₂O (red). n=3, mean ± SD; error bars not shown when less than the height of the symbol.

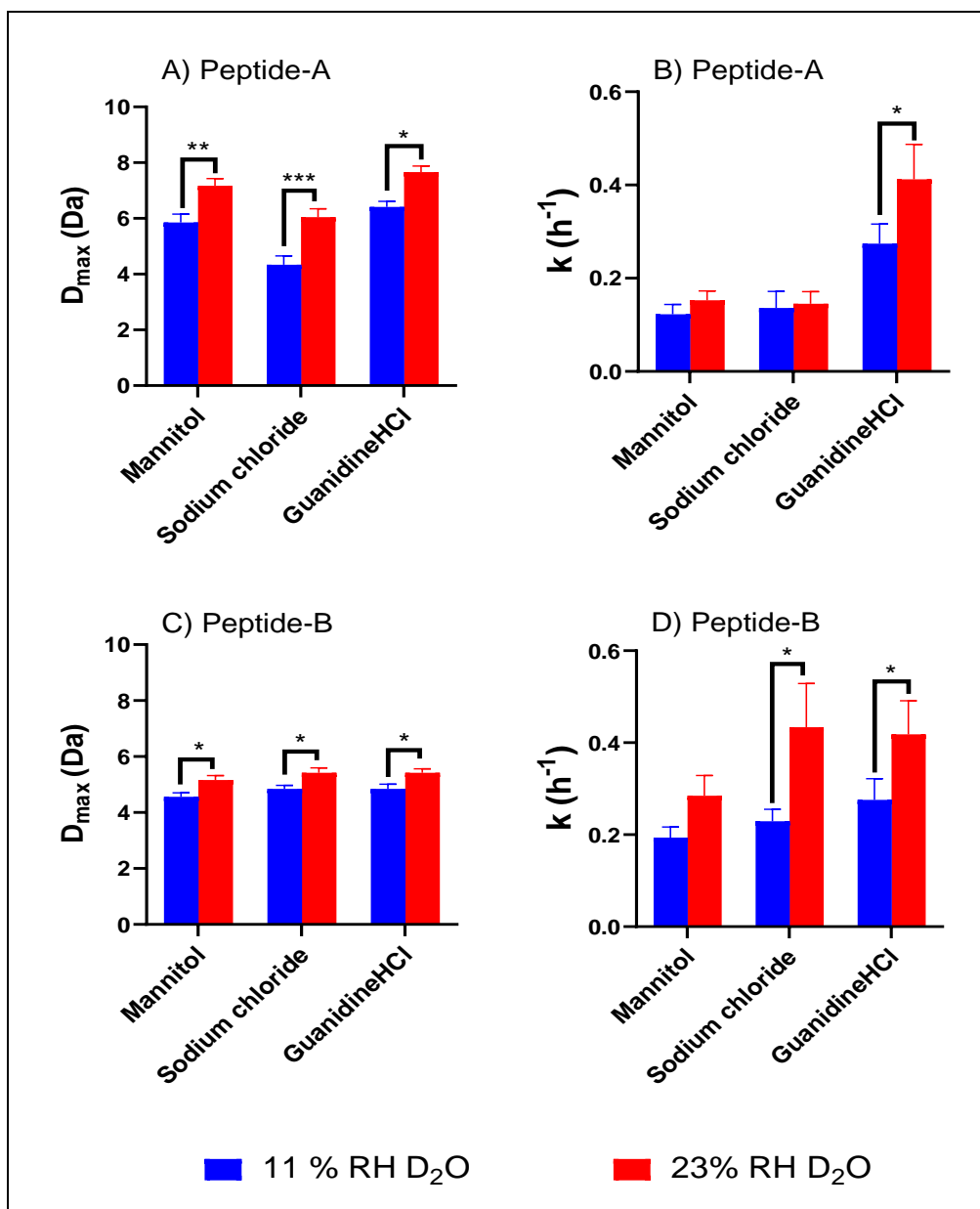


Figure C6. Comparison of ssHDX-MS kinetics at 11% RH D₂O and 23% RH D₂O (crystalline formulations). A) D_{max} (Peptide A), B) k (Peptide A), C) D_{max} (Peptide B), and D) k (Peptide B). Colors indicate different RH conditions: 11% RH D₂O (blue), 23% RH D₂O (red). n=3, mean ± SE; error bars not shown when less than the height of the symbol.

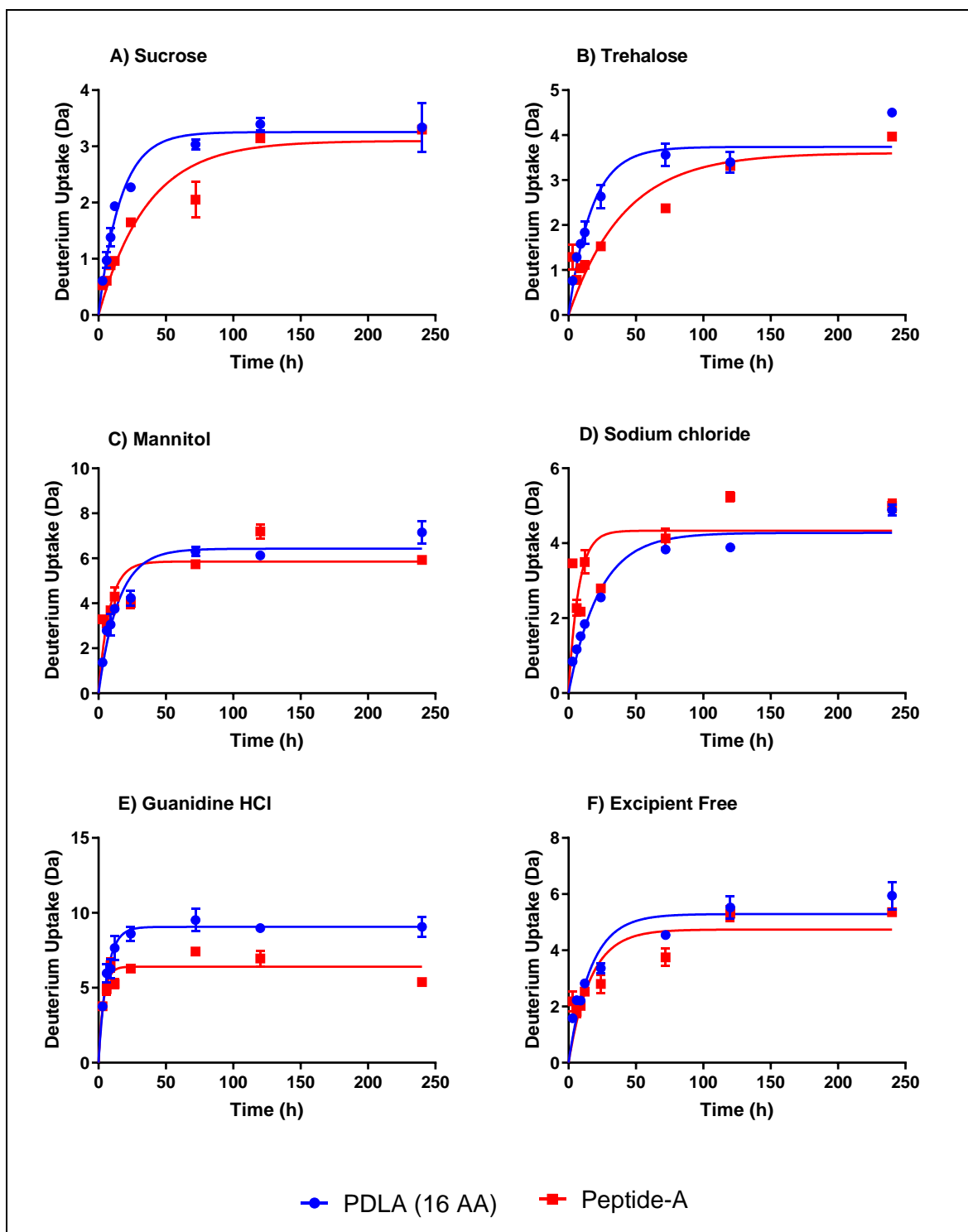


Figure C7. Comparison of ssHDX-MS of unstructured PDLA (16 aa) vs α -helical Peptide A at 11% RH. A) sucrose, B) trehalose, C) mannitol, D) sodium chloride, E) guanidine HCl, and F) excipient free, Colors indicate different peptides: PDLA (blue), Peptide-A (red). $n=3$, mean \pm SD; error bars not shown when less than the height of the symbol.

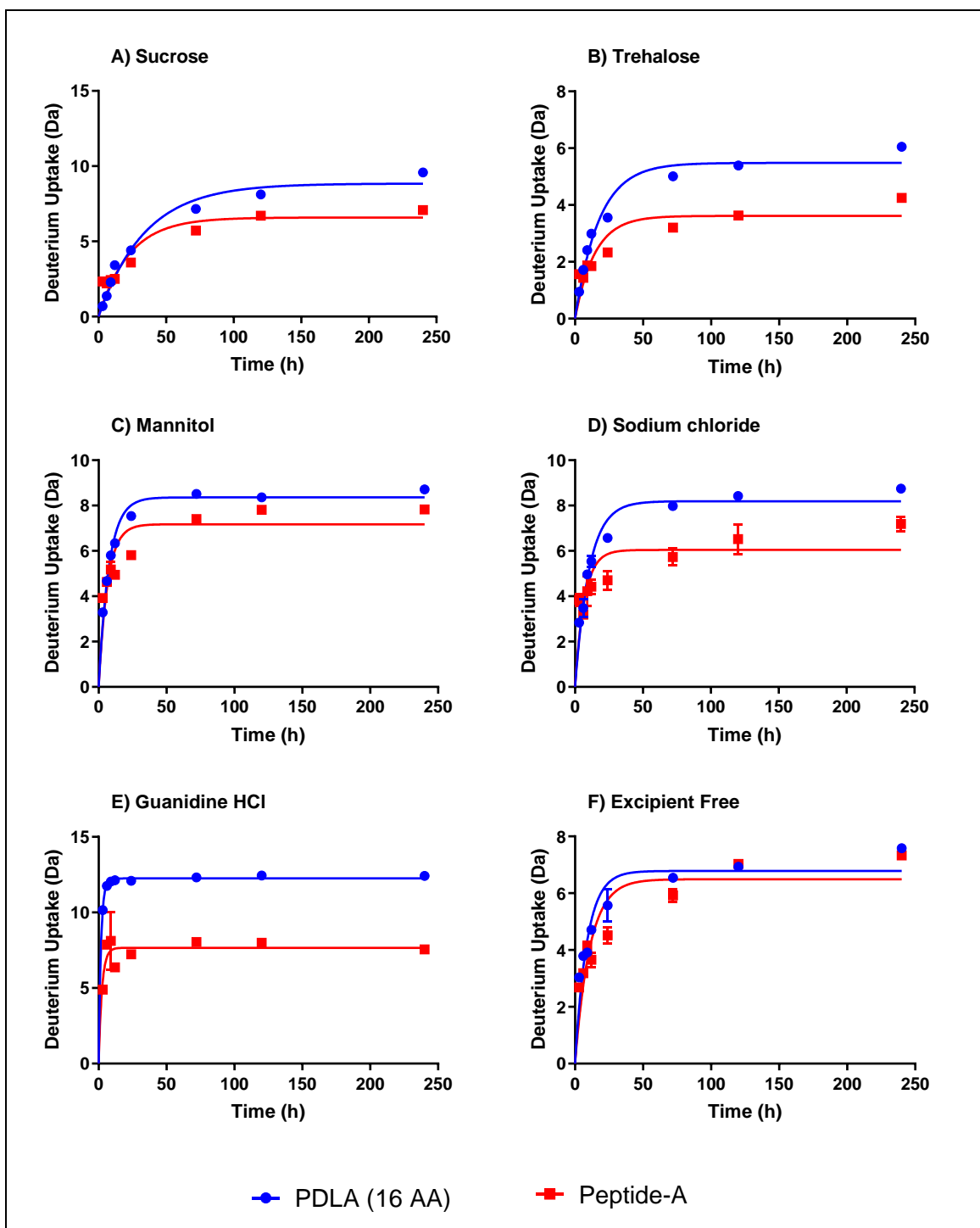


Figure C8. Comparison of ssHDX-MS of unstructured PDLA (16 aa) vs α -helical Peptide A at 23% RH. A) sucrose, B) trehalose, C) mannitol, D) sodium chloride, E) guanidine HCl, and F) excipient free, Colors indicate different peptides: PDLA (blue), Peptide-A (red). $n=3$, mean \pm SD; error bars not shown when less than the height of the symbol.

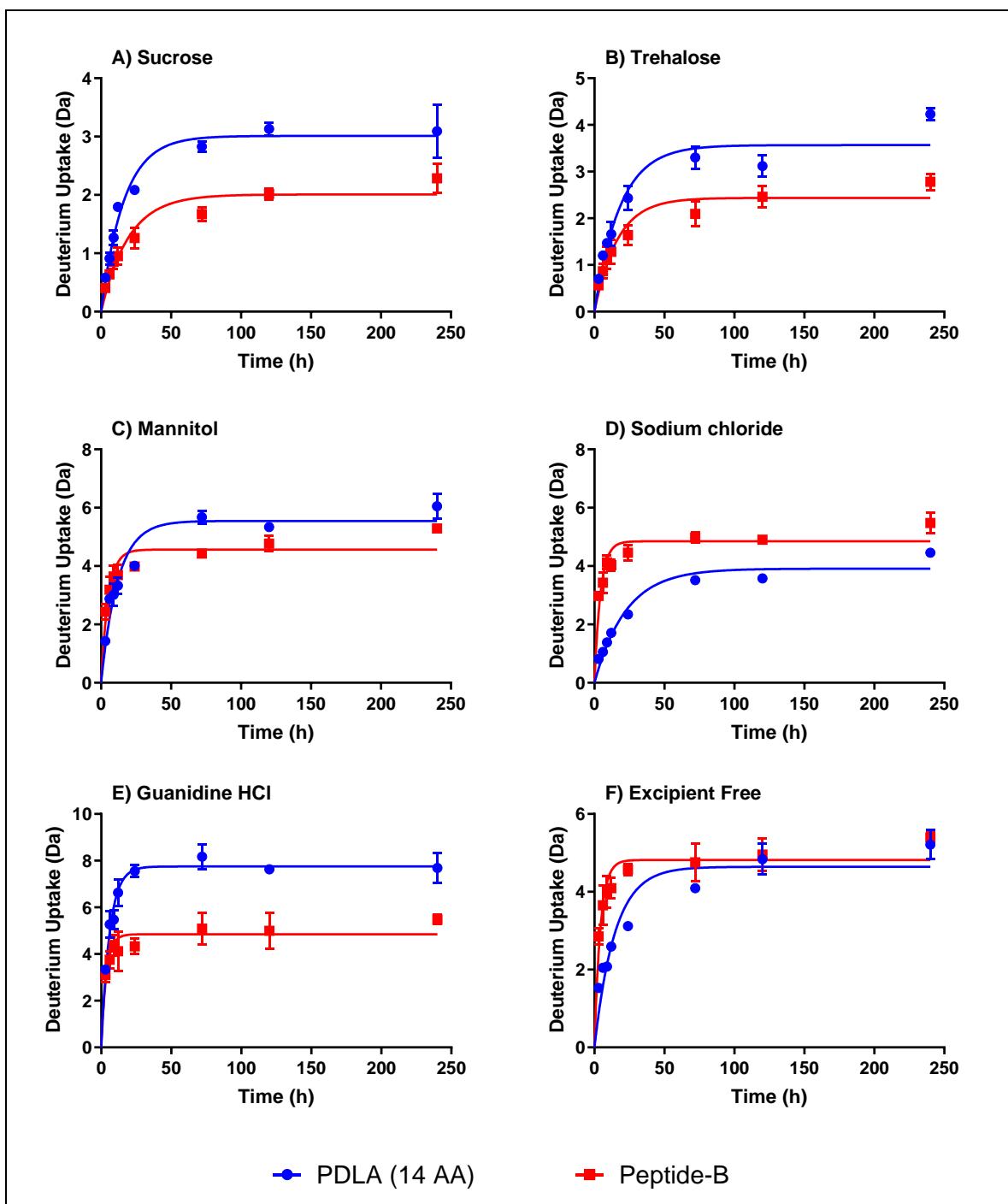


Figure C9. Comparison of ssHDX-MS of unstructured PDLA (14 aa) vs β -sheet Peptide B at 11% RH. A) sucrose, B) trehalose, C) mannitol, D) sodium chloride, E) guanidine HCl, and F) excipient free, Colors indicate different peptides: PDLA (blue), Peptide-B (red). $n=3$, mean \pm SD; error bars not shown when less than the height of the symbol.

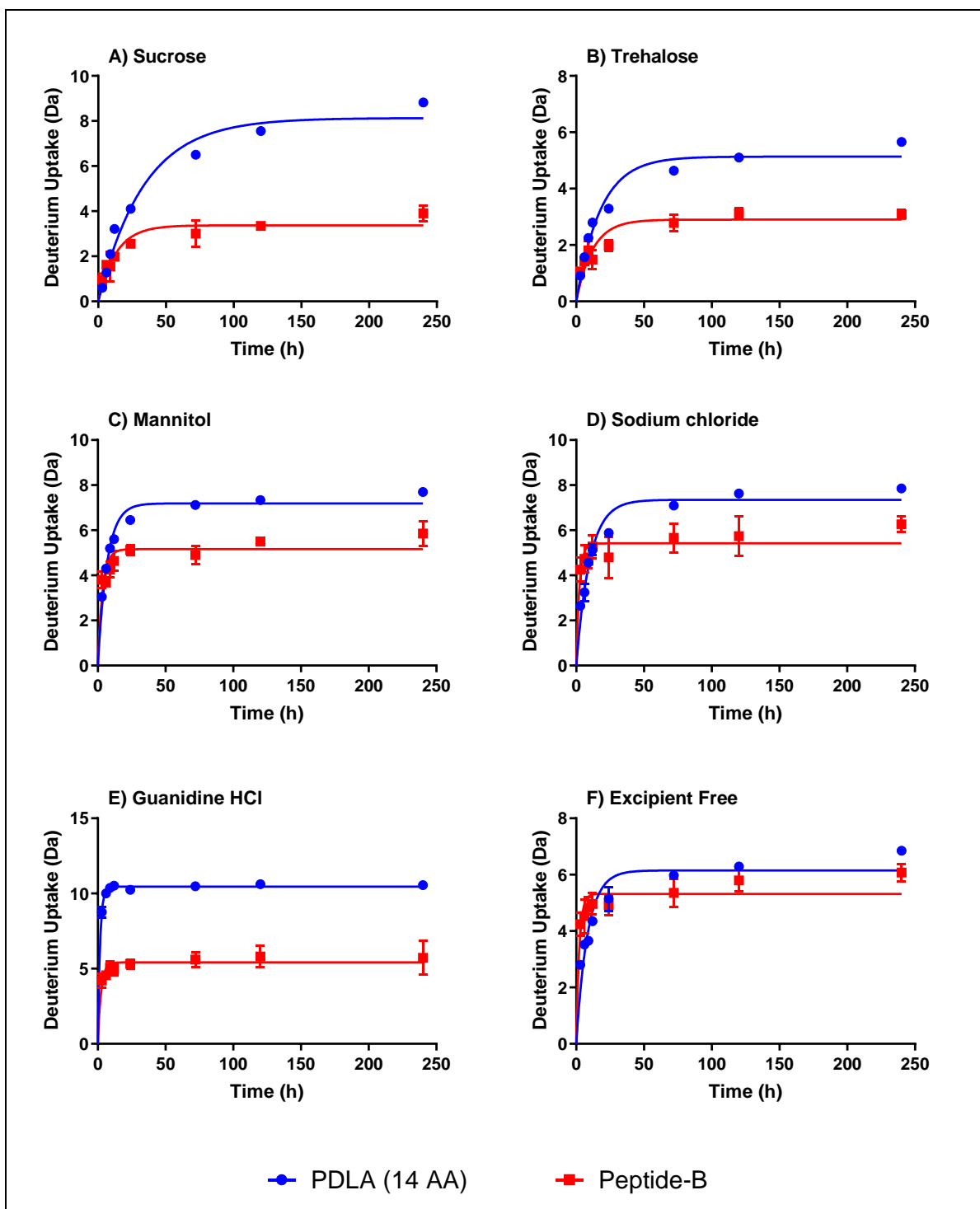


Figure C10. Comparison of ssHDX-MS of unstructured PDLA (14 aa) vs β -sheet Peptide B at 23% RH. A) sucrose, B) trehalose, C) mannitol, D) sodium chloride, E) guanidine HCl, and F) excipient free, Colors indicate different peptides: PDLA (blue), Peptide-B (red). $n=3$, mean \pm SD; error bars not shown when less than the height of the symbol.

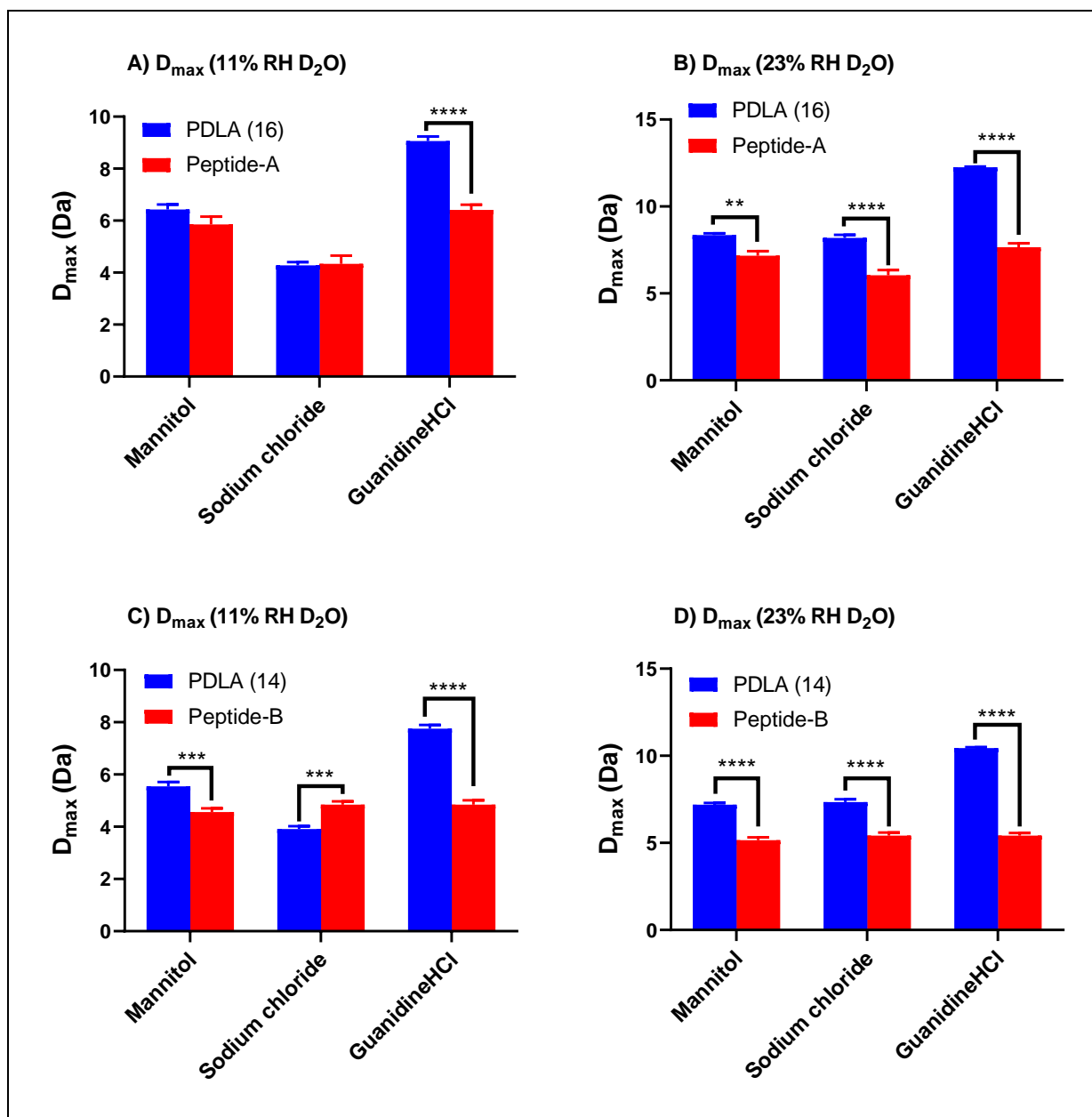


Figure C11. Comparison of maximum deuterium incorporation (D_{\max}) in ssHDX-MS for unstructured PDLA peptides vs structured Peptide A (α -helical) or Peptide B (β -sheet) formulations (crystalline). A) 16aa PDLA vs Peptide A (D_{\max} at 11% RH D_2O), B) 16aa PDLA vs Peptide A (D_{\max} at 23% RH D_2O), C) 14aa PDLA vs Peptide B (D_{\max} at 11% RH D_2O), and D) 14aa PDLA vs Peptide-B (D_{\max} at 23% RH D_2O). Colors indicate different peptides: PDLA (blue), Peptide A or Peptide B (red). $n=3$, mean \pm SE; error bars not shown when less than the height of the symbol.

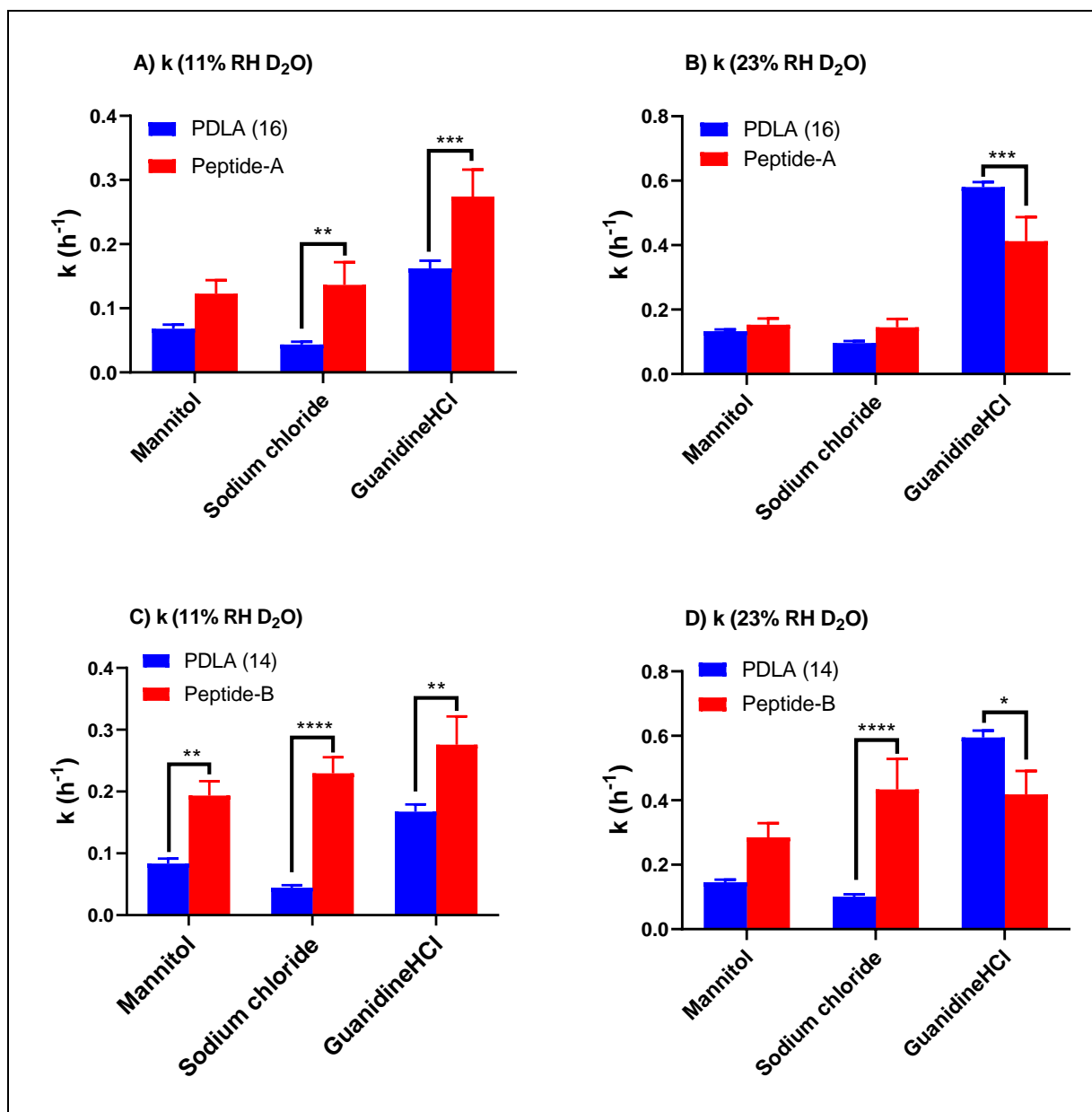


Figure C12. Comparison of ssHDX-MS kinetics of unstructured PDLA vs structured Peptide A or Peptide B formulations (crystalline). A) PDLA vs Peptide A (k at 11% RH D₂O), B) PDLA vs Peptide A (k at 23% RH D₂O), C) PDLA vs Peptide B (k at 11% RH D₂O), and D) PDLA vs Peptide B (k at 23% RH D₂O), Colors indicate different peptides: PDLA (blue), Peptide A or Peptide B (red). $n=3$, mean \pm SE; error bars not shown when less than the height of the symbol.

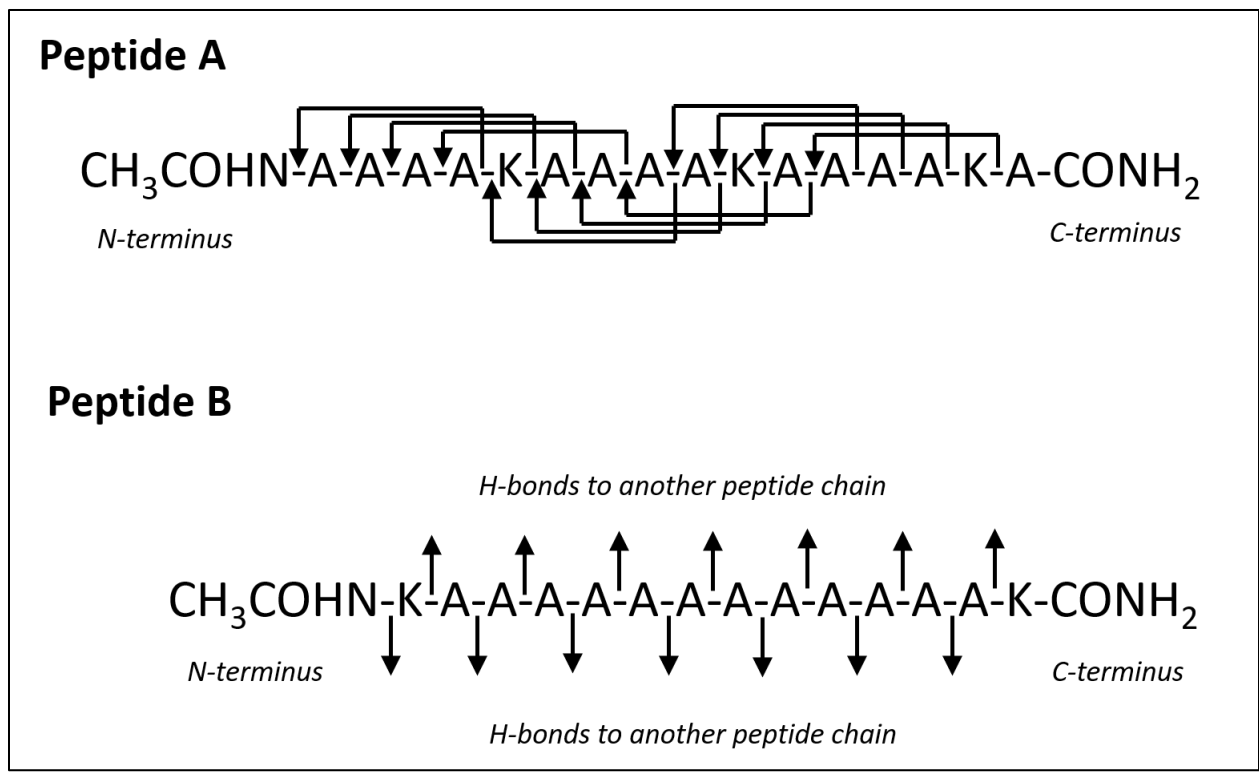


Figure C13. Possible structures and H-bond patterns of Peptides A and B. Peptide B may also form a β -hairpin with six hydrogen bonds (not shown).

Table C1. Effect of RH on the D_{\max} (Da) values of Peptide A and Peptide B formulations (n=3, mean \pm SE).

Formulation	Peptide-A		Peptide-B	
	11% RH D ₂ O	23% RH D ₂ O	11% RH D ₂ O	23% RH D ₂ O
Sucrose	3.1 \pm 0.1	6.6 \pm 0.3	2.0 \pm 0.1	3.4 \pm 0.1
Trehalose	3.6 \pm 0.2	3.6 \pm 0.2	2.4 \pm 0.1	2.9 \pm 0.1
Mannitol	5.9 \pm 0.3	7.2 \pm 0.3	4.6 \pm 0.1	5.2 \pm 0.2
Sodium chloride	4.3 \pm 0.3	6.0 \pm 0.3	4.8 \pm 0.1	5.4 \pm 0.2
Guanidine HCl	6.4 \pm 0.2	7.7 \pm 0.2	4.8 \pm 0.2	5.4 \pm 0.1
Excipient Free	4.7 \pm 0.3	6.5 \pm 0.3	4.8 \pm 0.1	5.3 \pm 0.1

Table C2. Effect of RH on the HDX rate constant values (k, h⁻¹) of Peptide A and Peptide B formulations (n=3, mean \pm SE).

Formulation	Peptide-A		Peptide-B	
	11% RH D ₂ O	23% RH D ₂ O	11% RH D ₂ O	23% RH D ₂ O
Sucrose	0.03 \pm 0.00	0.04 \pm 0.01	0.05 \pm 0.01	0.08 \pm 0.01
Trehalose	0.02 \pm 0.00	0.07 \pm 0.01	0.06 \pm 0.01	0.08 \pm 0.01
Mannitol	0.12 \pm 0.02	0.15 \pm 0.02	0.19 \pm 0.02	0.29 \pm 0.04
Sodium chloride	0.14 \pm 0.04	0.15 \pm 0.03	0.23 \pm 0.03	0.43 \pm 0.09
Guanidine HCl	0.27 \pm 0.04	0.41 \pm 0.08	0.28 \pm 0.05	0.42 \pm 0.07
Excipient Free	0.06 \pm 0.01	0.09 \pm 0.01	0.24 \pm 0.03	0.44 \pm 0.08

Table C3. Effect of secondary structure on the D_{\max} (Da) values of Peptide A formulations in comparison with corresponding unstructured PDLA peptides (n=3, mean \pm SE).

Formulation	11% RH D ₂ O		23% RH D ₂ O	
	PDLA (16 AA)	Peptide-A	PDLA (16 AA)	Peptide-A
Sucrose	3.3 \pm 0.1	3.1 \pm 0.1	8.8 \pm 0.2	6.6 \pm 0.3
Trehalose	3.7 \pm 0.1	3.6 \pm 0.2	5.5 \pm 0.1	3.6 \pm 0.2
Mannitol	6.4 \pm 0.2	5.9 \pm 0.3	8.4 \pm 0.1	7.2 \pm 0.3
Sodium chloride	4.3 \pm 0.1	4.3 \pm 0.3	8.2 \pm 0.2	6.1 \pm 0.3
Guanidine HCl	9.1 \pm 0.2	6.4 \pm 0.2	12.3 \pm 0.1	7.7 \pm 0.2
Excipient Free	5.3 \pm 0.2	4.7 \pm 0.3	6.8 \pm 0.2	6.5 \pm 0.3

Table C4. Effect of secondary structure on the D_{\max} (Da) values of Peptide B formulations in comparison with corresponding unstructured PDLA peptides (n=3, mean \pm SE).

Formulation	11% RH D ₂ O		23% RH D ₂ O	
	PDLA (14 AA)	Peptide-B	PDLA (14 AA)	Peptide-B
Sucrose	3.0 \pm 0.1	2.0 \pm 0.1	8.1 \pm 0.2	3.4 \pm 0.1
Trehalose	3.6 \pm 0.1	2.4 \pm 0.1	5.1 \pm 0.1	2.9 \pm 0.1
Mannitol	5.6 \pm 0.2	4.6 \pm 0.1	7.2 \pm 0.1	5.2 \pm 0.2
Sodium chloride	3.9 \pm 0.1	4.8 \pm 0.1	7.3 \pm 0.2	5.4 \pm 0.2
Guanidine HCl	7.8 \pm 0.1	4.8 \pm 0.2	10.5 \pm 0.0	5.4 \pm 0.1
Excipient Free	4.6 \pm 0.2	4.8 \pm 0.1	6.2 \pm 0.2	5.3 \pm 0.1

Table C5. Effect of secondary structure on the HDX rate constant values (k , h^{-1}) of Peptide A formulations in comparison with corresponding unstructured PDLA peptides ($n=3$, mean \pm SE).

Formulation	11% RH D ₂ O		23% RH D ₂ O	
	PDLA (16 AA)	Peptide-A	PDLA (16 AA)	Peptide-A
Sucrose	0.06 \pm 0.00	0.03 \pm 0.00	0.03 \pm 0.00	0.04 \pm 0.01
Trehalose	0.06 \pm 0.00	0.02 \pm 0.00	0.06 \pm 0.00	0.07 \pm 0.01
Mannitol	0.06 \pm 0.01	0.12 \pm 0.02	0.13 \pm 0.01	0.15 \pm 0.02
Sodium chloride	0.04 \pm 0.00	0.13 \pm 0.04	0.10 \pm 0.01	0.15 \pm 0.03
Guanidine HCl	0.16 \pm 0.01	0.27 \pm 0.04	0.58 \pm 0.02	0.41 \pm 0.08
Excipient Free	0.06 \pm 0.01	0.06 \pm 0.01	0.11 \pm 0.01	0.09 \pm 0.01

Table C6. Effect of secondary structure on the HDX rate constant values (k , h^{-1}) of Peptide B formulations in comparison with corresponding unstructured PDLA peptides ($n=3$, mean \pm SE).

Formulation	11% RH D ₂ O		23% RH D ₂ O	
	PDLA (14 AA)	Peptide-B	PDLA (14 AA)	Peptide-B
Sucrose	0.06 \pm 0.00	0.05 \pm 0.01	0.03 \pm 0.00	0.08 \pm 0.01
Trehalose	0.05 \pm 0.01	0.06 \pm 0.01	0.06 \pm 0.00	0.08 \pm 0.01
Mannitol	0.08 \pm 0.01	0.19 \pm 0.02	0.15 \pm 0.01	0.28 \pm 0.04
Sodium chloride	0.04 \pm 0.00	0.23 \pm 0.03	0.10 \pm 0.01	0.43 \pm 0.09
Guanidine HCl	0.17 \pm 0.01	0.28 \pm 0.05	0.60 \pm 0.02	0.42 \pm 0.07
Excipient Free	0.07 \pm 0.01	0.24 \pm 0.03	0.12 \pm 0.01	0.44 \pm 0.08

Table C7. Calculation of approximate number of structural H-bonds in myoglobin using protein sequence structure information from PDB

S.No.	Secondary structure	Sequence location	Number of amino acids	Approx. number of H-bonds
1	α -helix	4-18	15	11
2	α -helix	21-35	15	11
3	α -helix	37-40	4	1
4	3/10 helix	44-46	3	1
5	α -helix	52-57	6	2
6	α -helix	59-95	37	33
7	α -helix	101-118	18	14
8	α -helix	125-148	24	20
Total number of structural H-bonds (approx.)				93

Table C8. Number of protected amide bonds for myoglobin in various formulations, as measured in ssHDX-MS studies ^{1,2}

Row		Myoglobin
1	Number of exchangeable amide hydrogens (experimental) ¹	112
Protected amide groups, ssHDX-MS at 11% RH (Figure 3) ¹		
2	Mannitol formulation ^{a,b}	82.4 (74%)
3	Sucrose formulation	89.8 (80%)
Protected amide groups, ssHDX-MS at 43% RH (Figure 3B) ²		
5	Trehalose formulation	88.5 (79%)
6	Sorbitol formulation	77.7 (69%)
^a Number of protected amide groups is the difference between maximum deuteration levels in solution (D_{max}) and in ssHDX-MS. ^b Protected amide groups as a percentage of number of exchangeable amide hydrogens (Row 1) shown in parentheses.		

References:

1. Sophocleous, A. M.; Zhang, J.; Topp, E. M. Localized hydration in lyophilized myoglobin by hydrogen–deuterium exchange mass spectrometry. 1. Exchange mapping. *Mol. Pharmaceutics*. **2012**, 9, 718-726.
2. Moorthy, B. S.; Iyer, L. K.; Topp, E. M. Mass spectrometric approaches to study protein structure and interactions in lyophilized powders. *J. Vis. Exp.* **2015**, (98), No. e52503.

VITA

Rajashekar Kammari

EDUCATION

- **Doctor of Philosophy (Industrial and Physical Pharmacy)** Aug 2015 - Aug 2020
Purdue University West Lafayette, IN
- **Master of Science (Pharmaceutical Sciences)** Aug 2012 - May 2015
Butler University Indianapolis, IN
- **Bachelor of Pharmacy** Aug 2006 - Dec 2010
Osmania University (Nalanda College of Pharmacy) Nalgonda, India

RESEARCH SKILLS AND TECHNIQUES

- Formulation development: Protein/peptide formulations, lyophilization, and spray drying
- Biophysical characterization of proteins:
Mass spectrometry (ESI-Q-TOF): LC/MS, Peptide mapping, Hydrogen Deuterium Exchange (HDX), Chromatography: High Performance Liquid Chromatography (HPLC), Size Exclusion Chromatography (SEC)
Spectroscopy: UV-Visible, Circular Dichroism (CD), Fourier Transform Infrared (FTIR)
Other techniques: Freeze Dry Microscopy (FDM), Differential Scanning Calorimetry (DSC), Dynamic Vapor Sorption (DVS), Powder X-ray Diffraction (PXRD), Dynamic Light Scattering (DLS), Karl Fischer titration
- Molecular biology: Cell culture, Cell viability assays, Gel electrophoresis, Western blot, and Real-Time Polymerase Chain Reaction (RT-PCR)

RESEARCH EXPERIENCE

- Graduate Research Assistant, Purdue University** Aug 2015 - May 2020
- Evaluated the effect of formulation and process changes on the storage stability of recombinant protein (mAb/Fab) formulations produced by lyophilization, spray drying, MicroglassificationTM, and worked on developing solid-state hydrogen-deuterium exchange

mass spectrometry (ssHDX-MS) as a stability-indicating method for proteins in solid powders (NIIMBL collaboration project)

- Investigated the site-specific, reversible protein-protein interactions in high concentration monoclonal antibody formulations and developed a novel HDX-MS methodology for identifying interaction domains (Merck-Purdue Center for Measurement Science collaboration project)
- Designed and optimized lyophilization, spray drying cycles for protein formulations; conducted accelerated stability studies and applied novel biophysical characterization techniques to screen formulations and to study conformational changes
- Investigated the fundamental mechanism of ssHDX-MS and developed a mechanistic model by evaluating the effects of peptide/protein-matrix interactions, secondary structure (α -helix and β -sheet) and HDX reaction reversibility on deuteration kinetics

Summer Intern, Atrium (GlaxoSmithKline, King of Prussia, PA) May 2017 - Aug 2017

- Applied solid-state HDX-MS as a prediction tool for protein degradation propensity in lyophilized mAb formulations

Graduate Research Assistant, Butler University Aug 2012 - May 2015

- Developed and characterized polymeric nanoparticulate systems for the co-delivery of small molecular drugs and siRNA oligonucleotides
- Evaluated the nanoparticulate system efficiency in gene knockdown, cytotoxicity and apoptosis induction using *in vitro* cell culture models

REPRESENTATIVE PUBLICATIONS

- **Rajashekar Kammari**, Elizabeth M. Topp, Effects of Secondary Structure on Solid-State Hydrogen–Deuterium Exchange in Model α -Helix and β -Sheet Peptides, *Molecular Pharmaceutics*, 2020, 17 (9), 3501–3512.
- **Rajashekar Kammari**, Elizabeth M. Topp, Pre-Hydration and the Reversibility of Solid-State Hydrogen-Deuterium Exchange, *Molecular Pharmaceutics*, 2020, 17 (9), 3541–3552.
- **Rajashekar Kammari**, Elizabeth M. Topp, Solid-State Hydrogen Deuterium Exchange Mass Spectrometry (ssHDX-MS) of Lyophilized Poly-DL-Alanine, *Molecular Pharmaceutics*, 2019, 16 (7), 2935–2946.

- Karthik Balakrishna Chandrababu, **Rajashekar Kammari**, Yuan Chen, Elizabeth M. Topp, High-Resolution Mass Spectrometric Methods for Proteins in Lyophilized Solids, Chapter in Lyophilization of Pharmaceuticals and Biologicals. Humana Press, New York, NY, 2019, 353-375.
- **Rajashekar Kammari**, Nandita G. Das, Sudip K. Das, Nanoparticulate Systems for Therapeutic and Diagnostic Applications, Chapter in Emerging Nanotechnologies for Diagnostics, Drug Delivery and Medical Devices, Elsevier, Cambridge, MA, 2017, 105-144.

SELECTED PRESENTATIONS

- Characterization of Reversible Protein-Protein Interactions (PPI) in High Concentration mAbs Using Hydrogen/Deuterium Exchange Mass Spectrometry (HDX-MS), **Rajashekar Kammari**, Elizabeth M. Topp, Jainik Panchal, Brent Kochert, Valentyn Antochshuk, Smeet Deshmukh, Colorado Protein Stability Conference: 25th Anniversary, Breckenridge, CO, July 29- Aug 1, 2019.
- Solid-State Hydrogen/Deuterium Exchange Mass Spectrometry (ssHDX-MS) of Lyophilized Peptides, **Rajashekar Kammari**, Elizabeth M. Topp, Preclinical Form and Formulation for Drug Discovery, Gordon Research Seminar (GRS) and Gordon Research Conference (GRC), Waterville Valley, NH, June 8-14, 2019.
- Characterization of Protein-Protein Interactions (PPI) in High Concentration mAbs Using HDX-MS, **Rajashekar Kammari**, Elizabeth M. Topp, Merck-Purdue Symposium, Merck/Purdue Center for Measurement Science, West Point, PA, Nov 13, 2018.
- Reversibility Study of Solid-State Hydrogen/Deuterium Exchange Mass Spectrometry, **Rajashekar Kammari**, Elizabeth M. Topp, 15th Annual Garnet E. Peck Symposium, Purdue University, West Lafayette, IN, March 7, 2018.
- Solid-State Hydrogen/Deuterium Exchange Mass Spectrometry (ssHDX-MS) of Unstructured Peptides, **Rajashekar Kammari**, Elizabeth M. Topp, Midwest Chapter Annual Meeting, International Society of Lyophilization – Freeze Drying (ISL-FD), Chicago, IL, April 13, 2017.